

**Stellingen behorende bij het proefschrift  
"Groundwater modeling of large domains with analytic elements",  
W.J. de Lange.**

- 1 Modellen voor landelijk integraal water beheer zijn bedoeld voor meer-malig en veelzijdig gebruik en verdienen daarom een permanent en zorgvuldig onderhoud (dit proefschrift, p.19).
- 2 Modelleren met analytische elementen verschilt van modelleren met andere technieken omdat:
  - elk watervoerend pakket oneindig uitgestrekt is;
  - elk element zelfstandig werkt in het hele watervoerende pakket;
  - gekozen moet worden uit verschillende typen van elementen (naast de op te geven randvoorwaarde);
  - het combineren van elementen de betekenis heeft van het combineren van voor grondwater van belang zijnde eenheden (polders, rivieren, onttrekkingen, stuwwallen, aquifer afsluitingen);
  - het conceptuele model geformuleerd wordt in termen van grondwater-eenheden in plaats van in geohydrologische constanten (transmissiviteit, weerstand, etc.) (dit proefschrift, pp. 20, 21).
- 3 Modelleren met analytische elementen vereist gedegen kennis van de te gebruiken element types en van de mogelijke combinaties daarmee (dit proefschrift, p. 69).
- 4 Het gebruik van analytische elementen leidt tot een ongekennde flexibiliteit in het aanpassen van een model en versterkt het inzicht in het functioneren van het gemodelleerde systeem (dit proefschrift, pp. 125-138).
- 5 Na voltooiing van de voorziene ontwikkelingen zal de analytische elementen methode ongekennde mogelijkheden bezitten voor het modelleren van grondwaterstroming (dit proefschrift, p. 66-68).
- 6 De interactie tussen grote aantallen oppervlaktewateren en het onderliggende grondwater kan worden beschreven met eenvoudige formules voor de twee parameters in een Cauchy randvoorwaarde. Deze parameters zijn de voedingsweerstand en het gemodificeerde oppervlaktewater peil (maar niet het oppervlaktewater peil sec) (dit proefschrift, p. 148).
- 7 De voedingsweerstand is vrijwel lineair gerelateerd met de afstand tussen oppervlaktewateren voor afstanden die aanmerkelijk kleiner of aanmerkelijk groter zijn dan de spreidingslengte van het freatische watervoerend pakket, zijnde de wortel uit het produkt van de transmissiviteit en de weerstand van de onderliggende scheidende laag (dit proefschrift, p. 148).
- 8 De voedingsweerstand kan niet eenvoudig worden berekend met behulp van de drainageweerstand (dit proefschrift pp. 153, 155-156).

- 9 Berekening van de voedingsweerstand met behulp van een (computer-) model is alleen mogelijk indien dat model werkelijk stroming tussen de oppervlaktewateren en het bovenste watervoerend pakket simuleert (dit proefschrift, p. 158-160).
- 10 Het bestaande gebruik van de drainagedichtheid voor de bepaling van de representatieve afstand tussen willekeurig gesitueerde oppervlaktewateren in de formule voor de voedingsweerstand is aanvaardbaar indien (1) de grondwaterstroming hoofdzakelijk parallel (in het horizontale vlak) is nabij de oppervlaktewateren en (2) de voedingsweerstand bij benadering een lineaire relatie heeft met de afstand tussen de oppervlaktewateren (dit proefschrift, p. 196-200).
- 11 Zolang de hoek tussen twee rechte oppervlaktewateren kleiner is dan 180 graden stroomt er geen grondwater naar het kruispunt van deze wateren (contra conclusie van E.G. Youngs in Patterns of steady groundwater movement in bounded unconfined aquifers, Journal of Hydrology nr. 131 pp. 239-253, 1992) (dit proefschrift, p. 190-191).
- 12 De interactie tussen oppervlaktewater en grondwater wordt te vaak onbegrepen danwel onbegrijpelijk gemodelleerd.
- 13 Om zinvolle resultaten te kunnen leveren hoeft een model niet per se stroomlijnen en verplaatsingen te produceren die aan de hydrochemie beantwoorden (contra stelling 8 bij proefschrift P.J. Stuijzand, 1993).
- 14 Het is bij weinigen bekend dat Dupuit en Darcy ook formules hebben afgeleid die gebruikt zijn in stedelijke afvoerhydrologie. H. Mannes, Die Berechnung von Rohrnetzen staedtischer Wasserleitungen, R. Oldenburg Muenchen, 1912.
- 15 Een onderzoeker moet herhaaldelijk eigen werk over boord durven zetten.
- 16 Vanwege de kleinere halfwaardetijd verdient het aanbeveling om op computers relatief meer milieubelasting te heffen dan op auto's.
- 17 Het stellen van rechtmatigheid boven doelmatigheid door het rijk (nieuwjaarsrede 1994, J. de Jong, RIZA) leidt tot afname van de produktie bij verhoogde werkdruk. In extrema kan dit resulteren in overwerkte ambtenaren die niets produceren behalve een boekhouding met een accountantsverklaring.
- 18 De trein creëert een ouderwets gevoel van samenzijn.
- 19 Het schrijven van een proefschrift neemt meer tijd dan drie zwangerschappen.
- 20 Modelleren is model-leren.

GROUNDWATER MODELING OF LARGE DOMAINS  
WITH ANALYTIC ELEMENTS

657958

3190886

TR diss 2778

PROEFSCHRIFT

ter verkrijging van de graad van doctor aan  
de Technische Universiteit Delft op gezag van  
de Rector Magnificus Prof. ir K.F. Wakker  
in het openbaar te verdedigen  
ten overstaan van een commissie door  
het College van Dekanen aangewezen  
op dinsdag 25 juni 1996 te 13.30 uur

door

Willem Jan DE LANGE

civiel-ingenieur

geboren te Semarang (Indonesië)



Dit proefschrift is goedgekeurd door de promotor  
Prof. dr ir J.C. van Dam, Technische Universiteit Delft

Samenstelling promotiecommissie:

Rector Magnificus, voorzitter

Prof. dr ir J.C. van Dam	Technische Universiteit Delft, promotor
Prof. dr ir C. van den Akker	Technische Universiteit Delft
Prof. dr ir F.B.J. Barends	Technische Universiteit Delft
Prof. dr ir R.A. Feddes	Landbouwniversiteit Wageningen
Prof. dr ir O.D.L. Strack	University of Minnesota
Prof. dr ir P. van der Veer	Technische Universiteit Delft
Prof. dr ir W. Zijl	Vrije Universiteit Brussel

CIP-DATA KONINKLIJKE BIBLIOTHEEK, DEN HAAG

De Lange, Willem Jan

Groundwater modeling of large domains with analytic elements /  
Willem Jan de Lange .- Delft University of Technology, 1996 .- 237 p. :  
fig., tab.

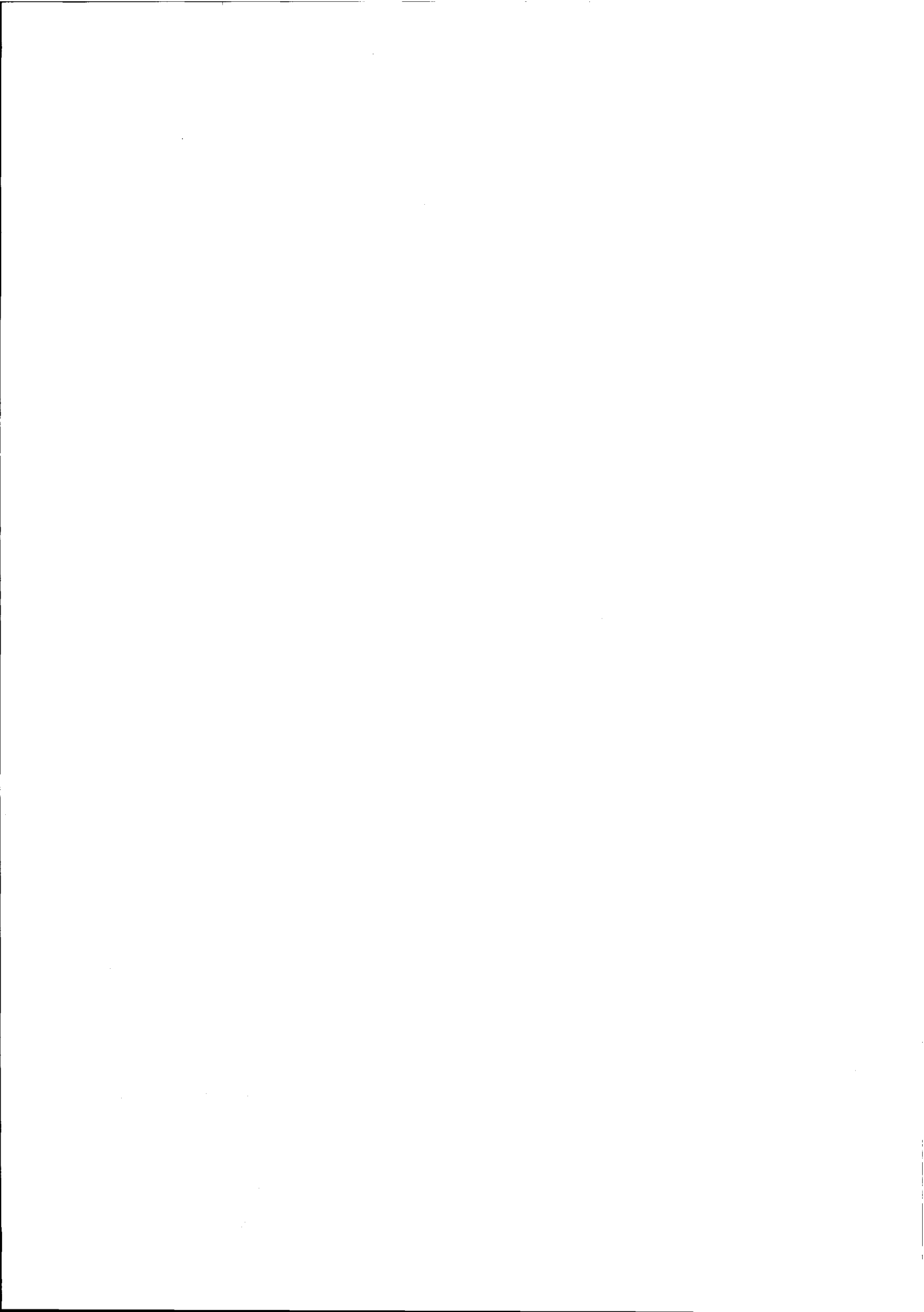
Thesis Delft.- With ref.- With summary in Dutch and English  
RIZA note 96.028.- ISBN 90-369-4569-0

Subject headings: analytical elementen method ; groundwater ; modeling ;  
interaction surface water - groundwater

Copyright (c) by W.J. de Lange, Lelystad, The Netherlands.  
All rights reserved. No part of this publication may be reproduced, stored  
in a retrieval system or transmitted in any form or by any means,  
electronic, mechanical, photocopying, recording or otherwise, without prior  
agreement and written permission of the copyright owner.



Aan mijn vrouw Elske,  
onze kinderen Jacob, Karin en Bart  
en aan mijn ouders.



## ACKNOWLEDGEMENTS

In the final part of my study at the Delft University of Technology, professor dr ir A.T. de Hoop (of the department of Electrical Engineering) introduced me in the boundary integral equation method, which was used to compute the changes over time in the shape and position of a sharp interface between fresh and salt groundwater in three-dimensional flow under semi-stationary conditions. This modeling technique required a modeling approach different from those used with the classical finite element and finite difference techniques. Here, my interest in physically based groundwater modeling was born.

The very first steps to the analytic element technique, which is the base of much of the work in this thesis, was made possible by drs J.W. Stellingwerff of the province of South-Holland. His open mind to test and use new ways to tackle groundwater problems has been stimulating for me.

A main part of this thesis is based on the modeling technique developed by professor dr ir O.D.L. Strack of the University of Minnesota. His enthusiastic support, his help and his explanations to understand the interactions between analytic elements has been of considerable importance during the development of the new modeling approach presented in this thesis.

Many colleagues of the Institute for Inland Water Management and Waste Water Treatment supported the development of the national groundwater model during many years. Especially, dr ir F.H.M. van de Ven is mentioned for his permanent and stimulating support in many respects during the years of this development.

During more than five years, many students and junior geohydrologists of several Universities in the Netherlands have cooperated enthusiastically in the search to the modeling approach presented in this thesis. I hope that they enjoyed it as much as I did.

The discussions with drs J.L. van der Meij and his colleagues of TNO-GG in Delft have been very fruitful. The response of dr ir L.F. Ernst in our correspondence is very appreciated. Ir G.A. Bruggeman is thanked for checking the reworked version of his derivation of the expression for the feeding resistance.

Special thanks are owed to dr. S.R. Kraemer for reading this thesis and for checking of the language.

By thanking mr. B. Jansen, mr. D. Brouwer and ms. S. Verbeek, I express my gratitude to the entire team of RIZA Design of the Institute for Inland Water Management and Waste Water Treatment for the final preparation of the figures and text.

The many discussions with professor dr ir J.C. van Dam helped to formulate the derived knowledge on modeling with the analytic element technique for the "not-insider". During many years, he was a willing ear for my new and sometimes very spontaneous ideas, some of which finally have grown to kernels in this thesis.

During all of my research life, I was supported by my parents and my wife Elske. To them and to my children I dedicate this thesis.

# Contents

<b>ACKNOWLEDGEMENTS</b>	<b>5</b>
<b>CONTENTS</b>	<b>7</b>
<b>1 SCOPE AND GIST OF THIS THESIS</b>	<b>13</b>
<b>2 INTRODUCTORY REMARKS TO THE MODELING OF LARGE DOMAINS WITH ANALYTIC ELEMENTS</b>	<b>17</b>
2.0 Summary	17
2.1 Modeling of large domains for national water management	17
2.2 The model of the Netherlands	18
2.3 Other models of large domains	19
2.4 On the application of the analytic element technique	20
<b>3 A PRACTITIONER'S DESCRIPTION OF STRACK'S ANALYTIC ELEMENT TECHNIQUE (1992)</b>	<b>23</b>
3.0 Summary	23
3.1 Introduction	23
3.2 The discharge potential	24
3.2.1 Basic equations	24
3.2.2 Extended applications of the discharge potential	28
3.3 Description of analytic elements	31
3.3.1 The point-sink (well).	31
3.3.2 The line-sink (river)	32
3.3.3 The dipole	35
3.3.4 The line-dipole (crack, drain, canal)	36
3.3.5 The non-connectable line-doublet (leaky wall, impermeable wall)	39
3.3.6 The connectable line-doublet (inhomogeneity)	42
3.3.7 The area-sink for surface conditions	44
3.3.8 The area-sink for the connection of aquifers	46
3.4 The extension to a semi-three-dimensional method	47
3.4.1 Computation of the vertical flow velocity	47
3.4.2 Vertical flow in other situations	48
3.5 Computational aspects	50
3.5.1 The solution technique	50
3.5.2 Solution technique for a model of elements with both specified and unknown strength	51
3.5.3 Dealing with coupled aquifers	51
<b>4. THE STATE OF THE ART OF THE ANALYTIC ELEMENT TECHNIQUE FOR THE MODELING OF LARGE DOMAINS</b>	<b>53</b>
4.0 Summary	53
4.1 Introduction	53

4.2	The main developments for modeling of large domains in 1993 and 1994	54
4.2.1	Minor and not applied developments	54
4.2.2	Curvilinear elements	54
4.2.3	Area-sinks to model the vertical flow through separating layers near a well	56
4.2.4	Implementation of variable density	59
4.2.5	Area-sink with a variable strength distribution	62
4.2.6	Reduction of needed computation effort (part 1); the superblock approach	63
4.3	An overview of the capabilities of the analytic element technique (march 1995)	64
4.3.1	Available analytic elements (march 1995)	64
4.3.2	Available modeling features due to the discharge potential	65
4.4	Expected developments	66
4.5	Some remarks on the use of the AEM in the computation of groundwater quality	68
<b>5.</b>	<b>PROPERTIES AND BEHAVIOUR OF ANALYTIC ELEMENTS IN MODELING</b>	<b>69</b>
5.0	Summary	69
5.1	Introduction	69
5.2	Single analytic elements	71
5.2.1	The well	71
5.2.2	The line-sink	74
5.2.3	The area-sink	77
5.2.4	The inhomogeneity	84
5.2.5	The leaky wall and the impermeable wall	89
5.2.6	The crack and the drain	94
5.3	Combinations of two analytic elements of different types in a single aquifer	106
5.3.1	A qualification of each combination of two types of analytic elements and a definition of error types	106
5.3.2	Combinations with wells	111
5.3.3	Combinations with line-sinks	118
5.3.4	Combinations with area-sinks	121
5.3.5	Combinations with inhomogeneities	124
5.3.6	Combinations with leaky or impermeable walls	124
5.3.7	Combinations with canals, cracks or drains	125
5.4	Combinations with many elements in a single aquifer	125
5.4.1	Example of area-sinks	125
5.4.2	Example of line-sinks and inhomogeneities	128
5.5	Combinations with elements in several aquifers	131
5.5.1	Example on the shape of leakage area-sinks	131
5.5.2	Example of the vertical transfer of effects in a three aquifer model	134

<b>6</b>	<b>A NEW EXPRESSION FOR THE CAUCHY BOUNDARY CONDITION DESCRIBING THE INTERACTION BETWEEN MANY SURFACE WATERS AND A REGIONAL AQUIFER</b>	<b>139</b>
6.0	Summary	139
6.1	Introduction	139
6.2	A simple expression for the Cauchy boundary condition and step one of its verification, comparisons with expressions for flow in the top aquifer only	143
6.2.1	Derivation of a simple expression for the Cauchy boundary condition based on one-dimensional flow in the top aquifer and a constant head in the regional aquifer	143
6.2.2	Summary of Bruggeman's (1972) derivation of an expression for the Cauchy boundary condition based on two-dimensional flow in the top aquifer and a constant head in the regional aquifer	149
6.2.3	Derivation of an expression for the Cauchy boundary condition based on one-dimensional flow in the top aquifer and a constant flux through the separating layer	151
6.2.4	Comparison of the simple expression for the Cauchy boundary condition with expressions for flow in the top aquifer only	153
6.3	Analysis of expressions for flow in both the top aquifer and the regional aquifer and step 2 of the verification of the simple expression for the Cauchy boundary condition	157
6.3.1	On the suitability of conceptual models describing flow in two aquifers for the derivation of the feeding resistance	157
6.3.2	The general, mathematical solution for a conceptual model with two aquifers	161
6.3.3	Derivation of an expression for the feeding resistance based on a conceptual model including both the top aquifer and the regional aquifer	162
6.3.4	Comparison of the expression for the feeding resistance based on flow in both the top aquifer and the regional aquifer with the simple expression presented in section 6.2.	167
6.4	An expression for the feeding resistance based on a conceptual model with surface waters connected to both the top aquifer and the regional aquifer and its comparison with a more practical expression	169
6.4.1	Derivation of an expression for the feeding resistance based on a conceptual model with surface waters connected to both the top aquifer and the regional aquifer	169
6.4.2	Comparison of the expression based on a conceptual model in which the surface waters are connected to both the top aquifer and the regional aquifer with a more practical expression	175
6.5	Concluding remarks	177

<b>7</b>	<b>ON THE DETERMINATION OF THE FEEDING RESISTANCE IN CASES WITH ARBITRARY SITUATED SURFACE WATERS</b>	<b>179</b>
7.0	Summary	179
7.1	Introduction	179
7.2	The drainage density	181
7.3	The representative feeding resistance in areas with predominantly parallel flow	184
7.3.1	The representative feeding resistance in an area between a straight surface water and a straight water divide forming a corner with an angle smaller than 90°	184
7.3.2	The representative feeding resistance in the situation of parallel flow in quadrangular areas bounded by surface waters	187
7.3.3	The representative feeding resistance for an arbitrary area with predominantly parallel flow bounded by surface waters making corners with angles smaller than 180°	190
7.3.4	Discussion of flow pattern analysis in literature	190
7.4	The feeding resistance in situations with predominantly axial-symmetric flow	191
7.4.1	The feeding resistance in a situation of axial-symmetric flow in a circular area	192
7.4.2	The feeding resistance for axial-symmetric flow in a triangular area bounded by path lines and a straight water divide	192
7.4.3	The feeding resistance for axial-symmetric flow in an arbitrary area bounded by path lines and water divides	196
7.5	The representative feeding resistance in an area with both axial-symmetric and parallel flow and a comparison with its determination in modeling practice	196
7.6	Examples of the calculation of the feeding resistance for an arbitrary area	198
7.7	Concluding remarks	201
<b>8.</b>	<b>ON THE MODELING OF LARGE DOMAINS WITH ANALYTIC ELEMENTS</b>	<b>203</b>
8.0	Summary	203
8.1	Introduction	203
8.2	The approach for modeling of large domains with analytic elements	203
8.2.1	Modeling with analytic elements using the concept of geohydrologic features	204
8.2.2	The approach to model large domains	205
8.3	An approach to build comparable models of different areas by different modellers	207
8.3.1	On the relation between the accuracy and the comparability of models	207
8.3.2	An approach to build comparable models of different areas (based on their scale and using geohydrological features)	209



<b>9. CONCLUSIONS</b>	<b>211</b>
9.1 Conclusions	211
9.2 Recommendations	213
<b>SUMMARY</b>	<b>215</b>
<b>SAMENVATTING</b>	<b>219</b>
<b>REFERENCES</b>	<b>223</b>
<b>LIST OF SYMBOLS</b>	<b>229</b>
<b>CURRICULUM VITAE</b>	<b>237</b>



# 1 SCOPE AND GIST OF THIS THESIS

In 1985, dr ir O.D.L. Strack, professor at the University of Minnesota, introduced his computer code called "single layer analytic element model" (SLAEM) in the Netherlands as part of a course on groundwater modeling. Ever since that moment, the analytic element "technique" - as preferred by the author, or "method" instead of "model" for use in the abbreviation "AEM" - has been used by several interested users in the Netherlands, one of them being the author. The technique showed results of a considerable different nature from those of any existing technique and was used first in the small systems of infiltration ditches and abstraction wells built by drinking water supply companies in the western coastal dune areas of the Netherlands. In the United States of America the technique was mostly applied in situations concerning one aquifer with infiltration, wells and rivers and often a "uniform flow field" was used.

In 1987, the author started the development of the NAGROM (NATionaal GROundwater Model) as one of the instruments for integrated water management of Rijkswaterstaat. Because a GIS (geographic information system) in geohydrology was not available at that moment, it was expected that the development of large models with one of the established techniques (finite element technique or finite difference technique) would become quite cumbersome. The solution for this problem was found in the direction of coupling of models. The principle of superposition which forms the basis of Strack's AEM principally enables coupling and refining of models. It was expected that using this technique large supra-regional models could be built by combining smaller, regional models. By combining the supra-regional models, the entire nation might be covered ultimately by one model.

However in 1987, only rather simple models of a single aquifer had been built with the AEM. Actually, a modeling approach for building multi-aquifer models or for the use of nested inhomogeneities did not exist. Also, basic items in groundwater modeling such as anisotropy and transient behaviour were not available at that time. Moreover, the theory on accounting for density differences, which is one of the most difficult items in groundwater flow was not expected to be included at all, because its three-dimensional behaviour can not be handled by a strictly two-dimensional technique. During the development of the NAGROM in the period 1987-1994, the AEM has grown out in such a way that it can handle these items. The modeling approach developed by the author for NAGROM is unique, even in the field of analytic element modeling. The development of NAGROM has triggered most of the work in this thesis.

During the development of NAGROM, the modeling approach has been expanded. It appeared that the regional models of NAGROM could be used as a framework for local models, because of the possibility to refine

parts in a model without changing the remaining model. In various modeling sessions, the existence of the boundary zone around the domain of interest appeared to be the main advantage of using NAGROM. Other reasons to choose the AEM for the modeling of large domains are the absence of numerical dispersion in the computation of the velocity as well as the analytically determined and therefore exact water balance within any volume.

The main line of the modeling approach of large domains with analytic elements has been developed for NAGROM and was based on practical experiences (De Lange, 1991). The models resulting from this approach are described in the reports on NAGROM (De Lange and Van der Meij, 1994). This thesis is largely complementary to these two references because it concerns the theoretical background of the modeling approach. In this modeling approach, three stages can be distinguished:

- 1 - the choice of the type of analytic element and the values of its parameters which depend on the simulated geohydrologic feature,
- 2 - the combination of analytic elements in single-aquifer models as well as in multi-aquifer models and
- 3 - the development of models covering large domains (5,000 to 10,000 km<sup>2</sup>) including many and detailed surface water systems.

The main parts of the first and the last stage have been reported in a RIZA note (De Lange, 1991) and are just mentioned in this thesis. The theory behind the second stage forms the first of the two main subjects of this thesis.

Analytic elements interact in a way that is different from that between elements in any other modeling technique. From the authors experience it is concluded that this interaction should be well understood when building a model, particularly a model covering a large domain. Single analytic elements of the source or sink type generate flow in the entire infinite domain. Other analytic elements (generally of dipole type) can only react to flow not generated by themselves. The analysis of the behaviour of single elements has led to several basic rules for modeling. The analysis of the combination of two elements of equal or different type resulted in several main rules for combinations. Also, some main rules have been determined for multi-aquifer modeling. The combination of different element types determines the behaviour of the model.

The second main subject in this thesis concerns the interaction between many surface waters and the groundwater in regional aquifers as it occurs in a country as rich of surface waters and drainage systems as the Netherlands. Dutch hydrologists have used for years several analytically derived expressions to model this interaction by a Cauchy boundary condition in areal elements. Generally, it is assumed that the two solutions most used lead to comparable results. In this thesis, it is shown that the differences between these solutions can not be neglected in many situations existing in practice. An extensive analysis has led to the decision of which of these solutions is to be preferred. Because the solution to be preferred is not simple to understand and to be used, a new analytic

solution is derived by the author, which is simple to understand and gives results that are strongly similar to those of the preferred existing solution. Because of its simplicity, the new solution appears to be more suitable for use in NAGROM than the existing ones. In all analytic solutions leading to a Cauchy boundary condition, the representative distance between the surface waters is a very important parameter. A theoretical basis is presented for a practical approach to derive this parameter in an area with arbitrary situated surface waters.

NAGROM is one of the instruments of Rijkswaterstaat for integrated water management in the Netherlands (Pulles, 1985). Its results have to be comparable over the entire country. NAGROM consists of connectable models that are and have been developed by different modellers at different times and places. The comparability of these different models is enabled by defining an input-based model accuracy (instead of relying on the output accuracy only). Each NAGROM model is defined at a certain scale. A definition of modeling scales is presented in this thesis. The model scale is related to the size of the domain of interest of the model. By modeling a standard amount of geohydrologic features in the domain of interest the degree of detail in the model can be defined.

An introduction to large scale modeling is given in chapter 2. The AEM is described in the form of a hydrologist's view in chapter 3 and concerns the analytic elements included in Strack's multi-aquifer computer code of 1992. The main elements that became available in 1993 and later are summarized in chapter 4. Chapters 3 and 4 are largely based on the existing theory of Strack (e.g. Strack, 1989a) and express some of the authors experiences with the technique. A main part of chapter 5 concerns the analysis of the behaviour of each type of analytic element described in chapter 3 individually and of the combinations of each one with one of the other types of elements. Chapter 5 concludes with a description of a number of combinations of more than two analytic elements. The modeling of the interaction between surface waters and groundwater by using a Cauchy boundary condition is analyzed in chapter 6. Chapter 7 describes a theoretical basis for the determination of the average distance between arbitrary situated surface waters for use in the Cauchy boundary condition. In chapter 8, it is illustrated how the theory of chapters 5, 6 and 7 has been used in NAGROM. Also, several aspects of the modeling of large domains are discussed, which are complementary to the description of the modeling approach of NAGROM (De Lange, 1991) and to the description of the NAGROM models (De Lange and Van der Meij, 1994).



## **2 INTRODUCTORY REMARKS TO THE MODELING OF LARGE DOMAINS WITH ANALYTIC ELEMENTS**

### **2.0 Summary**

A model of a large domain is generally developed for water management purposes and is used for scenario's concerning different aspects of groundwater. The idea of modeling of large domains is described regardless of the used modeling technique. Several aspects of modeling of large domains are discussed. The background of the model of the Netherlands is summarized and this model is put in the perspective of other models of large domains. Some aspects of the analytic element technique AEM are described with regard to modeling of large domains.

### **2.1 Modeling of large domains for national water management**

Regardless of the used modeling technique, the size of a large model for water management purposes is tens to hundreds of times larger than the modeling domain in the case of a common model for a case study. Models of large domains cover areas in the range of thousands of km<sup>2</sup>, whereas in common models the domains are generally in the range of tens to hundreds km<sup>2</sup> or smaller. The modeling domain is the area of interest in the model, which excludes the zone that forms the model boundary. Actually in terms of results, this boundary zone should not be considered as a part of the model.

In a model of a large domain (a large model), the coherence between the geohydrology of different regions becomes clear. For instance, large models include the regional water divides, rivers or faults which are often used as boundaries of common models. A large model accounts for changes in a water divide that occur due to changes in the model and for the groundwater flow that may cross a river or fault. A large model often covers areas for which the interests have been small or negligible, which may be the cause of a lack of data and of the absence of comparative studies.

A large model becomes also complicated due to the large amount of geohydrologic features (surface waters, separating layers, aquifer inhomogeneities, wells, etc., see section 3.1) to be included. The interactions between so many features are hard to understand and the model calibration may become cumbersome. A large model is preferably developed in parts of the size of common regional models, which are coupled afterwards. The coupling of models is a particular advantage of the AEM (section 2.4).

In general, models covering large domains are built for water management purposes. A model for (national) water management is not used for only one type of question and one situation such as the transport in

groundwater of a pollutant coming from a waste dump, but it should be applicable for many types of questions such as the effect of changes in vegetation (crops, forest) translated in terms of groundwater recharge on the flux in natural brooks, the effects of infiltration wells on the distribution of chloride in the groundwater, the effect of intensification of the agricultural drainage systems on the seepage in a wetland, etc. So, a model of a large domain for water management purposes may be used to compare the effects of different measures that occur in different places and originate from different reasons. These effects may be expressed in terms of different quantities (head, flux, travel time, concentration, mass load, size of affected area, etc.).

In a model for national water management, the results may be less detailed than needed for a particular question at local scale. The effects of the relatively coarse modeling on the results should be known and be considered in the evaluation of the results. Application of a large model at a more detailed level requires refinement and addition of information. It appears, that in the Netherlands the questions for national water management tend to require a more and more refined description of the groundwater flow at certain places (e.g. around natural areas which are relatively small). The existing schematization of NAGROM can easily be refined, because the analytic element technique is used.

## **2.2 The model of the Netherlands**

Since the late 1970's, the Ministry of Transportation and Public Works has carried out water management studies at the national level in the Netherlands by using the set of instruments (computer codes) of PAWN (= Policy Analysis for Water management in the Netherlands, Pulles 1985). Already in the first stage of PAWN, the groundwater flow in the unsaturated zone was included in a model for the water demand of agricultural crops but the groundwater flow in the saturated zone was actually left out completely (Rand Corporation, 1982). For the integrated water management studies that started in the late 1980's, the saturated groundwater flow had to be included in the set of PAWN instruments. This has led to the development of NAGROM (De Lange, 1991).

Because NAGROM is developed to be one of the instruments for national water management of PAWN, it is connected with the (renewed version of the) soil water model for the unsaturated zone MOZART (Arnold, 1995). The latter model simulates the soil water flow in the unsaturated zone by computing successive steady states (changes in time neglecting storage effects) and transient (including storage effects) conditions. The connection between MOZART and NAGROM (MONA) is being developed since 1994 and is based on the Cauchy boundary condition derived in chapter 6 that describes the interaction between one or more surface waters and the groundwater in an aquifer. In NAGROM the wet-season-average vertical flux to or from the unsaturated zone is computed using this boundary condition. This flux is assumed to be a first order approximation of the wet-season-average flux under successive steady states or transient



conditions as they are computed by the model for the unsaturated zone. Both models use the same Cauchy boundary condition with equal parameter values. MONA is still under development (1995).

NAGROM consists of about ten models of large domains (supra-regions), that can be coupled along the borders between any two models and that may ultimately form one nation-wide model (De Lange, 1991). NAGROM is the first groundwater model ever that covers more than 40,000 km<sup>2</sup> of mainly intensively drained and deltaic areas. Even the supra-regional models of NAGROM cover large domains (2,000 to 10,000 km<sup>2</sup>).

From the primary aim of NAGROM - to be a model for national water management - the following objectives are derived (De Lange, 1991):

- NAGROM should be accurate for scenario's at national level.
- The results of NAGROM should be comparable all over the country.
- Each use of NAGROM should be accepted by the local and regional water authorities and institutes to which the results are of concern.
- NAGROM should be maintained permanently.
- NAGROM should be generally available.

The first two objectives will be worked out in chapter 8 and the last three objectives are beyond the scope of this thesis.

During the development of NAGROM, the multi-aquifer modeling approach has been developed as well as many other extensions in the modeling with analytic elements (see chapter 5 and De Lange, 1991). Since 1990, several multi-aquifer models of analytic elements have been built besides NAGROM, which have mainly been based on the NAGROM modeling approach.

A model of analytic elements does not end at boundaries as it occurs in finite element or finite difference models, but it is bounded by a zone of analytic elements (the "boundary zone" or "surrounding zone") that separates the area of interest from the rest of the infinite aquifer. Analytic elements in a part of a model can be replaced by other elements without having to change the rest of the model. This enables to start with a coarse modeling and then refining step by step different parts all through the model. This refining can be repeated until the desired accuracy is reached. This approach is developed for NAGROM and has already been described in De Lange (1991). During the development of NAGROM, the distinct supra-regional models appeared to be very useful as a framework for refinements. The NAGROM models have been used to construct (by selection of the proper analytic elements) the boundary zone for smaller models. Refinements have been built in successfully for local scale models e.g. for the model of a silt depot in combination with a shelter-harbour near Weurt (Douben et al., 1994).

### **2.3 Other models of large domains**

When the development of NAGROM started in 1987, a large part of the Netherlands was covered by many models for the groundwater flow in the

saturated zone. Only two of these models can be considered as a model of a large domain; the model of the Central Graben in the southern part of the country (about 3,000 km<sup>2</sup>) (IWACO, 1987) and the model of the province of Drenthe (about 2,500 km<sup>2</sup>) (Province of Drenthe, 1985), which actually was not calibrated and consisted of four non-connected sub-models. None of these models could serve as a basis for a national groundwater model, because they were not generally available or they could not be connected to form large models as part of a national model. Since the start of NAGROM, several other large domain models have been developed in the Netherlands. The models of IWACO (IWACO, 1992) and RIVM (Pastoors, 1992) are based on the finite element technique and, therefore, they can not be coupled and refined in the elegant way it is possible in NAGROM. For the generation of a picture at national level, the results (in terms of the hydraulic head) of the RIVM sub-models are superimposed in the area of overlap and are pasted to form one cover of the entire country (model version 1993). The IWACO and RIVM models are filled automatically with data from databases using GIS-interfaces, which is different from the approach in NAGROM. At the start of NAGROM, no database or GIS was available and therefore, the NAGROM models are built manually based on expert-interpretations of maps. Recently (1994), the upper boundary of NAGROM has been rebuilt for the connection with the model of the unsaturated zone MONA (section 2.2) using GIS.

The actual models of IWACO and RIVM are not developed to be adapted afterwards for a new type of question. New questions may need an other schematization (e.g. a refinement) for which a complete new model should be generated. Then, the determination of the model boundaries and the calibration of the model have to be carried out again, which differs from the NAGROM modeling approach as sketched in section 2.2.

Models covering large domains outside the Netherlands have been built for particular purposes. Most of them have been used in arid areas where there is hardly any interaction between surface waters and groundwater. An example of this is the model of the Nubian aquifer in Egypt (Heinl and Brinkman, 1989), which has been built to compute the effects over time of withdrawals in a large (2,000,000 km<sup>2</sup>) groundwater basin at great depth.

#### **2.4 On the application of the analytic element technique**

The main difference between using the AEM and using other modeling techniques originates from the meaning of the elements, which will be summarized first. Analytic elements are analytic solutions with different meanings of the partial differential equation for groundwater flow in an infinite aquifer. Each analytic element is used to describe a feature in groundwater flow, such as an abstraction well, a river, a polder, an infiltration area, a domain with different transmissivity, a sheet pile wall, etc. Each analytic element can be used independently of other elements. Even a single analytic element such as a "well", a "line-sink" or an "area-sink" (see chapter 3) can be seen as a model, because it generates a flow and a head distribution in the entire infinite aquifer. Analytic elements are

combined based on the principle of superposition. In a model, the strengths of the elements are computed to meet the boundary conditions. Analytic elements may cross, overlap and be linked together and do not need to form closed meshes (see chapter 5).

Following from the difference in the meaning of the analytic elements, the modeling approach using this technique is also different from that using other techniques. In modeling with analytic elements, geohydrologic features have to be recognized and the appropriate type of analytic element has to be chosen, instead of giving each element in a finite element or a finite difference mesh the same, standard properties (except maybe at parts of the boundaries) such as the hydraulic conductivity and thickness of the layer.

An other important difference between the AEM and any other technique is (Strack, oral communication, 1994) that in a model of analytic elements, reality is discretized using elements that are exact solutions of the differential equation, while in finite difference and finite element techniques, the differential equation itself is discretized as well.

NAGROM is based on the AEM mainly because the technique enables flexible coupling and refining of existing models.

Refinement of a part of an existing model is easy, because (based on the superposition principle) each element can be taken out independently of the other elements and it can be replaced by other elements, even of different types. For instance, an area-sink describing a domain with many surface waters (see chapter 6) may be replaced by line-sink elements simulating the individual surface waters.

The boundary of a model of analytic elements is a zone of elements that globally simulate the behaviour of the geohydrologic features in that zone. The area of interest interacts directly with its boundary zone. Due to the characteristics of the AEM, coupling of models is natural; two sets of elements are combined based on superposition, which means here that parts of the boundary zones of both models are replaced by the actual areas of interest of both models.

A large model can be used as boundary zone model for a detailed model in a smaller domain. The detailed model is really built in the coarse model. This is strongly different from building a separate detailed model and taking the boundary conditions from a coarser model as is common in the classical techniques. This modeling aspect turns out to be useful especially when the area outside the domain of interest is complex.

In any volume in an AEM model, the water balance is accurate in the order of magnitude of the computer accuracy, independent of the size of the elements. This is important e.g. for the computation of transport of solvents, which requires to meet strictly fitting of the water balance (Douben et al., 1994). Also, at any point in the aquifers the three-dimensional velocity vector is analytically determined. By this, numerical dispersion in the computation of flow paths is virtually absent. These

aspects are important e.g. when dealing with changes in the density distribution in large coastal aquifers (subsection 4.2.4).

In 1987, two major drawbacks of the AEM were that it actually had never been applied in multi-aquifer models of large domains and that it was not clear at all how the effects of variable density in the groundwater in the coastal zone of the Netherlands could be included. Both of these drawbacks have lost their meaning since 1993. By the development of NAGROM, the applicability of the AEM has increased considerably: The building of multi-aquifer models covering large domains, the use of meshes of area elements to describe the interaction between groundwater and surface water and rules for the combination of these area elements with area elements for leakage between aquifers have been developed for NAGROM (see chapter 5). Also, the analytic solutions for curved line elements and for elements describing the vertical flow near wells have been implemented (chapter 4). In 1993, a solid and straight forward approach to include variable density effects has been developed (Strack 1994).

Still, new modules in the AEM are needed to include several basic geohydrologic features, such as a module to account for a gradually sloping base in a phreatic aquifer and a solid approach for computation of transient situations at a national level (section 4.5). In 1994 and 1995, Strack has developed theoretical solutions for these situations, which need to be explored further. The AEM will be strongly in development during the next five to ten years. It is expected by the author, that by these developments, the AEM will become one of the most powerful techniques for groundwater modeling, especially for the modeling of large domains.

### **3 A PRACTITIONER'S DESCRIPTION OF STRACK'S ANALYTIC ELEMENT TECHNIQUE (1992)**

#### **3.0 Summary**

In this chapter, the principles of the analytic element technique are recapitulated. The basics of the discharge potential are introduced and different applications are described. The types of analytic elements are discussed as far as they were implemented in 1992 in Strack's computer code and as far as they can be used in large scale modeling. The underlying mathematics are described only as far as needed to understand the behaviour of the analytic elements in a groundwater model. The principles of a multi-aquifer model and of three-dimensional tracing are described. Some words are spent on the derivation of the system of equations and its solution.

#### **3.1 Introduction**

The AEM has been found and developed by O.D.L. Strack and is presented in his book "Groundwater Mechanics" (Strack, 1989a). The main difference between the technique of Strack (and his followers) and other analytically-based techniques (e.g. Van den Akker, 1982) is the implementation of boundary conditions and the diversity of the elements. Strack's technique includes Neuman, Dirichlet and Cauchy boundary conditions and contains point, line (straight and curved) and areal source/sink elements as well as several types of line-dipole elements (section 3.3).

The AEM is different from boundary element techniques (e.g. Van der Veer, 1978) in the sense that analytic elements generate conditions at a point, line or area with effects in the entire aquifer of infinite extent whereas boundary elements generate conditions at the outer boundary of an area of concern and are not used outside that area.

The description of the analytic elements in this thesis is mainly based on documents of Strack (see references) but follows the author's experience in how this technique is used in modeling. Several applications mentioned in this description have been used for the first time by the author in the large scale groundwater model of the Netherlands NAGROM.

In principle, analytic elements are defined as analytic solutions of the two-dimensional Laplace (in area with recharge the Poisson) equation expressed in terms of the so-called discharge potential (section 3.2). Each type of analytic element has a different hydrological meaning (section 3.3). In the discharge potential several aquifer properties can be included, such as vertical variation in the horizontal hydraulic conductivity within an aquifer, impermeable horizontal laminae and differences in the density of groundwater (section 3.2).

A groundwater model can be seen as a combination of features in groundwater flow such as polders, infiltration areas, canals, rivers, separating layers, wells, inhomogeneities, etc. In modeling with the AEM, different types of features are represented by different types of analytic elements. The question "Which analytic element represents best the feature in question?" is typical in modeling with the AEM.

A model of analytic elements is formed by a well-chosen combination of elements of different types (chapter 5). Wells are represented by point-sinks (which also can be sources). Canals and rivers may be simulated by line-sinks. Area-sinks are used to model infiltration areas, polders, and other areal features. The interaction between aquifers is also simulated by area-sinks. Changes in the hydraulic conductivity, the thickness or the elevation of the aquifer base are simulated using line-doublets (sub-section 3.3.6).

The properties of analytic elements are specified by common geohydrologic parameters (resistance, hydraulic conductivity, etc.). Analytic elements may describe boundary conditions specified by the surface water level, or by the groundwater recharge. A problem expressed in terms of analytic elements is solved by computing the unknown strengths of the elements (section 3.5).

In this chapter, the description is limited to the elements available in the multi-layer version of Strack's computer code of 1992. The aim of this description is to provide a basis for the analysis (in chapter 5) of the combinations of analytic elements for use in large scale models. In chapter 4, the developments since 1993 will be described. In this chapter, all figures of streamlines and lines with equal head apply to (semi-) confined flow.

## **3.2 The discharge potential**

In the AEM, the discharge potential is a key parameter. The aquifer properties are included in the discharge potential (subsection 3.2.2) and all analytic elements are expressed in terms of the discharge potential (section 3.3). Therefore, the description of the AEM technique starts with the description of this parameter.

### **3.2.1 Basic equations**

An analytic element is represented by a solution of the Laplace (and in bounded domains with recharge the Poisson) equation for two-dimensional groundwater flow, in which the Dupuit-Forchheimer assumption is used, which is adapted to account for vertical flow by Strack (1984). The Dupuit-Forchheimer assumption implies that the flow is assumed to be mainly horizontal. This is valid in regional aquifers because their thickness is generally small compared to their extent. The mainly horizontal flow is expressed by a constant head over the entire aquifer thickness. This latter may be interpreted (Strack, 1984) in such a way that, in modeling practice, the resistance to vertical flow is neglected in the aquifers and is lumped in

the resistance value of the separating layers. The aquitards are simulated by separating layers in which the horizontal flow is neglected. In the first step of the theory of analytic elements, Strack (1989a) assumes the aquifers to be homogeneous and isotropic with steady flow. (In later steps, these restrictions are largely overcome).

In the case of flow under the Dupuit-Forchheimer assumption, the mass balance equation can be described by:

$$\frac{\partial Q_x}{\partial x} + \frac{\partial Q_y}{\partial y} = -\gamma \quad (3.1)$$

where  $Q_x$  and  $Q_y$  are the discharges per unit width [ $L^3/L.T$ ] in x- and y-direction respectively and  $\gamma$  is the vertical flux per unit area [ $L/T$ ]. Using  $Q_x$  and  $Q_y$ , Darcy's law is expressed by:

$$Q_x = -kh \frac{\partial \phi}{\partial x} ; Q_y = -kh \frac{\partial \phi}{\partial y} \quad (3.2)$$

where  $k$  is the hydraulic conductivity [ $L/T$ ],  $h$  is the thickness over which the groundwater flow occurs [ $L$ ] and  $\phi$  is the hydraulic head [ $L$ ].

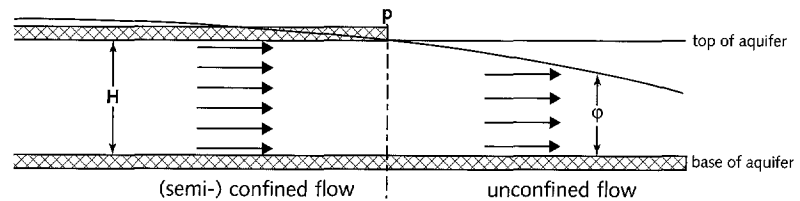


Figure 3.2.1 Scheme of flow under confined and unconfined conditions.

The thickness  $h$  over which the groundwater flow occurs is constant in the case of confined flow (figure 3.2.1, left hand side):

$$h = H \quad (3.3)$$

In the case of unconfined flow, the thickness  $h$  is variable and equal to the head  $\phi$  if the reference level is at the base of the aquifer (figure 3.2.1 right hand side):

$$h = \phi \quad (3.4)$$

In the case of semi-confined flow,  $h$  is equal to  $H$  similar as in the case of confined flow. Semi-confined flow is modeled in an approximate way and will be discussed in subsection 3.3.7.

Equation (3.2) can be rewritten as:

$$Q_x = - \frac{\partial \Phi}{\partial x} \quad Q_y = - \frac{\partial \Phi}{\partial y} \quad (3.5)$$

where  $\Phi$  is the discharge potential [ $L^3/T$ ]. The discharge potential (or just potential) is a key variable in the AEM. All expressions for the elements are in terms of the potential (section 3.3). Several properties of the aquifer such as thin impermeable layers, vertical variation of the horizontal hydraulic conductivity and density differences can be included by an appropriate expression for the potential (see subsection 3.2.2).

The discharge potential  $\Phi$  can be expressed in terms of  $k$ ,  $H$  and  $\phi$  in the case of confined flow by substitution of (3.2) and (3.3) in (3.5):

$$\Phi_c = kH\phi + C_c \quad (3.6)$$

and in terms of  $k$  and  $\phi$  in case of unconfined flow by substituting (3.2) and (3.4) in (3.5):

$$\Phi_u = 1/2k\phi^2 + C_u \quad (3.7)$$

The integration constants  $C_c$  and  $C_u$  can be used to satisfy the condition of continuity in  $\phi$ , at the boundary between confined and unconfined flow (see figure 3.2.1 point P). By choosing  $C_u = 0$  (Strack, 1989a), this leads to:

$$\Phi_c = kH\phi - 1/2kH^2 \quad (\phi \geq H) \quad (3.8)$$

$$\Phi_u = 1/2k\phi^2 \quad (\phi \leq H) \quad (3.9)$$

So, the potential  $\Phi$  describes groundwater flow under confined as well as under unconfined conditions. In confined situations  $\Phi_c$  is linearly related to  $\phi$ , in unconfined situations a quadratic relation is found, which may necessitate iteration during the solution (the computation of the unknown strengths). By substitution of (3.5) in (3.1), the Poisson equation (Laplace equation if  $\gamma = 0$ ) for two-dimensional flow in  $\Phi$  is derived.

$$\frac{\partial^2 \Phi}{\partial x^2} + \frac{\partial^2 \Phi}{\partial y^2} = \gamma \quad (3.10)$$

Because this is a linear differential equation, its solutions may be added and subtracted to derive new solutions (principle of superposition). The most simple solutions of this differential equation are the constant discharge potential (describing no flow), the discharge potential linearly varying in  $x$  and  $y$  (describing uniform flow) and the discharge potential quadratic in  $x$  and  $y$  (describing vertical inflow of water over an infinite area). The latter two solutions are treated extensively in Strack (1989a) and are called "uniform flow" and "rain". They can not be applied in large scale modeling because their effects do not vanish at large distances. Therefore, they will not be discussed in this thesis. Also, the analytic element called "pond" is not treated here, because its circular shape is unsuitable for use



in large multi-aquifer models and it can be seen a special case of an area-sink.

Each analytic element except the area-sink is a solution of the Laplace equation. Within the area-sink the Poisson equation holds, outside the element the Laplace equation holds. Each element is described in terms of  $\phi$ , so regardless whether the flow is unconfined or confined. Once the solution in  $\Phi$  has been computed and the values of  $k$  and  $H$  are known, the solution in  $\phi$  can be found unambiguously by applying the relation for either  $\phi \geq H$  or  $\phi \leq H$ . Therefore, analytic elements may be added and removed freely in a model.

Analytic elements generate continuous fields of both the potential  $\Phi$  and, when excluding areal recharge, the stream function  $\Psi$  [ $L^3/T$ ]. Similar to the Laplace equation in  $\Phi$ , the differential equation in terms of the stream function  $\Psi$  reads:

$$\frac{\partial^2 \Psi}{\partial x^2} + \frac{\partial^2 \Psi}{\partial y^2} = 0 \quad (3.11)$$

The potential and the stream function are related by the Cauchy-Riemann conditions:

$$\frac{\partial \Psi}{\partial x} = - \frac{\partial \Phi}{\partial y} ; \quad \frac{\partial \Psi}{\partial y} = \frac{\partial \Phi}{\partial x} \quad (3.12)$$

These conditions describe that streamlines are perpendicular to lines of equal potential. Assuming groundwater flow in a two dimensional space, analytic elements can be formulated in the complex plane ( $z = x + iy$ ). The potential  $\Phi$  and stream function  $\Psi$  can be combined in the complex potential  $\Omega$  by:

$$\Omega = \Phi + i\Psi \quad (3.13)$$

where:

$$\Omega = \text{complex potential } [L^3/T]$$

Using the complex variables  $\Omega$  and  $z$ , the mathematical expressions for the analytic elements become simple and clear to understand (section 3.3). The shape of both the potential  $\Phi$  and stream function  $\Psi$  is described in the infinite aquifer by a single expression for the complex potential  $\Omega$ .

A model in groundwater flow consists of a combination of analytic elements in one or several aquifers. Superposition of the complex potentials  $\Omega$  of all analytic elements leads to the complete solution in  $z$ . Then, the values of the stream function (except inside the area-sinks) and the potential can be computed at any point in any of the aquifers.

### 3.2.2 Extended applications of the discharge potential

Although it is a single variable, the potential  $\Phi$  may account for flow in an aquifer with a fresh water salt water interface, for flow in aquifers with impermeable horizontal laminae and for aquifers with vertically varying horizontal hydraulic conductivity. In order to give an idea on how this works, the formulas for these situations are presented. Their derivations can be found in Strack (1989a). The different situations described in this subsection can be merged when needed. Strack (1989a) shows some combinations. It is important to realize, that all solutions of equation (3.10) apply to these situations and their combinations.

#### Interface between fresh and salt groundwater

A sharp interface between salt and fresh groundwater is often found along coastlines, e.g. in the Dutch dune area along the North Sea coast. In the case of flow in an aquifer with a sharp interface between fresh and salt water, Strack assumed the salt water to be stagnant while the interface should be above the base of the aquifer.

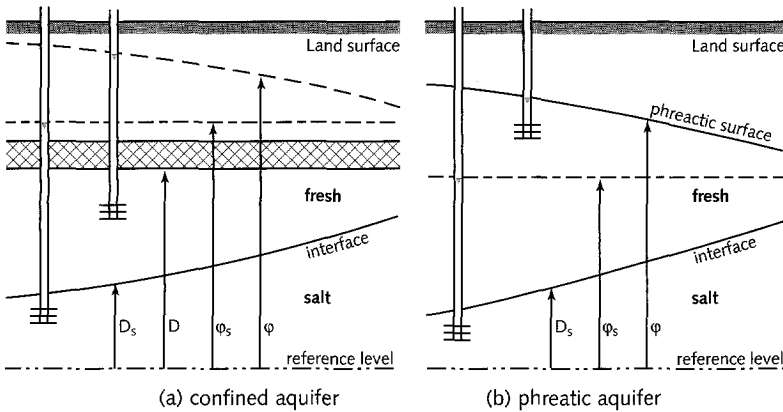


Figure 3.2.2. Definition scheme for an aquifer with a sharp interface.

The potential  $\Phi$  for this case is given by:

-for confined flow conditions (see figure 3.2.2-a):

$$\Phi = -k/2 v [\varphi - \varphi_s \rho_s / \rho_f - D/v]^2 + C_c \quad (\varphi \leq H) \quad (3.14)$$

-for unconfined flow conditions (see figure 3.2.2-b):

$$\Phi = -k/2 v [\varphi - H]^2 + C_u \quad (\varphi \geq H) \quad (3.15)$$

where:

$D$  = distance between the top of the aquifer and the reference level [L]

$C_c, C_u$  = integration constants for unconfined and confined situations respectively

$\varphi_s$  = head (in terms of  $\rho_s$ ) in the saline part of the aquifer [L]

$D_s$  = depth of the interface with respect to the reference level [L]

- $v$  = relative density, =  $(\rho_s - \rho_f)/\rho_f$  [-]
- $\rho_s$  = density of salt water [M/L<sup>3</sup>]
- $\rho_f$  = density of fresh water [M/L<sup>3</sup>]

In 1991, Strack implemented this potential in a special version of the AEM computer code, which has been applied to model a small coastal zone in the Netherlands (sandy dunes of Goeree). Comparison with a finite element model of the same area showed good agreement with respect to the position of the interface. Apart from the implementation of the interface in the AEM model by the author, both models have been built by dr W.J. Zaadnoordijk of IWACO Rotterdam.

In 1992, Strack (oral presentation) derived a solution for the case of a sharp interface with salt water flowing instead of being stagnant. This has not been developed further because Strack found in 1993 a solution for the implementation of three-dimensional variation of the density (chapter 4).

### Impermeable horizontal laminae

Impermeable laminae (figure 3.2.3) are impermeable horizontal planes of limited extension in the aquifer. They can be used to model relatively thin, horizontal layers with very high resistance.

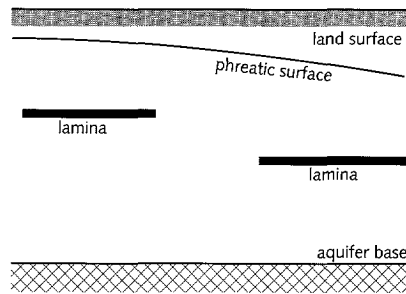


Figure 3.2.3 Impermeable laminae in an aquifer.

To include impermeable horizontal laminae in an aquifer, the potential  $\Phi$  is presented by:

- if the upper part of the aquifer is confined:

$$\Phi = 1/2k[\varphi_u - H]^2 + 1/2k\varphi_l^2 \quad (\varphi \leq H) \quad (3.16)$$

- if the upper part of the aquifer is unconfined:

$$\Phi = 1/2k[\varphi_u - H]^2 + 1/2kH\varphi_l + 1/2H^2 \quad (\varphi \geq H) \quad (3.17)$$

where the integration constants have been defined similar as in the derivation of expressions (3.8) and (3.9) and where:

- $\varphi_u$  = head in the upper part of the aquifer [L]
- $\varphi_l$  = head in the lower part of the aquifer [L]

Laminae are particularly appropriate in relatively simple models of small areas and have not been used yet in the model of the Netherlands. In Strack's book (1989a) more information on the use of these laminae is given.

*Vertically varying horizontal hydraulic conductivity in an aquifer*

Vertically varying horizontal hydraulic conductivity occurs for instance in chalk aquifers in the southern part of the Netherlands (South-Limburg). In such aquifers, leaching may create pores and cracks in the upper part of the aquifer leading to increased hydraulic conductivity. In the deeper part of the aquifer, the hydraulic conductivity does not change.

The potential  $\Phi$  can account for vertically varying horizontal hydraulic conductivity in aquifers with the equation (Girinski, 1946; see figure 3.2.4):

$$\Phi = \sum_{j=1}^{j=m-1} [k_j H_j (\varphi - \beta_j) - 1/2 k_j (\beta_{j+1} - \beta_j)^2] + 1/2 k_m (\varphi - \beta_m)^2 \quad (3.18)$$

where the integration constants are used similarly as in expressions (3.16) and (3.17) and where:

$$b_j = \text{base level of } j\text{-th layer [L]}$$

When  $b_m < \varphi < b_{m+1}$  the last term in (3.18) expresses the upper unconfined layer m. If the aquifer is entirely confined the last term vanishes.

This potential has been used in several test models in the area of South-Limburg. In this area, rivers cut deep in the chalk aquifers in which the hydraulic conductivity decreases strongly with depth. The effect of the variation in the hydraulic conductivity on the distribution of the groundwater heads was clearly demonstrated by the models.

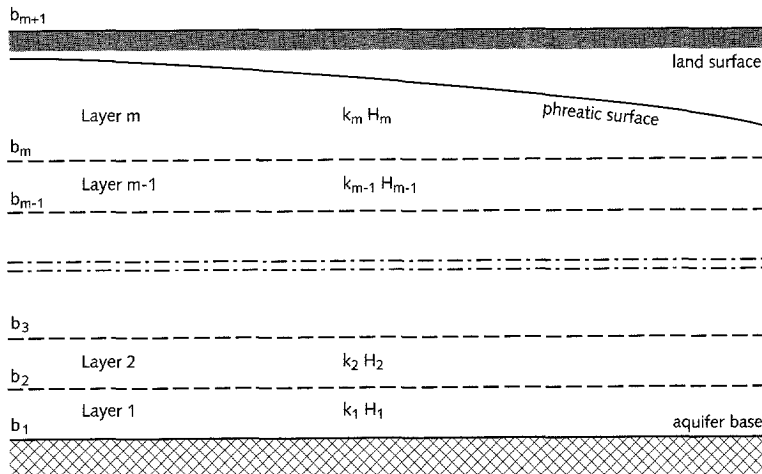


Figure 3.2.4. Vertically varying hydraulic conductivity in an aquifer.

### 3.3 Description of analytic elements

Starting with the classic well or "point-sink", the analytic elements are described in such an order that each element is an extension of one or more elements described before that element.

#### 3.3.1 The point-sink (well).

One of the most elementary examples of analytic elements is the point-sink or the fully penetrating well.

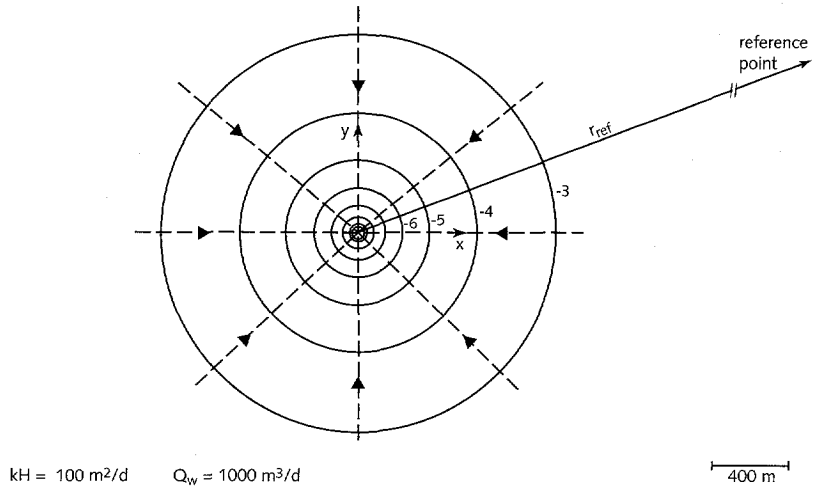


Figure 3.3.1. Lines of equal head (meters above reference level) and streamlines of a well element.

In radial coordinates  $(r, \theta)$  the potential is:

$$\Phi(r) = \frac{Q_w}{2\pi} \ln \left( \frac{r}{r_{ref}} \right) + \Phi_{ref} \quad (3.19)$$

where:

$r$  = distance between the well and the observation point [L]

$r_{ref}$  = distance between the well and the reference point [L]

$Q_w$  = discharge or strength of the well [L<sup>3</sup>/T]

$\Phi_{ref}$  = potential at the reference point [L<sup>3</sup>/T]

$\Phi(r)$  = potential at distance  $r$  from the well [L<sup>3</sup>/T]

This analytic element causes the potential value to change logarithmically with the distance to the sink, as presented in figure 3.3.1. The value  $\Phi_{ref}$  in a reference point at  $r = r_{ref}$  can be chosen arbitrarily.

Once the strength  $Q_w$  is given and the potential  $\Phi_{ref}$  at the reference point is defined, the potential distribution is determined in the entire aquifer. If, instead of the strength  $Q_w$ , a second potential value (e.g.  $\Phi(r_1)$  with  $r_1$  is a radius) in the aquifer is given,  $Q_w$  can be computed and the potential

distribution is also known. In Strack's computer codes, this second potential value is prescribed by default at the radius of the well ( $r_1 = r_w$ ), representing the head maintained in the well. So, either the strength or the head of a well can be specified, which form the Dirichlet and the Neuman boundary condition respectively. A Cauchy boundary condition (a linear relation between the strength and a head) is not implemented yet. It might be used e.g. to simulate a resistance to flow near the entrance of the well.

Using the complex orthogonal-radial conversion equation:

$$z = re^{i\Theta} \quad (3.20)$$

the Cauchy-Riemann conditions (3.12) can be rewritten as:

$$\frac{\partial \Phi}{\partial r} = - \frac{\partial \Psi}{r \partial \Theta} \quad (3.21)$$

By combination of (3.19) and (3.21), the expression of the stream function becomes :

$$\Psi(\Theta) = Q_w \Theta / 2\pi \quad (3.22)$$

So, the stream function jumps at  $\Theta = 2\pi$  along a line emanating from the well (Strack 1989a, p. 226). As can be seen in *figure 3.3.1*, the flow occurs from or to the well along lines emanating from the well. Substitution of (3.19) and (3.22) in (3.13) gives the function of the complex potential:

$$\Omega(z) = Q_w \ln(z-z_0) / 2\pi + \Phi_{ref} \quad (3.23)$$

where

$z-z_0$  = distance between well and observation point

This expression describes both the potential and stream function in the infinite aquifer for a fully penetrating well. It illustrates, how the geohydrological properties of an analytic element can be described completely in a single equation in the complex plane. The logarithmic function in (3.23) determines the shape of the potential and stream function field created by the element and is called the shape function of the element.

Wells are used in those cases where with drawal or suppletion of water occurs in a small area (a point) as compared to the size of the modeled domain. In subsection 5.2.1, it will be discussed how partially penetrating wells can be included in the AEM.

### 3.3.2 The line-sink (river)

Line-sinks are used to model inflow or outflow along a line. A line-sink can be seen as an infinite number of point-sinks (wells) along a straight line. Each point-sink represents a length  $d\delta$  of the line and has an extraction rate

of  $\sigma_{lin} d\delta$  (figure 3.3.2). The discharge of the line-sink is described by:

$$Q_l = \int_L \sigma_{lin} d\delta \quad (3.24)$$

where:

$Q_l$  = line-sink discharge [ $L^3/T$ ]

$\sigma_{lin}$  = line-sink strength per unit length, function of  $\delta$  [ $L^3/L.T$ ]

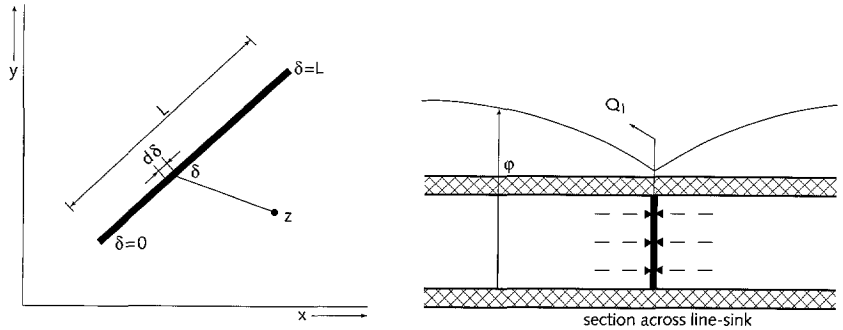


Figure 3.3.2. Definition scheme for a line-sink element.

Along a line, the strength can theoretically be distributed with functions of any order. In Strack's AEM, both the constant and linear strength distribution are implemented. Combination of (3.24) and (3.23) leads to:

$$\Omega(z) = \int_L \sigma_{lin} \ln(z - \delta)/2\pi d\delta + \Phi_{ref} \quad (3.25)$$

where:

$z - \delta$  = distance between observation point  $z$  and point of integration  $\delta$  [L]

The expressions for  $\Phi$  and  $\Psi$  are presented in Strack (1989a, pp. 287-288). As illustrated in figure 3.3.2 (right hand side), the value of the flux (stream function) jumps over the line-sink and the potential is continuous. Near the centre of the line-sink, the flow is perpendicular and the lines of equal head are parallel to the line-sink (figure 3.3.3). At the ends of the line-sink, the flow is approximately radial and the lines of equal head are approximately circular. At larger distance, the line-sink causes almost circular lines of equal head, because when looking from a large distance to the line-sink it behaves similar to a point-sink.

In analogy to the well, equation (3.25) describes the potential and stream function of the line-sink in the aquifer by its strength  $\sigma_{lin}$  and by its shape function.

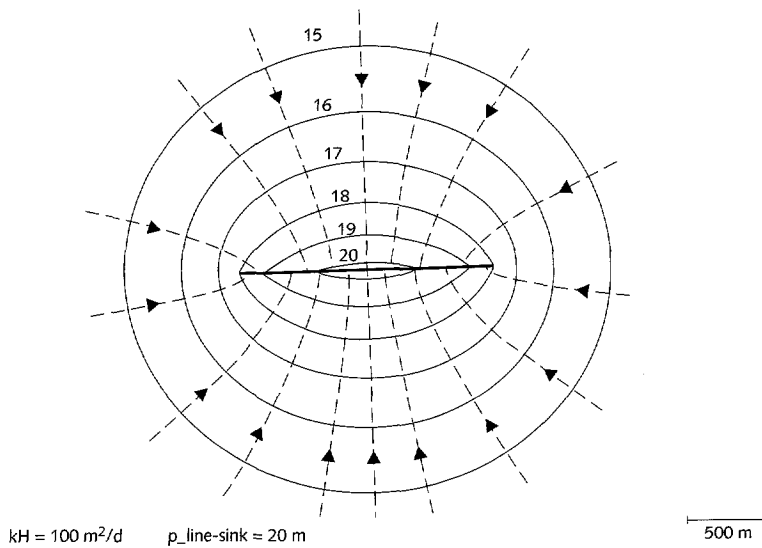


Figure 3.3.3 Lines of equal head (meters above reference level) and streamlines of a line-sink element.

In Strack's computer code, three boundary conditions (Dirichlet, Neuman, Cauchy) can be used with the line-sink (the Cauchy boundary condition since 1992). The head of a constant strength line-sink  $p$  is defined at the centre of the element, which is the so-called control point. The strength is computed in a way similar to that in the case of the well. Along the rest of the line-sink the head depends on the head in the neighbourhood (see also subsection 5.2.2). Therefore, a river with a gradually decreasing hydraulic head can be modeled using concatenated, relatively long head-specified line-sinks, if the distribution of the in- and outflow is of minor importance. On the other hand, a surface water generating a constant groundwater level can be simulated by a series of short head-specified line-sinks. They maintain the constant hydraulic head by adjustment of their strengths (see also the application of a canal, subsection 3.3.4).

A linear line-sink exists of line-segments with linearly varying strength. The heads in such an element are specified at the points between the segments and at the end points. The linear strength distribution per segment enables to account for variation in the inflow and outflow along the line-sink. This element enables to model inflow in and outflow from rivers more accurately than the element with constant strength.

In geohydrologic terms, a line-sink expresses a fully penetrating feature. In subsection 5.2.2, two ways to simulate a partially penetrating line-sink are discussed.

Line-sinks can be used to generate a "uniform flow" field in the surrounding zone of a regional model. For this purpose, the lengths of the line-sinks should be large as compared to the model area. In this way, a "head-specified" uniform flow is generated instead of the commonly used "flux-specified" uniform flow (see text with equation (3.10)).



### 3.3.3 The dipole

As the word says, a dipole consists of two poles, a sink and a source with equal but opposite strengths nearly at the same place (*figure 3.3.4*). This element does not express any useful element in geohydrologic practice.

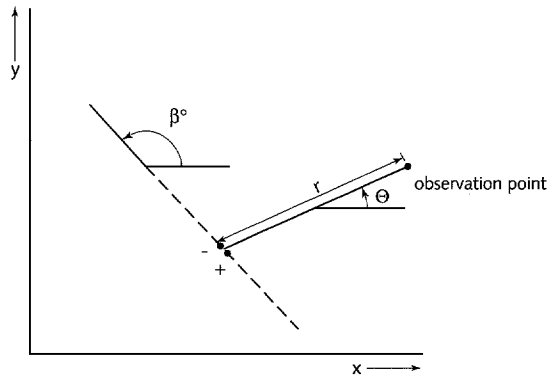


Figure 3.3.4 Definition scheme for a dipole.

However, it is treated here, because it forms an essential step in the theory of analytic elements. In the next sections, other useful types of analytic elements are derived based on the dipole.

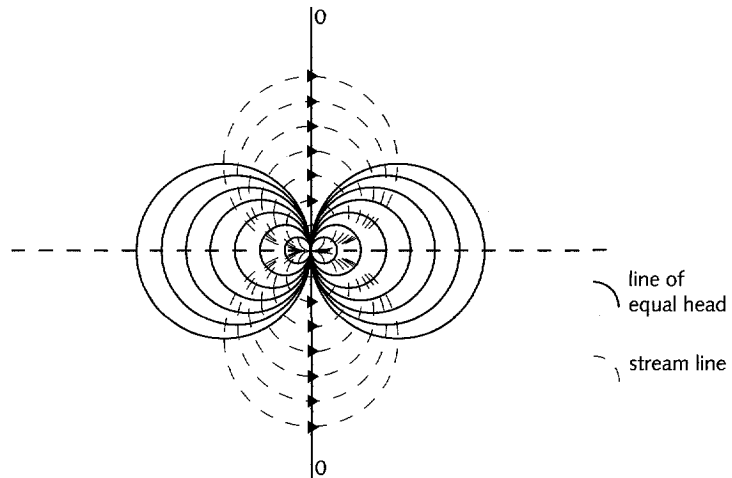


Figure 3.3.5. Lines of equal head (meters above reference level) and streamlines of the dipole-type analytic element.

As can be seen from *figure 3.3.5*, the lines of equal head of a dipole are circles eccentrically situated around each pole. Streamlines form a similar picture rotated 90 degrees around the centre of the dipole. The values of both the head and flux decrease with the distance to the dipole and are linearly dependent on the strength of the dipole. The strength of the dipole

is equal to the strength of the poles multiplied by the distance between the poles. These properties can be found from the formula for the potential of a dipole (Strack, 1989a):

$$\Phi(r, \Theta) = \Gamma_{\text{dip}} \cos(\Theta - \beta^\circ) / 2\pi r + \Phi_{\text{ref}} \quad (3.26)$$

and from the formula for the stream function:

$$\Phi(r, \Theta) = -\Gamma_{\text{dip}} \sin(\Theta - \beta^\circ) / 2\pi r \quad (3.27)$$

where:

$r$  = distance between dipole and observation point [L]

$\Gamma_{\text{dip}}$  = strength of the dipole [ $L^3/T$ ]

$\beta^\circ$  = orientation of the dipole [-].

Equation (3.27) can also be derived from equation (3.26), using equation (3.21). Substitution of (3.26) and (3.27) in equation (3.13), leads to the expression:

$$\Omega(z) = \Gamma_{\text{dip}} \exp(i\beta^\circ - \Theta) / 2\pi r + \Phi_{\text{ref}} \quad (3.28)$$

Again, a simple expression for  $\Omega$  is found. The dipole is described by its strength  $\Gamma_{\text{dip}}$  and by its shape function, which is reciprocal in  $r$ . A dipole does not extract any water, as the strengths of both poles are opposite and equal. However, these strengths do affect the potential and stream function.

### 3.3.4 The line-dipole (crack, drain, canal)

An infinite number of dipoles along a line is called a line-dipole or line-doublet (Strack, 1989a). At a line-dipole, the orientation of the dipoles is equal to the orientation of the line (*figure 3.3.6*) and at a line-doublet the orientation is perpendicular to the line (subsection 3.3.5). A line-dipole may represent a thin zone of very high hydraulic conductivity, as it can be found in cracks.

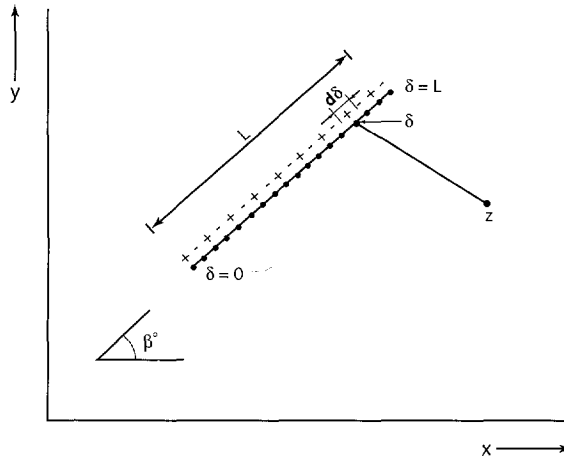


Figure 3.3.6. Definition scheme for a line-dipole element.

Similar to the derivation of the line-sink from the point-sink (well), the line-dipole is derived from the dipole. Integration of dipoles with strength  $\sigma_{\text{dip}} d\delta$  over length  $L$  and substitution in equation (3.28) leads to:

$$\Omega(z) = \int_L -\sigma_{\text{dip}} \exp(i\beta^\circ) / 2\pi(z-\delta) d\delta + \Phi_{\text{ref}} \quad (3.29)$$

where:

$z-\delta$  = distance between observation point  $z$  and point of integration  $\delta$  [L]

$\beta^\circ$  = orientation of line-dipole (equal to orientation of dipole) [-]

$\sigma_{\text{dip}}$  = strength per unit length, function of  $\delta$  [ $L^3/L.T$ ]

Across the element, the potential is continuous and the stream function jumps.

Strack's implementation is based on "Laurent expansions" (Strack, 1989a, pp. 462-466) around the line-dipole. The two "central expansions" generate a singular behaviour around the tips. At a user defined number of points "local expansions" can be generated, which affect the behaviour merely near these points. The more local expansions, the more detailed the flow conditions can be accounted for.

The order of the Laurent expansions can be defined by the user. It determines the degree of freedom of the element, which can be seen as the ability to account for differences in the flux and head along and across the element.

The coefficients in the expansion functions are computed according to the condition specified at a user defined number of control points. The number of control points must be larger than the number of points with a local expansion. The adjustment of the behaviour of line-dipoles appears to be difficult, because there is no direct relation between the behaviour and the steering parameters.

For geohydrological practice, the physics of the line-dipole can be described as follows. Each dipole at the line generates inflow and outflow. The one

pole of the first dipole abstracts water from the aquifer. The other pole generates outflow which directly is inflow of the next dipole. This repeats until the last dipole. The second pole of last dipole infiltrates water into the aquifer. The strength of the dipoles determines the flux through the line-dipole.

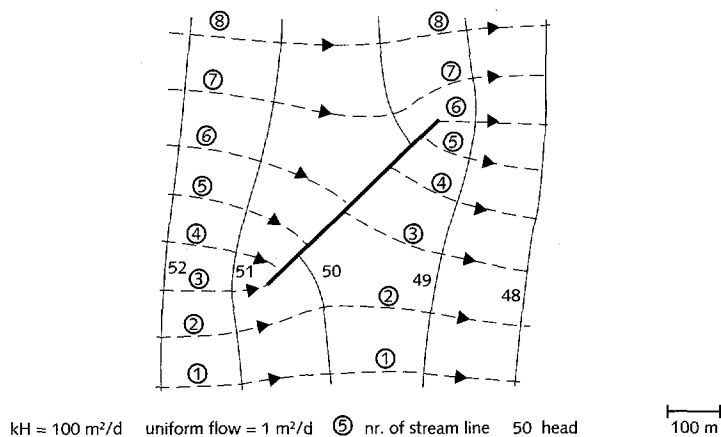


Figure 3.3.7. Lines of equal head (meters above reference level) and streamlines near a drain in uniform flow.

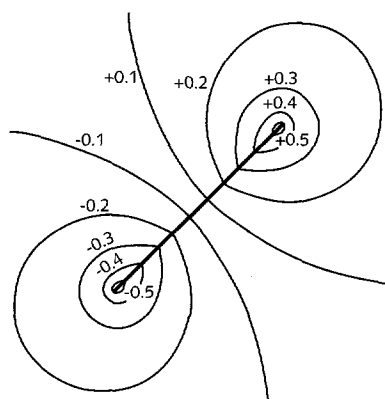


Figure 3.3.8 Difference in the head distribution between the cases of uniform flow with and without the drain of figure 3.3.7.

The dipoles along the line do not necessarily consist of a source and sink of equal strength but may generate a net abstraction or infiltration of water in the aquifer. In the lower part of the line-dipole of figure 3.3.7 (which is a drain, see later in this subsection), the groundwater flows into the line-dipole, in the upper part the groundwater flows out of the element.

A concentration of inflow and outflow occurs at both line ends. This can also be seen in the steep gradients near the tips in figure 3.3.8. Strack (1989a, pp 462-466) formulated these singularities in terms of complex

square-root functions. As the singularities occur at both ends, all elements with singularities at the tips are called double-root (DROOT) elements. The singular behaviour at the tips disables the possibility to connect these elements mutually.

In the AEM three different types of straight line-dipoles are distinguished:

- 1 - the canal, a line with prescribed head and infinite transmissivity;
- 2 - the drain, creating continuity of flow through a line with infinite transmissivity;
- 3 - the crack, creating continuity of flow through a line with specified transmissivity (so, with a width and a hydraulic conductivity).

Of these three line-dipoles, only the canal can abstract (or infiltrate) water from (or into) the aquifer. It can also be seen as a drain, in which a head specified well is added. A drain can be seen as a crack with an infinitely high transmissivity.

The canal generates flow in order to maintain the prescribed head in the aquifer. The drain and the crack do not abstract water from the aquifer and the head in these elements is determined by their environment. In a model with only these elements no flow will occur. Therefore, the drain in *figure 3.3.7* is defined in a uniform flow.

The strength distribution of the line-dipole depends on the distribution of the flux across the line as generated by the other elements in the model. *Figure 3.3.8* presents the difference in the head distribution between the cases of uniform flow with and without the drain of *figure 3.3.7*. In a general model, the effect shall be less symmetrical than in the case of *figure 3.3.8*, because the distribution of the flux near the element will not be as perfectly uniform as it is in the case presented in this figure.

A crack is developed to model thin features in groundwater flow such as cracks in rock. The transmissivity of a crack is defined (Strack, 1989a) as  $k_{cr}B_{cr}$ , which is the product of the hydraulic conductivity  $k_{cr}$  and the width  $B_{cr}$ . The thickness of the crack is equal to the aquifer thickness at the place of the crack.

To understand the definition of the transmissivity of a crack, consider a strip of a width  $b$  [L] in the aquifer. This strip can be seen as a tube characterized by three parameters; the width  $b$ , the hydraulic conductivity  $k_0$  and the thickness  $H_0$ . A crack is a similar tube with parameters width  $B_{cr}$ , hydraulic conductivity  $k_{cr}$  and thickness  $H_0$ , but it is simulated as a line of negligible width. The aquifer itself remains unchanged.

### **3.3.5 The non-connectable line-doublet (leaky wall, impermeable wall)**

A line of dipoles is called line-doublet if the orientation of the dipoles is perpendicular to the line (*figure 3.3.9*). The abstracting poles (plus sign, sink type) occur along one side and the injecting poles (minus sign, source

type) along the other side. The line-doublet withdraws water along one side and injects the same magnitude along the other side. So, in the aquifer, it is as if water flows continuously across the element, while a jump in the potential is created. In this section, non-connectable line-doublets (leaky wall and impermeable wall) are discussed. In the subsection (3.3.6) the connectable line-doublet is introduced.

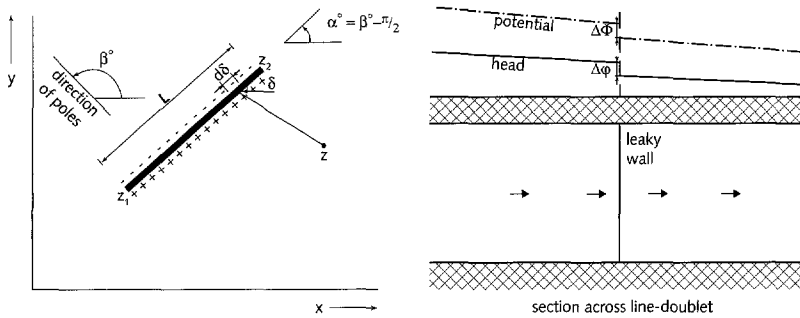


Figure 3.3.9. Definition scheme for a line-doublet element.

The equation for a line-doublet can be found in the same way as for the line-dipole and reads (Strack, 1989a):

$$\Omega(z) = i/2\pi \int_L \sigma_{dou} \exp(i\alpha^\circ) / (z-\delta) d\delta + \Phi_{ref} \quad (3.30)$$

where:

- $z-\delta$  = distance between observation point  $z$  and point of integration  $\delta$  [L]
- $\sigma_{dou}$  = strength of line-doublet as a function of  $\delta$  [ $L^3/L.T$ ]
- $\alpha^\circ$  = orientation of the line-doublet ( $\beta^\circ + \pi/2$ ) [-]

This equation is formally equal to (3.29); only the terms expressing the orientation of the dipoles ( $\beta^\circ$  and  $\alpha^\circ$ ) are different.

A line-doublet creates a jump in the potential  $\Phi$  (see figure 3.3.9), while the stream function (and the flux) remains continuous. From equations (3.8) and (3.9), it follows that  $\Phi = f(\varphi, k, H)$ . If  $k$  and  $H$  are constant across the line, the jump should be in the head  $\varphi$  and may describe a loss of head. Then, the resistance [T] of a line-doublet of type leaky wall (figure 3.3.10) can be defined as the loss of the head [L] divided by the flux [ $L/T$ ] across the element.

The behaviour of the element depends on the distribution of the flux across the element generated by the other elements in the model. Figure 3.3.11 presents the difference in the head distribution between the cases with and without the leaky wall in uniform flow in the case of figure 3.3.10. In general, the distribution of the effect will be different from that presented in figure 3.3.11, because in a real model the flux near the element will not be as constant as the uniform flow in this figure.

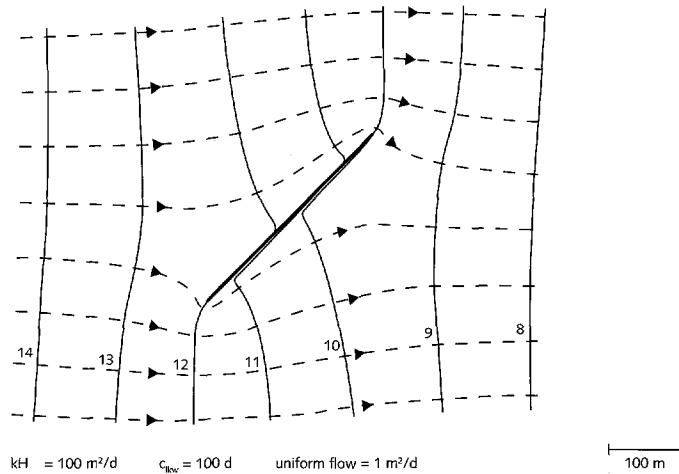


Figure 3.3.10. Lines of equal head (meters above reference level) and streamlines of a line-doublet element (leaky wall) in uniform flow.

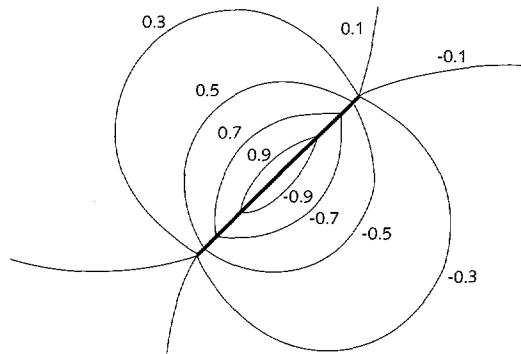


Figure 3.3.11 Difference in the head distribution between the cases of uniform flow with and without the leaky wall of figure 3.3.10.

The leaky wall element is generated by the same Laurent expansions as used in the case of the line-dipole (section 3.3.4). Adjustment of the behaviour of the element is as difficult as with line-dipoles. The resistance of the leaky wall is specified at the control points, which are distributed in the same way as with the line-dipole elements. The leaky wall may simulate a (leaky) sheet pile wall. It can also be used to simulate a local barrier in the transmissivity (e.g. ice-pushed ridges).

An impermeable wall is equal to a leaky wall with infinite resistance. However, a new type of element is defined because the mathematical elaboration of (3.30) becomes different from that of the leaky wall (Strack, 1989a). The flux across the element is zero, which is implemented in Stracks computer code by the condition of a constant value of the stream function. This leads to a particular constraint in the application of the

element: infiltration from the upper or lower boundary of the aquifer into the element is not allowed, because then the stream function can not be constant. The undesirable reaction of the element under such conditions appears clearly in any model.

From a modeling point of view, the behaviour of an impermeable wall is equivalent to the behaviour of a leaky wall with a very high resistance. In modeling, a leaky wall is preferred because it is not affected by any kind of infiltration.

### 3.3.6 The connectable line-doublet (inhomogeneity)

A line-doublet creates a jump in the potential  $\Phi$ , while the stream function (and the flux) remains continuous (see *figure 3.3.9*).

From equations (3.8) and (3.9), it follows that  $\Phi = f(\varphi, k, H)$ . In the case of a line-doublet of type inhomogeneity, the head  $\varphi$  remains constant across the line and a jump in the transmissivity  $kH$  is generated (*figure 3.3.12*).

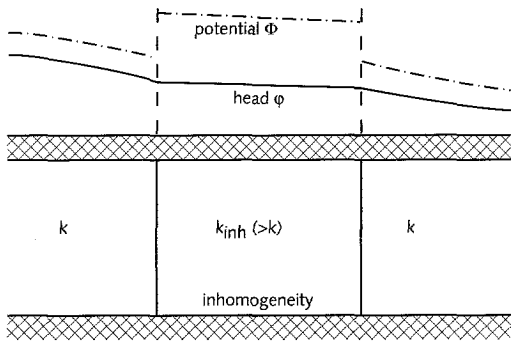


*Figure 3.3.12. Definition scheme for a line-doublet inhomogeneity.*

In Strack's AEM, the inhomogeneity is bounded by a closed string of straight elements called segments. *Figure 3.3.13* shows that streamlines can be computed very accurately at any point of an arbitrary boundary when using many segments. Along the boundary, the jump can be defined in any combination of a change in the hydraulic conductivity  $k_{inh}$ , the thickness  $H_{inh}$  and the base elevation  $B_{inh}$ , which are defined inside the element. Across the boundary of an inhomogeneity, the streamlines and the lines of equal head satisfy the physical laws of refraction.

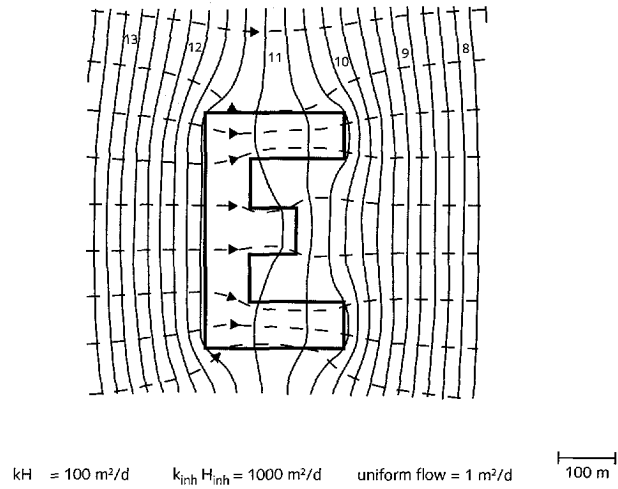
In *figure 3.3.14*, the difference in the head distribution between the cases of uniform flow with and without the inhomogeneity in the case of *figure 3.3.13* is presented. The behaviour of the element depends on the distribution of the flux across the element, which is generated by the other elements in the model, in this case uniform flow.



When only  $k_{inh}$  is different from the overall hydraulic conductivity  $k$ , the jump  $\sigma_{inh}$  [ $L^3/L.T$ ] in the potential (the strength of the line-doublet) may be expressed by (Strack, 1989a):

$$\sigma_{inh} = \Phi^- (k - k_{inh}) / k \quad (3.31)$$

where  $\Phi^-$  is the discharge potential at the outside of the boundary [ $L^3/T$ ]. In this case, the strength is linearly related to the outside potential and can be computed implicitly.



Figur 3.3.13. Lines of equal head (meters above reference level) and streamlines of an inhomogeneity element in uniform flow.

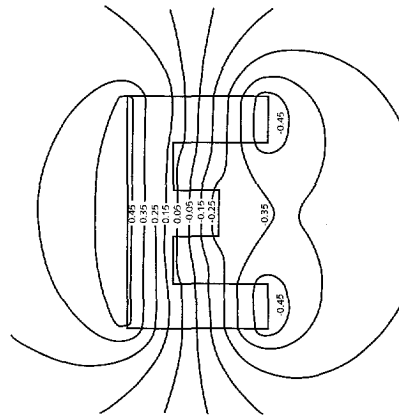


Figure 3.3.14 Difference in the head distribution between the cases of uniform flow with and without the inhomogeneity of figure 3.3.13

When the base or the thickness in an unconfined aquifer changes, the expression for the strength  $\sigma_{inh}$  is not linear in  $\Phi^-$  and iteration is necessary. If a model is applied for groundwater quantity problems only, the change in the transmissivity ( $k_{inh}$  and/or  $H_{inh}$ ) in (semi-) confined aquifers can be simulated by an inhomogeneity with only a different hydraulic conductivity  $k_{inh}$  keeping the thickness  $H$  constant in the model applying:

$$k_{inh} = \{ k_{inh} H_{inh} \}_{conc} / H \quad (3.32)$$

where the subscript  $_{conc}$  applies to the transmissivity in the conceptual model. In this way, iteration has been avoided in almost all models in NAGROM (section 3.1). This type of model should not be used for scenarios demanding flow paths or particle tracking, because the hydraulic conductivity in the inhomogeneities is only a model parameter. For these latter purposes, the thickness should be adjusted necessitating iteration. As an ultimate trick to avoid iteration, the porosity can be changed inside the inhomogeneity to generate the right flow velocities.

Only a jump in the base elevation (so hydraulic conductivity and thickness remaining constant) does not have any effect on the heads and the fluxes in a (semi-) confined aquifer. In these situations, a jump in the base is only relevant for the determination of streamlines. A jump in the base is geohydrologically important when phreatic flow occurs in the aquifer, because then it affects the transmissivity. A jump in the base in a confined aquifer with constant thickness and constant hydraulic conductivity does not affect the distribution of the head or of the flow in horizontal direction.

Strack and Haitjema (1981) compared an analytic solution for a circular inhomogeneity in uniform flow with a computed solution of an inhomogeneity with a boundary of 28 segments. They compared the results of an inhomogeneity with a linear strength distribution per segment to one with a second order (parabolic) strength distribution per segment. Application of the latter distribution appeared to give superior results and is used since then. The parabolic strength distribution demands an extra control point (point in which the specified conditions are fulfilled) for each segment. This control point is defined in the centre of each segment, while the other control points are defined at the endpoints of the segments.

### 3.3.7 The area-sink for surface conditions

Strack implemented the area-sink as an element on top or at the bottom of an aquifer generating a constant vertical inflow, outflow or through-flow over a quadrangular area.

Originally, Strack (oral communication, 1989) derived the formulas for the area-sink by integration of point-sinks over an area (cf. derivation of the line-sink in sub-section 3.3.2). However, the expression for the area-sink can be explained more easy by observing the potential and flux distributions inside, at and outside its boundary (see *figure 3.3.15*).

Consider an area-sink element with domain A and boundary C. In domain A, water is abstracted or infiltrated at a constant strength  $\gamma$  (figure 3.3.15, left).

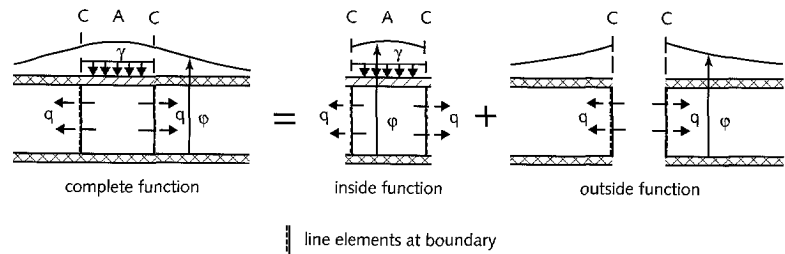


Figure 3.3.15. Definition scheme for area-sink elements.

In domain A, the Poisson equation (3.10) is valid leading to a solution with  $\gamma$  which is parabolic in  $x$  and  $y$ . Strack (oral communication, 1993) proved mathematically, that any kind of parabolic expression with  $\gamma$ , applied in the area-sink with constant strength, leads to one and the same distribution of the potential and stream function. This is due to the presence of line elements at the boundary of the area-sink, see hereafter. So, any arbitrary parabolic distribution with  $\gamma$  can be used.

The strength  $\gamma$  jumps at boundary C to  $\gamma = 0$  outside the area-sink. Continuity of the potential  $\Phi$  at boundary C requires jumps in both the potential and the stream function (figure 3.3.15, middle). Along each line-segment of boundary C, these jumps are generated by (figure 3.3.15, right) (1) a line-doublet (3.30) generating the jump in the potential function and by (2) a line-sink (3.24) generating the jump in the stream function.

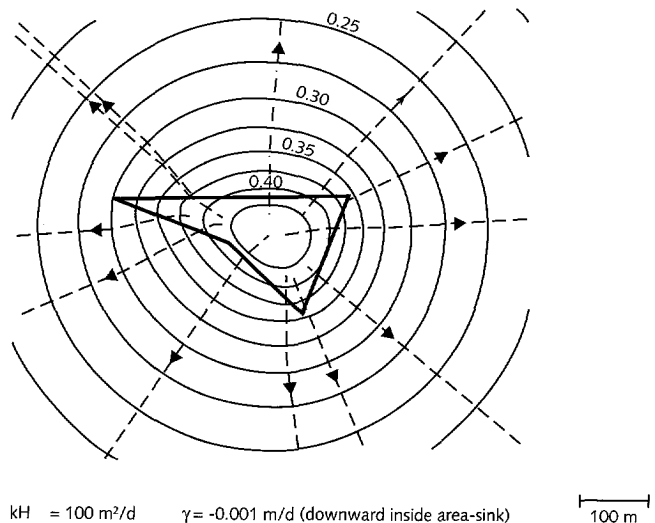


Figure 3.3.16. Lines of equal head (meters above reference level) and streamlines of an area-sink element.

So, the complete solution for the area-sink exists of two expressions:  
 - one for the inside, including the solution with strength  $\gamma$  (which is parabolic in some direction  $\chi$ ) and by the line-doublets and the line-sinks along boundary C:

$$\Omega(z) = i/2\pi \int_C \sigma_{\text{dip}}/(z-\delta) d\delta + 1/2\pi \int_C \sigma_{\text{lin}} \ln(z - \delta) d\delta + 1/2 \gamma \chi^2 + \Phi_{\text{ref}} \quad (3.33)$$

- and one for the outside, generated by the line-doublets and line-sinks along boundary C:

$$\Omega(z) = i/2\pi \int_C \sigma_{\text{dip}}/(z-\delta) d\delta + 1/2\pi \int_C \sigma_{\text{lin}} \ln(z - \delta) d\delta + \Phi_{\text{ref}} \quad (3.34)$$

of which all parameters have been explained before. The distributions from (3.33) and (3.34) are generated in the aquifer and are superimposed to the distribution generated by the other elements in the model.

At present, the surface area-sink (*figure 3.3.16*) can be specified by either the abstraction rate (Neuman boundary condition) or by the hydraulic resistance of a separating layer and the surface water level on top of that layer (Cauchy boundary condition). The latter condition can be used to model polder areas or lakes and is described by:

$$\gamma = (\varphi - p) / c \quad (3.35)$$

where:

$c$  = hydraulic resistance of separating top layer [T]

$p$  = surface water level [L]

$\varphi$  = head in the regional aquifer [L]

The strength  $\gamma$  is constant over the area-sink and is determined at the centre of the area, at the control point. In chapter 6, it is shown that (3.35) can be used to describe a more complex interaction between surface water and groundwater in areas, that are not polders or lakes.

### 3.3.8 The area-sink for the connection of aquifers

The Cauchy boundary condition is also used to describe the connection between two aquifers (*figure 3.3.17*) by:

$$\gamma = (\varphi_1 - \varphi_2) / c_2 \quad (3.36)$$

where  $\varphi_1$  and  $\varphi_2$  are the heads [L] in the upper and lower regional aquifer respectively and  $c_2$  is the resistance [T] of the separating layer in between the aquifers. The strength  $\gamma$  is constant over the area-sink and is determined at the centre of the area, at the control point.

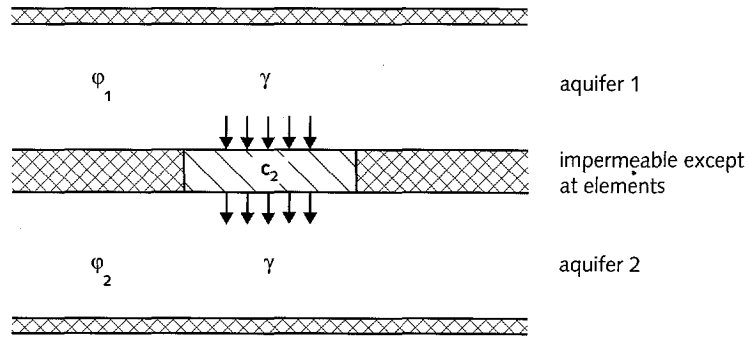


Figure 3.3.17. Two aquifers connected by leakage-type area elements.

This area-sink simulates vertical flow between the two aquifers and is called leakage area-sink. In fact, this is the element that changes a single layer model into a multi-layer model. At places, where these area-sinks are absent, no flow occurs and an impermeable separating layer is implicitly simulated (figure 3.3.17).

### 3.4 The extension to a semi-three-dimensional method

In the Dupuit-Forchheimer assumption, the head is constant over the vertical axes within the aquifer. Then, vertical flow may exist in the aquifer if the resistance in vertical direction is negligible (Strack (1984)). Vertical flow in an AEM model mainly is induced by elements and then occurs inside elements.

#### 3.4.1 Computation of the vertical flow velocity

Vertical flow in the AEM is based on the theory presented in Strack (1984). Analytic elements are defined in the complex (horizontal) plane and generate a two-dimensional field of the potential and stream function. In the derivation of the formulas, the Dupuit-Forchheimer assumption is used. Strack (1984) interpreted this assumption in such a way that the resistance to vertical flow in the aquifer is negligible. Because the vertical flow itself is not neglected, the analytic element technique can be extended to semi-three-dimensional flow.

The vertical flow velocity inside area-sinks is computed using the distinction between elements at the top and at the bottom of each aquifer. In figure 3.4.1, a flow velocity distribution inside an area-sink at the top of the aquifer is shown in a vertical section along a flow path. Continuity of flow leads to the velocity distribution in the vertical section. The flow velocity in horizontal direction follows from the inflow at the left boundary and the inflow along the top of the aquifer and increases from left to right below the area-sink.

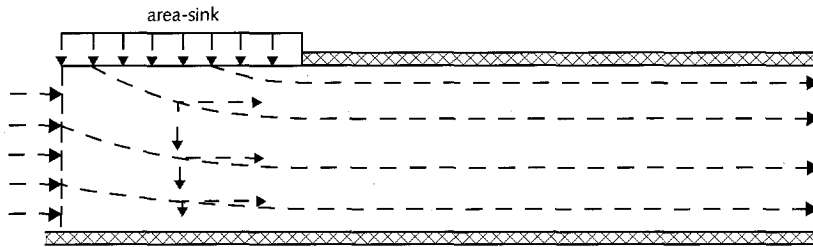


Figure 3.4.1. Flow velocity distribution in a vertical section partly below an area-sink along a path line using continuity of flow.

The vertical flow velocity decreases linearly from the infiltration rate at the top of the aquifer to zero at the bottom. This approach can also be used in cases with area-sinks both on top and at the bottom of the aquifer or only at the bottom of the aquifer.

Strack (1984) gives more examples of flow in vertical sections, as well as a comprehensive treatment of the theory behind it. He also shows that flow velocities computed in this way, in many cases, almost equal the exact three-dimensional solution.

### 3.4.2 Vertical flow in other situations

Vertical flow occurs at places where (figure 3.4.2):

- 1 - inflow or outflow occurs,
- 2 - the aquifer is phreatic,
- 3 - the base of the aquifer is not horizontal and also where
- 4 - the density varies (chapter 4).

Inflow or outflow occurs due to wells, line-sinks, canals (see figures 3.4.2. a and b) and area-sinks (subsection 3.4.1). Of all Strack's analytic elements, only area-sinks can be defined on top or at the bottom of the aquifer. The other types of elements are defined as fully penetrating elements. In the computation of streamlines, Strack assumed that the sink elements withdraw (or infiltrate) water from (to) the upper part of the aquifer. The vertical flow velocity inside the line-sink is derived as described for the area-sink in subsection 3.4.1. At the abstracting line-sink (figure 3.4.2 a), the streamlines jump upward, the jump itself decreasing with depth. Below the area-sink (figure 3.4.2 b), the streamlines bend in upward direction with the vertical flow velocity increasing in upward direction.

In phreatic aquifers, the vertical displacement concentrates at leaky walls and changes at boundaries of inhomogeneities (figures 3.4.2 c and d). The streamlines jump at the leaky wall and change direction at the boundary of the inhomogeneity. The vertical jump in the flow inside the leaky wall decreases with depth (as a consequence of the impermeable base). Inhomogeneities generating a change in the base cause vertical displacements in both confined and phreatic aquifers (figures 3.4.2 e and f).

The "semi-three-dimensional" analytic elements can be combined with fully three-dimensional analytic elements e.g. for partially penetrating wells and line-sinks (Haitjema, 1985) or three-dimensional ellipsoidal inhomogeneities (Fitts, 1991).

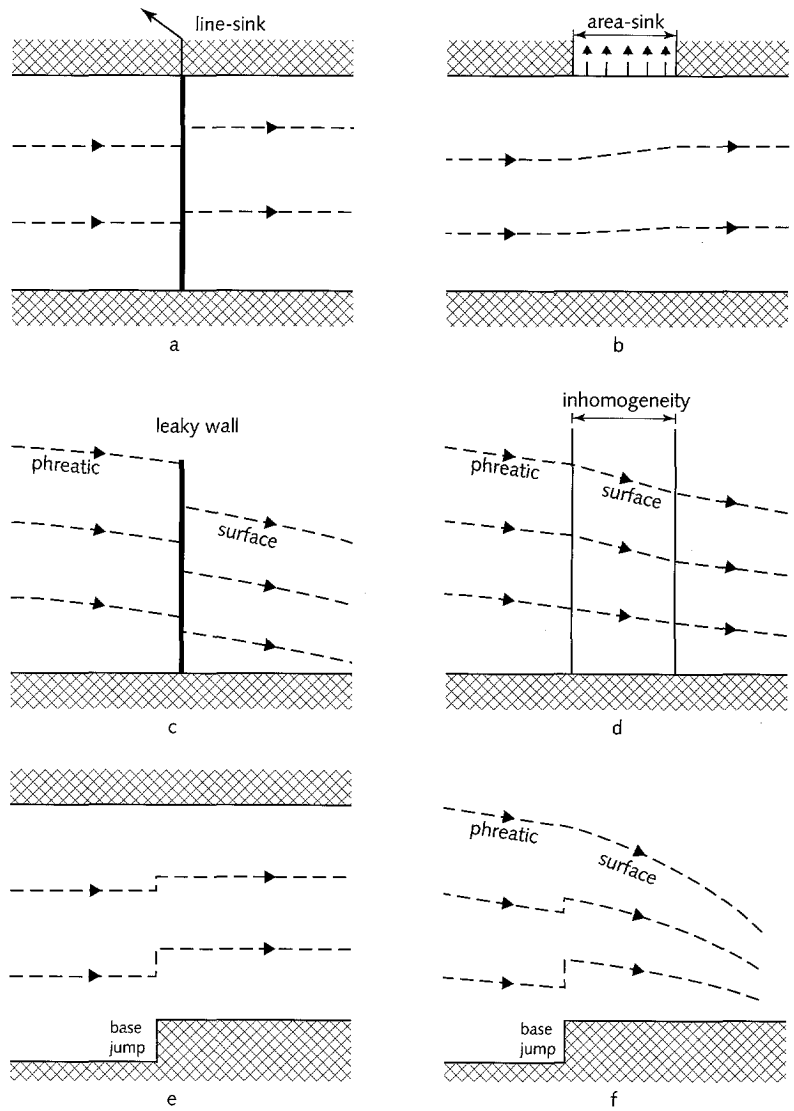


Figure 3.4.2 Schematic examples of causes of vertical flow in a model of analytic elements.

Stracks technique can account for velocity differences along the vertical axes, which are induced via the discharge potential. In an aquifer with vertical variation in the horizontal hydraulic conductivity (subsection 3.2.2), the horizontal flow velocity is uniformly distributed within each distinguished layer but is different per layer. In such an aquifer, the vertical velocity is determined from continuity of flow and is linearly distributed

within the layers. In aquifers with varying density (sub-section 4.2.4), the flow becomes really three-dimensional.

### 3.5 Computational aspects

In a model with analytic elements, the strengths of some elements are specified but the strengths of others are to be computed. For this computation, Strack developed a specific solution technique.

#### 3.5.1 The solution technique for models with only elements with specified strength

In an AEM model, the mathematical functions describing the analytic elements are solutions of the differential equation (3.10). The functions are superimposed to arrive at a solution. The model is said to be solved when the strengths of all elements are known. Then, the value of any variable at any position can be computed simply by superposition of the effects of the functions of all elements in the model. Next, this will be illustrated.

Each element is described by a linear relation between the strength and the corresponding potential distribution (section 3.3). The general expression for the potential in observation point  $P_m$  generated by analytic element  $j$  is:

$$\Phi_{m,j} = SF_{m,j} * S(j) + \Phi_{ref} \quad (3.37)$$

where:

- $\Phi_{m,j}$  = the potential in observation point  $P_m$ , generated by element  $j$  [ $L^3/T$ ]
- $SF_{m,j}$  = shape function ( $\ln(r)$ ;  $1/r$ ; etc) of element  $j$ , function of the distance to point  $P_m$  [-]
- $S_j$  = strength of element  $j$  [ $L^3/T$ ]
- $\Phi_{ref}$  = potential at the reference point  $P_{ref}$  [ $L^3/T$ ]

Superposition of all elements leads to the potential:

$$\Phi_m = \sum_{j=1}^{j=N} \{ SF_{m,j} * S(j) \} + \Phi_{ref} \quad (3.38)$$

where:

- $\Phi_m$  = the potential in an observation point  $P_m$  generated by all elements  $j$  in the model [ $L^3/T$ ]

Expression (3.38) describes the system of equations that is used to illustrate the solution technique of the AEM.

In this case, all strengths are prescribed (Neumann condition) so the model is solved already, assuming that the potential in the reference point is specified. Some of the  $\Phi$  functions, as presented in section 3.3, become



rather complicated, when they are formulated in expressions that can be handled by a computer. The computation of the shape functions  $SF_{m,j}$  appears to demand much computation time in models with a large number of elements. Also, computation effort is needed to determine whether the observed point is inside each of the elements or not. This shows up in the computation time needed for a grid of heads that is needed to draw contour lines.

### 3.5.2 Solution technique for a model of elements with both specified and unknown strengths

In a general model, not all the strengths of the analytic elements in a model will be known. In rivers, lakes, etc. a certain surface-water level is known but the corresponding fluxes are unknown. In such a case, the strengths of the analytic elements have to be computed. Corresponding to each of these unknown strengths a head or surface water level (Dirichlet condition), sometimes in combination with a resistance (Cauchy condition) must be specified (see section 3.3).

A problem formulated in terms of elements with only given potential values (derived from specified heads using e.g. (3.8) or (3.9) ), leads to the following set of equations (compare (3.38)):

$$\begin{aligned} \Phi(1) &= SF(1,1)*S(1) + SF(1,2)*S(2) + \dots + SF(1,M)*S(M) + \Phi_{ref} \\ \Phi(2) &= SF(2,1)*S(1) + SF(2,2)*S(2) + \dots + SF(2,M)*S(M) + \Phi_{ref} \\ .. &= .. + .. + .. + .. + .. \\ .. &= .. + .. + .. + .. + .. \\ \Phi(M) &= SF(M,1)*S(1) + SF(M,2)*S(2) + \dots + SF(M,M)*S(M) + \Phi_{ref} \end{aligned}$$

In matrix notation, this becomes:

$$\Phi = SF * S + \Phi_{ref} \tag{3.39}$$

which is a well-known set of equations, for which many solution techniques exist. Once the set is solved, the strengths are known and the problem is reduced to a problem as described in section 3.5.1.

In a case with elements of both given and non-given strengths, the number of equations in the matrix remains equal to the number of elements with non-given strength (assuming that the potential in the reference point is specified). The elements with given strength are included in the matrix  $\Phi$ . In  $\Phi$ , the potential values induced by all given strength elements in the centres of the non-given strength elements are accounted for.

### 3.5.3 Dealing with coupled aquifers

The matrix equation (3.39) holds for a single aquifer. In a multi-aquifer model, leakage elements are used (see subsection 3.3.8). This leads to differences with the finite element and finite difference techniques in the contents of the matrix of the shape functions.

In the hypothetical situation of a problem of two aquifers without connection, the matrix equation reads:

$$\begin{array}{|c|c|c|c|c|}
 \hline
 | & | & | & | & | \\
 | \Phi | & | & \mathbf{SF} & \mathbf{0} & | \mathbf{S} | \\
 | (aq 1) | & | & (aq 1) & & | (aq 1) | \\
 | & | & | & | & | \\
 | & = & | & * & | \\
 | & | & | & | & | \\
 | \Phi | & | & \mathbf{0} & \mathbf{SF} & | \mathbf{S} | \\
 | (aq 2) | & | & (aq 2) & & | (aq 2) | \\
 | & | & | & | & | \\
 \hline
 \end{array}$$

In the matrix of shape coefficients (containing the **SF** blocks) two fields with value zero (**0**) exist.

The leakage area-sinks connecting the aquifers, cause non-zero coefficients in these zero fields. These coefficients are symmetrically distributed along the upper-left-lower-right diagonal. Instead of the zero parts (**0**), the matrix contains the connection coefficients (**CC**), which describe the connection between both aquifers and arise from the equations for the leakage area-sinks:

$$\begin{array}{|c|c|c|c|c|}
 \hline
 | & | & | & | & | \\
 | \Phi | & | & \mathbf{SF} & \mathbf{CC} & | \mathbf{S} | \\
 | (aq 1) | & | & (aq 1) & aq(1&2) & | (aq 1) | \\
 | & | & | & | & | \\
 | & = & | & * & | \\
 | & | & | & | & | \\
 | \Phi | & | & \mathbf{CC} & \mathbf{SF} & | \mathbf{S} | \\
 | (aq 2) | & | & (aq 2&1) & (aq 2) & | (aq 2) | \\
 | & | & | & | & | \\
 \hline
 \end{array}$$

where

**CC** = the block containing the connection coefficients.

A problem of three or more aquifers can be treated in the same way. This can lead to a rather large matrix, which is not a band matrix, but it can easily be reduced in size. The matrix containing **SF** and **CC** is positive definit. Wassyn (1982) introduced a method to reduce this type of matrix to about a quarter of its size, without relevant loss or gain in computation time. This means that the size of the matrix to be solved is reduced with a factor four.

In a model with a large number of non-given elements, the computation of the inverse matrix needs much less time than the computation of the coefficients in the matrix. The need for numbercrunching computers is caused by the complicated shape functions, and not by the matrix inversion, which is opposite to what occurs when using other techniques.

## 4. THE STATE OF THE ART OF THE ANALYTIC ELEMENT TECHNIQUE FOR THE MODELING OF LARGE DOMAINS

### 4.0 Summary

In this chapter, the state of the art (march 1995) of Strack's AEM is described. The developments since 1992 consist of curved-line elements, area-sinks simulating the exact vertical leakage near an abstraction well, area-sinks with variable vertical flow and an extension of the discharge potential for density driven groundwater flow. These new developments are summarized with their present level of experience. Some of the developments expected in the near future are discussed and the remaining items needed in NAGROM are indicated. The expected capabilities of the AEM with respect to groundwater quality modeling are considered.

### 4.1 Introduction

Since 1989 several new extensions of the AEM have been developed and implemented that became available later than 1992. Because the chapters 3 and 5 have been conceived in 1992, these developments are only summarized here; they are not analyzed in chapter 5. For some of the developments the theory already existed in 1989 and for others a new theory had to be developed. Many of these developments were primarily initiated for NAGROM by the author and have been carried out by Strack.

In 1989, the primary needs for NAGROM with respect to the AEM concerned accounting for variable density, anisotropy, enclosures in aquifers, variation in the leakage near wells and for sloping layers. After several years (1989-1995) of development, most of these needs are satisfied:

- Anisotropy in the horizontal plane and enclosures in aquifers have successfully (section 5.2) been modeled in aquifers using curvilinear elements (subsection 4.2.2).
- The variation in the vertical flow through separating layers near wells can be modeled exactly with so-called Bessel area elements (subsection 4.2.3).
- A theory for variable density has been developed and elegantly implemented. It has been applied extensively in the coastal area of the Netherlands (subsection 4.2.4).
- In a large part of the Netherlands, sloping layers can be modeled using inhomogeneities as long as the model is used mainly for analysis of groundwater quantity. The need for an AEM tool for sloping layers still exists (1995) especially for situations with phreatic flow.

Because the computation effort needed for NAGROM has increased considerably, a new computation procedure will be introduced which has been developed partly (1995). In this approach, the model area is subdivided in so-called superblocs (subsection 4.2.6 and section 4.4). The

present version of NAGROM has primarily been developed for scenarios concerning groundwater quantity. Because the experience with the AEM for use in studies on groundwater quality is limited yet, only a short discussion is given of the expected capabilities of the technique.

## 4.2 The main developments for modeling of large domains in 1993 and 1994

### 4.2.1 Minor and not applied developments

The resistance in the Cauchy boundary condition (3.35) may depend on the head in the regional aquifer. For instance, the value may change when a part of the surface waters in an area falls dry. Therefore, the line-sink elements (for individual surface waters) and the area-sink elements (for lumped surface waters) have been implemented with a resistance value depending on the head in the regional aquifer, which are called multi-resistance area-sinks.

In 1991, Strack developed a doublet to simulate anisotropic inhomogeneities. The anisotropic behaviour was introduced by using the well-known transformation along the principal axes in the horizontal plane inside the inhomogeneity. This worked well for solitary inhomogeneities but the connection between inhomogeneities with different anisotropic properties appeared to be difficult. In the mean time, a practical solution was found by the author (see subsection 5.2.5) based on the application of curved line-elements (subsection 4.2.2) of type leaky wall. By finding this solution, the urgency disappeared and time came available to find a more fundamental solution to include anisotropy.

### 4.2.2 Curvilinear elements

The theory of curved line-elements or curvilinear elements existed several years (Strack (1986)) before the implementation in the AEM.

Curvilinear elements have been developed for the same types as the existing straight line elements described in chapter 3. Curvilinear elements consist of segments which are parts of hyperbolas. The segments can be chained to form open or closed curves. At the beginning and at the end of an open curvilinear element, Strack implemented straight segments to contain the function for the singularity similar to that in the case of the straight line-dipole elements in subsection 3.3.4. Closed curvilinear elements do not contain these functions.

The theory of curvilinear elements is based on the thought that the distribution function for the strength ( $\sigma_{in}$  in (3.25),  $\sigma_{dip}$  in (3.29),  $\sigma_{dou}$  in (3.30) or  $\sigma_{inh}$  in (3.31)) can be defined along any line as long as a real function can be defined along that line (Strack, 1986). Along a streamline such a real function can be found. Strack (1986) considered the flow in corners with angles of 90 degrees (figure 4.1). The streamlines in this case have the form of hyperbolas.

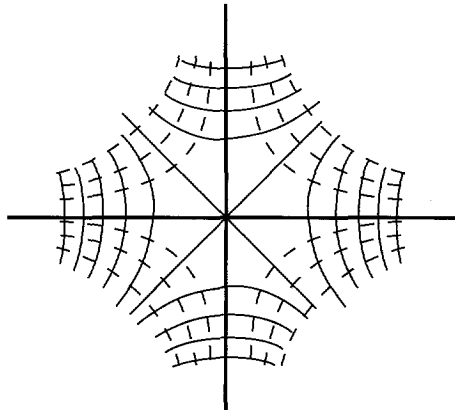


Figure 4.1 *Flownet in corners with angles of 90 degrees, used for the shapes of curvilinear elements (from Strack, 1986).*

As an example, the specification of a curvilinear element composed of two curved and two straight segments is presented in figure 4.2. Each hyperbolic segment is specified by its two nodal points (tips of the segment) and by an anchor point (point of intersection of the tangents at the tips). The end segments are only defined by two nodal points, because they are straight lines. In the case of a closed curvilinear element the singular behaviour is not needed and there are no end segments.

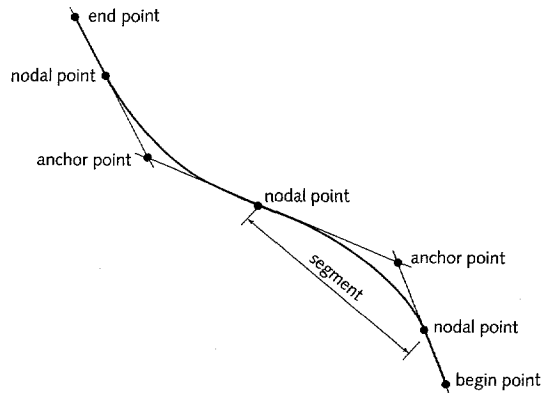


Figure 4.2 *Definition of a composed curvilinear element*

Continuity of the strength and its derivative at the connection of two segments requires that the tangents of both curves are equal there. Therefore, each anchor point should be on a straight line with the adjacent points in each direction. A curvilinear element may exist of relatively long and short segments. However, they should be connected via segments of which the length changes gradually. The conditions at the nodal points and the hyperbolic shape of the element lead to a sixth order polynomial function for the strength distribution.

The main advantages of curvilinear elements over straight line-elements are that they can account better for differences in the flux and head

distributions in the elements. This is the case because the form and length of the segments is flexible while the strength distribution is of an order higher than one. An example of the difference between straight and curvilinear elements can be found in figure 5.3.7 (subsection 5.3.2).

Other advantages of curvilinear elements are that they are developed to be chained, even segments of different type (e.g. line-sink type segments and leaky wall type segments) .

The main modeling experience (by the author in 1995) with curvilinear elements concerns the type of the leaky wall. Curvilinear leaky walls have been used to close an aquifer partly as well as completely over both short and long distances. These elements have also been used to generate anisotropy in models of large domains, which approach will be discussed in subsection 5.2.5.

#### 4.2.3 Area-sinks to model the vertical flow through separating layers near a well

The vertical flow through a separating layer near a well varies strongly with the distance to the well. Many area-sinks with constant strength (subsection 3.3.7) should be needed to model this variation. Each of these elements should have the properties of the area it covers. By this, local details might have to be included which do not belong to the scale of a model of a large domain (chapter 8). By using Bessel-area-elements (Strack, 1991a), the vertical flow near a well can be modeled accurately using elements with sizes that belong to the scale of models of large domains. In figure 5.3.4 in subsection 5.3.2, an example of the effect of a Bessel-area-element is presented.

A Bessel-area-element consists of one or more area-sinks bounded by one polygon and with given but in-place-varying strengths. The strengths of the area-sinks are determined by the properties of the aquifers and aquitards within the polygon and by the positions and the abstraction rates of the wells which have to be accounted for. In general, a Bessel-area-element is used in combination with leakage area-sinks (subsection 3.3.8).

The basic principles of the Bessel-area-element are rather straight forward, but the actual implementation in a computer code especially of the polygonal boundary appeared to be complex (Strack, 1991a).

The discharge potential  $\Phi$  in the case of flow to a well in a single semi-confined aquifer can be described by a modified Bessel function of order zero multiplied by a constant (Strack 1989, pp. 165-167).

$$\Phi = Q_w * K_0(r/\lambda) * \lambda / \{ 2 \pi r_w * K_1(r_w/\lambda) \} \tag{4.1}$$

where

$Q_w$  = the abstraction rate of the well [ $L^3/T$ ]

$r_w$  = well radius [L]

$\lambda = \sqrt{kHc}$ , characteristic length [L]  
 $kH$  = transmissivity of the aquifer [ $L^2/T$ ]  
 $c$  = resistance of the separating layer [T]  
 and  $K_0()$ ,  $K_1()$  are modified Bessel functions of the second kind and of order zero and one respectively (Abramowitz & Stegun, 1965).

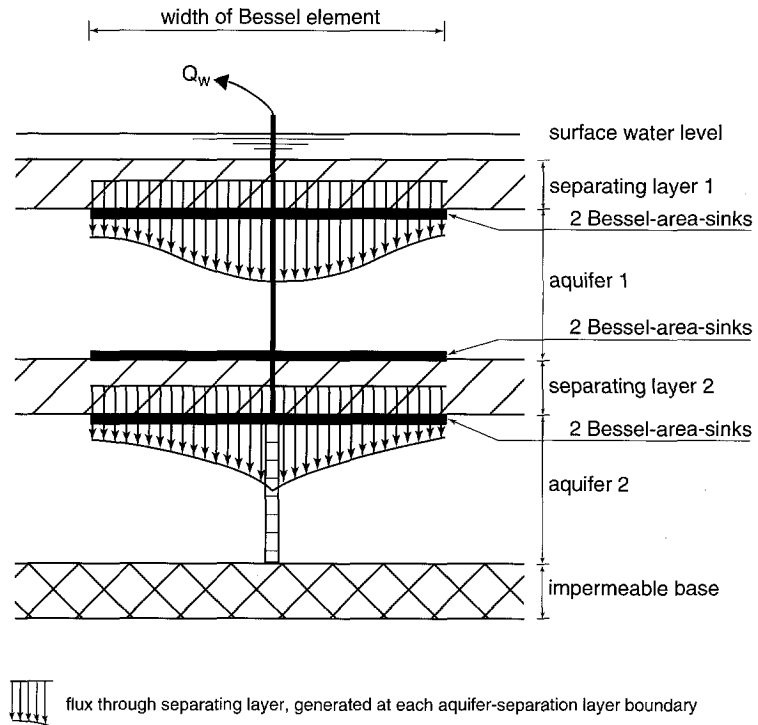


Figure 4.3 Scheme of area-sinks in a Bessel-area-element

The expression for the distribution of the strength  $\gamma$  of the Bessel-area-element is derived by combination of (4.1) and (3.10), which results in an expression with  $K_0(r/\lambda)$ . For different wells superposition is applied within each Bessel-area-element. In equation (4.1) only the geohydrologic properties ( $kH$  and  $c$ ) and the abstraction rate of the well are used. So, the strength is independent of the fluxes generated by the other elements (area-sinks, line-sinks, etc.) in the model. In fact, the Bessel-area-element can be seen as a "correction" element, that accounts for the non-constant distribution of the vertical flow near a well while the interaction between the actual flow in the model at that place is accomplished by the common constant-strength area-sinks.

A complete Bessel-area-element may consist of many area-sinks (figure 4.3). The vertical flow through each separating layer except the top layer is simulated by a specific combination of Bessel area-sinks at both sides. The vertical flow through the top layer is simulated by a specific combination of Bessel area-sinks at its lower side only. The number of elements depends on the number of separating layers. The elements are defined at each boundary between an aquifer and a separating layer. In a model with two

aquifers of which the upper one is semi-confined (*figure 4.3*), two Bessel elements form each specific (per layer) combination of Bessel area-sinks mentioned above and a total number of 6 Bessel elements is needed to simulate the vertical flow.

In a model of three aquifers of which the upper one is semi-confined, each specific combination of Bessel area-sinks needs 3 Bessel elements and there are 5 sides at which these combinations should be defined, so the total number of Bessel elements becomes 15. In a four aquifer model, this number grows to 28. In this, it is assumed that the geohydrologic properties in the observed area are constant. For each area with different geohydrologic properties, the same number of area-sinks should be specified.

Based on the theory of Strack (1989, pp 172-192), the vertical flow through the separating layers in a multi-aquifer system can be simulated by a specific combination of Bessel area-sinks in all aquifers with the same shape. In such a combination, the geohydrologic properties of all aquifers and separating layers at the location of the Bessel-area-element are included. These geohydrologic properties should be constant inside the polygon. A Bessel-area-element can account for the effects of a number of wells at different locations with different abstraction rates.

If the aim is to generate only a first order correction in the vertical flux through the separating layers near a well (e.g. in the case of a model for groundwater quantity), the number of area-sinks can often be reduced. Then, the need to use a area-sink in a complete Bessel-area-element depends on its effect on the flux and head distribution in the aquifer. The area-sinks with relatively small effect might be left out. From the authors experiences, it appears that in a model for quantitative problems, the correction can often be modeled using less Bessel area-sinks than needed to simulate the vertical flow near the well exactly.

By using the complete Bessel-area-element in a multi-layer model, the flux distribution near the well becomes three-dimensionally exact. Also, partially penetrating wells can be modeled by separating the pumped aquifer into two aquifers connected by leakage area-sinks and Bessel-area-elements.

The element has been used (see subsection 5.3.2) in models of large domains in situations where the sizes of Cauchy area-sinks are much larger than  $\lambda$  or where the effect of the well on the flux computed at the control point of the Cauchy area-sink is large.



#### 4.2.4 Implementation of variable density

In the coastal zones of the Netherlands, the density of the groundwater varies mainly as a result of the variation in the salinity. The variation of the density affects the groundwater flow in horizontal direction as well as in vertical direction. The density variation has to be included in the model of this area, because it causes significant effects on the groundwater flow. The classical approach with a sharp interface (see e.g. De Lange, 1986) is not appropriate, because the density varies gradually and not abruptly in the inland part of the Dutch coastal zone.

Maas and Emke (1989) presented an approach to include density variation in a (finite difference) computer program, in which actually only a single density can be defined. They implemented a source term in each element, that generates a correction for the density variation in the element. At the same time, Kontis and Mandle (1988) developed a similar approach in the USA. Strack (1991b) changed the approach of Maas and Emke (1989) to a new theory for variable density flow in terms of the discharge potential. The following presentation of the theory is mainly based on Strack (1992, oral presentation).

Variation in the density is not accounted for by a new type of analytic element but it is implemented via the discharge potential, similarly to the way it is described in subsection 3.2.2 for the sharp interface approach.

In a situation of groundwater with variable density, Darcy's law and the law of continuity can be described in terms of pressure (see e.g. Verruijt, 1982). By defining the hydraulic conductivity and the groundwater head in the regional aquifer in terms of the fresh water density, Darcy's law can be rewritten as (compare Diersch, 1988):

$$q_x = - k_x(\rho_f) \frac{\partial\phi(\rho_f)}{\partial x} \quad (4.2a)$$

$$q_y = - k_y(\rho_f) \frac{\partial\phi(\rho_f)}{\partial y} \quad (4.2b)$$

$$q_z = - k_z(\rho_f) \left\{ \frac{\partial\phi(\rho_f)}{\partial z} + v_{i_z} \right\} \quad (4.2c)$$

where:

- $i_z$  = unit vector in vertical direction [-]
- $k_x(\rho_f)$  = hydraulic conductivity in terms of  $\rho_f$  in x-direction [L/T]
- $k_y(\rho_f)$  = hydraulic conductivity in terms of  $\rho_f$  in y-direction [L/T]
- $k_z(\rho_f)$  = hydraulic conductivity in terms of  $\rho_f$  in z-direction [L/T]
- $q_x$  = specific discharge in x direction [L/T] (varying in x,y,z direction)

- $q_y$  = specific discharge in y direction [L/T] (varying in x,y,z direction)
- $q_z$  = specific discharge in z direction [L/T] (varying in x,y,z direction)
- $\phi(\rho_f)$  = groundwater head in terms of  $\rho_f$  [T] (varying in z direction)
- $\rho$  = density, varying with place [M/L<sup>3</sup>]
- $\rho_f$  = fresh water density [M/L<sup>3</sup>]
- $v$  = relative density  $(\rho - \rho_f) / \rho_f$  [-]

In the Dupuit-Forchheimer assumption,  $k_z(\rho_f)$  approaches infinity and  $q_z$  is a non-zero real value, so the expression between accolades in equation (4.2c) should approach zero. From this latter, the following expression for the head  $\phi(\rho_f)$  can be derived:

$$\phi(\rho_f) = - \int_{Z_r}^Z v(z) dz + \phi_{Z_{ref}}(\rho_f) \quad (4.3)$$

where:

- $\phi_{Z_{ref}}(\rho_f)$  = groundwater head at reference level in terms of fresh water density [L]
- $Z$  = observation level [L]
- $Z_{ref}$  = level of reference plane [L]

An expression for the total flux in the directions x and y is derived by integration of Darcy's law (4.2) over the thickness of the aquifer. Using the definition of the discharge potential  $\Phi$  in (3.5), Strack derived the following expression.

$$\Phi = k(\rho_f) \int_{Z_b}^{Z_t} \phi(\rho_f) dz + \Phi^* \quad (4.4)$$

where  $\Phi^*$  is a parameter which expresses the effect of the head distribution along the upper boundary  $Z_t$  and along the lower boundary  $Z_b$  of the aquifer. This parameter is constant in the case of flow in a (semi-)confined aquifer with piecewise horizontal upper and lower boundaries. Expressions can also be found for  $\Phi^*$  in the case with the phreatic surface as the upper boundary and with a sharp interface as the lower boundary (Strack, 1991b). In the case of flow in an aquifer with both the upper and lower boundary being horizontal, the discharge potential in (4.4) becomes:

$$\Phi = k(\rho_f)\phi(\rho_f, Z_t) Z_t - k(\rho_f)\phi(\rho_f, Z_b) Z_b + k(\rho_f) \int_{Z_b}^{Z_t} v(z) z dz \quad (4.5)$$

From (4.5) it can be concluded that the discharge potential can be analytically determined, if the distribution of  $v$  can be expressed by a continuous analytic function. In Strack's AEM, the distribution of  $v$  is implemented using a three-dimensional continuous distribution function based on the so-called multiquadric-biharmonic (MQ) method (Hardy, 1990), which reads:

$$v(x,y,z) = v_0 + \sum_{m=1}^M a_m \sqrt{\{[(x-x_m)^2 + (y-y_m)^2] \epsilon_{scale}^2 + (z-z_m)^2 + \Delta^2\}} \quad (4.6)$$

in combination with the condition:

$$\sum_{m=1}^M a_m = 0 \quad (4.7)$$

where the constants  $a_m$  ( $m = 1, M$ ) and  $v_0$  are to be computed from the condition that in the points of measurement  $(x_m, y_m, z_m)$  the computed relative density complies with the measured density. The scale parameter  $\epsilon_{scale}$  accounts for the different order of magnitude between vertical and horizontal distances in the aquifer. The parameter  $\Delta$  can be used to smooth the distribution, but should be equal to zero appearing from modeling practice. The MQ behaves reliable and predictable and it can be integrated for use in (4.5).

This theory has been verified with two analytic solutions for flow in a vertical plane by Bakker (1991). The particular case of flow across a jump in the transmissivity in groundwater with varying density has been studied in detail by Strack (1992a). For this case, a solution has been found in which the flow across the boundary of the inhomogeneity approaches the exact flow very well. All other analytic elements could be used directly in combination with the new discharge potential of (4.5).

The modeling with density-driven flow in the AEM goes as follows. By using the MQ, a continuous three-dimensional distribution of  $v$  is interpolated based on a set of three-dimensional, arbitrary-distributed data. In the next step, the discharge potentials (4.5) are computed at the control points of all analytic elements in the model, using boundary conditions in which the density is accounted for. After this, the solution is available in terms of the discharge potential. Then, the two-dimensional distribution of the discharge potential and the three-dimensional MQ distribution of the density are used to compute the pressure, the head in terms of  $\rho_f$ , the velocity in three dimensions, etc. in any point in the model.

The main advantages of the approach presented here are (1) the combination of three-dimensional flow and Dupuit-Forchheimer flow which enables to use the classical modeling approach of aquifers and aquitards and (2) the absence of numerical dispersion in a model with three-dimensional variable density which enables to compute flow paths exactly in models of large domains.

The experiences with models in which density-driven flow takes place has increased since 1993. The results of the NAGROM models of the northern and western coastal zone of the Netherlands have been reported in De Lange and Van der Meij (1994).

In modeling practice, the interpolation of three-dimensional density data based on real data appears to be the most difficult step in the modeling process, mainly because of the lack of knowledge of the real situation. The interpolation should be optimized with respect to the effects of the density variation on the groundwater flow.

The effects of the density variation in terms of fresh water heads grow with depth in areas with relatively high density. The effects of the density variation in terms of horizontal flow can be determined from the difference between the gradients in the freshwater head at a certain elevation in a model with variable density and in the same model with constant density. This follows directly from (4.2a), (4.2b) and Darcy's law for fresh water flow. The effects on the flow in vertical direction can also be determined using (4.2c) and Darcy's law. In terms of velocities, the effects of density variation appear to be relatively large in many areas in the coastal zone. The effects in the models of the coastal zone of the Netherlands show that the specific discharge may be strongly different in its direction (even flow in the opposite direction) and magnitude (up to a factor 1/3 or 3) from the discharge in a model with constant density.

Changes of the density distribution over time can be simulated by shifting the points of measurement ( $x_m, y_m, z_m$ ) over a distance computed from the three-dimensional velocity vector at these points and a certain time step in which the velocity distribution is assumed to be valid. In the new situation the interpolation of the density is carried out again, the groundwater flow is computed and the new velocities lead to the next shift. Experiences with this approach are limited yet (1995), but are very promising.

#### **4.2.5 Area-sink with a variable strength distribution**

The area-sink with constant strength (subsection 3.3.8) is simple to use in modeling but may lead to unexpected modeling errors or to the need of many relatively small elements in a model of a large domain (section 5.3). The variation of the vertical fluxes in reality can better be modeled by using a more sophisticated strength distribution. Strack (1992b) suggested the application of a modified version of the MQ (expression (4.6)) as distribution function for the strength of an area-sink. Strack (1993) suggested to use multi-logarithmic distributions rather than the modified MQ, because then the theory becomes more convenient for the implementation in the computer code. This element has been developed in 1994 and is called log-area-sink. It consists of an area bounded by a polygon in which the conditions are specified in several arbitrary situated control points. The strength (vertical flux) throughout the entire area-sink is defined by a multi-logarithmic distribution, which means that the strength is a combination of logarithmic functions. In the case of using the logarithmic distribution function,  $\Delta$  has a similar meaning as in expression (4.6), but is omitted ( $\Delta = 0$ ). In each element, the type of boundary condition at the control points can be one of the types of boundary conditions that is defined for the constant strength area-sink (subsections 3.3.7 and 3.3.8). In Strack's implementation the value of each parameter in

the boundary condition at a control point can be computed automatically from a predefined distribution. This predefined distribution is a MQ interpolation of the values specified in arbitrary situated points which for instance may be selected from a geohydrologic database.

As a test, the author used the log-area-sink to model the Mazure case (*figure 5.2.10-a*). Excellent agreement between the results of expression (5.12) (and its derivatives) and the computation results has been found in terms of the heads (and the horizontal and vertical fluxes) by using  $\Delta$  (expression (4.6)) equal to  $\lambda$  (expression (4.1)). The dependency of  $\Delta$  on  $\lambda$  causes that the specification of the area-sink becomes complex, because  $c$  (expression 4.1) and therefore  $\lambda$  is not constant within the element. Also,  $\lambda$  becomes complex in multi-aquifer models (Strack 1989a, pp. 172-176). To avoid this place dependent behaviour of the area-sink, the MQ distribution function (with  $\Delta = 0$ ) will be implemented also. After that implementation, tests will show which of the two distribution functions will be most favourable.

#### **4.2.6 Reduction of needed computation effort (part 1); the superblock approach**

Models of large domains such as they have been developed in the Netherlands (De Lange and Van der Meij, 1994) require considerable computing power. Combinations of such models and refinements in these models lead to an even greater required computing power. Therefore, Strack (1992c) developed an approach to decrease this requirement and by which these models can be used more flexible.

In this approach, the model is subdivided into squares in the horizontal plane the so-called super-blocks. In a computation, all analytic elements in each super-block are used as usual, but the effects of all analytic elements outside the super-block are included in a Taylor series expanded around the centre of the superblock. This means that for the computation of the head or the flux in a certain point within the super-block only a few elements and the Taylor series (which is computationally similar to including just one other element) are needed. So, instead of using several hundreds or thousands of elements in an aquifer in the computation of each point in a grid of heads, only several tens of elements are used.

During the first step in the development of the super-block approach (1993), the existing solution method is used to compute the unknown strengths (section 3.5). The coefficients in the Taylor series are determined from this solution in a second computation. In general, the time needed for the computation of a grid of heads after this step is reduced to about the time needed for a model that contains the average number of elements in a superblock.

The second step (future in 1995) in the development of superblocks will be described in section 4.4.

### 4.3 An overview of the capabilities of the analytic element technique (march 1995)

Because the number of types of analytic elements and the number of applications of the discharge potential have become considerably large, an overview of the most important applicabilities is given.

#### 4.3.1 Available analytic elements (march 1995)

In table 4.1, an overview is presented of the analytic elements available in 1995. The elements have been explained in sections 3.3 and 4.2. The point elements and the elements generating changes in areas are presented in part a of table 4.1. The available straight line elements in part b of table 4.1 are distinguished from the curved line elements in part c.

The strength distribution of the Bessel element (based on modified Bessel functions) has been discussed in subsection 4.2.3. The application of Laurent expansions in the definition of the strength has been discussed in subsection 3.3.4.

The curvilinear elements are curved versions of straight elements except the Qdrain, which is a drain additionally specified by its total strength  $[L^3/T]$ .

Table 4.1 Analytic elements available in 1995

#### a) non-line elements

NAME of analytic element	specified condition	strength distribution	shape and place in aquifer
Well (point-sink)	head, or strength	point	point, fully penetrating
Area-sink	strength, or resistance, or (multi-)resistance + head	constant	quadrangle on top or at bottom of aquifer
Bessel area-sink	strength	modified-Bessel functions	polygon on top or at bottom of aquifer
Logarithmic-area-sink	strength, or resistance, or (multi-)resistance + head	combination of logarithmic functions	polygon on top or at bottom of aquifer
Inhomogeneity (doublet)	jump in hydraulic conductivity, thickness, base and / or porosity	second order per segment	polygon, fully penetrating

### b) straight-line elements

NAME of analytic element	specified condition	strength distribution	shape and place in aquifer
Line-sink	head, or strength or (multi)-resistance + head	constant, or linear per segment	straight, fully penetrating
Leaky wall (line-dipole with double-root)	resistance	Laurent expansion	straight, fully penetrating
Impermeable wall (see leaky wall)	(infinite resistance)	Laurent expansion	straight, fully penetrating
Crack (see leaky wall)	transmissivity	Laurent expansion	straight, fully penetrating
Drain (see leaky wall)	(infinite transmissivity)	Laurent expansion	straight, fully penetrating
Canal (see leaky wall)	head (and infinite transmissivity)	Laurent expansion	straight, and fully penetrating

### c) curved-line elements

NAME of analytic element	specified condition	strength distribution	shape and place in aquifer
Line-sink (curvilinear)	head, or strength or (multi)-resistance + head	6th order	curved, fully penetrating
Leaky wall (curvilinear)	resistance	6th order	curved, fully penetrating
Impermeable wall (curvilinear)	(infinite resistance)	6th order	curved, fully penetrating
Crack (curvilinear)	transmissivity	6th order	curved, fully penetrating
Drain (curvilinear)	(infinite transmissivity)	6th order	curved, fully penetrating
Qdrain (curvilinear)	flux of entire element	6th order	curved, fully penetrating
Canal (curvilinear)	head	6th order	curved, fully penetrating

#### 4.3.2 Available modeling features due to the discharge potential

It has been presented in sections 3.2 and 4.2, that the discharge potential may account for several (solid and fluid) properties that are valid in the entire aquifer. Once the discharge potential is determined in which a

certain property can be included, all analytic elements can be used in that situation because they are all expressed in terms of the discharge potential. Therefore, the capability of the AEM to deal with aquifer-wide properties due to the discharge potential is presented separately in table 4.2.

In principle, all versions of the discharge potential can be combined, except (as foreseen in 1995) the solution for the anisotropy. Strack (1989a) shows some examples. At this moment most of the extended applications of the discharge potential are implemented in different special versions of the AEM computer code. The horizontal and impermeable laminae and the stepwise vertically varying hydraulic conductivity are not implemented yet in the multi-layer version.

Table 4.2. Properties accounted for by the discharge potential in 1995.

Description	Status
confined and unconfined flow	fully available
vertically varying horizontal hydraulic conductivity	available for single aquifer models
horizontal impermeable laminae	available for single aquifer models
sharp interface, salt water stagnant	prototype, tested
sharp interface, salt water flowing	theory
3-d variation in density	fully available, partly in development
sloping base / horizontal anisotropy	theory
transient flow	theory

#### 4.4 Expected developments

##### *Reduction of required computation effort (part 2); the superblock-solve approach*

In the next step (see part 1, subsection 4.2.6) of the development of the superblock approach (foreseen in 1996), a solution method based on the superblocks will be developed. This means, that for each superblock a set of equations and unknowns is set up, by which the interaction is described between all analytic elements in the superblock and the Taylor series expressing the elements outside the superblock. After this, the solution will be performed superblock after superblock by using some kind of a Gauss-Seidel procedure.

After the solution, each superblock contains the complete solution for its area and it can be treated as a separate sub-model. The use of individual super-blocks, the possibility of subdividing super-blocks in smaller superblocks and other new applications are to be considered as potentially important advantages of the AEM technique.

##### *Area-sink with strength distribution for leakage near line-sinks*

The vertical flow through separating layers close to a straight line-sink differs strongly with the distance to the element. Strack (1992d) outlined the theory for a "Bessel" area element for vertical flow near (linear) line-



sinks. It appears that the theory is largely similar to the theory for the Bessel element sketched in subsection 4.2.2. This element may become important for local models around streams. But to model streams the curvilinear line-sink may give the best results. The theory outlined by Strack may have to be extended for curvilinear line-sinks.

#### *Sloping base*

A sloping base in a phreatic aquifer affects directly the transmissivity and, therefore, affects the flux and head distribution. At present, this can only be modeled using inhomogeneities generating jumps in the base. Such base jumps appear to affect the flux and head distribution considerably in both the direction and magnitude by the direction of the segments across which the jump is generated and by the size of the base jump. Especially, a steep sloping base may demand many nested inhomogeneities (see subsection 5.4.2) and may lead to complex models only because of the slope in the base (Verhagen, 1992). For the model of the very southern part of the Netherlands, a solution to include a continuously sloping base is urgently needed, because too many small steps in the base are needed when using the available inhomogeneity element.

#### *Transient effects*

Transient effects have been considered to be of secondary importance to a groundwater model for national water management, because large amounts of data are needed and the computations may become very cumbersome. Also, for NAGROM as a part of PAWN (section 2.2) the transient effects are less important, because the connected model for the unsaturated zone MOZART (Arnold, 1995) accounts for the primary transient effects in the phreatic storage.

However, it is important that transient effects can be included in models of small domains. The phreatic and elastic storage of aquifers will be included in the AEM for use in NAGROM in order to analyse the differences between results of computations with and without storage and for the use in a refined part of NAGROM.

Zaadnoordijk (1988) has developed analytic elements for time dependent groundwater flow, which are not implemented in the Strack's AEM yet. Zaadnoordijk's approach requires to keep track of the history of the boundary conditions over time. So, to compute a head or flux at a certain time, the boundary conditions in all previous periods must be used.

Maas (1993, oral presentation) presented an approach to compute the response of the groundwater head to the variation in the recharge in terms of coefficients of a function. This approach is based on an impulse-response relation similar to the expression for the unit-hydrograph in surface water hydraulics. In this case, it is not necessary to compute the transient behaviour step by step.

Strack (oral communication, 1995) developed a theory in which the behaviour of the groundwater in time is described analytically. The boundary conditions (heads in rivers, abstraction rates of wells, infiltration rates, etc.) will be described as analytic functions in time (e.g. Fourier series, delta functions, etc). The elastic or phreatic storage responds to these boundary conditions and will be simulated by variable-strength area-sinks (subsection 4.2.5). The theory has been tested in a test situation and has to be extended further (1995).

#### **4.5 Some remarks on the use of the AEM in the computation of groundwater quality**

In the Netherlands, experiments with the AEM concerning problems on groundwater quality have been restricted to the classical aspects of tracing and travel time. At present, the AEM can compute processes that are directly related to travel times along flow paths of a single pollutant, such as advection, linear decay and retardation. Diffusion and longitudinal dispersion are not implemented yet, but have been explored in experimental versions of the AEM at the University of Minnesota (e.g. Maas, 1994).

In the AEM flow paths are computed without being affected by numerical dispersion due to element sizes or due to numerical differentiation of the head distribution. Also, in any volume (also (partly) inside elements) the water balance is perfect. This is in contrast to what happens in other techniques.

The AEM can be used to compute flow paths in aquifers with variable density. Also, density differences caused by pollution can be included.

When the module for transient effects is implemented, the AEM can account for the changes in the positions of particles over time which is the main source of horizontal transversal dispersion.

Eventually, the AEM will provide an analytically exact simulation of transport of a solvent in groundwater flow. The path lines of particles will be determined exactly (analytically) in time and place and can be combined with analytical descriptions for the longitudinal mechanical dispersion, the transversal dispersion based on transient effects and the molecular diffusion. The possibility of an implementation of linear chemical reactions is being studied.

## 5. PROPERTIES AND BEHAVIOUR OF ANALYTIC ELEMENTS IN MODELING

### 5.0 Summary

The properties and behaviour of the analytic elements implemented in the multi-aquifer version of the AEM (MLAEM) in 1992 are described with special attention to the interaction between elements.

First, single elements are analyzed. The well, line-sink, canal and area-sink generate flow and can be analyzed on their own. The inhomogeneity, leaky wall, impermeable wall, drain and crack do not generate flow by themselves. Therefore, they are analyzed in both a uniform and an axial-symmetric flow field. The analysis is focused on the distribution of the flow and the head in the vicinity of the elements.

Second, all combinations of two elements in a single aquifer are analyzed. A qualification with respect to the complexity of each combination is presented in a table.

Multi-aquifer models can lead to very complex combinations (De Lange and Van der Meij, 1994). A number of such combinations describing particular situations in the modeling of large domains is selected for the analysis.

### 5.1 Introduction

A groundwater model consists of a well-chosen combination of analytic elements. In a model, all analytic elements together are acting and reacting. Analytic elements may be nested, linked, crossed etc. (see section 5.3). This freedom in the choice of elements enables to develop models in which the shape and the type of each element is closely related to the shape and the type of the natural geohydrologic features (rivers, polders, etc., section 3.1). The reverse side of this medal appears to be that the behaviour of a combination of elements is not always as expected by the user. Therefore, it is a prerequisite for analytic element modeling to understand both the behaviour of each type of element on its own and the main interactions between analytic elements. It is an aim of the entire chapter 5 to present the behaviour of analytic elements in such a way that the appropriate types of analytic element can be chosen for many combinations of different geohydrological features.

In this chapter, the types of the analytic elements are dealt with in an order that a logical build up in the analysis. The names of the elements describe the modeling function in Strack's AEM programs, which are (cf. chapter 3):

- the well (point-sink)
- the line-sink

- the area-sink
- the inhomogeneity (connectable line-doublet)
- the leaky wall and the impermeable wall (non-connectable line-doublet)
- the canal, the crack and the drain (line-dipole)

Section 5.2 starts with the analysis of the well, the line-sink, the canal and the area-sink each on its own. The effects of these elements on other elements are described using the distributions of the flux across lines nearby each element. The inhomogeneity, the leaky wall, the impermeable wall, the crack and the drain generate flow only in reaction to existing flow. Therefore, the effects of these elements are analyzed in two basic flow fields being a uniform flow field and an axial-symmetric flow field generated by a well. As an exception, the curvilinear element of type leaky wall (subsection 4.2.2) is included, because only with this type of curvilinear element the modeling experience has grown sufficiently in 1992. This element is used in the analysis of a leaky wall in axial-symmetric flow. The discussion of each type of element is completed with some particular aspects concerning its applicability.

Based on the description of each individual element, the basic interactions between all combinations of two analytic elements of the types mentioned above are analyzed in section 5.3. A main point of attention herein is the so-called physical error, which is due only to a wrong combination of analytic elements and does not occur in other techniques.

The effects of interactions between more than two elements can often be deduced from the basic interactions between two types of elements. This is illustrated in the examples in section 5.4 which describe some combinations that are of particular interest in modeling of large domains. In each example, the specification of the elements is improved (with respect to the accuracy) step by step. These steps actually illustrate the process of calibration with analytic elements.

In multi-aquifer models of analytic elements, area-sinks of type leakage (subsection 3.3.8) are used to simulate the interaction between aquifers across separating layers. The transfer of the distribution of the flux in vertical direction by leakage area-sinks causes that the shapes of area-sinks should preferably be equal in vertical direction. As an example, a two-aquifer model is analyzed to show the effects of different meshes of leakage area-sinks on the head distributions in both aquifers.

Unless otherwise stated in the sections 5.3 and 5.4, the transmissivity in the examples is  $2500 \text{ m}^2/\text{d}$  with  $k = 50 \text{ m/d}$  and  $H = 50 \text{ m}$ , the surfacewater level  $p = 10\text{m}$  and the reference point is far outside the model area ( $x = 0 \text{ m}$ ,  $y = 10000 \text{ m}$ ) with a reference level of  $0 \text{ m}$ .

## 5.2 Single analytic elements

### 5.2.1 The well

In figure 5.2.1, the flux distributions across lines in the vicinity of a well are shown. The relative lengths of the cross-lines express the distribution of the flux in normal direction to each of these lines. The lengths of the cross-lines perpendicular to the horizontal lines are mutually comparable as well as the lengths of the cross-lines perpendicular to the vertical lines are. However, the lengths of the lines perpendicular to the horizontal lines are not comparable to the lengths of the lines perpendicular to the vertical lines. The lengths of the cross-lines along line 2 are almost negligible compared to the cross-lines along line 1. The distribution along line 3 is much smoother than along line 1. The variation in the distribution along line 4 is almost negligible compared to that along line 3. It can be concluded from figure 5.2.1, that the peak in the flux should be accounted for by elements in the close vicinity of the well only and can be neglected for elements at a greater distance.

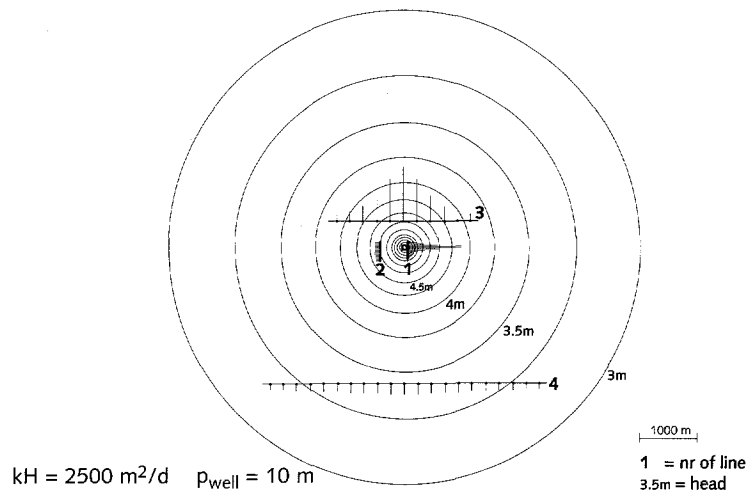


Figure 5.2.1 Distribution of the flux generated by a well across several lines of observation (see text).

In fact, the distribution of the flux along each line in figure 5.2.1 represents the effect (in terms of fluxes) of the well on an analytic element at the place of that line. The latter element may generate a reaction dependent on this effect e.g. a jump in the head generated by a leaky wall in reaction to flow generated by a well as shown in figure 5.3.7. This will be discussed further in section 5.3. The distribution of the flux may lead to define the distances between the control points or line-segments of the reacting element near the well.

By combination of equations (3.2), (3.3), (3.19) and some basic goniometric expressions, the distribution of the flux across a line near a

well can be derived :

$$Q_n = Q_w a_w / 2\pi r^2, \text{ with } r^2 = a_w^2 + x^2 \quad (5.1)$$

where:

$r$  = distance between a point on the considered line and the well [L]

$a_w$  = distance between the considered line and the well [L]

$x$  = coordinate on the considered line with the origin at the point of projection of the well [L]

$Q_n$  = normal flux per unit length across the line [L<sup>3</sup>/L.T]

$Q_w$  = abstraction rate of the well [L<sup>3</sup>/T]

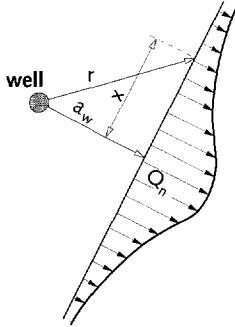


Figure 5.2.2 Scheme for the derivation of expression (5.1).

In some situations, the distances between the control points or line-segments of the reacting element near the well can be related to the point of inflexion of the flux distribution, which is at the place where the second derivative of  $Q_n$  equals zero. The second derivative (or the curvature) of  $Q_n$  is given by:

$$\frac{d^2 Q_n}{dx^2} = \frac{-Q_w (a_w^3 - 3a_w x^2)}{\pi (a_w^2 + x^2)^3} \quad (5.2)$$

The point of inflexion of the flux distribution becomes:

$$x = a_w / \sqrt{3} \quad (5.3)$$

Between the two points of inflexion of *figure 5.2.2*, the flux distribution is convex and outside these points it is concave. Also, the changes in the flux between these points are stronger than outside. Therefore, these points are often used as segmentation points. In modeling practice, also other elements affect the flux across the line(-segment) and often the coordinate of the segmentation point is rounded off to  $x = a_w$ .

The adaption of the distribution of line-segments of an element to the flux distribution generated by the well can be illustrated using an inhomogeneity. Because the parabolic strength distribution along each line-segment of an inhomogeneity can properly account for either the

convex or the concave part of the flux distribution, a control point between two line-segments of an inhomogeneity (subsection 3.3.6) might be defined at the point of inflexion. This will be explained further in subsection 5.3.2.

### Applicability

In Strack's AEM, the well is defined as a fully penetrating well. Haitjema and Kraemer (1988) developed an analytic element generating fully three-dimensional flow to a partially penetrating well, in a confined aquifer which might be, but is not yet implemented in Strack's computer programs.

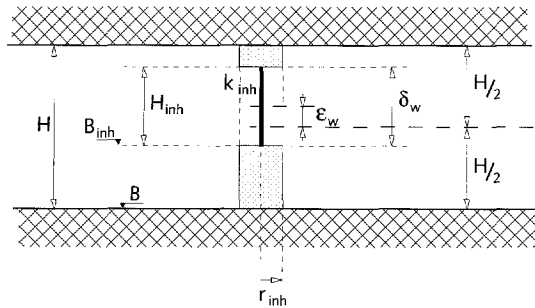


Figure 5.2.3 Modeling a partially penetrating well by using an approximately circular inhomogeneity e.g. as presented in figure 5.2.15.

A partially penetrating well (figure 5.2.3) can be simulated also by a combination of a well and an approximately circular inhomogeneity (e.g. figure 5.2.15). The parameters of the inhomogeneity can be found as follows. The inhomogeneity accounts for the length and depth of the partial penetration by a local jump in the base and in the top of the aquifer and for the radial resistance by a reduction of the local transmissivity. The effect of the radial resistance in terms of the extra drawdown (compared to in the case of a fully penetrating well) of the head at the well boundary can be found in literature (e.g. CHO-TNO, 1964, p 82) and has the form of:

$$\phi_{w,\text{partial}} - \phi_{w,\text{full}} = F(\delta_w, \epsilon_w, H, r_w) Q_w / 2\pi kH \quad (5.4)$$

where  $\phi_{w,\text{partial}}$  and  $\phi_{w,\text{full}}$  are the heads at the well radius in the case of a partially respectively fully penetrating well [L],  $F(\phi_w, \epsilon_w, H, r_w)$  [-] is a (not simple) function given in the reference,  $H$  is the thickness of the aquifer [L],  $\delta_w$  length of the well screen [L],  $\epsilon_w$  is the eccentricity of the well screen [L] (figure 5.2.3) and  $r_w$  is the well radius [L]. Assuming that the inhomogeneity (figure 5.2.3) is a circle around the well (in the horizontal plane) with radius  $r_{\text{inh}}$ , the lowering generated by the inhomogeneity can simply be found using expression (3.19).

$$\phi_{w,\text{partial}} - \phi_{w,\text{full}} = \frac{Q_w}{2\pi} \left[ \frac{1}{k_{\text{inh}} h_{\text{inh}}} - \frac{1}{kH} \right] \ln \left( \frac{r_{\text{inh}}}{r_w} \right) \quad (5.5)$$

where  $k_{inh}H_{inh}$  is the transmissivity inside the inhomogeneity [ $L^2/T$ ],  $r_{inh}$  is the radius of the inhomogeneity [ $L$ ] and  $\phi_{w,inh}$  is the head at the well radius in the case with the inhomogeneity. By stating that the lowering generated by the inhomogeneity should account for the extra lowering needed to simulate the radial resistance, both formula's can be combined to an expression for  $k_{inh}H_{inh}$ .

$$k_{inh}H_{inh} = kH / [ 1 + F(\delta_w, \epsilon_w, H, r_w) / \ln(r_{inh}/r_w) ] \quad (5.6)$$

In general, partial penetration is of interest in local models only. For regional models, the effects of the partial penetration can often be neglected. In the latter models, often a single fully penetrating well is used even to simulate a field of partially penetrating wells.

### 5.2.2 The line-sink

The flux across a line parallel to and near a stand-alone line-sink generating a constant (or linearly) distributed flux is almost constant (or linear), except near the ends of the element (figure 5.2.4, line (1) ).

The distribution of the flux across a line at a certain distance from a tip of the line-sink (figure 5.2.4, line (2) ) approaches that in the case of a well. The distribution is symmetric if the line of observation is parallel or perpendicular to the line-sink. At a large distance from the line-sink (figure 5.2.4 line (3) ), the head and flux distribution become more even similar to that in the case of a well.

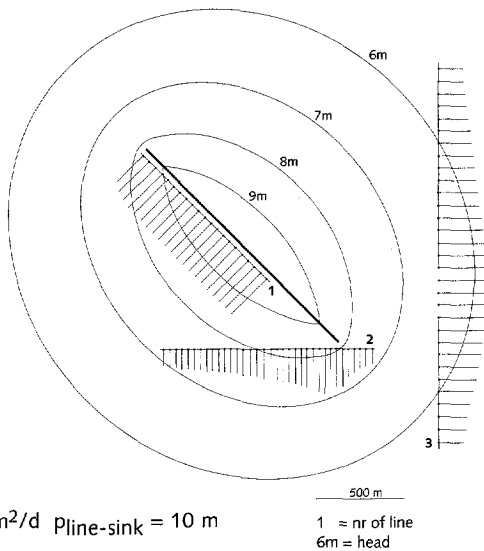


Figure 5.2.4 Distribution of flux generated by a line-sink across several lines.

The head generated along such a line-sink is not constant (figure 5.2.5). Along the line-sink, the further away from the centre of the line-sink, the



more the head approaches the head generated by the other elements in the model or, in this case, the level at the reference point.

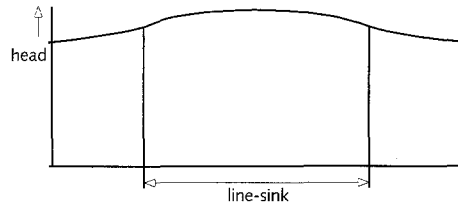


Figure 5.2.5 Head distribution along line 1 parallel to a line-sink in figure 5.2.4.

Similarly to the derivation of expression (3.24), the expression for the flux across a line at a certain distance of a line-sink can be found by integration of the effects of an infinite number of infinitesimal small wells with strength  $\sigma_{lin}d\delta$  along the line of the element. So, in the case of a line-sink (5.1) is reworked to:

$$Q_n = \int_L \sigma_{lin} a(\delta) / [2\pi r(\delta)^2] d\delta \quad (5.7)$$

where  $Q_n$  is valid at a certain point along the considered line,  $\sigma_{lin}$  is the strength of line-sink per unit length [ $L^3/(L.T)$ ] and  $a(\delta)$  and  $r(\delta)$  take the place of  $aw$  and  $r$  in expression (5.1) (figure 5.2.2). Defining the origin  $O$  at the point of intersection in lengthened lines of the line-sink and the considered line, the solution of (5.7) is found by application of basic trigonometric functions and straight forward integration:

$$Q_n = \frac{\sigma_{lin} \sin(\Delta^\circ)}{4\pi} \ln \frac{\delta_2^2 - 2y\delta_2 \cos \Delta^\circ + y^2}{\delta_1^2 - 2y\delta_1 \cos \Delta^\circ + y^2}$$

$$\frac{\sigma_{lin} \cos \Delta^\circ}{2\pi} \left[ \arctan\left(\frac{\delta_2 - y \cos \Delta^\circ}{y \sin \Delta^\circ}\right) - \arctan\left(\frac{\delta_1 - y \cos \Delta^\circ}{y \sin \Delta^\circ}\right) \right] \quad (5.8)$$

where:

- $\Delta^\circ$  = angle between line-sink and considered line [-]
- $\delta_1$  = distance from origin  $O$  to farthest tip of line-sink [L]
- $\delta_2$  = distance from origin  $O$  to closest tip of line-sink [L]
- $y$  = distance from origin  $O$  to point of determination of  $Q_n$  [L]

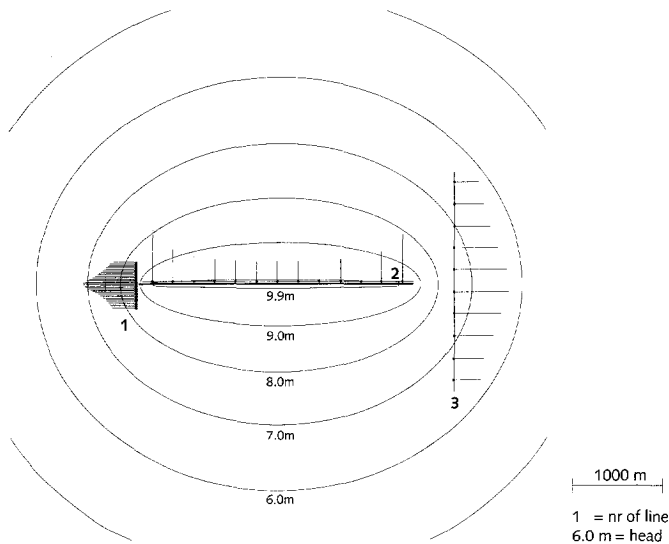
However, this expression does not lead to a simple solution of the point of inflexion. Therefore, the rule developed for the well in subsection 5.2.1 is also used for lines near the tip of a line-sink, which means that the line-segments of an element close to that tip are as long as the distance between that tip and the element.

## Applicability

Haitjema and Kraemer (1988) presented also a solution for a partially penetrating line-sink. In principle, a partially penetrating line-sink can be simulated in a way similar to that presented for a partially penetrating well (figure 5.2.3), but the determination of the parameter values of the inhomogeneity becomes more complex.

## The canal

At the tips of a canal, the double-root functions (subsection 3.3.4) generate more pronounced flow patterns than what occurs at the tip of the line-sink (figure 5.2.6, line 1). The flow at the tip of a canal approaches the flow a well even more than in the case of the line-sink. Contrary to the case of a line-sink, the strength of a canal varies along the element (figure 5.2.6, line 2) in such a way that it generates a constant head inside the element. In order to generate this constant head, the flux near the tips of the element is much stronger than in the middle. At some distance of the element the lines of equal head are smooth and the flux across a line (figure 5.2.6, line 3) is more evenly distributed similar to that in the case of the line-sink.



$$kH = 2500 \text{ m}^2/\text{d} \quad p_{\text{canal}} = 10 \text{ m}$$

Figure 5.2.6 Distribution of flux across several lines generated by a canal

The lines of equal groundwater head of 9.9 m in figure 5.2.6 indicate an almost constant head just outside the element. The difference between the constant head along the canal presented in figure 5.2.7 and the varying head along the line-sink of figure 5.2.5 is obvious.

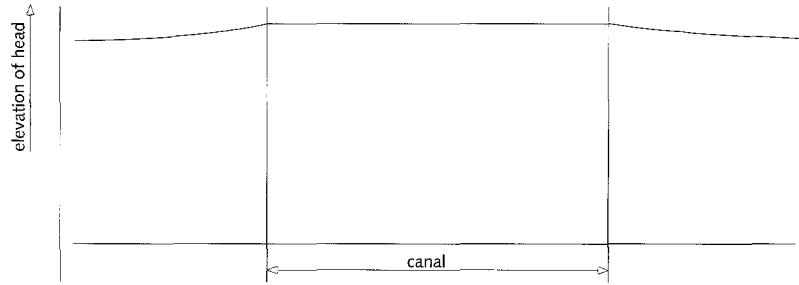


Figure 5.2.7 Head distribution along a line parallel to a canal similar to line (2) in figure 5.2.6.

The derivation of an expression for the flow across a line in the vicinity of a canal is not straight forward, because the strength of the element is not constant. The line-segments or distances between control points of an element in the vicinity of a canal should be at most as great as in the case of the line-sink.

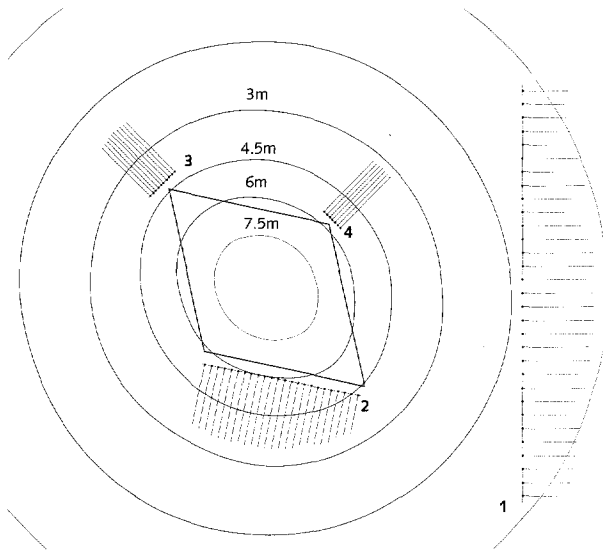
#### *Applicability*

A canal can be used to model a narrow surface water imposing a constant head along its entire length. A canal can also be used to model the strong groundwater flow around weirs in a surface water.

### 5.2.3 The area-sink

At a large distance from an area-sink, the head and flux distribution (line (1) in figure 5.2.8) become similar to those in case of the well. The flux distributions generated by an area-sink across its sides are similar to parabolic distributions (subsection 3.3.7). This is shown in figure 5.2.8, line (2) for a line parallel to and near a side. Across a line near a sharp or an obtuse corner, the flux distribution remains more even (lines (3) and (4) in figure 5.2.8).

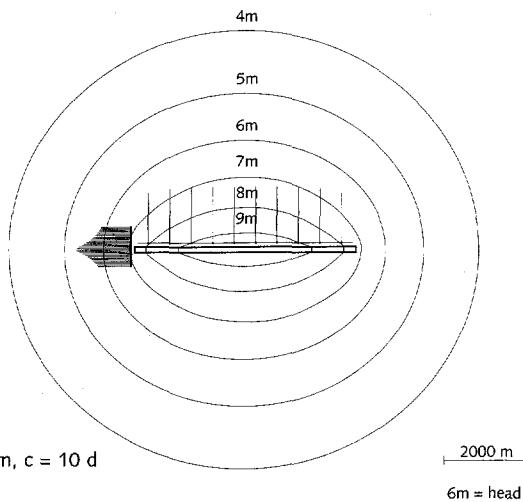
The head and flux distributions near an elongated area-sink (figure 5.2.9) become similar to the distributions near a line-sink.



$kH = 2500 \text{ m}^2/\text{d}$  Parea-sink = 10 m,  $c = 500 \text{ d}$

4000 m  
1 = nr of line  
6m = head

Figure 5.2.8 Flux distribution generated by an area-sink across several lines.



$kH = 2500 \text{ m}^2/\text{d}$   
Parea-sink = 10 m,  $c = 10 \text{ d}$

2000 m  
6m = head

Figure 5.2.9 Flux distribution near an elongated area-sink.

In principle, the expression for the flux across a line in the vicinity of an area-sink can be found in a way similar to that for the expressions (5.7) and (5.8) for the line-sink, so by integration over the surface of the area-sink. Because the integration is not solved yet, this line of investigation is not explored further. It also appears that area-sinks generate rather smooth distributions of the flux across lines in their vicinity except in the case shown in figure 5.2.9. Therefore, the distances between control points or the lengths of line-segments of elements affected by an area-sink can often be taken equal to the length of the closest side(s) of the area-sink.

Because the area-sink consists of four line elements surrounding an area with a constant inflow or outflow (subsection 3.3.7), its shape is only limited by the maximum differences in length of these line elements allowed by the computer accuracy. In practice, these differences are almost never exceeded. So, the shape of area-sinks is almost completely free.

### *Applicability*

The following part of this subsection applies to area-sinks generating a Cauchy boundary condition (3.35) on top of a single aquifer.

In models of large well drained areas such as NAGROM, the entire model domain is covered by area-sinks generating a Cauchy boundary condition (3.35) for the interaction between the surface waters and the groundwater (chapter 6). It appears from the author's experiences, that the size of the area-sinks determines largely the accuracy of the model as well as the needed computation effort. Considering the computation effort needed in the large models mentioned above, an optimum between size of area-sinks and the accuracy is needed. In the following, a relation between the sizes of area-sinks with a Cauchy boundary condition and the model accuracy will be derived.

At the control point of an area-sink (the centre of gravity of the element, subsection 3.3.7), the flux through the element is equal to the difference between the surface water level and the head in the aquifer divided by the value of the hydraulic resistance. Further away from the control point, the head in the aquifer approaches the heads in the neighbourhood of the element and deviates more from the head at the control point. So, the difference between the constant surface water level and the head in the aquifer is not constant over the area-sink. Because the strength is constant over the entire area-sink, the resistance in the element belonging to the computation results can not be constant (equation (3.35)). So, the model accuracy should be considered in terms of the accuracy of the resistance following from the computed results which should be compared with the specified resistance.

Another way of thinking about the accuracy in terms of the Cauchy boundary condition is to state that actually the resistance should be constant (as specified) over the area-sink, and the flux distribution should be adapted to this by using a smaller element. The constant flux generated by such an element can be seen as a first order approximation of the variable flux. Next, the accuracy of a model of a stand-alone area-sink is analyzed. The largest variations in the difference between the surface water level and the groundwater head along flow lines below the area-sink are found along the flow line that crosses the control point. If the variation along this flow line is acceptable, it will be acceptable all over the element. So, the accuracy in terms of the Cauchy boundary condition along that flow line may give a good indication of the accuracy over the entire area-sink. In the following, the distributions of the head and flux

generated by different sizes (in the direction of flow) of the area-sink are compared with the same distributions generated by an exact solution.

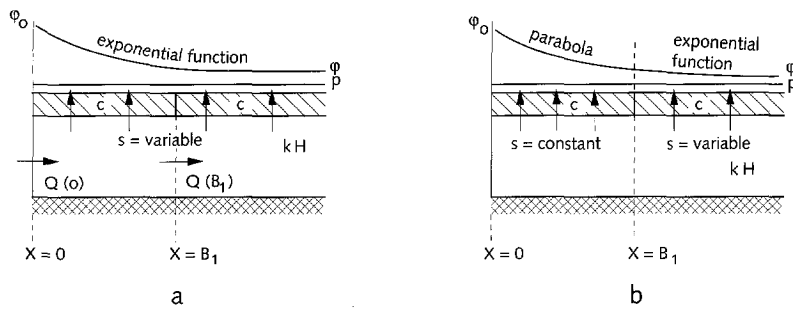


Figure 5.2.10 Cauchy boundary condition on top of an aquifer; (a) with variable flux, (b) with partly ( $0 \leq x < B_1$ ) constant and partly ( $x \geq B_1$ ) variable flux.

In figure 5.2.10-a, a classical case of groundwater flow in a section is presented (Mazure, 1936). This section is assumed to follow the flow line below the control point of the area-sink mentioned above. For the Mazure case, the section is assumed to be straight while the effects of curved flow lines are neglected (semi-two dimensional flow).

At the left boundary ( $x = 0$ ) the head in the aquifer is given. The Cauchy boundary condition on top of the aquifer generates changes in the horizontal and vertical flow and extends to infinity at the right hand side. The flow across the separating layer on top of the aquifer varies over the entire aquifer. The differential equation between  $x = 0$  and  $x = \infty$  is (Verruijt, 1982):

$$\frac{d^2\phi}{dx^2} = \frac{\phi - p}{\lambda^2} \quad (5.9)$$

where

- $p$  = surface water level [L]
- $\phi$  = head in the aquifer [L]
- $\lambda$  = characteristic length =  $\sqrt{(kHc)}$  [L]
- $c$  = hydraulic resistance of the separating layer [T]
- $k$  = hydraulic conductivity of the aquifer [L/T]
- $H$  = thickness of the aquifer [L]

The general solution is expressed by:

$$\phi = p + C_1 \exp(-x / \lambda) + C_2 \exp(x / \lambda) \quad (5.10)$$

where  $C_1$  and  $C_2$  are integration constants [L]. The boundary conditions are described by:

$$\begin{aligned} \phi(x = 0) &= \phi(0) \\ \phi(x = \infty) &= p \end{aligned} \quad (5.11)$$

where  $\varphi(0)$  is the groundwater head specified at  $x = 0$  [L]. These boundary conditions lead to  $C_1 = (\varphi(0) - p)$  and  $C_2 = 0$ , to that the complete solution in the exact case of *figure 5.2.10-a* becomes (Mazure, 1936):

$$\varphi = p + (\varphi(0) - p) \exp(-x / \lambda) \quad x \geq 0 \quad (5.12)$$

In the other case of *figure 5.2.10-b*, an area-sink with constant strength is defined between  $x = 0$  and  $x = B_1$ . The variable flux applies for  $x \geq B_1$ . (In a model, this can be done by taking the elements at the right of the area-sink small enough to satisfy the desired accuracy.) The differential equation between  $x = 0$  and  $x = B_1$  is:

$$\frac{d^2\varphi}{dx^2} = \frac{s}{kH} \quad 0 \leq x \leq B_1 \quad (5.13)$$

where  $s$  is the constant flux through the area-sink [L/T]. Because  $s$  is constant over  $0 \leq x \leq B_1$ , integration over this part leads to:

$$\varphi = sx^2/2kH + C_3x + C_4 \quad 0 \leq x \leq B_1 \quad (5.14)$$

where  $C_3$  and  $C_4$  are integration constants. It is assumed that the general solution for  $x > B_1$  is described by (5.10). At  $x = B_1$  continuity of the flow and the head in the aquifer leads to two conditions and with the conditions (5.11) the four integration constants can be solved.

$$\begin{aligned} C_1 &= -(sB_1/kH + C_3) \lambda \exp(B_1 / \lambda) \\ C_2 &= 0 \\ C_3 &= (p - \varphi(0))/(B_1 + \lambda) - (s/kH)(B_1^2/2 + B_1 \lambda)/(B_1 + \lambda) \\ C_4 &= \varphi(0) \end{aligned} \quad (5.15)$$

*Figure 5.2.11* shows for different values of  $B_1 / \lambda$  and  $0 \leq x \leq B_1$ , the ratio between the heads computed in the exact case of *figure 5.2.10-a* and the heads computed in the case with the area-sink of *figure 5.2.10-b*. For  $B_1 / \lambda \leq 1$ , the ratio is about equal to 1, expressing that the heads ( $0 \leq x \leq B_1$ ) are almost equal in both cases. So, the distribution of the head is sufficiently accurate as long as the width of the area-sink (in the main direction of the groundwater flow) does not exceed the characteristic length. For  $B_1 \geq 3 \lambda$ , the ratio differs considerably from 1, expressing that the case with the area-sink leads to inaccurate heads.

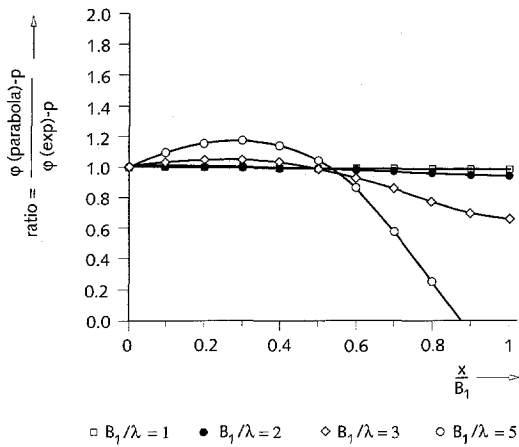


Figure 5.2.11 Ratio between heads at  $x/B_1$  calculated from (5.15) and (5.12) for different values of  $B_1/\lambda$ .

The value of the constant flux between  $x = 0$  and  $x = B_1$  is determined in the middle at  $B_1/2$  in the control point of the area-sink (subsection 3.3.7). The flux of the area-sink is based on the Cauchy boundary condition (3.35), which becomes:

$$s = [\varphi(B_1/2) - p] / c \quad 0 \leq x \leq B_1 \quad (5.16)$$

where  $\varphi(B_1/2)$  is the head [L] in the aquifer at the control point of the area-sink  $x = B_1/2$ .

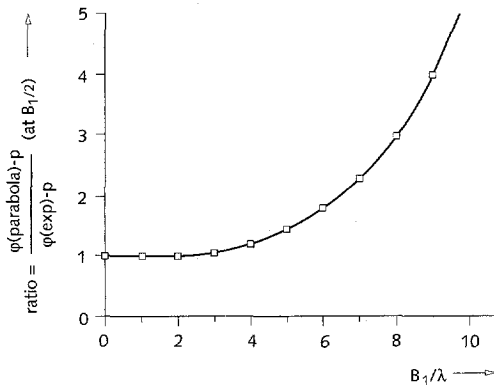


Figure 5.2.12 Ratio between heads at  $B_1/2$  calculated from (5.15) and (5.12) for different values of  $B_1/\lambda$ .

In order to determine the flux of the area-sink, the accuracy of the head  $\varphi(B_1/2)$  at the control point of the area-sink ( $x = B_1/2$ ) is analyzed. In figure 5.2.12, the same ratio of heads as in figure 5.2.11 is presented for different values of  $B_1/\lambda$ , but this time as they occur at  $x = B_1/2$ . The ratio is about 1 for  $B_1/\lambda \leq 3$ , which means that (in this situation) the head in the aquifer at the control point of the area-sink is about exact as long as the width  $B_1$  of the area-sink is smaller than  $3\lambda$ .



Next, the head  $\phi(B_1/2)$  is used to compute the constant flux of the area-sink between  $x = 0$  and  $x = B_1$  similar to in the way it occurs in the AEM. According to the results in figure 5.2.12, this head in the case with the area-sink is about equal to that in the exact case if  $B < 3\lambda$ . Therefore, the solution of the exact case (5.12) can be used to describe  $\phi(B_1/2)$  as long as  $B < 3\lambda$ . Then, the total flux through the area-sink (per unit width perpendicular to the section)  $S(0, B_1)$  between  $x = 0$  and  $x = B_1$  becomes:

$$S(0, B_1) = B_1 s = B_1 (\phi(0) - p) \exp(-B_1/2\lambda) / c \quad B < 3\lambda \quad (5.17)$$

This total flux through the area-sink is compared with the total flux  $S(0, B_1)$  through the separating layer between  $x = 0$  and  $x = B_1$  in the exact case (figure 5.2.10-a). The latter total flux is found by calculating the difference between the inflow in the aquifer at  $x = 0$  and the outflow at  $x = B_1$ . Darcy's law (3.2) in combination with (5.10) and (5.12) leads to :

$$Q(0) - Q(B_1) = kH(\phi(0) - p)[1 - \exp(-B_1/\lambda)]/\lambda \quad (5.18)$$

where:

- $Q(0)$  = total flux at  $x = 0$  per unit width perpendicular to the section [L<sup>2</sup>/T]
- $Q(B_1)$  = total flux at  $x = B_1$  per unit width perpendicular to the section [L<sup>2</sup>/T]

The relative difference  $E$  between the fluxes is defined by:

$$E = (Q(0) - Q(B_1) - S(0, B_1)) / (Q(0) - Q(B_1)) \quad (5.19)$$

Combination of (5.17), (5.18) and (5.19) leads to:

$$E = 1 - B_1/2\lambda / \sinh(B_1/2\lambda) \quad (5.20)$$

In table 5.1, the values of  $E$  are given for several values of  $B_1/2\lambda$  (with  $B_1 < 3\lambda$ ). From the values in this table it is concluded that, when  $B_1$  is about  $\lambda$  the error in the total flux through the area-sink is 4%, which is generally acceptable in models.

Table 5.1. Relative error  $E$  in terms of the flux.

$B_1/2\lambda$	.1	.5	1.	1.5
$\sinh(B_1/2\lambda)$	.1002	.521	1.17	2.13
$E$	.002	.04	.145	.296

The above analysis can be generalized to a rule for the maximum size of area-sinks in the main direction of flow. For the accuracy in the total flux through the area-sink (table 5.1) as well as in the head distribution in the aquifer below the entire area-sink (figure 5.2.11), the maximum size should be about  $\lambda$ . So, the length of any area-sink in the direction of flow should be about equal to  $\lambda$  in order to derive a commonly accepted

accuracy. This rule will be applied in subsections 5.3.4 and 5.4.1. Olsthoorn and Moorman (1991) derived the same rule from several test computations with a model of area-sinks.

#### 5.2.4 The inhomogeneity

The behaviour and the effects of an inhomogeneity are analyzed in both a uniform and an axial-symmetric flow field. In both cases, it will be shown that the behaviour of the inhomogeneity in a model depends on whether the transmissivity inside the element is higher or lower than outside the element.

##### *The inhomogeneity in a uniform flow field*

The effect on the flow of an inhomogeneity with a relatively low transmissivity is fundamentally different from that of an inhomogeneity with a relatively high transmissivity. To illustrate this, the following expression of Strack and Haitjema (1981) for the ratio between the flux inside and outside a cylindrical inhomogeneity in a uniform flow field (figure 5.2.13) is used:

$$Q_{x,in}/Q_{x,out} = 2k_{inh}/(k + k_{inh}) \quad (5.21)$$

where:

- $k_{inh}$  = hydraulic conductivity inside the inhomogeneity [L/T]
- $k$  = hydraulic conductivity outside the inhomogeneity [L/T]
- $Q_{x,in}$  = flux component in x-direction per unit width (in y-direction) inside the inhomogeneity [L<sup>2</sup>/T]
- $Q_{x,out}$  = flux component in x-direction per unit width (in y-direction) outside the inhomogeneity [L<sup>2</sup>/T]

This expression shows that if  $k_{inh} \gg k$  the flux inside  $Q_{x,in}$  approaches the limit of  $2Q_{x,out}$ . So, the effect of an increase of the hydraulic conductivity on the flow is limited. This means that the jump to be generated by the different line-segments of the inhomogeneity is limited. Once, the distribution of the segments has been determined accurately for a jump in the transmissivity, it is very likely that the same distribution will do also if that jump is increased.

If  $k_{inh} \ll k$  the flux inside  $Q_{x,in}$  approaches the limit of 0. In any situation, a decrease of the transmissivity inside the inhomogeneity causes further decrease of the flow across the line-segments. This means that the jump to be generated by the line-segments of the inhomogeneity is not limited. Therefore, any decrease of transmissivity may cause a need to adapt the distribution of the line-segments.

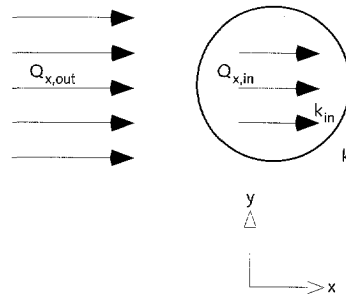


Figure 5.2.13 Definition scheme for a cylindrical inhomogeneity in a uniform flow field.

#### Applicability

The effect of an inhomogeneity in a uniform flow field has already been presented in *figure 3.3.14*. In that figure, the effect is shown of a domain in which the transmissivity is higher than in the rest of the aquifer. The boundary of that inhomogeneity consists of numerous line-segments, so that the jump in the transmissivity is modeled almost perfectly. However in a common situation, as few line-segments as possible are used in a model. This implies that the distribution of line-segments should be adapted to the distribution of the flux through the boundary of the inhomogeneity.

In *figure 5.2.14*, two cases of a square inhomogeneity in uniform flow are presented in which the transmissivity is low compared to the transmissivity of the aquifer. In the situation of *figure 5.2.14-a*, only one line-segment is used per side. In the corners, peaks in the flow occur, which can not be accounted for by the segments of this figure. These peaks should be modeled using short line-segments as shown in *figure 5.2.14-b*.

The line-segments (with a parabolic strength distribution, subsection 3.3.6) in normal direction to the uniform flow (segments 1) can easily account for the flow crossing these segments. Across the sides in the direction of the uniform flow, inflow as well as outflow occurs. The single line-segments of *figure 5.2.14-a* can not properly account for the distribution of the flux across the segment, which is shown by the distributions of the head. In such a case, at least two segments should be used (*figure 5.2.14-b*): one generating the distribution of the outflow (segments 2) and one generating the distribution of the inflow (segments 3).

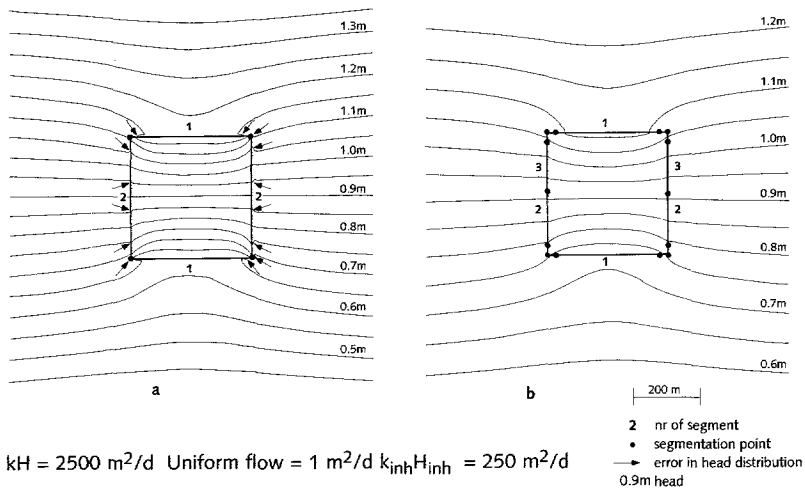


Figure 5.2.14 Square inhomogeneity in uniform flow with (a) one line-segment per side and (b) line-segments adapted to the flow across the boundary.

### The inhomogeneity in an axial-symmetric flow field

In the situation of an inhomogeneity in an axial-symmetric flow field, an approximately circular inhomogeneity around a well is used (figure 5.2.15). In this case, the analytic solution for the abstraction rate of a head-specified well is found using the fact that the total difference in head between the well and the reference point equals the sum of all differences in head in the intermediate stretches:

$$Q_{w,inh} = 2 \pi (\varphi_{ref} - \varphi_w) / \left[ \frac{1}{k_{inh}H_{inh}} \ln \frac{r_{inh}}{r_w} + \frac{1}{kH} \ln \frac{r_{ref}}{r_{inh}} \right] \quad (5.22)$$

where

- $\varphi_{ref}$  = head at the reference point [L]
- $\varphi_w$  = head at the well radius [L]
- $k_{inh}H_{inh}$  = transmissivity within the inhomogeneity [ $L^2/T$ ]
- $r_w$  = well radius [L]
- $r_{ref}$  = distance from the well to the reference point [L]
- $r_{inh}$  = radius of the inhomogeneity [L]
- $Q_{w,inh}$  = abstraction rate of a well inside a circular inhomogeneity [ $L^3/T$ ]

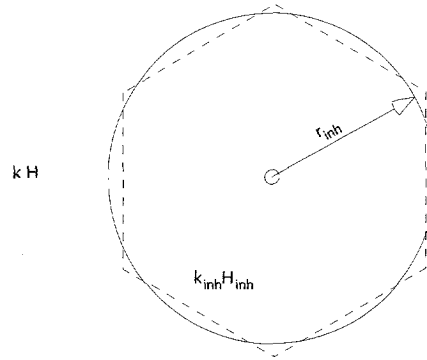


Figure 5.2.15 Scheme for a circular inhomogeneity approximated by a hexagon of line-segments with a well in the centre.

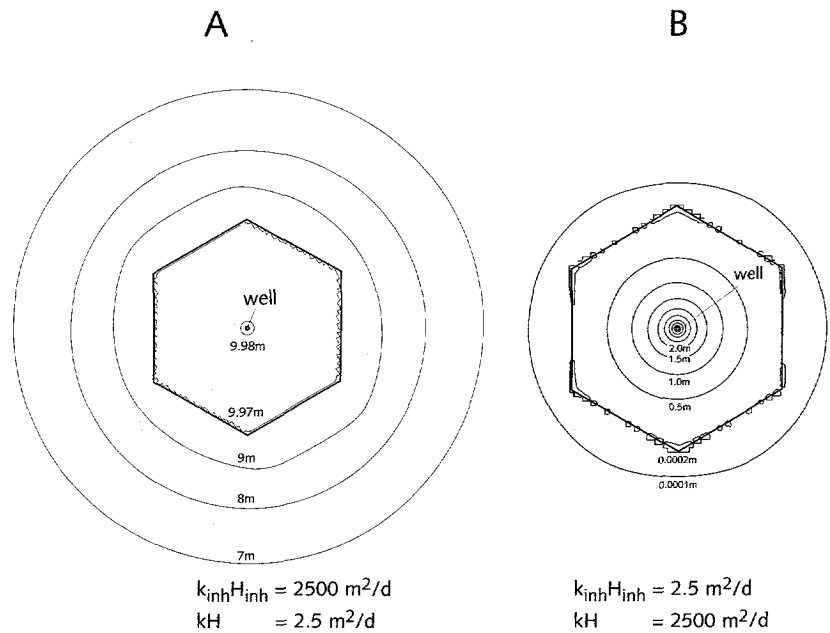


Figure 5.2.16 Inhomogeneity as defined in figure 5.2.14 with very high (a) and very low transmissivity, relative to the outside transmissivity.

The basic expression for the abstraction rate of a well  $Q_w$  in a confined aquifer can be found by taking  $k_{inh}H_{inh} = kH$  in expression (5.22), which complies with expression (3.19). The ratio between  $Q_w$  and  $Q_{w,inh}$  then becomes:

$$\frac{Q_w}{Q_{w,inh}} = \frac{kH}{k_{inh}H_{inh}} \frac{\ln(r_{inh}/r_w)}{\ln(r_w/r_{ref})} + \frac{\ln(r_{ref}/r_{inh})}{\ln(r_{ref}/r_w)} \quad (5.23)$$

So, when  $k_{inh}H_{inh}$  becomes large (figure 5.2.16-a), the ratio between  $Q_w$  and  $Q_{w,inh}$  approaches the value of the second term of the right hand side of this expression, which is independent of  $k_{inh}H_{inh}$ . On the other hand, when  $k_{inh}H_{inh}$  becomes small (figure 5.2.16-b), the ratio between

$Q_w$  and  $Q_{w,inh}$  becomes large, so the flux into the inhomogeneity is strongly obstructed from the boundary. To the inside this obstruction can only be generated by many line-segments. This means that the approach for the adaption of segments to the flow across the boundary of the inhomogeneity described above for the case of uniform flow also holds in the case of axial-symmetric flow and most likely will be valid in any flow situation.

At this point, it is interesting to see what the equivalent transmissivity  $T_{eq}$  [ $L^2/T$ ] will be that is defined as the transmissivity between the well and the reference point which gives the same difference in the heads at the well radius and at the reference point with the abstraction rate of the well  $Q_{w,inh}$ :

$$T_{eq} = \{Q_{w,inh} \ln(r_{ref}/r_w)\} / \{2\pi(\varphi_{ref} - \varphi_w)\} \quad (5.24)$$

By combination of (5.22) and (5.24),  $1/T_{eq}$  becomes:

$$\frac{1}{T_{eq}} = \frac{\ln[r_{inh}/r_w]}{k_{inh}H_{inh} \ln[r_{ref}/r_w]} + \frac{\ln[r_{ref}/r_{inh}]}{kH \ln[r_{ref}/r_w]} \quad (5.25)$$

From (5.25), it follows that the equivalent transmissivity equals the length-(along the radius to the reference point)-weighted harmonic mean of the transmissivities inside and outside the inhomogeneity. In general,  $r_w$  is small and  $r_{ref}$  is large compared to  $r_{inh}$ . If  $\ln(r_{inh}/r_w)$  is in the same order of magnitude as  $\ln(r_{ref}/r_{inh})$ , a relatively low transmissivity inside or outside the inhomogeneity makes the relatively high transmissivity of minor importance for the equivalent transmissivity. So, in a given situation, the groundwater flow is mainly sensitive for variations in the lowest transmissivity, which can occur inside as well outside the inhomogeneity.

As said before, groundwater flow is more affected by changes in relatively high resistances in the aquifer (the low transmissivities) than by changes in relatively low resistances in the aquifer (the high transmissivities). This rule is opposite to the rule for the combined effect on the groundwater flow of different resistances in a separating layer. The average resistance of a separating layer over a certain area is determined by the area-weighted harmonic mean of the resistances. According to this, the groundwater flow is most affected by changes in the lowest resistance of a separating layer.

As a consequence of the rule for modeling derived above, an inhomogeneity with relatively high transmissivity is easier to be modeled than an inhomogeneity with a low transmissivity. This agrees with the modeling experiences of the author and has become an important rule in modeling with inhomogeneities.

## Applicability

In *figure 5.2.16-a*, an inhomogeneity with an very high transmissivity (1000 times higher than the aquifer transmissivity) is presented. The inhomogeneity can easily account for this difference in transmissivity. In *figure 5.2.16-b*, an inhomogeneity with an very low transmissivity (1000 times lower than the aquifer transmissivity) is presented.

Taking into account the large change in the gradient of the head, *figure 5.2.16* shows small distortions in the distribution of the head near the boundary. The small distortions point out that the jump in transmissivity is about the maximum that can be generated by the segments. Computations with smaller jumps did not give these distortions and larger jumps cause larger distortions. From the authors modeling experience it is concluded that in a general model an inhomogeneity can generate a lower transmissivity of a factor up to 100, if the distribution of the line-segments is adapted carefully for the flow distribution across the boundary of the inhomogeneity.

### 5.2.5 The leaky wall and the impermeable wall

The leaky wall affects only the flow component in normal direction to the element. The properties and the behaviour of the impermeable wall can be deduced from the analysis, in this subsection, of a leaky wall of which the hydraulic resistance is taken infinite. This subsection deals with the behaviour of a leaky wall in a uniform and in an axial-symmetric flow field.

#### *The leaky wall in a uniform flow field*

The effect of a leaky wall is directly related to the ratio of the resistance of the element  $c_{lkw}$  and the resistance along a flow path around the element starting at one side in the middle of the element and ending at the other side in the middle of the element ( $L_{lkw}/k$ ), because this ratio describes which part of the flow will cross the element or will flow around it. The ratio is expressed by the coefficient  $v$  (valuator):

$$v = c_{lkw} k / L_{lkw} \quad (5.26)$$

in which:

$c_{lkw}$  = hydraulic resistance of the leaky wall against horizontal flow [T]

$k$  = horizontal hydraulic conductivity of the aquifer [L/T]

$L_{lkw}$  = length of the leaky wall [L]

If  $v < 1$ , most of the groundwater will flow across the element (*figure 5.2.17-a*) and the element actually has virtually no effect on the groundwater flow.

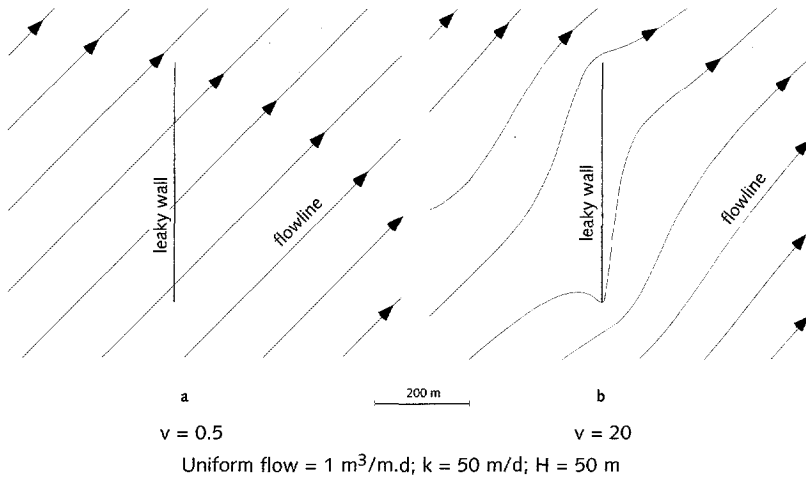


Figure 5.2.17 A leaky wall in uniform flow; in case (a)  $v = .5$  and in case (b)  $v = 20$ .

If  $v > 10$ , the leaky wall behaves almost like an impermeable wall; almost all the groundwater flows around the element since the resistance along that path is much lower than along the path across the element (figure 5.2.17-b). In case  $1 < v < 10$  the groundwater flow is affected by the element but still a relevant part may flow across it.

It follows from expression (5.26), that the effect of the leaky wall is not related to the transmissivity of the aquifer but to its hydraulic conductivity  $k$  only. This is important to consider in the cases where equation (3.32) is applied to avoid iteration.

#### The leaky wall in an axial-symmetric flow field

The situation of a leaky wall in axial-symmetric flow can only be observed clearly using a circular element (figure 5.2.18), because the element acts only in the direction normal to the flow. Therefore, as an exception, in the next part of this subsection use is made of the curvilinear element (subsection 4.2.1) to illustrate the analysis.

The expression for the flux  $Q_w$  of a head specified well in the centre of the circular leaky wall is derived in a similar way as in the case of expression (5.22).

$$Q_w = 2\pi kH (\phi_{ref} - \phi_w) / [ \ln(r_{ref}/r_w) + c_{lkw}k/r_{lkw} ] \quad (5.27)$$

where:

$r_{lkw}$  = distance from the well to the concentric circular leaky wall [L].

Equation (5.27) reduces to the common well formula (cf. (3.19) with (3.6)), if  $r_{lkw}$  approaches to infinity or  $c_{lkw}$  approaches to zero. The term  $c_{lkw}k/r_{lkw}$  is similar to the right hand side of expression (5.26), but here the distance between the well and the leaky wall appears. The larger this



distance, the more the abstraction rate of the well approaches the abstraction rate of a well in the case without the leaky wall.

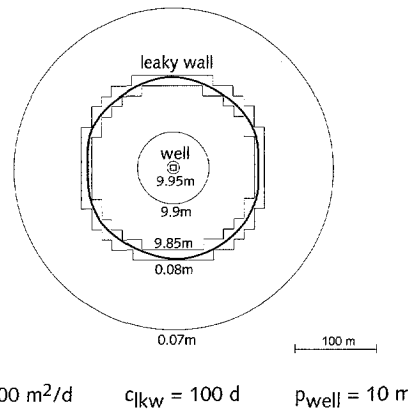


Figure 5.2.18 A well in the centre of a circular leaky wall.

This analysis can be used in cases where the leaky wall is used to isolate (a part of) a model. When looking at a model of analytic elements from a relatively very large distance, the model reduces to a point and the flow pattern generally looks similar to that in the case of a single well. So, the well may be seen as a representation of a model when looking at a large distance. Then, the behaviour of the leaky wall surrounding the model area (like the well in figure 5.2.18) can be estimated by using expression (5.27).

#### Applicability 1

In NAGROM, leaky walls (straight droot and curvilinear elements) have been used to model elongated deep troughs filled with boulder clay, which partly cut off the aquifer (De Lange and Van der Meij, 1994). The resistance of the element expresses the effect of the reduced transmissivity below the trough. The relation between the resistance of the leaky wall  $c|_{kw}$  and the properties of the trough in the aquifer is derived as follows.

As presented in figure 5.2.19, the trough is assumed to have a triangular shape. Right of the lowest point of the triangular trough, the thickness  $H(x)$  of the aquifer can be expressed by:

$$H(x) = (2H_{tr}/B_{tr}) x + H - H_{tr} \quad 0 \leq x \leq B_{tr}/2 \quad (5.28)$$

where

$H_{tr}$  = maximum thickness of the trough [L]

$B_{tr}$  = width of the trough at the top of the aquifer [L]

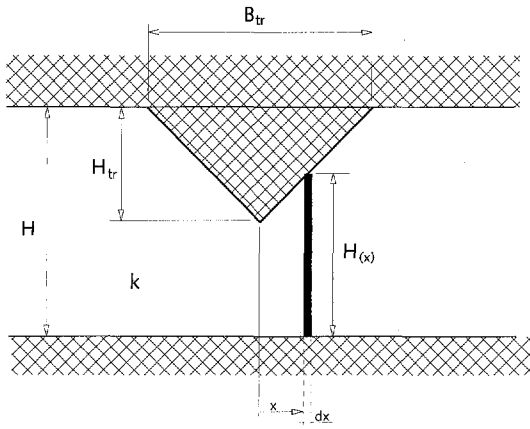


Figure 5.2.19 Scheme for the determination of the resistance of a leaky wall simulating a deep impermeable trough.

The transmissivity  $T''$  at  $x$  inside the strip  $dx$  under the trough is

$$T'' = k H(x) = k'' H \quad (5.29)$$

The specific resistance to groundwater flow  $c''$  [T] inside this strip of width  $dx$  at place  $x$  is determined using  $H$  as the thickness, because the leaky wall element acts over the entire thickness  $H$ .

$$dc'' = H/T'' dx \quad (5.30)$$

The specific resistance to groundwater flow  $c'$  [T] inside strip  $dx$  in the case without the trough is:

$$dc' = H/T dx \quad (5.31)$$

where  $T (= kH)$  is the transmissivity of the aquifer [ $L^2/T$ ]. The difference between the specific resistance with and without the trough inside the strip  $dc$  becomes:

$$dc = dc'' - dc' = (1/k'' - 1/k) dx \quad (5.32)$$

Assuming a symmetric shape of the trough, the difference in the resistance over the entire trough  $C_{tr}$  becomes:

$$C_{tr} = 2 \int_0^{B_{tr}/2} dc \quad (5.33)$$

Using  $k'' = kH(x)/H$  (from expression (5.29)) and expressions (5.28) and (5.32), integration leads to the following expression:

$$C_{tr} = B_{tr}/k \{ (H/H_{tr}) \ln |H/(H-H_{tr})| - 1 \} \quad (5.34)$$

in which  $C_{tr}$  becomes 0 for  $H_{tr} = 0$  and  $C_{tr}$  becomes  $\infty$  for  $H_{tr} = H$ . The total difference in the resistance is to be generated by the leaky wall, so  $C_{lkw} = C_{tr}$ .

### *Applicability 2*

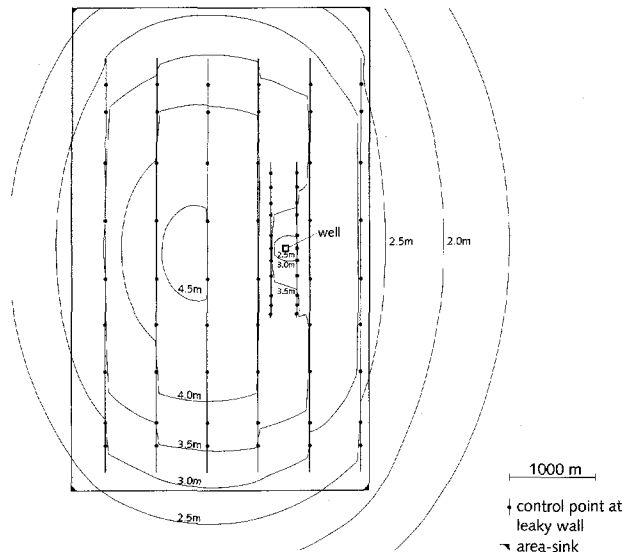
Curvilinear leaky walls have been used in NAGROM to model anisotropic behaviour in the horizontal plane in a certain domain (De Lange and Van der Meij, 1994). The anisotropic behaviour is generated by the leaky walls because the flow across the elements is affected and the flow along the element is not. In this way, the resistance to horizontal flow in the model is different in both directions and, therefore, the effective hydraulic conductivity is different.

The leaky wall accounts for the difference between the high and the low hydraulic conductivity by generating resistance to the flow in the direction of the lowest hydraulic conductivity. Again, the value of the resistance of the leaky wall is determined by the difference of two resistances. The resistance of the leaky wall is determined for the length  $L_{k_{low}}$  [L] (index indicates  $k_{low}$ ) in the direction of the lowest hydraulic conductivity  $k_{low}$  [L/T] over which the element is assumed to act (*figure 5.2.20*). The desired resistance in the direction of the lowest hydraulic conductivity is  $L_{k_{low}}/k_{low}$ . The actual resistance in the model is caused by the high hydraulic conductivity  $k_{high}$  [L/T] and is  $L_{k_{low}}/k_{high}$ .

The difference between these resistances should be generated by the leaky wall, which results in:

$$C_{lkw} = L_{k_{low}}/k_{low} - L_{k_{low}}/k_{high} \quad (5.35)$$

A change in the distance  $L_{k_{low}}$ , e.g. because of refinement of the model, causes a change in the hydraulic resistance of the leaky wall. It is concluded that anisotropic behaviour can easily be simulated by parallel leaky walls because the parameters of each leaky wall can be specified quite easily using expression (5.35).



$H = 50 \text{ m}$                        $k = 50 \text{ m/d}$   
 $Q_{\text{well}} = 5000 \text{ m}^3/\text{d}$               area-sink:  $\gamma = -.0006 \text{ m/d}$   
 $k_{\text{low}} = 12.5 \text{ m/d}$ , generated by  $c_{lkw} = 30 \text{ d}$ , except for the short leaky walls close to well  
 where  $c_{lkw} = 10 \text{ d}$

Figure 5.2.20 Curvilinear leaky walls used to model anisotropy

### 5.2.6 The crack and the drain

A crack (figure 5.2.21) or a drain (figures 3.3.7 and 3.3.8) causes a change in the transmissivity in its own direction only. The transmissivity in normal direction to the crack or drain is not changed. Only the flow component in the direction of the crack or drain is affected, because the crack is a jump in the stream function (Strack, 1989). At both tips a concentration of flow is generated (figure 5.2.21, line (1)). The inflow into the upstream part of the element is equal to the outflow from the downstream part (figure 5.2.21, line (2)).

The forthcoming analysis of the properties and the behaviour of the crack (which includes the drain by taking an infinitely large transmissivity) is based on numerous numerical experiments, some assumptions that are more or less physically based and the basics of groundwater hydrology. The behaviour of the crack is analyzed step by step in both uniform and axial-symmetric flow.

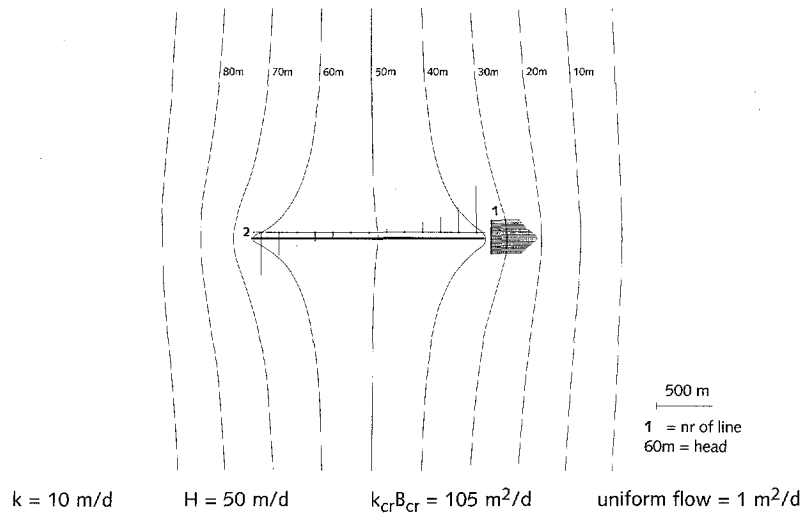


Figure 5.2.21 Flux distribution across lines near a crack in a uniform flow field.

#### The crack in a uniform flow field

The effects on the groundwater flow generated by a crack in uniform flow (figure 5.2.21) can not be directly characterized by the hydraulic conductivity of the crack because of the following. Parallel to in the case of an inhomogeneity with a relatively high hydraulic conductivity, a high hydraulic conductivity of a crack has a limited effect on the groundwater flow because the maximum flux to the element is limited. Considering a certain gradient in the head in the direction of the crack, the flux through a strip including that crack is not straight forwardly related with the sum of the hydraulic conductivities of both the aquifer and the crack in that strip. As will be shown in the next analysis, the flux through the strip will generally be smaller than following from the gradient in the head and the sum of the transmissivities. The total hydraulic conductivity in that strip, including the hydraulic conductivity of the crack, is not really effective on the groundwater flow but only by a (not a priori known) part of it. Therefore, the hydraulic conductivity of a crack can hardly be used to determine its effect on the groundwater flow. The effect of the crack can be characterized well by the maximum flux inside the element, which occurs in the middle of the element in the case of a crack in uniform flow.

Numerous test computations showed, that the maximum flux in a crack in uniform flow largely depends on its transmissivity  $k_{cr} B_{cr}$  compared to its length  $L_{cr}$  multiplied by the hydraulic conductivity of the aquifer  $k$ . The effect of a crack can be neglected, if  $k_{cr} B_{cr}$  is much smaller than  $k L_{cr}$  (e.g.  $0.1 k L_{cr}$ ). Then, the crack does not change the distributions of the head and flux significantly. The test computations have led to the following relations:

- 1 - In a crack with relatively high transmissivity  $k_{cr}B_{cr}$  compared to  $kL_{cr}$ , the flux in the middle of the crack is equal to the length of the crack multiplied by the component of the uniform flow in the direction of the crack, or:

$$Q_{cr,m} = L_{cr} U_s, \text{ if } (k_{cr}B_{cr} / kL_{cr}) \gg 1 \quad (5.36)$$

where:

- $k$  = horizontal hydraulic conductivity of the aquifer [L/T]
- $k_{cr}B_{cr}$  = transmissivity of the crack [ $L^2/T$ ]
- $L_{cr}$  = length of the crack [L]
- $Q_{cr,m}$  = flux in the middle of the crack [ $L^3/T$ ]
- $U_s$  = flux component (per unit width) of the undisturbed uniform flow in the direction of the crack [ $L^2/T$ ]

- 2 - In a crack with a relatively low  $k_{cr}B_{cr}$  compared to  $kL_{cr}$ , the flux in the middle of the crack is equal to the component of the uniform flow in the direction of the crack multiplied by the transmissivity of the crack and divided by the hydraulic conductivity of the aquifer, or:

$$Q_{cr,m} = U_s k_{cr}B_{cr} / k, \text{ if } (k_{cr}B_{cr} / kL_{cr}) \ll 1 \quad (5.37)$$

- 3 - The flux in the middle of the crack is not influenced by the thickness of the aquifer nor by the flux in normal direction to the crack.

In figure 5.2.22, the relation resulting from the test computations is presented. X and Y are the dimensionless parameters on the x-axis and y-axis respectively and are defined as:

$$X = k_{cr}B_{cr} / kL_{cr} \quad (5.38a)$$

$$Y = Q_{cr,m} / U_s L_{cr} \quad (5.38b)$$

Because of the relative simplicity of the curve in figure 5.2.22, it was found that the curve can be described by:

$$Y = X / (1 + X) \quad (5.39)$$

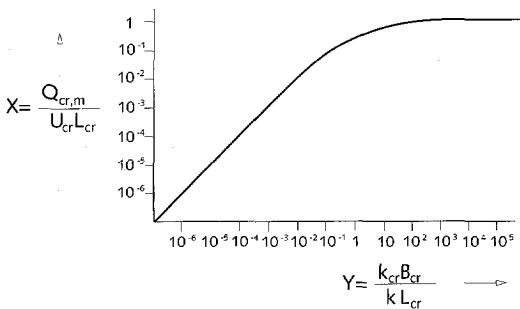


Figure 5.2.22 Relation between parameters influencing the flux in the middle of a crack in uniform flow.

Combination of (5.38) and (5.39) leads to:

$$Q_{cr,m} = \alpha_c L_{cr} U_s \quad (5.40a)$$

where:

$$\alpha_c = k_{cr} B_{cr} / (k_{cr} B_{cr} + k L_{cr}) \quad (5.40b)$$

This formula agrees with all the conclusions drawn from the test computations mentioned above and is illustrated in tables 5.2.a - 5.2.d. Strack (1981, p12) derived an exact solution for the flux distribution through the entire crack, while the width of the crack varied according to an analytic function. In the middle of a crack with constant width his expression becomes equal to (5.40).

Table 5.2 Comparison of fluxes computed by the AEM and by formula (5.40) with variation in (a)  $L_{cr}$ , (b)  $k_{cr} B_{cr}$ , (c)  $k$ , and (d)  $U_s$ . The standard values are  $L_{cr} = 200$  m,  $k_{cr} B_{cr} = 1000$  m<sup>2</sup>/d,  $k = 10$  m/d,  $U_s = 1$  m/d.

(a)						
$L_{cr}$	1	10	100	200	1000	10000
$Q_{cr,m}$ AEM	0.999	9.9	92.2	171	541	1030
$Q_{cr,m}$ (5.40)	0.999	9.9	90.9	167	500	909

(b)									
$k_{cr} B_{cr}$	.001	.01	.1	1.0	10	100	1000	10000	100000
$Q_{cr,m}$ AEM	.001	.01	.1	1.0	10.5	74	171	197	200
$Q_{cr,m}$ (5.40)	.001	.01	.1	.99	9.5	67	167	196	200

(c)									
$k$	.001	.01	.1	1	10	100	1000	10000	100000
$Q_{cr,m}$ AEM	200.	200	197	171	74	10.6	1.02	.1	.01
$Q_{cr,m}$ (5.40)	200	200	196	167	67	9.5	.99	.1	.01

(d)				
$U_s$	.1	1	10	100
$Q_{cr,m}$ AEM	17.1	171	1711	17112
$Q_{cr,m}$ (5.40)	16.7	167	1667	16667

It follows from (5.40) that the flux in the crack is limited when its length becomes large (actually, when  $k L_{cr}$  becomes much larger than  $k_{cr} B_{cr}$ ). Then (5.40) turns into (5.37), which can be written as:

$$Q_{cr,m} = U_s k_{cr} B_{cr} / k \quad (5.41)$$

It follows from expression (5.41) that, in case of the increase of the length of a long crack, the transmissivity of the crack limits the inflow, outflow and through flow, which also become independent of the length. It follows from expression (5.36) that in the case of the increase of a high transmissivity of a crack, the length of the crack and the strength of the flow component in the direction of the crack limit the inflow, outflow and

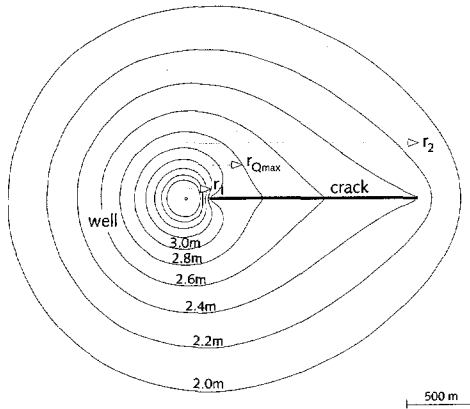
through flow, which become independent of the hydraulic conductivity. This illustrates that the effect of a crack on the groundwater flow can not simply be determined from its transmissivity only.

*The crack in an axial-symmetric flow field*

Next, a crack in axial-symmetric flow towards a well (figure 5.2.23) is analyzed. Again, numerous test computations have been carried out to derive a relation between the parameters and the behaviour of the crack. In this, expressions for the maximum flux through the crack are derived, starting with the expression for the crack in uniform flow. The results of the derived expressions are verified with the results of computations.

The shape of the crack is a line so it has a length but no width. The width remains undefined in the axial-symmetric case. Therefore, the element can be used in the axial-symmetric analysis without adaption of its shape while the hydraulic conductivity  $k_{cr}B_{cr}$  remains constant over the element.

Next, the place of the maximum flux through a crack in axial-symmetric flow is determined and after that an expression for that maximum flux. From an analysis of the derivation of the expression (5.40), it was expected that the maximum flux in a crack in axial-symmetric flow might have a relation with the undisturbed flow in the direction of the element similar to what occurs in the case of a crack in uniform flow.



$k = 10 \text{ m/d}$        $H = 50 \text{ m}$   
 $k_{cr}B_{cr} = 105 \text{ m}^2/\text{d}$        $p_{well} = 10 \text{ m}$

*Figure 5.2.23 Crack in the originally axial-symmetric flow field generated by a well.*

In the case of a crack in uniform flow, the total inflow over one half of the length of the crack equals the total outflow over the other half. In other words, the integral of all inflow over the distance between one tip and the point of maximum flux inside the crack equals the integral of all outflow over the distance between the other tip and that point. The maximum flux inside the crack in uniform flow occurs in the middle of the element and



expression (5.40) shows that the maximum flux is directly (linearly) related to the undisturbed flow in the direction of the crack.

The undisturbed flow occurs along the crack only if its effects on the flow are absent, so in the imaginary situation that the crack is replaced by just a line. The integral of that undisturbed flow over the distance between one tip and the middle point of that line equals the integral of that undisturbed flow over the distance between the other tip and the middle point. So, by stating that both integrals in the last sentence are equal, the point of maximum flux of the crack can be found.

This relation is used to determine the place of the maximum flux of a crack in axial-symmetric flow. The comparison between the computed results and the results of the derived expression for the maximum flux in the crack (table 5.3) will show that the derived expression is acceptable.

The undisturbed flux  $U_s(r)$  [ $L^2/T$ ] in the imaginary case of a not-effective crack (just a line) in an axial-symmetric flow field is dependent on the distance  $r$  to the well expressed by:

$$U_s(r) = Q_w / 2\pi r \quad (5.42)$$

Consider the line (representing the not-effective crack) situated along a radius between the distances  $r_1$  and  $r_2$  from the well. Next, the point  $r_p$  can be determined at which the integral of  $U_s(r)$  over the distance between one end of the crack and that point equals the integral over the distance between the other end and that point. Integration of the flux over  $r_2 - r_p$  leads to:

$$Q_{2-m} = \int_{r_p}^{r_2} Q_w / 2\pi r \, dr \quad (5.43)$$

with the solution:

$$Q_{2-m} = Q_w / 2\pi \ln (r_2 / r_p) \quad (5.44)$$

where:

- $r_p$  = distance from the well to point P [L]
- $r_1$  = distance from the well to the closest tip of the line [L]
- $r_2$  = distance from the well to the farthest tip of the line [L]
- $Q_w$  = abstraction rate of the well [ $L^3/T$ ]

Similarly, the integration over part  $r_p - r_1$  gives:

$$Q_{m-1} = Q_w / 2\pi \ln (r_p / r_1) \quad (5.45)$$

where  $r_1$  is distance from the well to the closest tip of the crack [L]. At  $r_p$  the equation  $Q_{2-m} = Q_{m-1}$  is used, leading to:

$$r_p = \sqrt{(r_1 r_2)} \tag{5.46}$$

So, at  $r = r_p$  the flux  $U_s(r)$  along one part of the line equals the flux along the other part of the line. Based on the analysis described above, it is assumed that the maximum flux in a crack at the place of the line between  $r_1$  and  $r_2$  (figure 5.2.23) occurs at  $r_{Q_{mx}} = r_p$ . Combination of (5.46) with (5.42) gives:

$$U_s(r_{Q_{mx}}) = Q_w / 2\pi\sqrt{(r_1 r_2)} \tag{5.47}$$

Table 5.3 Comparison of the maximum flux in a crack computed by the AEM and by expression (5.48) with variation in (a)  $L_{cr}$ , (b)  $k_{cr}B_{cr}$ , (c)  $k$ , and (d)  $r_1$ , with  $L_{cr} = 200$  m,  $k_{cr}B_{cr} = 1000$  m<sup>2</sup>/d,  $k = 1$  m/d,  $r_1 = 100$  m.

(a)\*1

$L_{cr}$	1	10	100	1000
$Q_{cr,m}$ AEM	.07	.68	4.56	9.36
$Q_{cr}(r_{Q_{mx}})$ (5.48)	.07	.68	4.58	8.97

(b)

$k_{cr}B_{cr}$	.001	.01	.1	1	10	100	1000	10 <sup>4</sup>	10 <sup>5</sup>
$Q_{cr,m}$ AEM	.00004	.0004	.004	.04	4	.28	6.6	7.6	7.7
$Q_{cr}(r_{Q_{mx}})$ (5.48)	.00004	.0004	.004	.04	4	.26	6.7	7.9	8.0

(c)

$k$	.001	.01	.1	1	10	100	1000	10 <sup>4</sup>	10 <sup>5</sup>
$Q_{cr,m}$ AEM	.008	.08	.76	6.6	28.4	37.5	37.5	37.5	37.5
$Q_{cr}(r_{Q_{mx}})$ (5.48)	.008	.08	.79	6.7	26.6	37.9	39.6	39.7	39.7

(d)\*2

$r_1$	5*3	10	20	50	100	500	1000
$Q_{cr,m}$ AEM	40.9	22.8	15.1	9.55	6.6	2.07	1.1
$Q_{cr}(r_{Q_{mx}})$ (5.48)	25.8	20.2	15.3	9.95	6.7	2.0	1.1

\*1 If  $L_{cr} > 1000$  m the crack is too close to the reference point due to its length  
 \*2 If  $r_1 > 1000$  m, the crack is too close to the reference point due to the distance to the well  
 \*3 Crack very close to the well.

Test computations (table 5.3) showed, that the maximum flux in the crack can be described by using expression (5.40), in which  $U_s$  is replaced by  $U_s(r_{Qmx})$  derived in expression (5.47).

$$Q_{cr}(r_{Qmx}) = \alpha_c Q_w L_{cr} / 2\pi\sqrt{(r_1 r_2)} \quad (5.48)$$

where:

$Q_{cr}(r_{Qmx})$  = maximum flux through the crack [ $L^3/T$ ]

Expression (5.48) can be rewritten into:

$$Q_{cr}(r_{Qmx}) = \beta_c Q_w \quad (5.49a)$$

with

$$\beta_c = \alpha_c L_{cr} / 2\pi\sqrt{(r_1 r_2)} \quad (5.49b)$$

The presence of  $\alpha_c$  in (5.49b) indicates that the effect of the crack on the groundwater flow is based on a relation between the transmissivity of the crack and its length (multiplied by the hydraulic conductivity of the aquifer) similar to that in the case of uniform flow. So, the same conclusions apply in both flow situations with respect to these parameters of the crack.

The ratio  $L_{cr}/\sqrt{(r_1 r_2)}$  becomes  $\sqrt{(L_{cr}/r_1)}$  if  $L_{cr} \gg r_1$  and becomes  $L_{cr}/r_1$  if  $L_{cr} \ll r_1$ . This means that  $r_1$  divided by a certain factor has the same effect on the maximum flux in the crack as  $L_{cr}$  multiplied with the same factor. With respect to this effect, the distance to the well is of equal importance as the length of the crack.

#### *Applicability*

It is interesting to analyse the effects of several cracks in the neighbourhood of a head-specified well on its abstraction rate in order to examine the possibility of using these cracks in the simulation of anisotropic behaviour.

The derivation of the expressions for this analysis starts with a description of the effect of the crack on the transmissivity in the annular domain between  $r_2$  and  $r_1$  (figure 5.24) in the case that the crack is along a radial. (Later on the case of a crack arbitrary situated within an annular domain will be discussed.) The transmissivity representing the effect of the crack in the annular domain is used to derive the equivalent transmissivity between the well and the reference point similar to that in the case of the inhomogeneity (expression (5.20)). Using this equivalent transmissivity, the expression for the effect of the crack on the abstraction rate of the well can be found, because the head is specified both at the well radius and at the reference point. The derivation ends up with an expression for the relation between the abstraction rate of a well in an aquifer without cracks and the abstraction rate of a well with  $n$  cracks in its neighbourhood.

If the head of the well is specified, the crack affects the abstraction rate of the well. This abstraction rate can be determined in an approximate way

by assuming continuity of flow across the concentric circle around the well over  $r_{Qmx}$  (all groundwater flow goes towards the well):

$$Q_{w,1} = Q(r_{Qmx}) + Q_{cr}(r_{Qmx}) \quad (5.50)$$

where:

$Q(r_{Qmx})$  = the flux through the concentric circle at  $r = r_{Qmx}$  (figure 5.2.24), outside the crack [ $L^3/T$ ]

$Q_{w,1}$  = the abstraction rate of the well affected by a single crack (index 1) [ $L^3/T$ ]

This expression can be combined with expression (5.49a) by taking into account that  $Q_w$  in (5.49a) is affected by the single crack, so  $Q_{w,1} = Q_w$ .

$$Q_{w,1} = Q(r_{Qmx}) / (1 - \beta_c) \quad (5.51)$$

From the results of test computations (e.g. as presented in the tables 5.3 and 5.4), it has been concluded that generally the maximum flux through the crack is several orders of magnitude smaller than the abstraction rate at the well. This means that most of the groundwater flows outside the crack through the circle at  $r_{Qmx}$  and is not affected by the crack. As a first order approximation, the flux  $Q(r_{Qmx})$  is described by an expression for axial-symmetric flow through the circular domain at  $r_{Qmx}$  outside the crack (figure 5.2.24) assuming that the effect of the crack on this flux is negligible.

$$Q(r_{Qmx}) = 2\pi kH [\varphi(r_2) - \varphi(r_1)] / \ln(r_2/r_1) \quad (5.52)$$

The flux to the well  $Q_{w,1}$  can be described by an expression for axial-symmetric flow through the annular domain around the well (figure 5.2.24) including the effect of the crack by using a representative transmissivity  $T_{an}$ , according to:

$$Q_{w,1} = 2\pi T_{an} [\varphi(r_2) - \varphi(r_1)] / \ln(r_2/r_1) \quad (5.53)$$

where:

$T_{an}$  = representative transmissivity in the annular domain including the effect of the crack [ $L^2/T$ ]

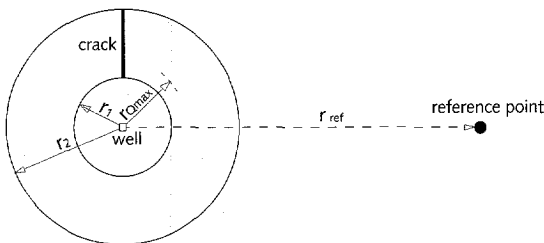


Figure 5.2.24 Scheme for derivation of the equivalent transmissivity

Substitution of (5.52) and (5.53) in (5.51) leads to:

$$T_{an} = kH / (1 - \beta_c) \quad (5.54)$$

The annular domain can be seen as an annular inhomogeneity around the well representing the effect of the crack on the abstraction rate of the well. Similar to the definition in expression (5.24), the equivalent transmissivity  $T_{eq}$  in the domain between the reference point and the well is defined by:

$$T_{eq} = Q_{w,1} \ln(r_{ref}/r_w) / [2\pi(\phi_{ref} - \phi_w)] \quad (5.55)$$

The expression for  $T_{eq}$  in terms of transmissivities for the case with the annular domain of *figure 5.24* is derived similarly to expression (5.25).

$$\frac{1}{T_{eq}} = \frac{1}{kH} + \left[ \frac{1}{T_{an}} - \frac{1}{kH} \right] \frac{\ln [r_2/r_1]}{\ln [r_{ref}/r_w]} \quad (5.56)$$

Combination of (5.56) and (5.54) leads to:

$$T_{eq} = \gamma_c kH \quad (5.57a)$$

with:

$$\gamma_c = 1 / \left[ 1 - \beta_c \frac{\ln [r_2/r_1]}{\ln [r_{ref}/r_w]} \right] \quad (5.57b)$$

At this point, a relation between the abstraction rate of the well in the case with a crack  $Q_{w,1}$  and in the case without a crack  $Q_{w,0}$  can be found based on the equivalent transmissivity and the heads specified at the well radius and at the reference point. In the situation without a crack the flux to the well is expressed by the standard well formula:

$$Q_{w,0} = 2\pi kH [\phi_{ref} - \phi_w] / \ln(r_{ref}/r_w) \quad (5.58)$$

Combination of (5.55), (5.57a) and (5.58) leads to:

$$Q_{w,1} = \gamma_c Q_{w,0} \quad (5.59)$$

Table 5.4 shows a comparison of the results of equation (5.59) with the results computed with Strack's AEM. The results of the formula's and the AEM compare well for the entire range of values of the parameters.

From table 5.4, it can be concluded that the abstraction rate of the well is hardly affected by changes in the length or in the transmissivity of the crack. When the distance between the (closest point of the) crack and the well becomes small some effect is determined. If the well is really

connected to the crack the effect may become considerable. Of course, a change in the hydraulic conductivity of the aquifer (table 5.4, part c) causes a change in the abstraction rate of the well.

Table 5.4 Comparison of the well flux computed by the AEM and by expression (5.59) with variation in (a)  $L_{cr}$ , (b)  $k_{cr}B_{cr}$ , (c)  $k$ , and (d)  $r_1$ , with  $L_{cr} = 200$  m,  $k_{cr}B_{cr} = 1000$  m<sup>2</sup>/d,  $k = 1$  m/d,  $r_1 = 100$  m.

(a)\*1

$L_{cr}$	1	10	100	1000
$Q_w$ AEM	45.47	45.48	45.66	47.6
$Q_w$ (5.59)	45.47	45.48	45.70	47.0

(b)

$k_{cr}B_{cr}$	.001	.01	.1	1	10	100	1000	10 <sup>4</sup>	10 <sup>5</sup>
$Q_w$ AEM	45.47	45.47	45.4	45.5	45.6	45.7	45.9	45.9	45.9
$Q_w$ (5.59)	45.47	45.47	45.4	45.5	45.6	45.7	46	46.1	46.1

(c)

$k$	.001	.01	.1	1	10	100	1000	10 <sup>4</sup>	10 <sup>5</sup>
$Q_w$ AEM	.046	.46	4.59	45.9	457	4550	45500	4.5 10 <sup>4</sup>	4.5 10 <sup>5</sup>
$Q_w$ (5.59)	.046	.46	4.61	46.0	457	4550	45500	4.5 10 <sup>4</sup>	4.5 10 <sup>5</sup>

(d)\*2

$r_1$	5*3	10	20	50	100	500	1000
$Q_w$ AEM	61.7	51.8	48.3	46.5	45.9	45.5	45.46
$Q_w$ (5.59)	52.4	50	48.1	46.6	46.0	45.5	45.46

\*1 \*2 \*3 see table 5.3

In cases where the direction of the crack is not along a radial, it appeared from test computations that the effect of the crack on the abstraction rate of the well remains about the same as that of a crack along the radial that fits in the same annular domain. This means that expression (5.59) can be used also for an arbitrary situated crack.

The effects of several cracks on the abstraction rate of a well can be added as long as the cracks act independent. This is confirmed by test computations of one of which the results are presented in table 5.5.

In table 5.5, the flux of a well is presented for five cases in which respectively 0, 1, 2, 3 and 4 cracks are situated close to the well. The four cracks are defined along the +x, +y, -x and -y direction respectively, so their effects are as independent as possible. The crack in figure 5.2.23 has a transmissivity that is relatively large with respect to the product of its length and the hydraulic conductivity of the aquifer ( $\alpha_c$  in expression

(5.40 b) ), which means that the effect of the crack is not limited by its transmissivity but by its length (see the analysis in the paragraph following expression (5.41)). From the distribution of the heads in this figure, it is concluded that this crack acts within a quarter of the domain. Because the four cracks in the computations are shorter than in the case of figure 5.2.23 and are situated along the main axes, they act also within a quarter of the domain and act independently.

Table 5.5 Computed abstraction rates of wells affected by 0,1,2,3,4 independently acting cracks

$k_{cr}B_{cr}=1000 \text{ m}^2/\text{d}$ ,  $L_{cr}=100 \text{ m}$ ,  $k=10 \text{ m}/\text{d}$ ,  $r_{ref}=1000 \text{ m}$ ,  $r_w=1 \text{ m}$ ,  $H=50 \text{ m}$ ,  $\phi_{ref}-\phi_w=10 \text{ m}$

well identifier	nr. of cracks	abstraction rate in $\text{m}^3/\text{d}$ $r_1 = 10 \text{ m}$	abstraction rate in $\text{m}^3/\text{d}$ $r_1 = 50 \text{ m}$	abstraction rate in $\text{m}^3/\text{d}$ $r_1 = 100 \text{ m}$	abstraction rate in $\text{m}^3/\text{d}$ $r_1 = 500 \text{ m}$
$Q_{w,0}$	0	546.7	545.7	545.7	545.7
$Q_{w,1}$	1	565.9	549.7	547.3	545.85
$Q_{w,2}$	2	584.1	553.6	548.8	545.97
$Q_{w,3}$	3	597.8	557.1	550.3	546.07
$Q_{w,4}$	4	610.3	560.5	551.8	546.16

The factor by which the abstraction rate changes due to the addition of each crack appears to be almost constant (table 5.6). From this it is concluded that the effect on the abstraction rate of the well of addition of each additional crack can be estimated by recurrent use of (5.59).

Table 5.6 Comparison of  $\gamma_c$  following from the computed values in table 5.5 with the result of expression (5.57b).

$k_{cr}B_{cr}=1000 \text{ m}^2/\text{d}$ ,  $L_{cr}=100 \text{ m}$ ,  $k=10 \text{ m}/\text{d}$ ,  $r_{ref}=1000 \text{ m}$ ,  $r_w=1 \text{ m}$ ,  $H=50 \text{ m}$ ,  $\phi_{ref}-\phi_w=10 \text{ m}$

Ratio of wells	$\gamma_c$ , $r_1 = 10 \text{ m}$	$\gamma_c$ , $r_1 = 50 \text{ m}$	$\gamma_c$ , $r_1 = 100 \text{ m}$	$\gamma_c$ , $r_1 = 500 \text{ m}$
$Q_{w,1}/Q_{w,0}$	1.037016	1.007330	1.002932	1.000274
$Q_{w,2}/Q_{w,1}$	1.032161	1.007094	1.002740	1.000219
$Q_{w,3}/Q_{w,2}$	1.023454	1.006322	1.002733	1.000183
$Q_{w,4}/Q_{w,3}$	1.020910	1.006103	1.002725	1.000164
average $\gamma_c$ from AEM computations	1.028365	1.006712	1.002782	1.000210
$\gamma_c$ from (5.57)	1.025285	1.007551	1.002369	1.000124
relative error (see text)	0.003004	0.000832	0.000412	0.000086

This means that  $\gamma_c$  should be raised to the power equal to the number of cracks in the annular domain around the well.

$$Q_{w,i} = \gamma_c^i Q_{w,0} \quad i = 1,2,\dots \quad (5.60)$$

where  $i$  is the number of independently acting cracks inside one annular domain around the well.

In table 5.6, the results of expression (5.60) are compared with the average factor resulting from test computations. The last row of table 5.6 represents the relative error, which is defined as  $[\gamma_c \text{ computed} - \gamma_c (5.57)]/\gamma_c (5.57)$ . Considering the complexity of the problem and the possible inaccuracies in

the computed values, the relative errors indicate a good agreement between the computed values and the results of (5.60).

Cracks in different annular domains generate different values of  $\gamma_c$ . From the analysis above it is admissible that their effects can also be included using the recurrent relation (5.60) with different  $\gamma_c$ 's for different annular domains, as long as they act independently.

This analysis shows that the effects of arbitrary situated cracks on the abstraction rate of a well can be predicted as long as the cracks act independently. The actual effects of the cracks on the abstraction rate of the well are relatively small as long as the cracks are not really close to the well. In general the effects are even so small that they can be neglected compared to the inaccuracies generated by the other elements in a model of analytic elements (compare table 5.1).

Because cracks increase the transmissivity in one direction, several parallel cracks might be used to generate anisotropic behaviour in axial symmetric flow. The effect of each of the parallel cracks on the axial-symmetric flow can be determined by using its effect on the transmissivity in the annular domain in which the anisotropy should be generated. The representative transmissivity generated by all cracks in this annular domain should be equal to the desired representative transmissivity following from the desired anisotropy. Doing this, the properties of the cracks are defined in such a way that the desired anisotropy is generated. However, it is a rather complex procedure to find the right properties of the crack. The procedure is very sensitive to the distance between the well and the closest crack. From modeling experience, it is concluded that it is a hard job to use cracks for anisotropic behaviour and that leaky walls are to be preferred to model anisotropic behaviour.

### **5.3 Combinations of two analytic elements of different types in a single aquifer**

#### **5.3.1 A qualification of each combination of two types of analytic elements and a definition of error types**

The analysis of the individual elements in section 5.2 can be used to analyse the interaction between each two types of elements described in chapter 3. In a model, each analytic element can be specified independently of all the other elements. But, not every specification makes sense. In order to derive a proper model, elements should be specified according to rules that are based on underlying mathematics and physical reality. In section 5.3, each possible combination of two types of analytic elements is described and analyzed.



Analytic elements can be combined in six different ways:

- 1 - nested \* = one within the other,
  - 2 - at the same place = covering each other completely,
  - 3 - crossed \* = (partly) overlapping each other
  - 4 - linked \* = be connected at tips (lines) or at sides (areas),
  - 5 - close = close together but not connected
  - 6 - free = far away from each other
- (\* = case presented in figure 5.3.1).

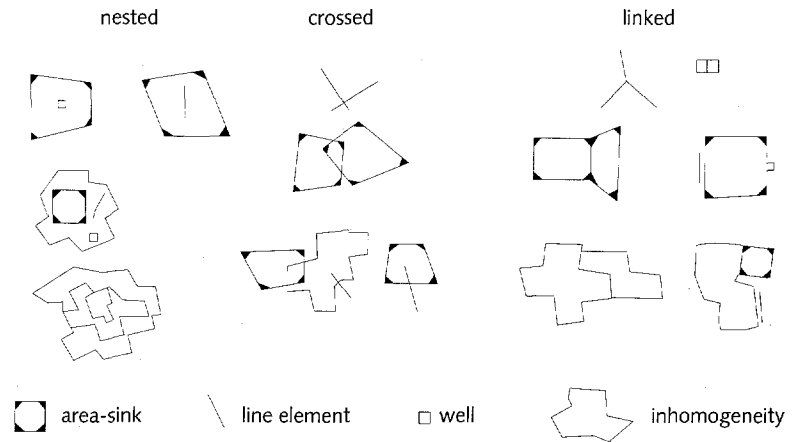


Figure 5.3.1. Examples of nested, crossed and linked elements

In modeling practice, it appears that elements are "close" together if the distance between their control points (chapter 3) is smaller than about  $L/100$ , where  $L$  is the length of a line-segment or the length of the largest diagonal of an area-sink. Elements are situated "free" if the distance between their control points is larger than about  $L$ . In this, the effects of elements with extreme strengths are taken into account. In between these situations, the interaction between elements gradually changes from free to close. Free elements can easily be combined and therefore these combinations are not discussed further in this section.

Based on both the theory and the authors experience, some general rules for the combination of analytic elements can be given:

- 1 - Elements with a given strength can easily be combined with each other.
- 2 - Two different heads prescribed at control points close together express physically impossible boundary conditions (except near weirs).
- 3 - DROOT type elements (cracks, drains, canals, leaky walls and impermeable walls) are difficult to combine.
- 4 - Free elements easy to combine.

All combinations of two analytic elements have been tested and qualified in table 5.7. If, in this entire section, two head-specified elements are discussed, these heads are presumed to be different. In the case of nested elements, each two elements can be interchanged as long as it is possible by their shapes.

In the next parts of this section, the combinations are discussed following the rows of table 5.7. So, the well (all types of table 5.7) is discussed in combination with all types of elements, the line-sink (all types) in combination with all types of elements except the well, the area-sink (all types) in combination with all types of elements except the well and the line-sink, etc. The canal is discussed together with the crack and the drain because in most combinations these elements act more similar than the canal and the line-sink (as compared in subsections 5.2.6 and 5.2.7). This is because of the strength distributions defined along these elements (subsection 3.3.4).

In complicated situations, the leaky and impermeable walls as well as the cracks, drains and canals should be replaced by curvilinear elements (subsection 4.2.2), which are more flexible and reliable in modeling than the original droot elements of subsections 3.3.4 and 3.3.5. However, these original elements are dealt with in subsection 5.3.

When modeling with analytic elements, three types of errors may occur. The following types of errors are listed in increasing order of importance of the geohydrological knowledge and in decreasing order of importance of the computation technique.

- Numerical errors occur due to numerical problems, which in the case of the AEM can be problems of not converging series in the computation of mathematical functions, problems in finding points of intersection, problems due to the rounding off of numbers, etc. Numerical errors can be solved by the developer of the technique only and are not dealt with in this thesis.
- Physical errors are due to wrongly chosen types or sizes of analytic elements or to wrong combinations of analytic elements and do not exist in modeling with other techniques. These errors show up in the form of heads and/or fluxes which are impossible in natural conditions, e.g. heads are computed outside the possible range of values. Physical errors form a main subject in this section. The most important ones are shown together with an indication of how they can be solved.
- Modeling errors are caused by using wrong geohydrological constants, wrong geohydrologic schematization or too coarse distributions of elements. In general, these errors may occur regardless the modeling technique. The aspect of distribution of elements is treated explicitly in section 5.4 and the relation between schematization and analytic elements is discussed in chapter 8.

Both the physical and modeling errors are visible in distributions of the head and flux. They may occur at the same place and can only be recognized by understanding the cause of these errors. In general, a combination of elements can be checked by analyzing both the head distribution (or distributions in adjacent aquifers) and the element strengths. A general rule for finding the cause of errors is that most of the unexpected behaviour of elements occurs inside or near the elements themselves. Causes of errors are rarely found at large distance of the place where they show up.

### 5.3.2. Combinations with wells

#### *Wells and wells*

The combination of wells is classical knowledge (see e.g. Raudkivi & Callander 1976, Bear 1979, Strack 1989). Wells with given strength can be combined in any way. Wells with opposite strength or different heads generate a dipole-like behaviour when placed close together (subsection 3.3.3). Head-specified wells cannot be put at the same place, because they generate conflicting boundary conditions.

#### *Wells and line-sinks*

Combinations of wells and line-sinks are easy to perform, except if the control point of a head-specified line-sink is close to a head-specified well. This will be illustrated by the following example.

A head-specified well close to the control point of a head-specified line-sink will cause a dipole-like behaviour (both heads are assumed to be different, subsection 5.3.1); the strength of both the line-sink and the well will become extreme in order to maintain the specified heads at their control points. Along the line-sink, the extreme strength remains constant (or linear) and often causes a physical error.

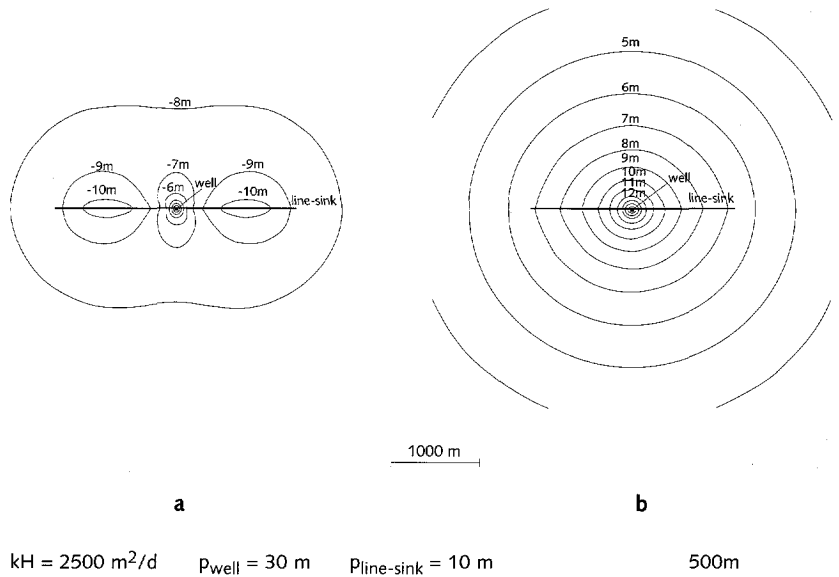


Figure 5.3.2. A well and a line-sink causing a physical error (a) and the same problem modeled without this error (b).

Table 5.7. A qualification of combinations of analytic elements.

elem-ent	combin-ation	well	line-sink	area-sink	inh	res	imp	crk	drn	can
		q h	q h	q h						
well q	ne	. .	+ 0	+ 0	+	!	!	-	-	-
	sp	+ +	. .	. .	.	.	.	.	.	.
	cr	. .	. .	. .	.	.	.	.	.	.
	li	+ +	+ 0	+ 0	-	!	!	-	-	-
	cl	+ +	+ 0	+ 0	0	-	-	0	0	-
well h	ne	.	+ !	+ 0	+	!	!	-	-	!
	sp	!	. .	. .	.	.	.	.	.	.
	cr	.	. .	. .	.	.	.	.	.	.
	li	-	+ 0	+ 0	-	!	!	-	-	!
	cl	0	+ 0	+ 0	0	-	-	-	-	-
line-sink q	ne		+ +	+ +	+	!	!	0	0	0
	sp		+ +	. .	-	!	!	+	+	0
	cr		0 0	0 0	0	+	!	-	-	-
	li		+ +	+ +	0	!	!	0	0	0
	cl		+ 0	+ 0	0	-	-	0	0	0
line-sink h	ne		!	+ 0	+	!	!	0	0	!
	sp		!	. .	-	!	!	+	+	!
	cr		!	0 0	0	+	!	-	-	!
	li		+	+ +	0	!	!	0	0	!
	cl		0	+ 0	0	-	-	0	0	0
area-sink q	ne			+ +	+	0	!	0	0	0
	sp			+ +	.	.	.	.	.	.
	cr			+ 0	0	0	!	0	0	0
	li			+ 0	+	+	+	+	+	+
	cl			+ 0	+	+	+	+	+	+
area-sink h	ne			!	+	0	!	-	-	!
	sp			!	.	.	.	.	.	.
	cr			!	-	-	!	-	-	!
	li			0	+	+	+	+	+	0
	cl			0	+	+	+	+	+	0
inh	ne				+	0	0	0	0	0
	sp				+	.	.	.	.	.
	cr				!	!*	!*	!*	!*	!*
	li				+	!	!	!	!	!
	cl				+	0	0	0	0	0

Tabel 5.7. (continued)

elem-ent	combin-ation	well	line-sink	area-sink	inh	res	imp	crk	drn	can
		q h	q h	q h						
res	ne					!	!	!	!	!
	sp					!	!	!	!	!
	cr					.*	-	.*	.*	.*
	li					!	!	!	!	!
	cl					+	+	+	+	+
imp	ne						!	!	!	!
	sp						!	!	!	!
	cr						.*	!	!	!
	li						!	!	!	!
	cl						+	+	+	+
crk	ne							!	!	!
	sp							!	!	!
	cr							0*	0*	0*
	li							!	!	!
	cl							+	+	+
drn	ne								!	!
	sp								!	!
	cr								0*	0*
	li								!	!
	cl								+	+
can	ne									!
	sp									!
	cr									!
	li									!
	cl									+

\* (1995) these elements need to be adapted for these combinations.

Legend

- |                          |   |
|--------------------------|---|
| inh = inhomogeneity      | res = leaky wall                                |
| imp = impermeable wall   | crk = crack                                     |
| drn = drain              | can = canal                                     |
| q = specified strength   | h = specified head (+ resistance for area-sink) |
| ne = nested              | + = easy combination                            |
| sp = at the same place   | 0 = combine with care                           |
| cr = crossed/intersected | - = tricky combination                          |
| li = linked              | ! = physically or mathematically wrong          |
| cl = close               | . = impossible because of element shape         |

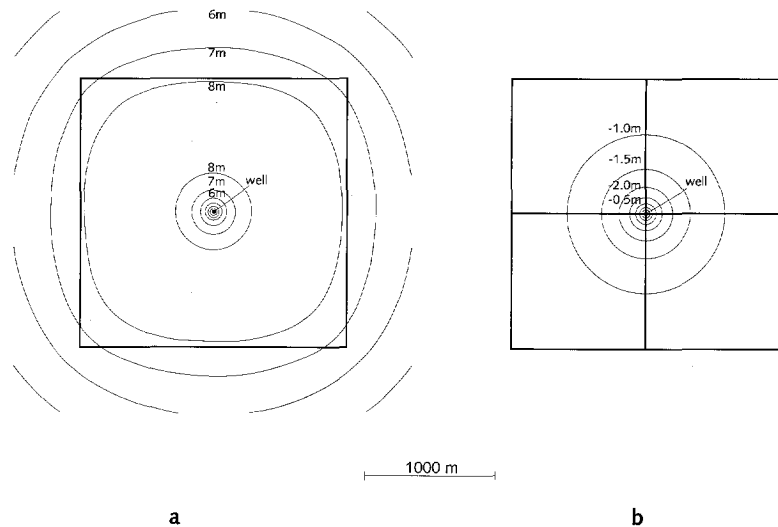
In *figure 5.3.2-a*, a head-specified well is placed close to the control point of a head-specified line-sink. (For this example, Strack's AEM program had to be misled because, since 1991, such a short distance between control points with specified heads is not allowed in the program.) The head of the line-sink is 10 m and the head of the well is 30 m. In this situation, the computed heads should be between the reference level 0 m and the level of the well 30 m. But in the case of *figure 5.3.2-a*, heads much lower than 0 m are computed at the ends of the line-sink. Also, at larger distance from the elements the groundwater flows toward both elements instead of flowing away from the elements. The pattern of the isolines in *figure 5.3.2-a* is typical for a physical error. In modeling practice, it is said that the model is "blown up" locally, because too extreme values occur in the head and flow distribution.

The situation of *figure 5.3.2-a* can be explained as follows. If the line-sink had been stand-alone, it should have generated a flow into the aquifer as its head of 10 m is above the reference level. By the addition of the well a much higher head (of about 30 m) is generated close to the control point of the line-sink, which causes the line-sink to abstract (large amounts of) water. Because the strength along the line-sink is constant, this abstraction rate occurs also at places along the line-sink where the head in the vicinity is not so high and where the flow should be not so extreme.

The physical error is overcome by adding control points and by putting them at sufficient distance, e.g. by splitting up the line-sink. Then, no extreme fluxes are computed and reasonable heads are found (*figure 5.3.2-b*). Also, the application of (in this case at least two) linear line-sinks will lead to an increase of the accuracy because the flux in the element can adapted better to the changes occurring.

#### *Wells and area-sinks*

The behaviour of a well combined with an area-sink is highly comparable to that in the case described above with a line-sink. All combinations of area-sinks and wells are easy to implement except if the control points of a head-specified well and a "Cauchy" (specification of both the surface water level and the resistance, subsection 3.3.7) area-sink are close together.



$kH = 2500 \text{ m}^2/\text{d}$   $p_{\text{well}} = 10 \text{ m}$   $p_{\text{area-sink}} = 0 \text{ m}$   $c_{\text{area-sink}} = 400 \text{ d}$  1000m

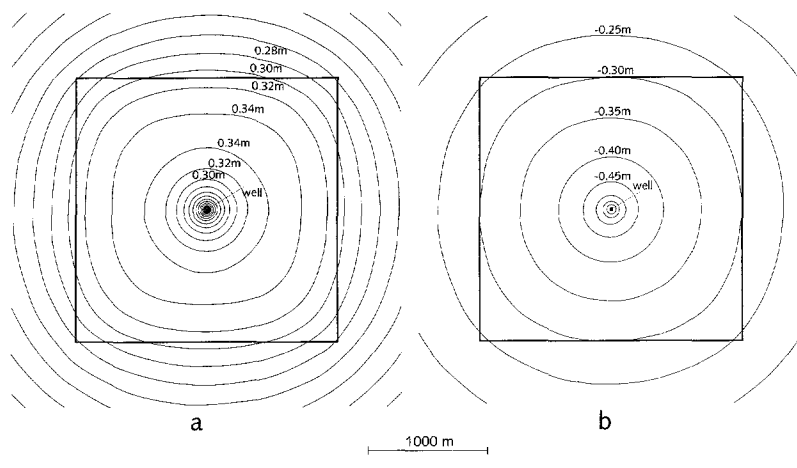
Figure 5.3.3 A well and an area-sink causing a physical error (a) and the same problem modeled without this error (b).

As an example of this latter case, a well with head  $-10 \text{ m}$  is placed close to the control point of an area-sink ( $2000 \times 2000 \text{ m}^2$ ) with a surface water level of  $0 \text{ m}$  (equal to the reference level) above a layer with a resistance of  $400 \text{ d}$  (figure 5.3.3-a). The computed heads should be in between  $-10 \text{ m}$  (well) and  $0 \text{ m}$  (reference level / surface water level). However, figure 5.3.3 shows computed heads far above the reference level which indicate a physical error.

The causes of this error are similar to that in the case with the line-sink. The head in the aquifer generated by the well close to the control point causes the area-sink to generate a strong infiltration. Because of its constant strength, the area-sink generates strong infiltration also further away from the well and causes a head above the reference level.

The physical error of figure 5.3.3-a is overcome by putting the control points of the elements at sufficient distance, e.g. by splitting up of the area-sink into four parts (figure 5.3.3-b). The accuracy of this "model" can be improved further by refining the area-sinks around the well.

In fact, the example of figure 5.3.3 shows a well in a semi-confined aquifer. In this situation, the vertical flow through the separating layer varies strongly with the distance to the well. An area-sink with constant strength can not account for this properly and should be refined around the well. But even then, the strength distribution generated by the area-sinks will not be exact. To model this variation of flux near a well exactly, the so-called Bessel-element (subsection 4.2.3) has been developed. This element generates the exact distribution of the vertical flow through the separating layer.



$$kH = 2500 \text{ m}^2/\text{d} \quad Q_{\text{well}} = 1600 \text{ m}^3/\text{d} \quad P_{\text{area-sink}} = 0 \text{ m} \quad c_{\text{area-sink}} = 400\text{d}$$

Figure 5.3.4 A well and an area-sink causing a physical error (a) and the same problem modeled properly with a Bessel element (b).

Figure 5.3.4 shows an example of this. Figure 5.3.4-a shows the head distribution generated by the area-sink of figure 5.3.3-a and by a well with a given abstraction rate of  $1600 \text{ m}^3/\text{d}$ . The specification of the well is changed, because the Bessel element has been developed yet to account for wells with given abstraction rate only. The abstraction rate is taken about equal to the abstraction rate of the well in the case of figure 5.3.3-b, because in that case the abstraction rate will be more accurate than in the case of figure 5.3.3-a. The strength of the area-sink in the case of figure 5.3.4-a is smaller than in the case of figure 5.3.3-a, because the rate of the well in this case is smaller than the abstraction rate of the well in that case. Therefore, the "dipole-effect" between the well and the area-sink is smaller, but figure 5.3.4-a still shows the physical error with heads above 0 m.

Figure 5.3.4-b shows the exact distribution of the head. From the comparison of figures 5.3.4-b and 5.3.3-b, it can be concluded that the refinement of figure 5.3.3-b does not lead to an accurate result yet, so a modeling error remains in this latter figure. If only constant strength area-sinks are used to model this situation (figure 5.3.3-b), further refinement of the area-sink mesh is needed to approach the accuracy of figure 5.3.4-b.

### Wells and inhomogeneities

Wells and inhomogeneities combine well if the distribution of the line-segments of the inhomogeneity is adapted for the presence of the well. A head-specified well should not be placed at the boundary of an inhomogeneity because then the well is replaced close to the boundary of the inhomogeneity by Strack's program and it is not a priori known whether that means inside or outside that boundary. In such a case, the



strength of the head-specified well is computed belonging to the transmissivity in its vicinity which means both inside and outside the inhomogeneity.

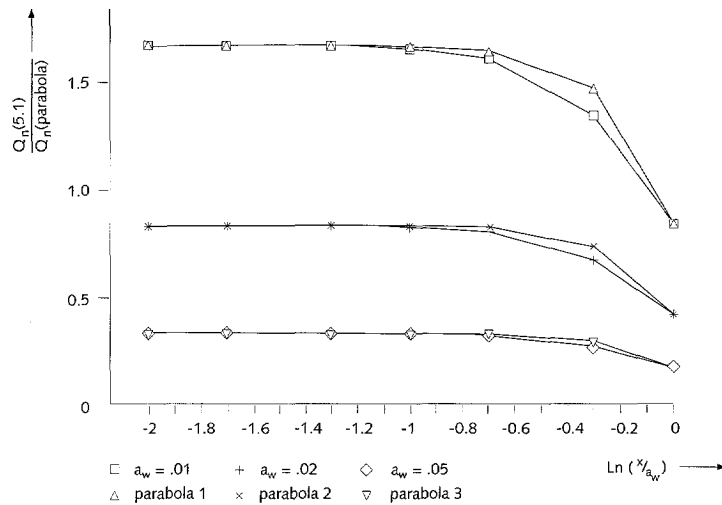


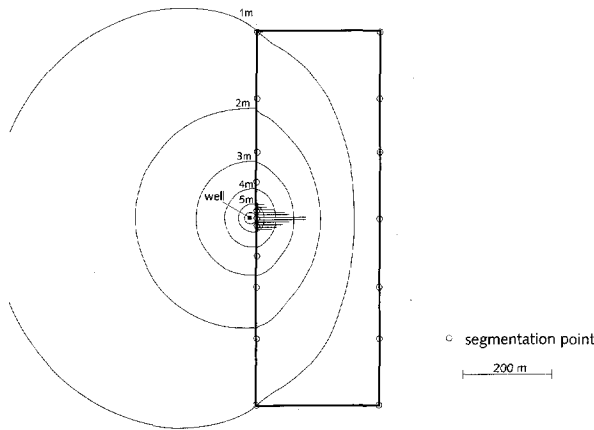
Figure 5.3.5 Ratio between the flux distribution of (5.1) and a parabolic strength distribution between  $x/a_w = .01$  ( $\ln(x/a_w) = -2$ ) and  $x = a_w$  ( $\ln(x/a_w) = 0$ ).

The strength distribution of each inhomogeneity segment is parabolic in terms of the jump in the potential (expression (3.30) and figure 3.3.9). The corresponding flux distribution is linear (because the flux is the derivative of the potential). Obviously, this flux distribution can match the distribution generated by the well (expression (5.1)) only by using small elements close to projection point of the well.

A theory to adapt the strength distribution of the inhomogeneity for a well in its vicinity is known (Strack, oral communication, 1991), but is not implemented yet. Next, it will be shown that the peak in the flux distribution across a line-segment (see figure 5.2.1) can be accounted for accurately using a parabolic distribution in terms of the flux, which means a third order strength distribution of the line-segments of the inhomogeneity. In figure 5.3.5, the ratio between the flux across a line-segment generated by the well (according to expression (5.1)) and a well-chosen parabolic distribution is presented along  $0 \leq x \leq a_w$ , where  $x = 0$  is the point closest to the well as shown in figure 5.2.2 and  $a$  is equal to the distance between the well and the line-segment. From figure 5.3.5, it can be concluded that the flux distribution close to projection point of the well can be approximated quite well by the parabolic distribution of the flux (which follows also directly from (5.1) for  $x \leq a_w$ ).

In figure 5.3.6., a well ( $h = 10$  m) is situated near an inhomogeneity in which the transmissivity is ten times lower ( $250 \text{ m}^2/\text{d}$ ) than outside. The distribution of the control points near the well is as described above and leads to a good result in the head and flux distribution.

From modeling experience and from the example of *figure 5.3.6*, it follows that the segmentation of the present inhomogeneities (with a parabolic distribution for the jump in the potential) should be symmetrical around the point of projection of the well (*figure 5.2.2*) and that the segments starting from there should extend to about the point of inflexion, which is generally approximated at  $x = a_w$ . For  $x \leq a_w$ , the flux distribution becomes smoother and smoother and can be modeled using longer and longer line-segments. As a general rule following from modeling practice, the length of each next line-segment can be increased by a factor 2.



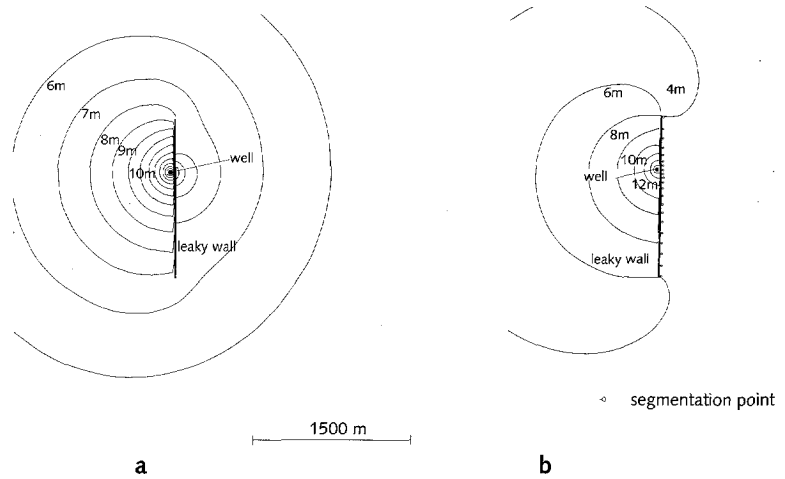
$$kH = 2500 \text{ m}^2/\text{d} \quad k_{\text{inh}}H_{\text{inh}} = 250 \text{ m}^2/\text{d} \quad p_{\text{well}} = 10 \text{ m}$$

*Figure 5.3.6* Accounting for a well near an inhomogeneity by adapting the lengths of the line-segments.

### Wells and leaky or impermeable walls

Except if the elements are positioned "free", a well close to a leaky or impermeable wall is tricky or physically wrong in a model (subsection 5.3.1), .

In *figure 5.3.7*, a well with a head of 30 m is placed close to a leaky wall (subsection 3.3.5) with a resistance of 1000 d. As the length of the leaky wall is 1500 m and  $k = 50 \text{ m}/\text{d}$  the value of  $v$  defined in expression (5.26) is about 30 and so the analytic element should be almost impervious. However, the computed head distribution in *figure 5.3.7-a* shows considerable leakage through the leaky wall near the well. Adaption of the number of control points does not lead to better results in terms of the enclosing effect of the leaky wall. From this and from other experiences it is concluded, that a real peak in the distribution of the flux (see subsection 5.2.1) can hardly be accounted for by the strength distribution of a straight leaky wall as described in subsection 3.3.5. However, using the curvilinear element of type leaky wall (subsection 4.2.2), proper modeling results can be derived as shown near the well in *figure 5.3.7-b*.



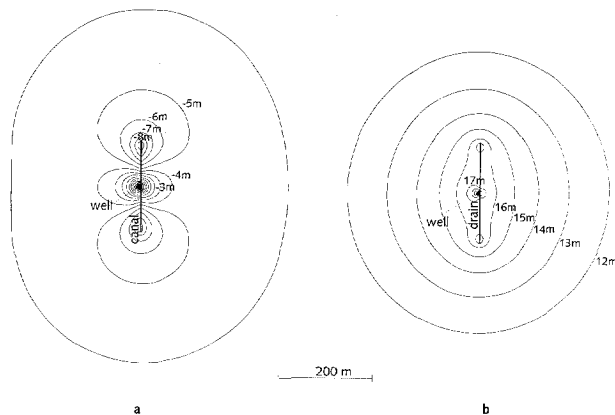
$$k = 50 \text{ m/d} \quad H = 50 \text{ m} \quad c_{lkw} = 1000 \text{ d} \quad p_{\text{well}} = 30 \text{ m}$$

Figure 5.3.7 Distribution of the head generated by a well (a) near a leaky wall and (b) near a curvilinear element type leaky wall.

In figure 5.3.7-b, the (straight) line-segments of the curvilinear element are distributed using the rule for the distribution of the line-segments of the inhomogeneity mentioned above. It can be concluded from the distribution of the heads in figure 5.3.7-b, that the curvilinear element of type leaky wall really generates an (almost) impermeable barrier and accounts accurately for the distribution of the flux generated by the well.

#### Wells and canals, cracks or drains

In general, wells and canals, cracks or drains should be combined with care, except when the elements are modeled "free".



$$kH = 2500 \text{ m}^2/\text{d} \quad p_{\text{well}} = 30 \text{ m} \quad p_{\text{canal}} = 10 \text{ m}$$

Figure 5.3.8 Behaviour of a head-specified well close to a canal (a) and close to a drain (b).

A head-specified well close to a canal may lead to physical errors similar to that in the case of a head-specified line-sink, because in both cases two different heads are specified close together. In *figure 5.3.8-a*, a well with head 30 m is defined closely to a canal with head 10 m. The canal reacts similar to the line-sink in the case of *figure 5.3.2-a*, but the effects in terms of heads and fluxes are relatively larger, because the canal in *figure 5.3.8-a* is about 10 times shorter than the line-sink in *figure 5.3.2*. Increasing the length of the canal causes an increase of the "blowing-up" effect. Similarly to in the case of the leaky wall (DROOT-type) in *figure 5.3.7-a*, the problem of *figure 5.3.8-a* can be modeled properly by using a curvilinear element.

In subsection 5.2.6, the effect of the crack on the abstraction rate of the well has been analyzed. The combination of a well and a crack or drain is complex only, because of the strength distribution inside the crack or drain. In *figure 5.3.8-b*, a head-specified well close to a drain is shown. In this case the well is situated in the middle of the element, which generates a flow distribution inside the drain that is different from that in the case of the crack in *figure 5.2.23*. In the drain at both sides of the well, both inflow and outflow takes place. In *figure 5.3.8-b*, the distribution of the head (about constant) along the drain shows that the behaviour is as expected.

### 5.3.3 Combinations with line-sinks

#### *Line-sinks and line-sinks*

Line-sinks can be combined easily in any way except in two cases. The first case concerns two head-specified line-sinks of which the control points are close to each other. In such a situation, the reaction of each of the line-sinks is similar to the reaction of the line-sink in *figure 5.3.2-a* (physical error), because each line-sink acts similar to the well in this figure with respect to the other line-sink.

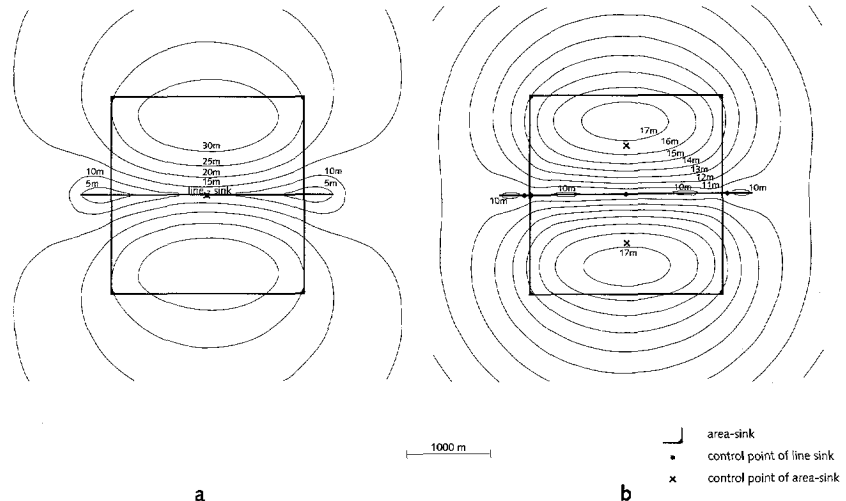
The second case concerns two head-specified line-sinks overlapping (crossing) each other. Then, two surface water levels are specified the overlapping part, which is physically impossible. The strengths of both line-sinks are superimposed and do not comply with the specified conditions. Actually, line-sinks should not overlap at all in a model, because such situations do not exist in reality.

#### *Line-sinks and area-sinks*

Line-sinks and area-sinks can be combined easily except in the cases with specified heads "close" or "at the same place".

When the control points of a head-specified line-sink and of a "Cauchy" (subsection 5.3.2 part "wells and area-sinks") area-sink are close together, extreme fluxes are computed in both elements which lead to errors in the head and flux distribution (physical error). This behaviour is shown in *figure 5.3.9-a*, where the control points of a line-sink (with head of 10 m) and of a Cauchy area-sink (with surface water level 20 m and resistance of 40 d) are

placed close together. The heads in the aquifer should be in between 0 m (reference level) and 20 m (surface water level). The computed heads in figure 5.3.9-a exceed the expected range significantly and indicate a physical error. The cause of this error is similar to that in the case of the area-sink and the well in figure 5.3.3-a. This error is removed by placing the control points of the elements further away from each other. In figure 5.3.9-b, both the area-sink and the line-sink are divided into two equal parts.



$$kH = 2500 \text{ m}^2/\text{d} \quad P_{\text{line-sink}} = 10 \text{ m} \quad P_{\text{area-sink}} = 20 \text{ m} \quad C_{\text{area-sink}} = 40 \text{ d}$$

Figure 5.3.9 A line-sink and an area-sink causing a physical error (a) and the same case modeled without that error (b).

In reality, surface waters often cross polder areas. Then, a modeling option might be that line-sinks overlap area-sinks. This should be avoided because the heads in the elements are generally different and actually two boundary conditions at the place of the line are defined in such a situation, which is physically impossible.

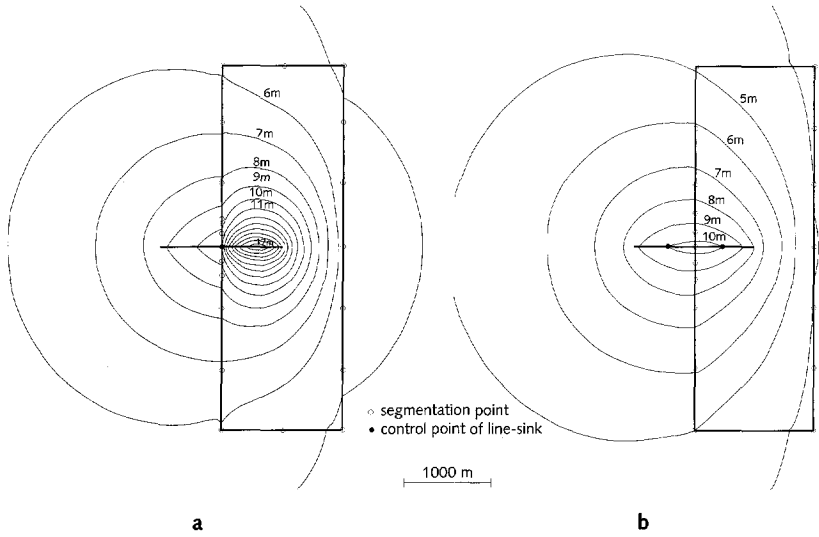
#### Line-sinks and inhomogeneities

A line-sink and a line-segment of an inhomogeneity can be put at the same place (because it has been tested), but then the same occurs as in the case of the well and the inhomogeneity. The line-sink is replaced by Strack's program and it is not a priori known whether that means inside or on outside that boundary outside the inhomogeneity. This situation should be avoided in modeling.

Line-sinks linked with or close to the boundary of an inhomogeneity should be modeled with care. The distribution of the line-segments of the inhomogeneity should be in accordance with the distribution of the flux across the line-segments generated by the line-sink. This latter distribution has been discussed in subsection 5.2.2.

If a line-sink is approximately parallel and close to a line-segment of an

inhomogeneity, the strength distribution of the line-segment can account well for the flow distribution generated by the line-sink. In this case, the line-segment of the inhomogeneity can be about as long as the line-sink. If a line-sink in normal direction to a line-segment of an inhomogeneity is close the line-segment, the distribution of the line-segments should be similar to that in the case with a well, because the flow near a tip of a line-sink is comparable to that near a well.



$$kH = 2500 \text{ m}^2/\text{d} \quad k_{inh}H_{inh} = 250 \text{ m}^2/\text{d} \quad p_{line-sink} = 10 \text{ m}$$

Figure 5.3.10. A line-sink crossing the boundary of an inhomogeneity with a physical error (a) and without physical error (b).

In general, a line-sink should not cross a boundary of an inhomogeneity, because then the constant strength of the head-specified line-sink is neither belongs to the transmissivity outside nor to the transmissivity inside the inhomogeneity. As an example, figure 5.3.10-a shows the computed heads generated by a line-sink with head 10 m crossing the boundary of an inhomogeneity of which the transmissivity inside is ten times lower than outside. The computed heads should be in between this head and the reference level of 0 m.

Inside the inhomogeneity, the computed head is higher than 10 m (physical error). This is caused by the following. The flux outside the inhomogeneity needed to generate the 10 m is much greater than the flux needed inside the inhomogeneity. This great flux generates values of the head that are higher than the surface water level which show a physical error. After splitting up the line-sink at the boundary of the inhomogeneity, the strengths in both parts are computed according to the transmissivities inside and outside the inhomogeneity and the physical error overcome (figure 5.3.10-b).

### *Line-sinks and leaky or impermeable walls*

Line-sinks may cross leaky walls but not impermeable walls because in the latter case the no-flux condition inside the element is disturbed (see subsection 3.3.5). Also in this case, the effect of the leaky wall becomes not clear, because the line-sink generates a "hole" in the leaky wall.

Line-sinks may not overlap leaky or impermeable walls, because then mathematical inconsistencies occur. If the tip of the line-sink is very close to a leaky or impermeable wall, both elements can hardly be combined similar to the case of a well close to a wall (subsection 5.3.2). If the line-sink is almost parallel to a leaky or impermeable wall, the combination is less difficult than if the elements are perpendicular to each other. In the case of parallel elements, the line-sink generates a smooth flow distribution at the place of the leaky or impermeable wall.

### *Line-sinks and canals, cracks or drains*

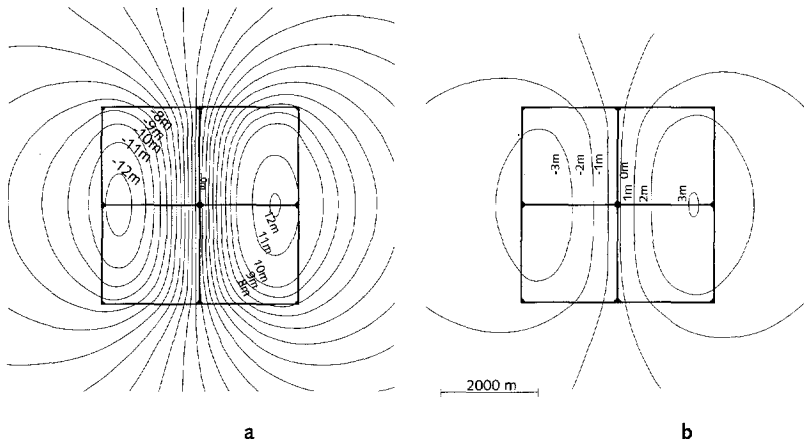
Line-sinks may (partly) overlap cracks, drains or canals or be nested and linked with these elements (as long as no head conflicts occur), but the meaning of such combinations in reality is difficult to determine. A head-specified line-sink crossing a canal leads to a physical error, similar to the case of two head-specified line-sinks but the effects in terms of heads and fluxes will be more pronounced.

A head-specified line-sink at the same place as a drain forms a canal. Also, a line-sink can be at the same place as a crack. In general, these combinations will lead to good results.

## **5.3.4 Combinations with area-sinks**

### *Area-sinks and area-sinks*

Area-sinks can be defined on top or at the bottom of an aquifer. Here, only cases with area-sinks on top are discussed, which are similar to cases with area-sinks at the bottom. The behaviour of combinations of area-sinks at both top and bottom of the aquifer will be discussed in section 5.5.



(a)  $kH = 25 \text{ m}^2/\text{d}$  (b)  $kH = 2500 \text{ m}^2/\text{d}$   
 $c_{\text{area-sink}} = 1000 \text{ d}$  left-hand-side:  $p_{\text{area-sink}} = -10 \text{ m}$  right-hand-side:  $p_{\text{area-sink}} = 10 \text{ m}$

Figure 5.3.11 Computed heads in the case with the width of area-sinks in the main flow direction much larger than (a) and about equal to (b) the characteristic length.

Area-sinks with given strengths can easily be combined in any way. Cauchy area-sinks can easily be close together or linked. Two Cauchy area-sinks may not be nested, may not be crossed and may not be at the same place because these situations are physically impossible.

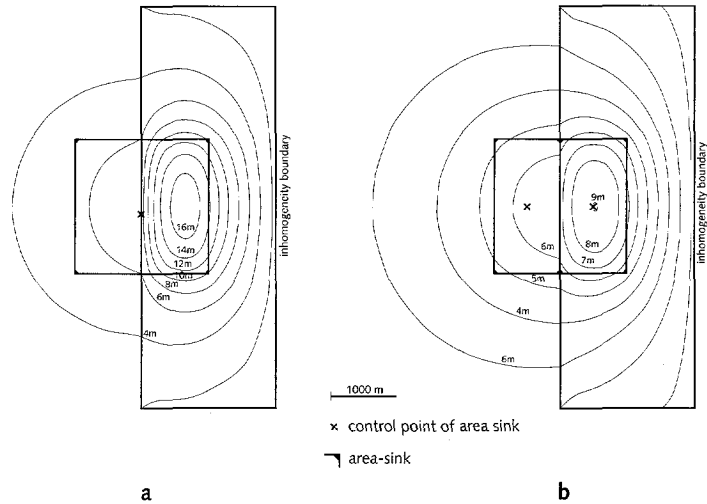
In subsection 5.2.3, the size of an area-sink is related to the accuracy of its strength and the head in the aquifer below the element. The size of the area-sink is specified in terms of the width of the element in the main direction of the flow in the aquifer. The preferred width of the element (with respect to the accuracy) can directly be used in a model with a mesh of area-sinks.

In figure 5.3.11, two models of area-sinks with different ratios of  $L/\lambda$  (see subsection 5.2.3) are presented, where  $L$  is interpreted as the width of the area-sink in the main direction of the flow and  $\lambda$  is defined in expression (4.1). The surface water levels of both left and right area-sinks are  $-10 \text{ m}$  and  $10 \text{ m}$  respectively. The reference level is  $0 \text{ m}$  and the reference point is at the right hand side of the area-sinks, which explains the non-symmetric head distribution in figure 5.3.11. In the case of figure 5.3.11-a, the transmissivity is 100 times smaller than in the case of figure 5.3.11-b and  $L/\lambda$  is about 13. According to the analysis of subsection 5.2.3 (table 5.1), the error in the flux of the area-sinks will be large. The computed heads in the aquifer are above the highest and below both the lowest specified surface water levels, indicating a physical error. In the case of figure 5.3.11-b, the ratio  $L/\lambda$  is about 1.3 and good results are found in the fluxes of the area-sink (compare table 5.1) and in the presented head distribution.



### Area-sinks and inhomogeneities

Area-sinks can easily be combined in any way with inhomogeneities, except when the elements are partly overlapping (crossing) each other. Because the strength of the area-sink is either valid outside or inside the inhomogeneity, it is always wrong and a physical error can be expected. Figure 5.3.12-a shows an example of this.



$$kH = 2500 \text{ m}^2/\text{d} \quad k_{\text{inh}}H_{\text{inh}} = 125 \text{ m}^2/\text{d} \quad P_{\text{area-sink}} = 10 \text{ m} \quad c_{\text{area-sink}} = 400 \text{ d}$$

Figure 5.3.12 An area-sink crossing an inhomogeneity (a) and the same domain covered by two area-sinks (b).

The inhomogeneity generates a transmissivity that is 20 times lower inside than outside. The area-sink partly overlaps the inhomogeneity and is defined with a surface water level of 10 m. Inside the inhomogeneity, the computed heads are higher than 16 m (physical error). The reason for this is that the strength of the element belongs mainly to the conditions outside the inhomogeneity (because the control point of the area-sink is just outside the inhomogeneity) and this strength is too large inside the inhomogeneity. By adapting the strength distribution of the area-sink by splitting up the element into two parts covering the area inside and the area outside the inhomogeneity as shown in figure 5.3.12-b, the two strengths lead to a result without physical error.

### Area-sinks and leaky or impermeable walls

In general, area-sinks cause less pronounced behaviour at the corners than line-sinks at the tips (see subsection 5.2.3). Therefore, leaky and impermeable walls can be combined more easily with area-sinks than with line-sinks.

Area-sinks can be used with leaky-walls in any combination. If the presence of the leaky wall causes large differences with respect to the flow generated by the area-sink only, it can be desirable to split up area-sinks in a way similar to that in the case of figure 5.3.9-b.

Impermeable walls do not allow vertical flow on top of or at the bottom of their place (subsection 3.3.5). So, area-sinks (including those with given strengths) may not overlap with impermeable walls. In other situations these elements can be used similarly to leaky walls.

#### *Area-sinks and canals, cracks or drains*

Area-sinks can be used with cracks, drains and canals in any combination, except if two different (subsection 5.3.1) heads are specified at the same place. The latter occurs if a Cauchy area-sink overlaps a canal with a different level. The effects are most pronounced when the control points nearly coincide and give results comparable to those presented in *figure 5.3.9-a* for area-sinks and line-sinks. If a crack, drain or canal causes large effects in the flow, it may be desirable to adjust the strength distribution generated by the area-sinks e.g. by refinement.

### **5.3.5 Combinations with inhomogeneities**

#### *Inhomogeneities and inhomogeneities*

Inhomogeneities can easily be nested and linked but cannot be crossed. In the latter case, the inhomogeneities should be redesigned in such a way that they do not cross. If a line-segment of an inhomogeneity is defined at the same place as a line-segment of another inhomogeneity, the coinciding control points can be merged, because only one jump in transmissivity is meant at that boundary. Control points of different inhomogeneities close together affect each other strongly and should be modeled with care or should be avoided.

#### *Inhomogeneities and leaky or impermeable walls*

Inhomogeneity boundaries that cross leaky and impermeable walls should be modeled with care. The larger the jumps in both elements the more accurate the strength distributions should be to account for the effects by both elements. The effects at the tips of leaky and impermeable walls

desire careful adjustment of the boundary of the inhomogeneity in case they are close together.

#### *Inhomogeneities and canals, cracks or drains*

Canals, cracks and drains crossing inhomogeneity boundaries can be treated largely similar as line-sinks crossing inhomogeneity boundaries. The effects at the tips of cracks, drains and canals desire careful adjustment of the inhomogeneity in case they are close together.

### **5.3.6 Combinations with leaky or impermeable walls**

#### *Combinations of leaky or impermeable walls*

Leaky and impermeable walls can only be combined free or close together. The tip effects demand careful modeling in any combination. To concatenate these

elements, they should be replaced by line-segments of curvilinear elements (see subsection 4.2.2).

### Combinations of leaky or impermeable walls with canals, cracks or drains

Leaky and impermeable walls and canals, cracks or drains can only be combined free or close together. Impermeable walls should not be crossed at all by canals, cracks or drains because the impermeable walls does not allow any inflow or outflow. Canals, cracks and drains crossing leaky walls are largely similar to cases with line-sinks crossing leaky walls and is not allowed.

### 5.3.7 Combinations with canals, cracks or drains

Crossing of canals, cracks and drains is tricky in any case. Crossing of canals cause two heads (with different levels) at one place and is physically wrong. By modeling canals closely together with different levels, the tip effects may simulate the groundwater flow around a weir. To concatenate these elements, they should be replaced by line-segments of curvilinear elements (see subsection 4.2.2).

## 5.4 Combinations with many elements in a single aquifer

### 5.4.1 Example of area-sinks

Area-sinks do not set constraints to the presence or the shape of adjacent area-sinks, because each element is defined independently of an other area-sink. Therefore, a mesh of area-elements can be strongly different from meshes in models based on the finite element or the finite difference technique. schematization of the upper boundary are presented in figure 5.4.1.

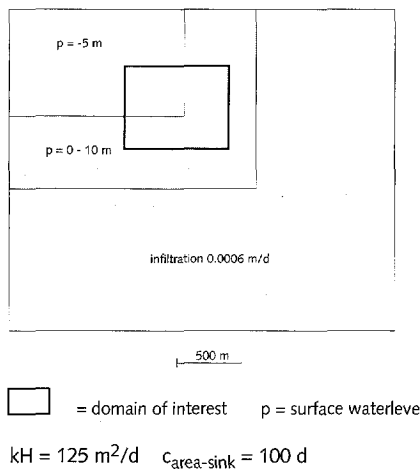


Figure 5.4.1 Model schematization and the domain of interest.

In an aquifer with a rather low transmissivity of  $125 \text{ m}^2/\text{d}$ , groundwater flows from an infiltration area (downward flux of  $.0006 \text{ m/d}$ ) via an intermediate area with sloping surface water levels ( $p$ , between 0 and 10 m)

to a deep polder (with a surface water level of -5 m). Except in the infiltration area, a separating layer with a small resistance of 100 d is present on top of the aquifer. In the domain of interest (figure 5.4.1), relatively strong flow occurs with steep gradients in the groundwater head.

In the first model, a coarse mesh of area-sinks (average size of about 2 km<sup>2</sup>) is used (figure 5.4.2). The polder is covered by three elements (level of -5 m) and in the intermediate region the surface water levels are averaged to 5 m. The general head distribution in the whole model is reasonable. The minimum and maximum heads and the 0 and -1 m isolines are approximately at the right place and the overall picture is smooth as expected. The gradient in the head distribution near the jump in the surface water levels is too small considering the actual value of  $\lambda$  (115 m). The inaccuracies are caused by the widths of the elements in the main direction of flow (see subsection 5.2.3) which are larger than 10  $\lambda$ .

Because the jump in the surface waters is not reflected in a proper way in the head and flux distribution, the area-sinks near this jump are refined in the second model (figure 5.4.3). The intermediate region is subdivided into a region with surface water levels at 6 m near the infiltration area and at 3 m near the jump.

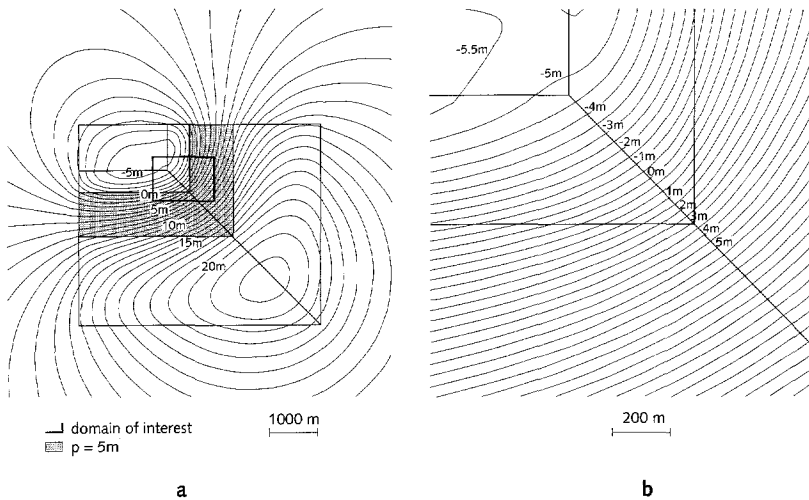


Figure 5.4.2 First model with a coarse mesh of area-sinks.

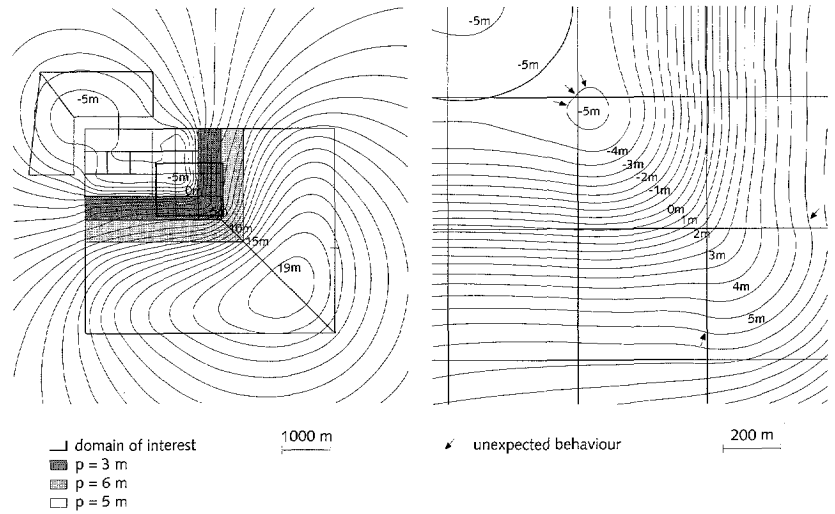


Figure 5.4.3 Second model with refined mesh of area-sinks.

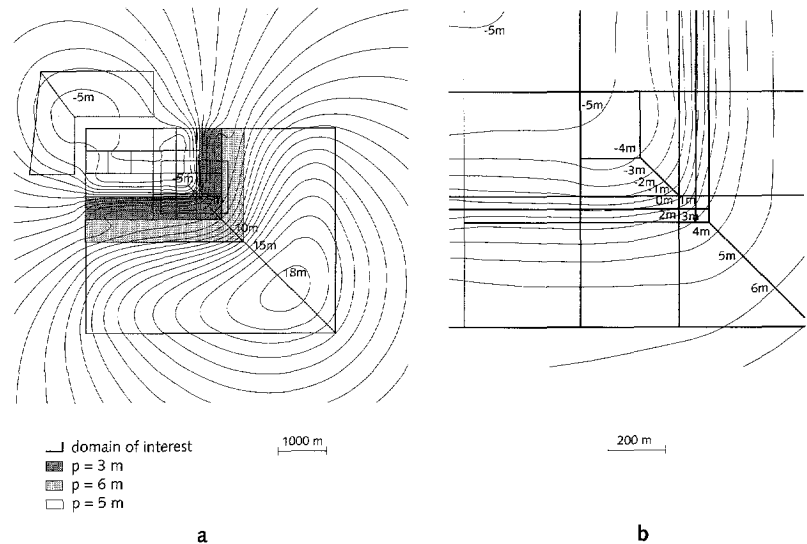


Figure 5.4.4 Third model with a fine mesh of area-sinks in the domain of interest.

The width in the main direction of flow of the area-sinks in the refined area is about  $600\text{ m}$ , which is about  $5\lambda$ . By these changes in the model, the head distribution near the jump in the surface water levels has become more pronounced than in the first model. However, the isolines of the head indicate that the flow in the domain of interest is not reliable yet (arrows in figure 5.4.3-b). The maximum head in the model is lowered from  $22\text{ m}$  in figure 5.4.2 to  $19\text{ m}$  in figure 5.4.3, which means that the refinement has considerable effects on the entire model.

In the third model, the elements near the jump in the surface waters (figure 5.4.4) are refined further down to widths (about  $60\text{ m}$ ) in the

direction of the main flow smaller than  $\lambda$  (about 115 m). The head distributions in the polder and near the infiltration area changed not much compared to those in the second model (maximum and minimum levels remain about the same). In the domain of interest, the head distribution (e.g. the 0 m isoline) follows the corner (of 90 degrees) closely. Also, the fluxes in the domain of interest will be reliable, which follows from the analysis in subsection 5.2.3.

Concluding remarks.

- The first model is much too coarse because the computed head distribution is too flat near the jump in the surface waters and the isolines do not follow the place of the jump.
- The head distribution in the entire model area changes in the second model. So, the changes in this model provide an important increase of the accuracy of the entire area.
- In the third model, changes occur mainly in the part in which the refinement is made. So, the accuracy is further improved mainly locally in the domain of interest.
- The example shows that refinements are easy to implement in a model of analytic elements.

#### 5.4.2 Example of line-sinks and inhomogeneities

This model describes groundwater flow in an unconfined aquifer with a sloping base. The elevation of the base causes a change in the saturated thickness and therefore in the transmissivity of the aquifer. The elevation in the base is changed step by step using three nested inhomogeneities generating three jumps in the base (*figure 5.4.5*). The natural groundwater recharge is simulated by an area-sink with specified downward flow of 0.0006 m/d over the entire region. The two rivers in the area are modeled by 12 line-sinks with specified heads (*figure 5.4.5*). The line-sinks have been split up close to the inhomogeneity boundaries in order to avoid the physical error presented in *figure 5.3.10-a*. In the consecutive steps in this example, the line-sinks remain the same.

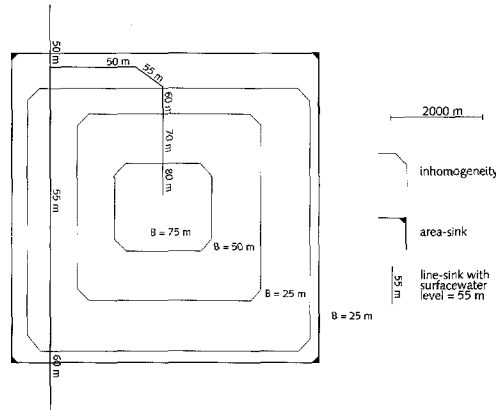
In the first model (*figure 5.4.6*), the boundaries of the inhomogeneities are modeled as coarse as possible, which means that control points are defined at the corners only. The computed head distribution shows physical errors at the long line-segments of the inhomogeneity (see arrows in *figure 5.4.6*). The strength distribution of these line-segments can not account for the variation in the actual flow. The edges in the isolines are typical of this physical error.

In the second model (*figure 5.4.7*), the line-segments of the inhomogeneity are divided at the points where the line-sinks cross the boundary of the inhomogeneity and also long segments have been split up. After doing this, the distribution of the head does not show obvious errors.

A further refinement of the inhomogeneity is shown in *figure 5.4.8*. All line-segments have been split up further. There is no obvious difference between the head distribution in this third model and that in the second model.

In figure 5.4.9, the differences in the head between the third and second model are shown, which are really minor. From this, it is concluded that the second model is a good optimum between accuracy and computation effort.

Based on this example and on extensive experience, the following conclusion can be drawn with respect to errors in the computed results. If a model does not clearly show physical errors, there is only a small chance that relevant physical errors have not been recognized in the model. The remaining errors may appear later only in those parts of the model in which almost no flow occurred during the calibration.



$k = 1 \text{ m/d}$     $B = \text{base in m}$     $H = \text{computed head} - \text{base}$     $\gamma_{\text{area-sink}} = -.0006 \text{ m/d}$

Figure 5.4.5    Model schematization.

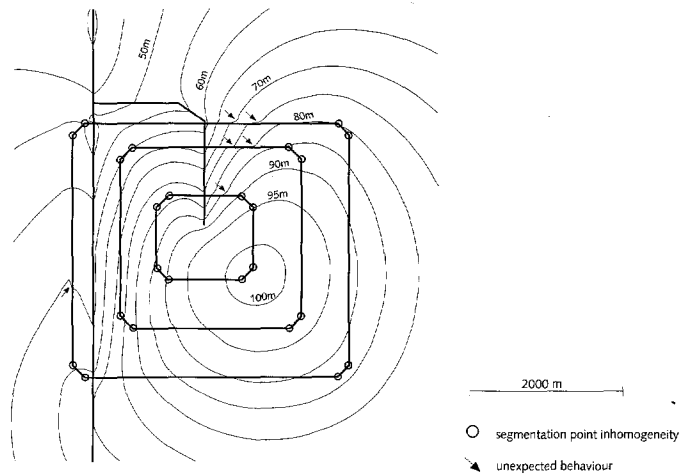


Figure 5.4.6    Computed head distribution in the first model.

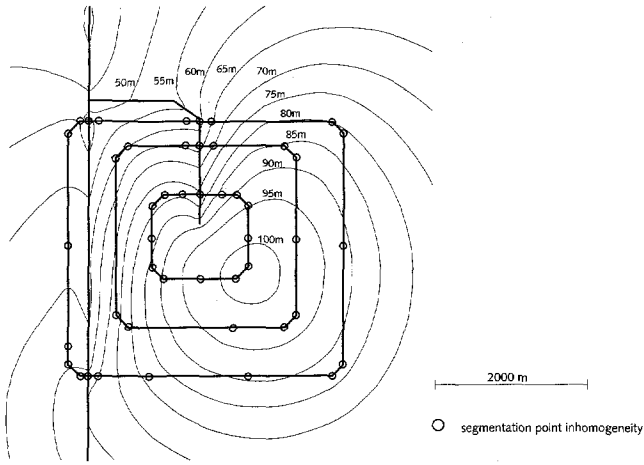


Figure 5.4.7 Computed head distribution in the second model.

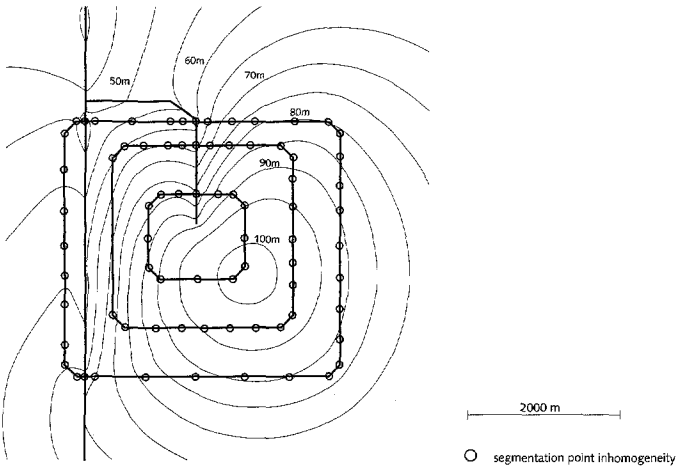


Figure 5.4.8 Computed head distribution in the third model.

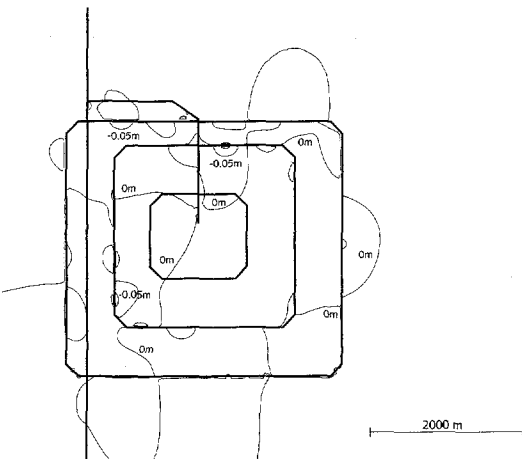


Figure 5.4.9 Differences in head between the second and third model.



## 5.5 Combinations with elements in several aquifers

### 5.5.1. Example on the shape of leakage area-sinks

In a multi-aquifer system without abstractions, the distribution of the vertical flow is generated by the boundary conditions on top of the system. In such a system, it seldomly occurs that the vertical flux at the top of the aquifer is in opposite direction to the flux at the bottom of that aquifer. In general, the flux at the bottom of an aquifer will be smaller but in the same direction as the flux at the top.

The vertical flux is constant per area-sink and jumps at the boundary of each area-sink. In *figure 5.5.1*, a section with area-sinks at separating layers is shown which have different shapes at the different levels.

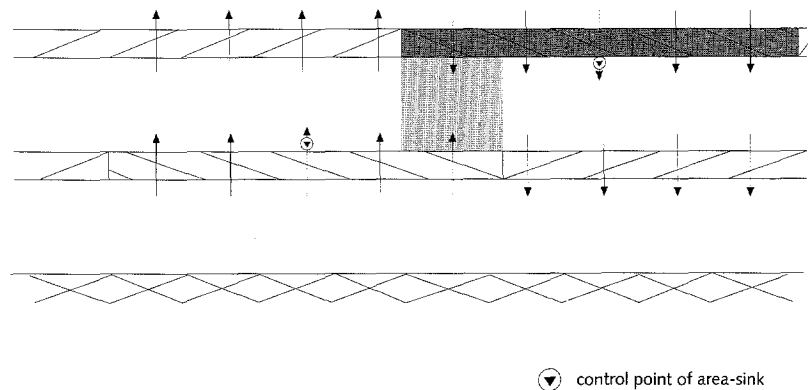


*Figure 5.5.1* Scheme of section with area-sinks layers with different shapes at the different levels.

In the centre part of *figure 5.5.1*, the flux through the area-sinks on top and at the bottom of the upper aquifer is in opposite direction due to the overlap of the analytic elements and not due to conditions based on reality. At that place in the aquifer, unexpectedly high values in the groundwater head occur (physical error), because of the influx from both sides of the aquifer. These fluxes in opposite direction originate from the analytic element distribution only and not from boundary conditions, transmissivities and resistances of the multi-aquifer system. Because a model should not generate situations with opposite flow by itself, the scheme of *figure 5.5.1* is principally wrong. If such situations should occur in a model they should originate from the boundary conditions and the transmissivities and resistances in the model and not from accidental occasions. Therefore, it is stated that meshes of area-sinks should be equal in the different separating layers of a multi-aquifer model. The example in this subsection illustrates the effect of this physical error in a large model and how it should be overcome.

In the example, the results of a model with non-equal area-sink meshes (the first model) is compared with the results of a similar model with equal area-sink meshes (the second model). The results have been exaggerated by taking  $L/\lambda > 3$  in order to show the different behaviour of both models. The models are



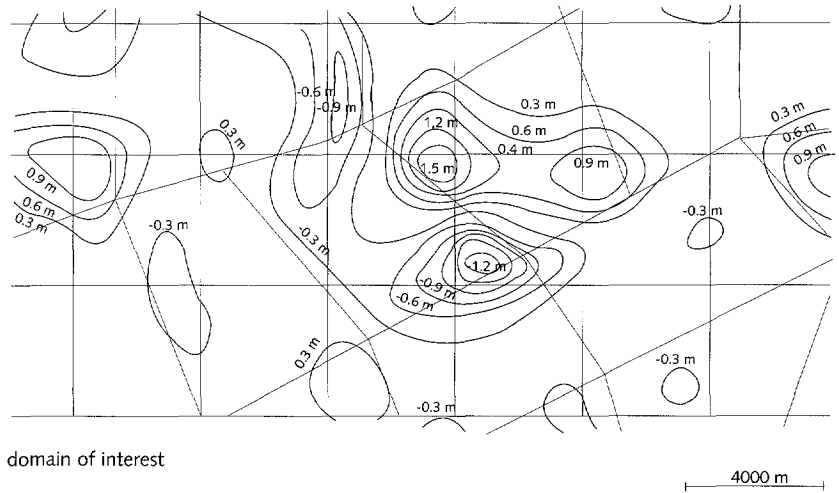


Figure 5.5.4 Computed differences in the head across the separating layer in the domain of interest of the first model (see text).

The differences in the head are in the order of magnitude of 1 m. Such differences across a layer with a resistance of 100 d result in a vertical flow of .01 m/d, which is impossible under Dutch circumstances. The distribution of extreme values is strongly related to the overlaps of the area-sinks on top of the upper aquifer and between the two aquifers.

In the second model both area-sink meshes are equal. In figure 5.5.5, the differences in head across the separating layer in between the aquifers in the second model are presented, also in the area of observation. The computed differences in the head are in the order of magnitude of .01 m, which comply with the flow rates through such a layer with a resistance of 100 d under Dutch conditions.

The effects generated by the difference in the shapes of the area-sinks in the first model are unacceptable and very acceptable in the second model. From this example and from the experiences of the author, it is concluded that the meshes of leakage area-sinks in a model should be equal (particularly in cases where flow paths are to be computed).

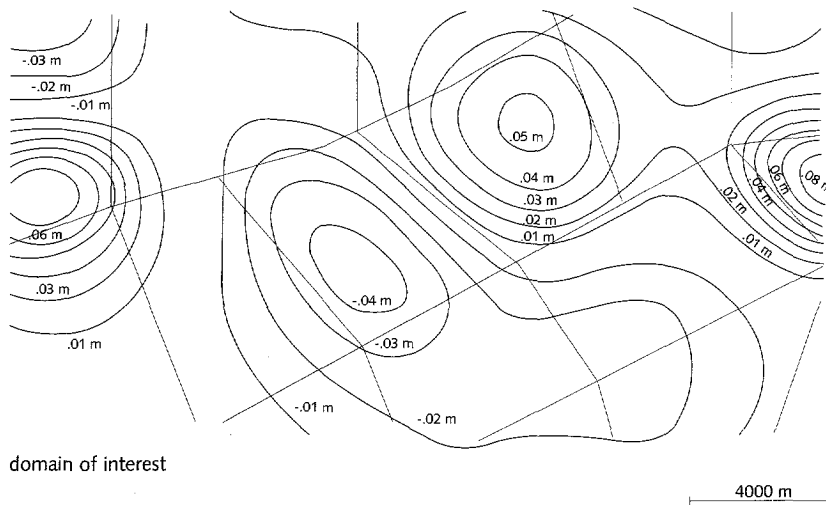


Figure 5.5.5. Computed differences in the head across the separating layer in the domain of interest of the second model.

### 5.5.2. Example of the vertical transfer of effects in a three aquifer model

In a model with three aquifers, the transfer of effects through leakage area-sinks will be shown in terms of the head distributions.

The vertical fluxes are generated by a well in the middle aquifer and transferred by equal meshes of area-sinks simulating the separating layers. The domain of interest (figure 5.5.6) is surrounded by a wide zone of elements. In the domain of interest, the widths of the area-sinks in the direction of flow are smaller than the largest  $\lambda$  (see Strack, 1989 pp. 172-176) in each aquifer in order to comply with the rule  $L/\lambda \leq 1$  (subsection 5.2.3).

In the lower aquifer, the transmissivity of 2000 m<sup>2</sup>/d is diminished considerably to 20 m<sup>2</sup>/d in the south-west half space (figure 5.5.7), which simulates the presence of a zone with a very low permeability. The resistance of the separating layer on top of this aquifer is 5000 d in the south-west half space (figure 5.5.7) and 5000 d in the north-east half space.

In the middle aquifer with a transmissivity of 600 m<sup>2</sup>/d the well withdraws groundwater (30,000 m<sup>3</sup>/d) in the centre of the model (figure 5.5.6). The resistance of the separating layer on top of this aquifer is divided in a south-east domain in figure 5.5.8 with high resistance of 10,000 d and a north-west domain with intermediate resistance of 1000 d.

In the entire upper aquifer, the transmissivity is 1200 m<sup>2</sup>/d. In the north-west domain in figure 5.5.9, the resistance of 500 d of the top layer is lower than that in the south-east domain where it is 5000 d. For the sake of simplicity, the surface water levels are taken at 0 m (equal to the reference level) in all elements of figure 5.5.6.

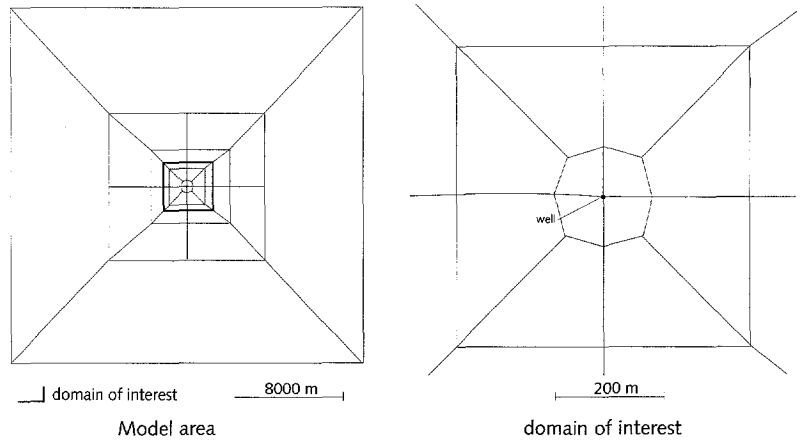


Figure 5.5.6 Mesh of area-sinks in the model area (left) and in the domain of interest (right) with a well.

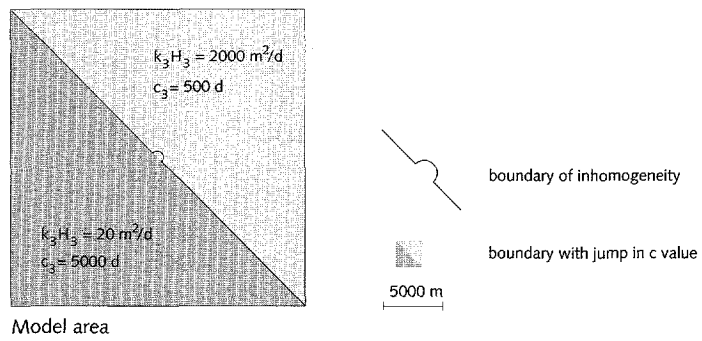


Figure 5.5.7 Transmissivity values in the model area in the lower aquifer and resistance values of the separating layer on top of this aquifer.

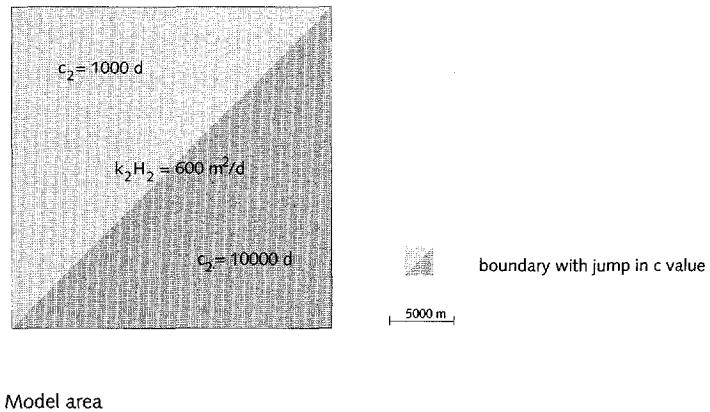
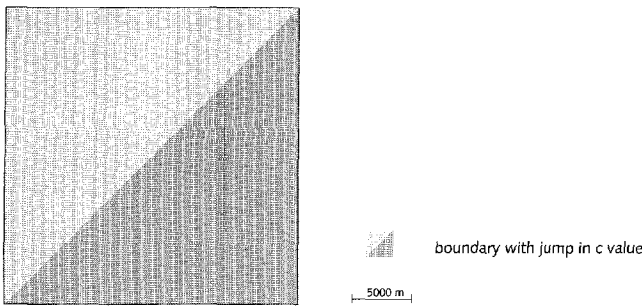


Figure 5.5.8 Transmissivity values in the model area in the middle aquifer and resistance values of the separating layer on top of this aquifer.



Domain of interest

Figure 5.5.9 Transmissivity values in the model area in the upper aquifer and resistance values of the top layer.

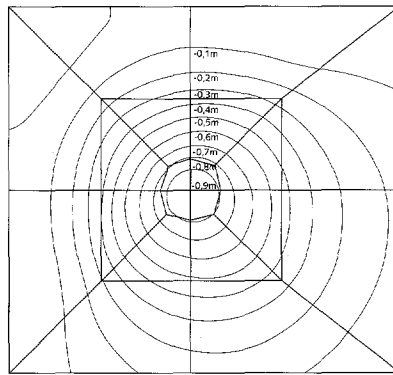
The computed head distribution in the upper aquifer (figure 5.5.10) shows the effect of the difference in the distribution of the resistances of the upper two separating layers. The lowering in the head is less in the domain of the lower resistances, the north-west space in figure 5.5.9.

In the lower aquifer, the effect of the inhomogeneity with the low transmissivity is clearly present in the head distribution of figure 5.5.11.

In the middle aquifer, the head distribution shows the effects of the well combined with the reactions in both adjacent aquifers (figure 5.5.12). In the north-west quadrant, the low resistances of both separating layers above the middle aquifer cause the smallest lowering in the head.

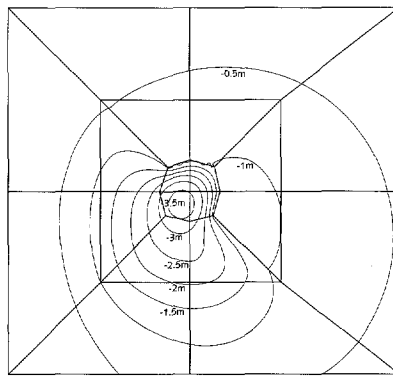
The relatively small lowering in the north-east quadrant is caused by the higher transmissivity in the lower aquifer. In the south-west and south-east quadrants, the opposite occurs as can be seen from the lowering of the head in these directions.

This example shows that the distribution of the head (and also of the flux) in the middle aquifer of a three aquifer model is visibly related to the elements and their properties in the adjacent aquifers and separating layers. Errors in the head or flux may be caused by the analytic elements in all three aquifers. Often the relation can be found between these errors and a specific combination of elements in one of the three aquifers.



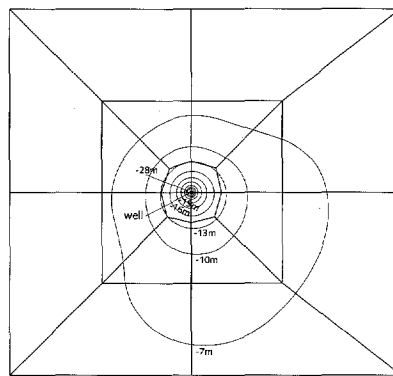
Domain of interest

Figure 5.5.10 Computed head distribution in upper aquifer in the domain of interest.



Domain of interest

Figure 5.5.11 Computed head distribution in the lower aquifer in the domain of interest.



Domain of interest

Figure 5.5.12 Computed head in the middle aquifer in the domain of interest.





## 6 A NEW EXPRESSION FOR THE CAUCHY BOUNDARY CONDITION DESCRIBING THE INTERACTION BETWEEN MANY SURFACE WATERS AND A REGIONAL AQUIFER

### 6.0 Summary

In the model of the Netherlands (De Lange, 1991), large numbers of surface waters in intensively drained regions are lumped over relatively large areas using a Cauchy boundary condition. In this chapter, this boundary condition actually describes the interaction between the flow from or to many parallel equidistant surface waters in a phreatic top aquifer and the groundwater flow in the upper regional aquifer. The flow between these aquifers crosses a separating layer, which is included in the Cauchy boundary condition. New and simple expressions are derived for the two constants in this condition. The results of these simple expressions are compared with the results of other existing (Bruggeman, 1972) and new expressions based on different conceptual models including one with two aquifers. From these comparisons, it is concluded with respect to the simple expressions that: (1) the simplifications used in the derivation are acceptable; (2) the condition applied at the separating layer is preferred; (3) the behaviour of the interaction can be analyzed more clearly by using this new expression than by the existing accurate solution of Bruggeman (1972).

Apart from this, it is shown that with a simple modification the new expressions can be used in the case in which the surface waters are in direct contact with both the top aquifer and the upper regional aquifer, as when they cut through the separating layer.

### 6.1 Introduction

In the general potential theory, a Cauchy boundary condition is a linear relation between the potential and its normal derivative (Bear, 1972). In groundwater flow analysis, the Cauchy condition (expression (3.35)) at the upper boundary expresses the relation between the leakage through a separating layer at the bottom of a surface water and the head in the aquifer below that layer (Bear and Verruijt, 1987). In groundwater modeling, the Cauchy boundary condition is commonly used to simulate individual surface waters, lakes, etc with known resistances at their bottoms (McDonald and Harbaugh, 1984).

NAGROM covers the entire country of the Netherlands, 43,000 km<sup>2</sup>, of which large regions are intensively drained. These areas occur mainly in the lower part of the country (*figure 6.1.1*) and contain up to several hundreds of surface waters per km<sup>2</sup>. NAGROM is used for national water management in which the individual effects of many of the surface waters are not of interest. Therefore, these effects are lumped in Cauchy boundary conditions applied over relatively large areas. In NAGROM, a Cauchy boundary condition expresses the interaction between many surface waters

in a phreatic top aquifer and the groundwater in the upper aquifer of the model (figure 6.1.2, upper part). For use in the model of the Netherlands, simple expressions for the constants in the Cauchy boundary condition have been derived. During the analysis of the applicability of the simple expressions for the constants, comparisons have been carried out with other expressions, the most important of which are presented in this chapter.



Figure 6.1.1 Area below mean sea level in the Netherlands.

For more than twenty years, Cauchy boundary conditions have been used in the Netherlands to model the interaction between surface water(s) and groundwater (Ernst, 1978; Van Drecht, 1982; Querner, 1993). Their derivations are mainly based on older conceptual models in vertical cross-sections that have been used to determine the required spacing between parallel drains (Hooghoudt, 1936; Kirkham, 1958; Ernst, 1962; Dagan, 1964).

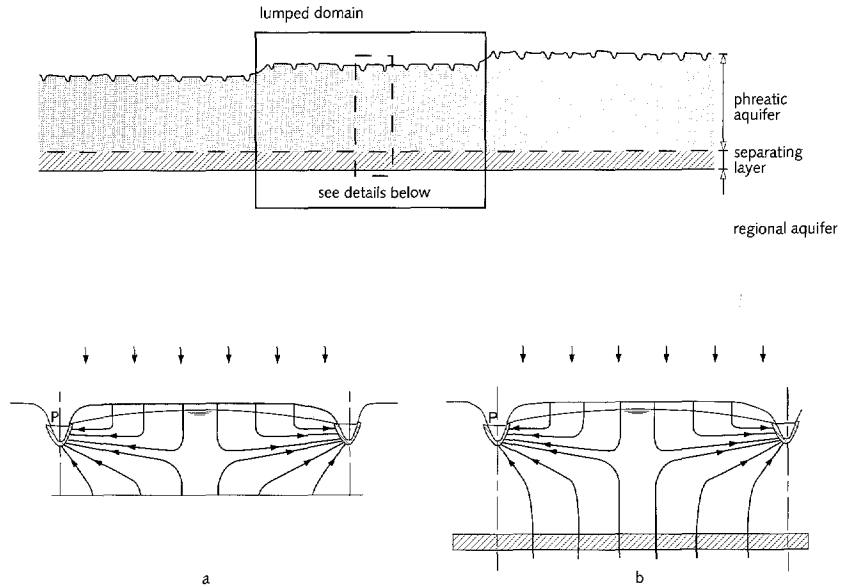


Figure 6.1.2 Conceptual models for the Cauchy boundary condition based on (a) the drainage resistance and (b) the feeding resistance.

Two conceptual models for the Cauchy boundary condition (comparable with expression (3.35)) will be distinguished. The main difference between these models concerns the meaning of the resistance between the surface waters and the groundwater in the upper aquifer of the model.

In the first conceptual model, the (phreatic) top aquifer is the upper aquifer in the groundwater flow model (figure 6.1.2-a). So, this Cauchy boundary condition describes the interaction between the surface waters and the groundwater in the phreatic aquifer over a certain area. The resistance between the surface waters and the top aquifer is called the drainage resistance (Ernst, 1962). Ernst (1978) presents applications of the drainage resistance and develops expressions to include nested systems of surface waters of different dimensions and, therefore, with different effects in the interaction between those surface waters and the groundwater in the aquifer. The drainage resistance is commonly used in the Netherlands, but apart from Ernst (1978) applications have not been published in the international literature.

In the second conceptual model, the (upper) regional aquifer underlying the top aquifer is the upper aquifer in the groundwater flow model (figure 6.1.2-b). The flow in the top aquifer and through the layer separating this aquifer and the regional aquifer is described by the Cauchy boundary condition. The representative resistance between the surface waters and the regional aquifer is called the feeding resistance (Province of Drenthe, 1985).

In the context of types of resistance, the words "drainage" and "feeding" are just part of the names and are not related with the direction of the flow. In both conceptual models, the boundary conditions can be dependent on the flux to or from the surface waters, such as it may occur due to falling dry of a part of the surface waters.

In the following, only the conceptual model for the feeding resistance will be used, except if mentioned otherwise. Apart from this, the analysis in this chapter applies only for equidistant and parallel surface waters generating similar interactions with the groundwater in the regional aquifer. In chapter 7, it will be shown, how this Cauchy boundary condition can be used in situations with arbitrary situated surface waters.

In this chapter, a new and simple expression for the Cauchy boundary condition is presented in the form of new expressions for the two constants in this condition. To provide a solid basis for this new expression, the simplifications used in its derivation are justified and the boundary condition describing the flow through the layer separating the top aquifer and the regional aquifer is verified.

The justification of the simplifications used in the derivation is carried out by comparison of the results of the new expression with the results of an expression derived for a similar conceptual model but without these simplifications (Bruggeman, 1972).

The verification of the lower boundary condition starts with a comparison of the results of the new expression with the results of an expression derived for a similar situation except that the condition at the lower boundary is changed (constant flux instead of variable flow through the separating layer in figure 6.1.2-b). From this comparison, it appears that these expressions may lead to strongly different results. So, only one of the boundary conditions at the lower boundary should be used.

In both comparisons mentioned above, it is concluded that only one constant in the Cauchy boundary condition (the feeding resistance) is needed in a comparison.

In order to judge which of the conditions at the lower boundary should be used, an analytic expression for the feeding resistance is derived for the situation with both the top aquifer and the regional aquifer. In general, the results of this latter expression agree well with the results of the new and simple expression.

In the search to the right conceptual model for the derivation of the expression for the situation with both the top aquifer and the regional aquifer, several conceptual models had to be rejected. Because some of these conceptual models have been used (by others) to compute the value of the drainage resistance numerically, they are summarized and the reason of their rejection is described.

As an extension of the derivation of the expression for the situation with both the top aquifer and the regional aquifer mentioned above, an analytic expression for the feeding resistance has been derived for the situation in which the surface waters are in direct contact with the regional aquifer, so when they cut through the separating layer. This expression is used to show that in this case the feeding resistance can often be found by using a simple formula in which the new expression for the feeding resistance is used.

The derivations of the expressions for the feeding resistance in this chapter are rather complex. Therefore, the derivations are separated from the comparisons between different expressions.

As an exception, all expressions, equations, formula's, etc. in this chapter are indicated as (6,s,n), where s is the number of the section and n is the number within that section.

## **6.2 A simple expression for the Cauchy boundary condition and step one of its verification, comparisons with expressions for flow in the top aquifer only**

### **6.2.1 Derivation of a simple expression for the Cauchy boundary condition based on one-dimensional flow in the top aquifer and a constant head in the regional aquifer**

The Cauchy boundary condition is used to include the interaction between the surface waters and the upper regional aquifer in the actual ground-water model. This interaction determines the flow from (or to) the surface waters to (or from) the regional aquifer via the top aquifer and the separating layer (*figure 6.2.1-a*). In the conceptual model used in the derivations, the surface waters are assumed to have equal dimensions and to be parallel and equidistant. In section 6.1, Ernst's (1978) solution to deal with surface waters of different dimensions has been mentioned and in chapter 7 arbitrary situated surface waters are dealt with. The conceptual model applies to vertical sections between any two of the parallel and equidistant surface waters.

In the forthcoming derivation of the simple expressions for the constants in the Cauchy boundary condition, the differential equation applied is valid in the top aquifer between the borders of the surface waters, which necessitates the derivation of boundary conditions at these borders. In the derivation of the differential equation, the head in the regional aquifer is assumed to be constant, which is interpreted in the way that the effects of the individual surface waters on the groundwater flow in the regional aquifer can be neglected in terms of the local head.

The Dupuit-Forchheimer assumption is used, which results in expressions for the constants in the Cauchy boundary condition in which the resistance to vertical flow is neglected. In order to account for this resistance, two terms are added in the constants in the Cauchy boundary condition, which

partly are based on terms derived by other authors (Ernst, 1962; Van Drecht, 1983).

*The conceptual model*

In the conceptual model of figure 6.2.1-a, the Cauchy boundary condition applies to the groundwater flow in the top aquifer and through the separating layer between the centre of a surface water and the groundwater divide. The underlying regional aquifer is the upper aquifer of the actual groundwater flow model.

In the following derivation, the Dupuit-Forchheimer assumption is used in combination with the assumption that the thickness of the top aquifer is constant. Van Drecht (1983) presents a numerical approach to cope with a situation with a variable thickness. Bear (1979, pp. 181 - 183) describes several analytic solutions for the latter situation, which can not be used here because they lead either to solutions which are too complex (elliptic integrals) or apply to situations that are not valid here.

The head in the regional aquifer below the top aquifer is assumed to be constant. This assumption is valid if the flux coming from each individual surface water is small compared to the flux in the regional aquifer.

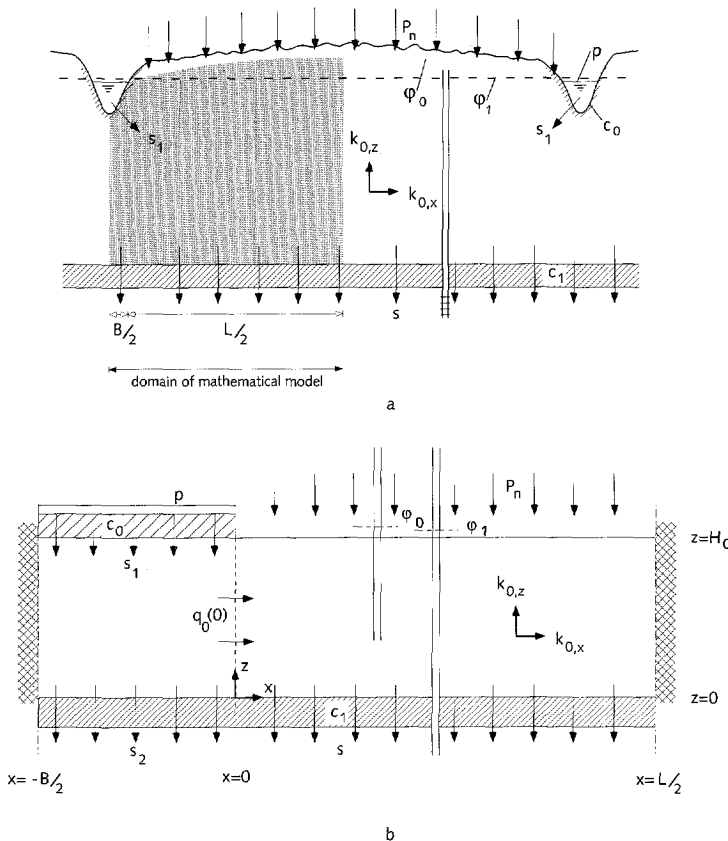


Figure 6.2.1 Conceptual (a) and mathematical (b) model for the Cauchy boundary condition with the feeding resistance.

Between  $x = 0$  and  $x = L/2$  (figure 6.2.1-b), the following differential equation holds.

$$\frac{d^2\phi_0}{dx^2} + \frac{P_n}{k_{0,x}H_0} - \frac{\phi_0 - \phi_1}{\lambda_0^2} = 0 \quad 0 \leq x \leq L/2 \quad (6.2.1)$$

where:

- $c_1$  = resistance of the separating layer [T]
  - $H_0$  = (representative) thickness of the top aquifer [L]
  - $k_{0,x}$  = hydraulic conductivity of the top aquifer in horizontal direction [L/T]
  - $L$  = distance between the surface waters [L]
  - $P_n$  = natural recharge [L/T]
  - $\lambda_0 = \sqrt{c_1 k_{0,x} H_0}$  = the characteristic length [L]
  - $\phi_0$  = head in the top aquifer [L]
  - $\phi_1$  = (constant) head in the regional aquifer [L]
- and  $x = 0$  is defined at the border of the surface water (figure 6.2.1).

#### Boundary conditions

The principal boundary conditions are based on assumptions of symmetry around the centres of the surface waters ( $x = -B/2$ ) and around the water divides between the surface waters ( $x = L/2$ ), leading to:

$$\frac{d\phi_0}{dx} = 0 \quad \text{at } x = -B/2 \text{ and at } x = L/2 \quad (6.2.2)$$

where:

- $B$  = width of the surface water [L]

Because the differential equation (6.2.1) applies to  $x \geq 0$ , the flow and the boundary conditions for  $x \leq 0$  are transformed into a boundary condition at  $x = 0$  (figure 6.2.2). Because  $B$  is generally small (compared to  $L$  and  $\lambda_0$ ), it is assumed that the flux through the bottom of the surface water  $s_1$  and below that place the flux from the top aquifer to the regional aquifer  $s_2$  are constant over the small width  $B$  and can be determined using the average groundwater head in the top aquifer. Assuming a parabolic distribution of the groundwater head, the average groundwater head  $\phi_{0,Bav}$  will be at  $x = -B/6$ .

$$s_1 = (p - \phi_{0,Bav})/c_0 \quad \text{and} \quad s_2 = (\phi_{0,Bav} - \phi_1)/c_1 \quad (6.2.3)$$

where  $p$  is the surface water level [L],  $c_0$  is the resistance of the bottom layer of the surface water [T] and  $s_1$  and  $s_2$  are positive in downward direction (figure 6.2.1). The horizontal flow  $q_0(0)$  [L/T] at  $x = 0$  can be approximated using:

$$q_0(0) = k_{0,x} \times \{\phi_{0,Bav} - \phi_0(0)\} \times 6/B \quad (6.2.4)$$

where  $\varphi_0(0)$  is the head at  $x = 0$ . Continuity of flow over  $-B/2 \leq x \leq 0$  leads to

$$(s_1 - s_2) \times B/2 = q_0(0)H_0 \quad (6.2.5)$$

Combination of (6.2.3), (6.2.4) and (6.2.5) leads to

$$q_0(0) = (p - \varphi_0(0))/c_0'' + (\varphi_1 - \varphi_0(0))/c_1'' \quad (6.2.6)$$

where:

$$c_0'' = c_0 \times (1 + \beta) \times 2H_0/B \quad (6.2.7)$$

$$c_1'' = c_1 \times (1 + \beta) \times 2H_0/B \quad (6.2.8)$$

$$\beta = [(B/2\lambda_0')^2 + (B/2\lambda_0')^2]/3 \quad (6.2.9)$$

where  $\lambda_0'$  ( $= \sqrt{c_0 k_{0,x} H_0}$ ) can be called the minor characteristic length [L]. The first term in the right hand side of (6.2.6) describes the flow from or to the surface water and the second term the flow to or from the regional aquifer. In general,  $\beta$  vanishes for small surface waters.

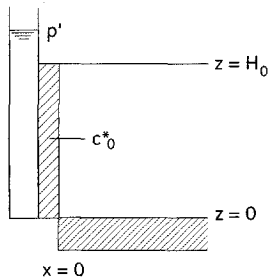


Figure 6.2.2 Mathematical model for the derivation of the boundary condition at  $x = 0$ .

Equation (6.2.6) can be rewritten in a boundary condition at  $x = 0$  (figure 6.2.2).

$$\frac{p' - \varphi_0(0)}{c_0^*} = q_0(0) = -k_{0,x} \frac{d\varphi_0}{dx} \quad (6.2.10)$$

where:

$$p' = (pc_1 + \varphi_1 c_0)/(c_1 + c_0) \text{ and } c_0^* = c_0 \times (1 + \beta) \times 2H_0/B \times c_1/(c_1 + c_0) \quad (6.2.11)$$



### Derivation of the solution and the feeding resistance

With the boundary conditions (6.2.2) at  $x = L/2$  and (6.2.10) at  $x = 0$ , the differential equation (6.2.1) can be solved, leading to:

$$\varphi_0 = \varphi_1 + P_n c_1 + \{p' - \varphi_1 - P_n c_1\} \times \{\exp((L-x)/\lambda_0) + \exp(x/\lambda_0)\} / \{\exp(L/\lambda_0) + 1 + (k_{0,x} c_0^* / \lambda_0) (\exp(L/\lambda_0) - 1)\} \quad (6.2.12)$$

With this solution, an expression can be found for the coefficients in the Cauchy boundary condition. This condition describes a linear relation between the difference between the surface water level and the head in the regional aquifer, and the flux from or to the regional aquifer by:

$$s_{L,av} = (p^* - \varphi_1) / c^* \quad (6.2.13)$$

where  $c^*$  is the feeding resistance [T],  $p^*$  is the modified surface water level [L] and  $s_{L,av}$  is the average flux over  $L$  through the separating layer [L/T]. In fact, (6.2.13) represents the principal definition of both the feeding resistance and the modified surface water level. In this definition, both the seepage through the separating layer  $s$  and the head  $\varphi_1$  in the regional aquifer can be either constant or averaged over the distance between the surface waters  $L$ . In this subsection and in subsection 6.2.2,  $\varphi_1$  is taken constant and in subsection 6.2.3,  $s$  is taken constant. The water balance between  $x = 0$  and  $x = L/2$  is described by:

$$s_{L,av} L = q_0 2H_0 + P_n L \quad (6.2.14)$$

Using (6.2.14), (6.2.10) and (6.2.12) with  $x = 0$  (to calculate  $q_0(0)$ ), the following expressions are found for the constants in (6.2.13):

$$c^* = c_0(1 + \beta)L/B + (c_0 + c_1)L/2\lambda_0 \operatorname{ctnh}(L/2\lambda_0) \quad (6.2.15)$$

$$p^* = p + P_n(c^* - c_1 - c_0) \quad (6.2.16)$$

These expressions are based on the Dupuit-Forchheimer assumption and, therefore, the resistance to vertical flow in the top aquifer is not included in the feeding resistance yet.

### Accounting for two-dimensional flow

In the Dupuit-Forchheimer assumption the resistance to flow in vertical direction in the aquifer is neglected, but not the vertical flow itself (Strack, 1984). The effects of the resistance to vertical flow in the top aquifer can be included in the feeding resistance by two additions.

The first addition concerns the effect on the feeding resistance by the contraction of flow lines near the surface water. Ernst (1962, 1978) suggests that this effect can be approximated by the radial resistance  $c_{rad}$

[T], which simply can be added to the feeding resistance described by (6.2.15).

$$c_{rad} = r_{rad}L \quad (6.2.17)$$

where  $r_{rad}$  is the specific radial resistance [T/L]. Ernst (1962) derived expressions for  $r_{rad}$  based on flow to a small surface water cutting in an aquifer of infinite thickness, which can be seen as a first approximation of the effect of the contraction of the flow in reality. With a minor simplification and assuming that the hydraulic conductivity for radial flow ( $k_r$ ) in an anisotropic medium is the geometric mean of the hydraulic conductivities in the principal directions ( $k_r = \sqrt{k_{0,x}k_{0,z}}$ ), the expressions for  $r_{rad}$  as presented by Ernst (1962, pp. 25-26) can be written as:

$$\left. \begin{aligned} r_{rad} &= \ln(4H_0/\pi B) / \pi a k_{0,x} && \text{if } H_0 \geq \pi B/4 \\ r_{rad} &= \ln(4) / \pi a k_{0,x} && \text{if } H_0 < \pi B/4 \end{aligned} \right\} \quad (6.2.18)$$

where  $a (= \sqrt{k_{0,z}/k_{0,x}})$  is the anisotropy factor [-] and  $k_{0,z}$  is the hydraulic conductivity of the top aquifer in vertical direction [L/T].

The second addition accounts for the effect of the vertical hydraulic conductivity  $k_{0,z}$  in the entire top aquifer by taking its reciprocal value as the vertical resistance per unit thickness of the aquifer. This resistance is assumed to occur over the representative thickness  $H_0$  and is added to the resistance of the separating layer, which is called the lumped resistance of the separating layer  $c_1'$  [T]:

$$c_1' = c_1 + H_0/k_{0,z} \quad (6.2.19)$$

Including these additions the expressions for  $c^*$ ,  $p^*$  and  $\lambda_0$  become:

$$c^* = c_0(1 + \beta)L/B + r_{rad}L + (c_0 + c_1')L/2\lambda_0 \operatorname{ctnh}(L/2\lambda_0) \quad (6.2.20)$$

$$p^* = p + P_n(c^* - c_1' - c_0) \quad (6.2.21)$$

$$\lambda_0 = \sqrt{c_1' k_{0,x} H_0} \quad (6.2.22)$$

If  $L$  is very small,  $c^*$  becomes almost equal to  $c_0 + c_1'$ , which expresses the situation with vertical flow through the layer at the bottom of the surface water which acts in series with the separating layer. In fact, the effect of the top aquifer vanishes in this case.

If  $L/2\lambda_0 > 3$ ,  $c^*$  is approximately linearly related to  $L$ , so (6.2.20) reduces to  $c^* = CL$ , where  $C = c_0(1 + \beta)/B + r_{rad} + (c_0 + c_1')/2\lambda_0$ . Combination of this relation with (6.2.13) and (6.2.14) leads to an expression for  $q_0(0)$  in which  $L$  vanishes.

$$q_0(0) = (p - \phi_1 - P_n(c_1' + c_0)) / (2H_0C) \quad \text{if } L/2\lambda_0 > 3 \quad (6.2.23)$$

This expression shows that the flux  $q_0(0)$  to or from the surface water is approximately constant over  $L$  for  $L/2\lambda_0 > 3$ . This actually means that the flux from or to the surface water reaches its maximum at about  $L = 6\lambda_0$ .

Then, the area at the distance larger than this value of  $L$  is not affected by the surface water any more.

### 6.2.2 Summary of Bruggeman's (1972) derivation of an expression for the Cauchy boundary condition based on two-dimensional flow in the top aquifer and a constant head in the regional aquifer

Bruggeman's (1972) expressions for the constants in the Cauchy boundary are presented for the analysis of the effects of the simplifications used in the derivation of expressions (6.2.20) and (6.2.21), such as the Dupuit-Forchheimer assumption, the boundary condition at  $x = 0$  (expression (6.2.10) ) and the addition of terms for the resistance to vertical flow (expressions (6.2.17) and (6.2.19) ). Because the derivation of these expressions has not been generally published, it is summarized here. In Bruggeman's conceptual model, the boundary conditions are different from those used in subsection 6.2.1. Therefore, they are presented before the actual solution is treated.

#### *Conceptual model*

Bruggeman (1972) derived expressions for the constants in the Cauchy boundary condition in the case of a conceptual model with two-dimensional flow in the top aquifer and with the surface water expressed by a condition on the top boundary at  $-B/2 < x < 0$  (figure 6.2.1). The differential equation is used in the entire domain ( $-B/2 \leq x \leq L/2$ ,  $0 \leq z \leq H_0$ ). In this differential equation, the natural recharge  $P_n$  is omitted first and is added in a second step.

$$k_{0,x} \frac{\partial^2 \phi_0}{\partial x^2} + k_{0,z} \frac{\partial^2 \phi_0}{\partial z^2} = 0 \quad -B/2 \leq x \leq L/2 \quad (6.2.24)$$

#### *Boundary conditions*

The conditions at the vertical boundaries are based on symmetry of the flow in the top aquifer (figure 6.2.1). Equation (6.2.2) is rewritten for two-dimensional flow.

$$\frac{\partial \phi_0}{\partial x} = 0 \quad \text{for } 0 \leq z \leq H_0 \quad \text{at } x = -B/2 \text{ and } x = L/2 \quad (6.2.25)$$

Again, the vertical flux  $s_1$  through the bottom of the surface water is assumed to be constant over the width  $B$ . Along the rest of the upper boundary a zero flux condition is defined.

$$\frac{\partial \phi_0}{\partial z} = \frac{s_1}{k_{0,z}} \quad \text{for } -B/2 \leq x \leq 0 \quad \text{at } z = H_0 \quad (6.2.26)$$

$$\frac{\partial \phi_0}{\partial z} = 0 \quad \text{for } 0 \leq x \leq L/2 \text{ at } z = H_0 \quad (6.2.27)$$

Afterwards,  $s_1$  is replaced by a Cauchy boundary condition, which includes the surface water level and the resistance to the flow from the surface water, according to:

$$s_1 = (p - \phi_{0,Bav})/c_0 \quad (6.2.28)$$

where  $\phi_{0,Bav}$  is the average groundwater head over  $-B/2 \leq x \leq 0$  at  $z = H_0$ , which is analytically determined. Across the lower boundary, the flux depends on the difference in the head across the separating layer.

$$k_{0,z} \frac{\partial \phi_0}{\partial z} (x,0) = \frac{\phi_0(x,0) - \phi_1}{c_1} \quad \text{for } -B/2 \leq x \leq L/2 \text{ at } z = 0 \quad (6.2.29)$$

where again  $\phi_1$  is the constant head in the regional aquifer.

#### *Derivation of the solution*

The differential equation is solved by using finite Fourier transformation over the independent variable  $x$  and applying the boundary conditions. The resulting equation for  $\phi_0(x,z)$  includes  $s_1$ . After this solution the natural recharge  $P_n$  is added along the entire upper boundary ( $-B/2 \leq x \leq L/2$ ). This generates an increase in the head  $\phi_0(z)$  constant in  $x$  with the value of  $P_n \times (c_1 + (H_0 - z)/k_{0,z})$ . To correct for this flow between  $x = -B/2$  and  $x = 0$ ,  $s_1$  is replaced by  $s_1 - P_n$ , leading to the expression:

$$\begin{aligned} \phi_0(x,z) = & \phi_1 + \left[ P_n + \frac{(s_1 - P_n)B}{L+B} \right] * \left[ c_1 + \frac{H_0 - z}{k_{0,z}} + \frac{s_1 - P_n}{\pi^2 k_{0,z}} a(L+B) \right] * \\ & * \sum_{n=1}^{\infty} \frac{1}{n^2} \sin \frac{n\pi B}{L+B} \cos \frac{n\pi x}{L+B} F(n,z) \end{aligned} \quad (6.2.30)$$

where:

$$F(n,z) = \frac{(n\alpha_1 + 1)e^{n\alpha_2} + (n\alpha_1 - 1)e^{-n\alpha_2}}{(n\alpha_1 + 1)e^{n\alpha_3} - (n\alpha_1 - 1)e^{-n\alpha_3}} \quad (6.2.31)$$

$$\alpha_1 = \frac{2\pi k_{0,x} c_1}{a(L+B)} ; \alpha_2 = \frac{2\pi(H_0 - z)}{a(L+B)} ; \alpha_3 = \frac{2\pi H_0}{a(L+B)} \quad (6.2.32)$$

### Derivation of the feeding resistance

The feeding resistance is determined using (6.2.13). For this equation,  $s_{L,av}$  is derived from the water balance between  $x = -B/2$  and  $x = L/2$ :

$$s_{L,av} = \{P_n L + s_1 \times B\} / (L + B) \quad (6.2.33)$$

In this equation  $s_1$  is found using (6.2.28) in which  $\varphi_{0,Bav}$  is determined by integration of (6.2.30) between  $x = -B/2$  and  $x = 0$  at  $z = H_0$ , leading to:

$$s_1 = (p - \kappa_1 P_n - \varphi_1) / \kappa_2 \quad (6.2.34)$$

where:

$$\kappa_1 = c_1' L / (L + B) - \kappa_3 B / k_{0,z} \quad (6.2.35)$$

$$\kappa_2 = c_0 + c_1' B / (L + B) + \kappa_3 B / k_{0,z} \quad (6.2.36)$$

and:

$$\kappa_3 = \frac{a(L+B)^2}{\pi^3 B^2} \sum_{n=1}^{\infty} \frac{1}{n^3} \sin^2 \frac{n\pi B}{L+B} F(n,0) \quad (6.2.37)$$

The average flux  $s_{L,av}$  through the separating layer is determined using the water balance equation (6.2.33). Finally with (6.2.34) and after reworking the result into the form of (6.2.13), this leads to:

$$c^* = c_0 L / B + c_0 + c_1' + \kappa_3 (B+L) / k_{0,z} \quad (6.2.38)$$

$$p^* = p + P_n (c^* - c_1' - c_0) \quad (6.2.39)$$

In the derivation of this expression for  $c^*$ , no approximations have been used and because of that, this solution can particularly be used to determine the accuracy of the implementation of the two-dimensional effects in the expressions based on one-dimensional flow equations (6.2.20) and (6.2.21). The summation in (6.2.37) converges slowly. In general, more than thirty terms are needed. In several computations for the comparison in subsection 6.2.4, more than 3000 terms were needed. Also, the expression (6.2.38) for  $c^*$  is difficult to apply in mathematical analysis such as will be presented in subsection 7.3.1.

### 6.2.3 Derivation of an expression for the Cauchy boundary condition based on one-dimensional flow in the top aquifer and a constant flux through the separating layer.

The case of this subsection is presented in order to show the effects of a different boundary condition at the separating layer. In this case, the flow across the separating layer is changed from variable to constant (figure 6.2.1). So, the head in the regional aquifer will not be constant.

The derivation of the expressions for the constants in the Cauchy boundary condition is similar as it is done in subsection 6.2.1.

Between  $x = 0$  and  $x = L/2$  in *figure 6.2.1*, the following differential equation holds, leading to:

$$\frac{d^2\phi_0}{dx^2} = \frac{s - P_n}{k_{0,x}H_0} \quad 0 \leq x \leq L/2 \quad (6.2.40)$$

where  $s$  is the constant flux through the separating layer [L/T]. For the description of the flow in the domain  $x \leq 0$ , the boundary condition (6.2.10) is used again. In the derivation of this boundary condition, the flow  $s_2$  between  $x = -B/2$  and  $x = 0$  through the separating layer is assumed to be constant, which complies with  $s$  being constant. At  $x = L/2$ , again boundary condition (6.2.2) has been used. Combination of these boundary conditions and (6.2.40) leads to:

$$\phi_0 = (s - P_n)/2H_0 \times \{(x^2 - Lx)/k_{0,x} - c_0^*L\} + p' \quad (6.2.41)$$

In the Cauchy boundary condition (6.2.13), a single value for the head in the regional aquifer is needed. For this, the average head between  $x = 0$  and  $x = L/2$  is used. So, (6.2.13) is changed into (see also explanatory text with (6.2.13) ):

$$s = (p^* - \phi_{1,Lav})/c^* \quad (6.2.42)$$

where  $\phi_{1,Lav}$  is the average head over  $0 \leq x \leq L/2$  in the regional aquifer [L]. The flux  $s$  to the regional aquifer between  $x = 0$  and  $x = L/2$  can be found using:

$$s = (\phi_{0,Lav} - \phi_{1,Lav})/c_1 \quad (6.2.43)$$

where  $\phi_{0,Lav}$  is the average of  $\phi_0$  over  $0 \leq x \leq L/2$ . The expression for  $\phi_{0,Lav}$  is derived using (6.2.41) and (6.2.11) for  $c_0^*$ .

$$\phi_{0,Lav} = p' + (P_n - s) \times (L^2/12k_{0,x}H_0 + c_0^*L/2H_0) \quad (6.2.44)$$

Combination of (6.2.42), (6.2.43) and (6.2.44) leads to:

$$c^* = c_0(1 + \beta)L/B + c_0 + c_1 + (c_0 + c_1) L^2/12\lambda_0^2 \quad (6.2.45)$$

$$p^* = p + P_n(c^* - c_1 - c_0) \quad (6.2.46)$$

Similar to what is done in the derivation of (6.2.20) and (6.2.21), the two corrections for the effects of the resistance to vertical flow (6.2.17) and (6.2.19) can be included, leading to:

$$c^* = c_0(1 + \beta)L/B + c_0 + c_1' + c_{rad} + (c_0 + c_1') L^2/12\lambda_0^2 \quad (6.2.47)$$

$$p^* = p + P_n(c^* - c_1' - c_0) \quad (6.2.48)$$

This expression for the feeding resistance appears to be strongly related to a solution of Ernst (1962) for the drainage resistance. The differences between the conceptual models for the drainage resistance and the feeding resistance have been presented in section 6.1 (figure 6.1.2).

Ernst's (1962) solution for the drainage resistance  $c_{\text{drain}}$  is based on the difference  $\Delta\phi_0$  between the highest groundwater level (at the water divide in between the surface waters) and the surface water level. In fact, his solution is an addition of resistances to vertical flow, to rotational flow (expressed by the radial resistance) and to horizontal flow respectively:

$$c_{\text{drain}} = \Delta\phi_0/P_n = H_0/k_{0,z} + c_{\text{rad}} + L^2/8k_{0,x}H_0 \quad (6.2.49)$$

Opposite to Van Drecht's (1983) statement, this original Ernst formula does not include a term with the entrance resistance  $c_0$ . Using Ernst's approach of adding resistances, Van Drecht (1983) changed Ernst's expression for the drainage resistance to an expression for the feeding resistance simply by the addition of  $c_0$  and  $c_1$ .

Expressions (6.2.47) and (6.2.49) show that the addition of  $c_0$  and  $c_1$  is not straightforward. These constants are left out in (6.2.47) in order to arrive at an expression comparable to (6.2.49). Then (6.2.47) becomes equal to (6.2.49) except for the term with  $L^2$ . This latter term appears with  $1/12$  in (6.2.47) and with  $1/8$  in (6.2.49). In his derivation, Ernst used the maximum head in the top aquifer, whereas for (6.2.47) the average head in the top aquifer has been used. It follows directly from the parabolic shape of the head in the top aquifer that its maximum is  $3/2$  times as high as its average, which explains the difference.

From the similarities in the expressions (6.2.47) and (6.2.49) mentioned above, it is concluded that a constant flux through the separating layer has been implicitly assumed in Van Drecht's adaption of Ernst's expression. Also, it is concluded that the terms with  $c_0$  and  $c_1$  in Van Drecht's expression for the feeding resistance are considerably different from those in (6.2.47).

#### **6.2.4 Comparison of the simple expression for the Cauchy boundary condition with expressions for flow in the top aquifer only**

##### *Context and premises*

In this subsection, the new expressions (6.2.20) and (6.2.21) for the constants in the Cauchy boundary condition (6.2.13) are compared with Bruggeman's (1972) expressions (6.2.38) and (6.2.39) in order to show the effects of the simplifications used in the derivation, such as the one-dimensional flow and the boundary condition at  $x = 0$ . After that, the expressions (6.2.20) and (6.2.21) are compared with the expressions (6.2.47) and (6.2.48) in order to show the effect of using the different boundary condition at the separating layer.

The expressions for  $p^*$  ( (6.2.21), (6.2.39) and (6.2.48) ) are equal and only lead to different results if the values of  $c^*$  are different. Therefore, the comparison is restricted to the expressions for the feeding resistance  $c^*$  ( (6.2.20), (6.2.38) and (6.2.47) ) only.

The primary variable in the comparison between the different feeding resistances is the distance between the surface waters  $L$ . In practice, the geohydrologic constants  $c_0$ ,  $c_1$ , etc. in the expressions for  $c^*$  are roughly estimated over relatively large areas compared to the rather accurate determination of the distance between the surface waters. Also, it is important to know how the feeding resistance will change due to a change in the surface water network which also is expressed in terms of  $L$ . It can be concluded from (6.2.20) and (6.2.47) that  $c^*$  is partly but not completely related to  $L/\lambda_0$ . Also, the relation between  $c^*$  and  $L/\lambda_0$  does not appear clearly from (6.2.38) or from the expressions for  $c^*$  that will be derived in section 6.3. Therefore, the distance parameter is not made dimensionless.

The results of the comparisons are presented in the figures 6.2.3 and 6.2.4. The x-axes in these figures represent the distance between the parallel surface waters. The y-axes in these figures express the ratio between the two feeding resistances in each comparison.

Table 6.2.1 Parameter values applied in the comparisons

parameter		low value	standard value	high value
$c_0$	d	.01	1	100
$c_1$	d	.1	10	1000
$k_{0,z}$	m/d	.1	1	10
$k_{0,x}H_0$	$m^2/d$	$.1 \times .5$	$1 \times 5$	$10 \times 50$
$B$	m	.1	2	10

In the diagrams in figures 6.2.3 and 6.2.4, the ratio between each two feeding resistances is presented for three different values of all geohydrologic constants, which are given in table 6.2.1. The "standard" values of the geohydrologic constants are chosen such that all terms in expression (6.2.20) are effective; there is not a single term dominating the other terms in the expression of feeding resistance. The other two values of the geohydrologic constants are taken considerably larger and smaller than the standard values.

*The effect of the simplifications in the derivation of the new expression for the feeding resistance shown by comparison with Bruggeman's expression*

Figure 6.2.3 shows the ratio between the feeding resistances of (6.2.38) and (6.2.20), which is chosen in order to show the larger differences between both feeding resistances as a ratio smaller than 1. This ratio is in the range of 0.9 to 1.1 in most of the diagrams for any distance between the surface waters  $L$ . This means that the values of the feeding resistances in the two approaches are almost equal. All graphs start close to 1 and



become constant for large values of  $L$ . From the equality of both expressions, it is concluded (see remarks with expression (6.2.21)) that also Bruggeman's expression becomes linear with  $L$  for large values of  $L$ .

The largest differences between both expressions appear for low values of  $k_{0,z}$  (figure 6.2.3-d) and large values of  $k_{0,x}H_0$  (figure 6.2.3-b), which originates from the terms  $c_1'$  and  $r_{rad}$  in (6.2.20) that account for the two-dimensional effects. The larger the thickness of the aquifer or the smaller the vertical hydraulic conductivity becomes the more the effects of the approximations for the resistance to vertical flow in (6.2.20) will show up.

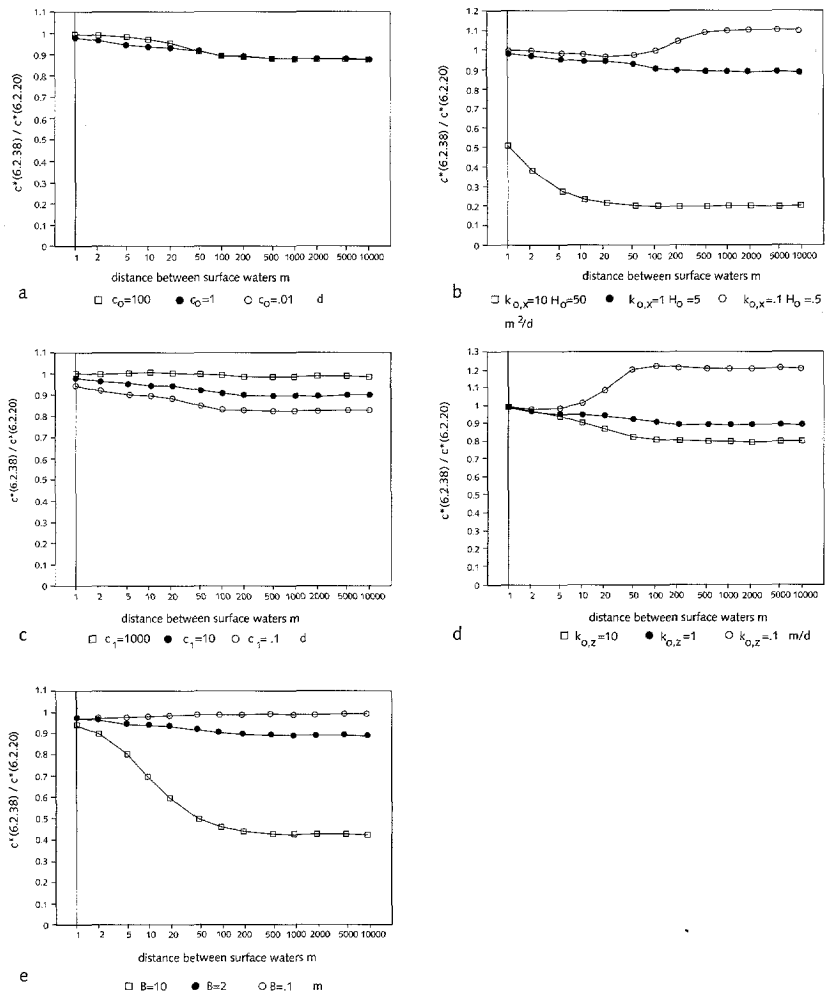


Figure 6.2.3 Ratios between the feeding resistances (6.2.38) and (6.2.20).

The differences showing up for large values of  $B$  (figure 6.2.3-e) originate from the assumptions used in the derivation of the boundary condition at  $x = 0$  (e.g.  $s_2$  being constant over width  $B$ ).

It is concluded that the simplifications in the derivation of the simple expression for the feeding resistance are justified by the results of this comparison.

*The effect of a different boundary condition in the new expression for the feeding resistance shown by comparison with the expression for the case with constant flux across the separating layer*

In figure 6.2.4, the ratio between the expressions (6.2.20) and (6.2.47) is presented, which is chosen in order to show the larger differences between both feeding resistances as a ratio smaller than 1.

In all diagrams of figure 6.2.4, the results of (6.2.20) and (6.2.47) appear to be comparable for  $L \leq 6 \lambda_0$ . The parameter values given in table 6.2.1 lead to the following values for  $\lambda_0$ :  $\lambda_0 = 8.7$  m for standard values,  $\lambda_0 = 87$  m for high  $k_{0,x}H_0$ ,  $\lambda_0 = 0.8$  m for low  $k_{0,x}H_0$ ,  $\lambda_0 = 71$  m for high  $c_1$ ,  $\lambda_0 = 5$  m for low  $c_1$ ,  $\lambda_0 = 7.2$  m for high  $k_{0,z}$  and  $\lambda_0 = 17$  m for low  $k_{0,z}$ .

From analysis of the expressions (6.2.20) and (6.2.47), it becomes clear why the results of these expressions will be different for  $L \geq 6 \lambda_0$ . When  $L$  becomes larger than  $6 \lambda_0$  then (6.2.20) is linear in  $L$  while the last term of (6.2.47) is quadratic in  $L$ . All differences between these feeding resistances due to other parameter variations are minor compared to this difference.

It is concluded from figure 6.2.4 and the above analysis that a different condition at the lower boundary leads to significantly different results of the feeding resistance.

In reality, the distribution of the flux through the separating layer will be neither equal to the distribution generated by the constant head nor equal to the distribution generated by the constant flux. The real distribution depends on the characteristics of both the top aquifer and the regional aquifer and of the separating layer. Therefore, an expression for the feeding resistance based on a two-aquifer schematization is presented in the next section. The results of that expression (6.3.29) will be compared with the results of the simple expression for the feeding resistance. By that comparison it will be shown, that the boundary condition used in the derivation of this simple expression based is to be preferred above the expression based on a constant flux to the regional aquifer.

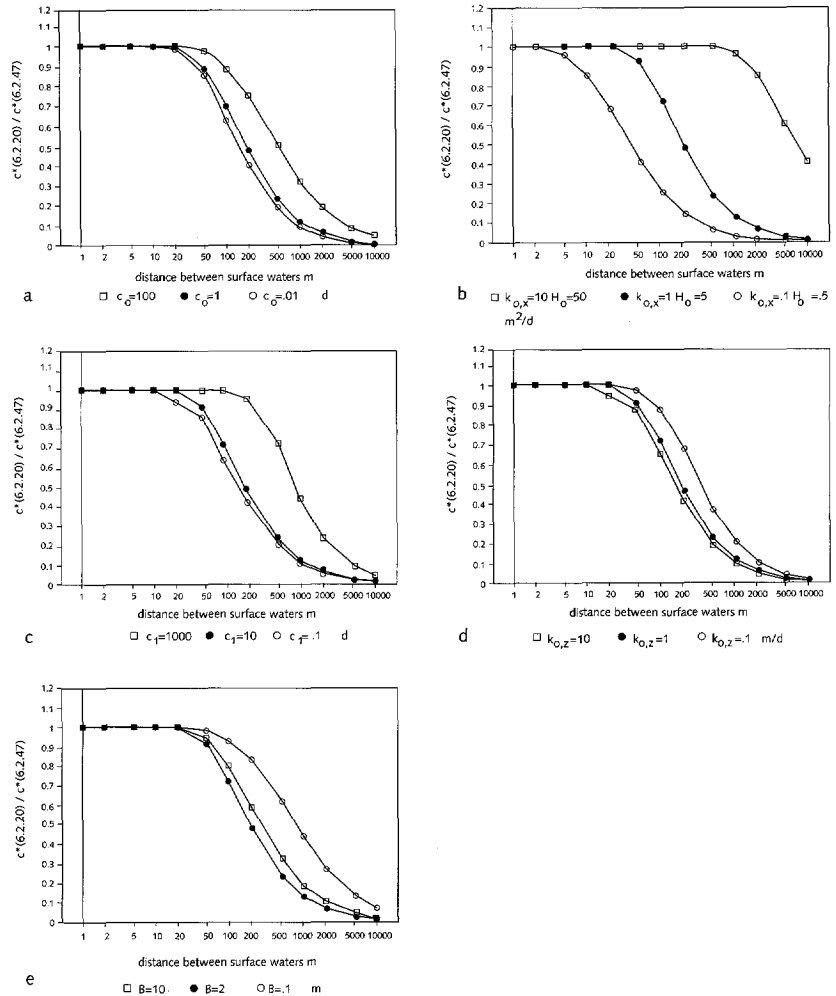


Figure 6.2.4 Ratios between the feeding resistances (6.2.20) and (6.2.47).

### 6.3 Analysis of expressions for flow in both the top aquifer and the regional aquifer and step 2 of the verification of the simple expression for the Cauchy boundary condition

#### 6.3.1 On the suitability of conceptual models describing flow in two aquifers for the derivation of the feeding resistance

In section 6.2, it has been concluded that in reality neither the flux through the separating layer between the top aquifer and the regional aquifer is constant nor the head in the regional aquifer is constant and, therefore, neither of the expressions for the feeding resistance derived in that section are perfect. In order to verify the boundary condition used in the new expression for the feeding resistance (derived in subsection 6.2.1), this expression is compared with an expression for the feeding resistance based on a conceptual model including flow in both the top aquifer and the regional aquifer. To be suitable for the derivation of the feeding resistance, a conceptual

model should describe the principle of a Cauchy boundary condition in a groundwater model, which is (see section 6.1) the interaction between the surface waters in the top aquifer and the groundwater in the upper regional aquifer of the model. In the practice of computing the effects of different scenarios, the Cauchy boundary condition is meant to account for the changes in the flux to or from the regional aquifer due to changes in the flow conditions, e.g. a different surface water level or a different abstraction by a well in the regional aquifer.

In the conceptual models with two aquifers described in this section, the upper aquifer represents the top aquifer in which the surface waters act (figure 6.2.1-a) and the lower aquifer represents the upper regional aquifer which is the actual upper aquifer of the groundwater model. In a suitable conceptual model, there should be an exchange of groundwater between the surface waters and the regional aquifer or - which is the same - between both aquifers.

Several analytic solutions for axial-symmetric cases with wells in multi-aquifer profiles have been presented by various authors (e.g. Huisman, 1972, Maas 1986). The general solution of the differential equation describing (semi-) two-dimensional flow in two aquifers is a classical solution (e.g. Huisman, 1972), but particular solutions of this differential equation, as they are needed here, are rare (see later in this subsection).

During the search for a suitable conceptual model, several conceptual models with two aquifers had to be rejected. These models are discussed here in order to prevent using them in the computation of the feeding resistance.

In these models, the boundary conditions in both the top aquifer and the regional aquifer are based on assumptions of symmetry. As will be shown next, these models describe particular cases of groundwater flow which are not suitable for the derivation of the feeding resistance. The rejected conceptual models are presented together with their practical meaning and the reason why they are not suitable for the derivation of the feeding resistance. The discussion is without a presentation of the solutions in terms of the feeding resistance (which can be obtained from the author).

The enumeration starts with one of the few existing solutions for a two-aquifer system with semi-two-dimensional flow derived by Ernst (1983). After that, the other rejected conceptual models are described.

#### *The Ernst (1983) case*

Ernst (1983, pp. 8-10) presents a solution for a case of groundwater flow in a system of two aquifers separated by a separating layer (figure 6.3.1-a). Ernst defines a constant inflow at the upper boundary (e.g. natural recharge) and zero flow across the base. In the top aquifer, the boundary conditions at the vertical sides are based on symmetry similar to that in the cases of section 6.2. In the regional aquifer, Ernst assumed that there is no horizontal flow

under the surface waters. Ernst did not explicitly describe the outlet of the flow system. In his solution, an integration constant remains, which should have been worked out as a condition that describes the flow to the surface waters.

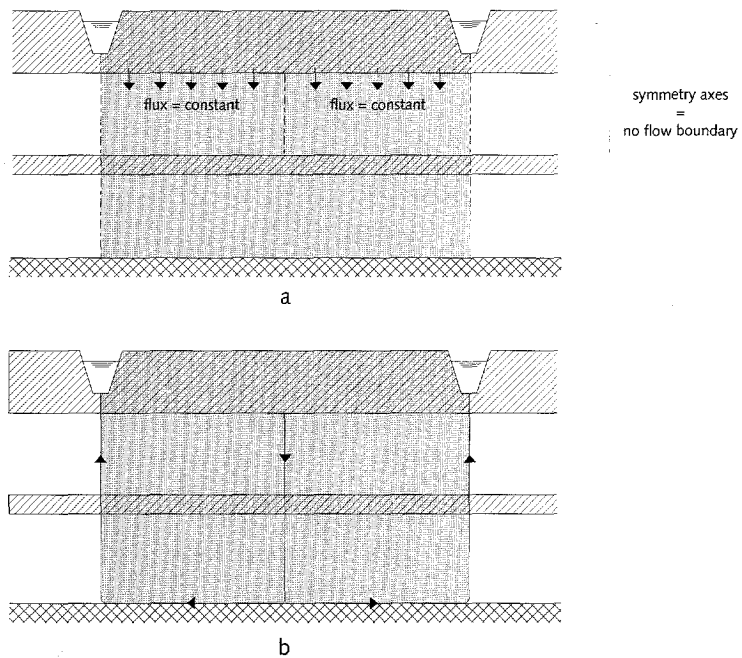


Figure 6.3.1 Conceptual model (a) of Ernst (1983) and the author's interpretation of the schematized flow situation (b).

In the regional aquifer, the no flow boundary conditions determine the outermost streamline of the flow system connected with the top aquifer (figure 6.3.1-b). All the groundwater flowing down through the separating layer flows up again at another place inside the outermost streamline. The combination of this flow system and another flow system in the regional aquifer (as Ernst suggests) does not change the fact that the water in the flow system remains inside that outermost streamline. In other words, there is no net flow from the surface waters to the regional aquifer.

As mentioned in subsection 6.3.1, the Cauchy boundary condition should describe the exchange of groundwater between the surface waters and the regional aquifer (being the top aquifer of the actual groundwater model). The present conceptual model does not describe this exchange, so it can not be used for the derivation of the feeding resistance.

*Other symmetric cases*

In *figure 6.3.2*, two conceptual models with symmetric flow in both of the two aquifers are presented. The boundary conditions in the top aquifer represent the surface waters and the axis of symmetry similar to the case of *figure 6.2.1*. For the sake of simplicity the natural recharge is omitted, because it does not affect the feeding resistance (see (6.2.20), (6.2.38) and (6.2.47)). In the regional aquifer, the boundary conditions are an impermeable base, a no flow boundary and a constant head boundary.

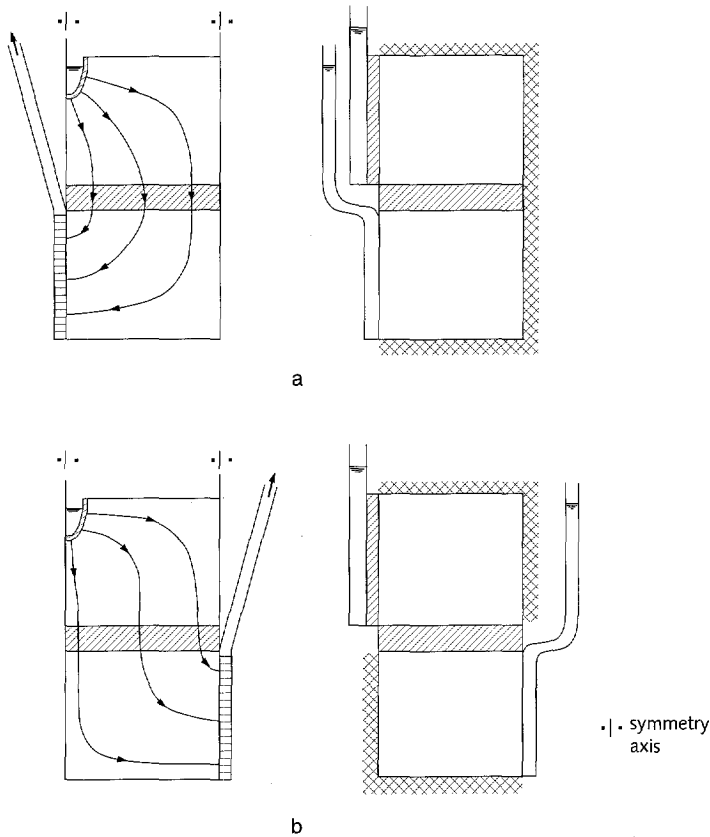


*Figure 6.3.2* Conceptual models with two aquifers and boundary conditions describing symmetric flow; prescribed head condition in the lower aquifer (a) below the surface waters and (b) below the middle between the surface waters.

Both models in *figure 6.3.2* are based on symmetry along the vertical boundaries. Next to each model, a model with boundary conditions mirror-wise can be placed and this can be repeated over and over. Then, it is easy to see that the constant head boundary simulates an internal vertical boundary in the regional aquifer, simulating an infinitely-long head-specified line-sink (or line-source) in the direction perpendicular to the section. The groundwater in such line-sinks is generated by man-made conditions and will flow to or from the surface of the system. The constant head boundary does not simulate the interaction between the surface

water and the regional aquifer, because in reality this interaction does not occur by way of line-sinks. Therefore, both conceptual models are not suitable for the derivation of the feeding resistance. Actually, the groundwater system is again bounded by flow lines similar to those in figure 6.3.1.

### 6.3.2 The general, mathematical solution for a conceptual model with two aquifers

The derivation of the expression for the feeding resistance based on the case with two aquifers starts from the classical differential equation describing the flow in a two aquifer system. Next, the derivation of the general solution (so without implementation of boundary conditions) of this differential equation is presented which also can be found in the literature (Huisman, 1972, pp.37-38).

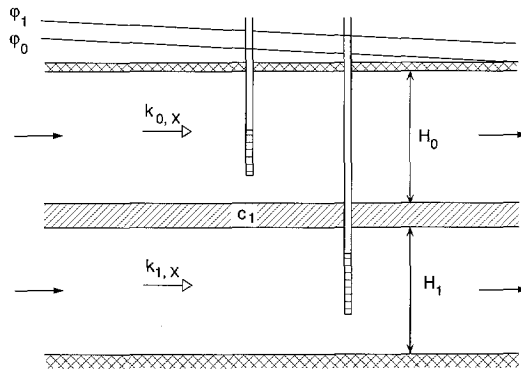


Figure 6.3.3 Conceptual model for flow in two infinite aquifers

As mentioned in subsection 6.3.1, the natural recharge can be omitted in the derivation, because it does not affect the feeding resistance. In the rest of section 6.3, the effects of the resistance to vertical flow are not taken into account, because all cases are based on the Dupuit-Forchheimer assumption. Then the flow in the top aquifer can be described by :

$$\frac{d^2\phi_0}{dx^2} - \frac{\phi_0 - \phi_1}{\lambda_1^2} = 0 \quad (6.3.1)$$

where  $\lambda_0$ ,  $\phi_0$ ,  $\phi_1$  have been explained in section 6.2. The flow in the regional aquifer is described by:

$$\frac{d^2\phi_1}{dx^2} - \frac{\phi_1 - \phi_0}{\lambda_1^2} = 0 \quad (6.3.2)$$

where:

$$\lambda_1^2 = k_{1,x} H_1 c_1 \quad (6.3.3)$$

and

$H_1$  = thickness of the regional aquifer [L]

$k_{1,x}$  = hydraulic conductivity in horizontal direction in the regional aquifer [L/T]

$\lambda_1$  = characteristic length in the regional aquifer [L]

Subtraction of (6.3.1) from (6.3.2) leads to:

$$\frac{d^2 (\varphi_1 - \varphi_0)}{dx^2} - \frac{\varphi_1 - \varphi_0}{\lambda_{01}^2} = 0 \quad (6.3.4)$$

where:

$$\lambda_{01}^2 = \frac{\lambda_0^2 \lambda_1^2}{\lambda_0^2 + \lambda_1^2} \quad (6.3.5)$$

and  $\lambda_{01}$  is the combined characteristic length [L]. The general solution of (6.3.4) is:

$$\varphi_0 - \varphi_1 = C_1 e^{-x/\lambda_{01}} + C_2 e^{x/\lambda_{01}} \quad (6.3.6)$$

Combination of (6.3.6) and (6.3.1) and integrating twice gives the general solution for  $\varphi_0$ .

$$\varphi_0 = \frac{\lambda_{01}^2}{\lambda_0^2} (C_1 e^{-x/\lambda_{01}} + C_2 e^{x/\lambda_{01}}) + C_3 x + C_4 \quad (6.3.7)$$

The general solution for  $\varphi_1$  is found by subtracting (6.3.6) from (6.3.7).

$$\varphi_1 = \frac{\lambda_{01}^2}{\lambda_1^2} (C_1 e^{-x/\lambda_{01}} + C_2 e^{x/\lambda_{01}}) + C_3 x + C_4 \quad (6.3.8)$$

Equations (6.3.7) and (6.3.8) are the general solution of the differential equation describing flow in two aquifers. The integration constants depend on the conditions at the vertical boundaries in both aquifers. The differences between the cases described in subsections 6.3.3 and 6.3.4 apply to differences in these boundary conditions.

### 6.3.3 Derivation of an expression for the feeding resistance based on a conceptual model including both the top aquifer and the regional aquifer

The expression for the feeding resistance is based on a conceptual model that includes both the top aquifer and the regional aquifer. This conceptual model should comply with the basic principle of the Cauchy boundary condition, which is the exchange of groundwater between the surface waters and the regional aquifer being the top aquifer of the actual groundwater model. The boundary conditions following from the conceptual model are



derived in a way that is more or less similar to that in subsection 6.2.1. After solving for the integration constants, the expression for the feeding resistance is found.

#### Conceptual model

Consider a top aquifer and a regional aquifer connected by way of a separating layer (figure 6.3.4). As argued in subsection 6.3.1, the natural recharge is omitted in this conceptual model. In the model presented in figure 6.3.4, the groundwater flows from the surface waters to the deeper groundwater system, or in the opposite direction. The surface waters are connected with the top aquifer via a layer generating the entrance resistance (compare with figure 6.2.1). The thickness of the top aquifer is assumed to be constant (as in subsection 6.2.1).

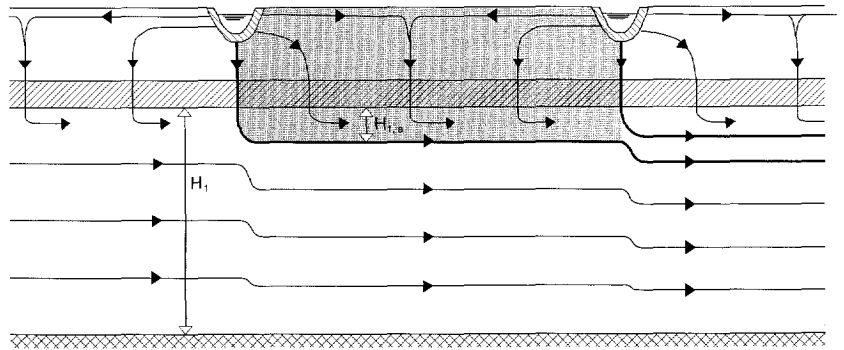


Figure 6.3.4 Conceptual model with two aquifers for the derivation of the feeding resistance

In the regional aquifer in figure 6.3.4, one particular flow line separates the groundwater coming from the surface waters via the top aquifer and the groundwater entering the section via the left boundary in the regional aquifer. This separating flow line starts in the centre of the surface water at the upstream side (left side in figure 6.3.4). Between the surface waters, the part of the regional aquifer above this flow line is considered in the derivation of the solution for the feeding resistance. In the derivation, the thickness of the part of the regional aquifer above this flow line  $H_{1,a}$  is assumed to be constant. At the right boundary, the head in the regional aquifer is specified (taken as the reference level). Similar conceptual models can be placed adjacent to this model. In this conceptual model, there is a real interaction between the surface waters and the groundwater in the regional aquifer.

From continuity of flow it follows that the ratio between  $H_{1,a}$  and the thickness of the entire regional aquifer  $H_1$  equals the ratio of the flux above the separating flow line and the flux through the entire aquifer. So, the value of  $H_{1,a}$  in the following formulas for the feeding resistance is not only determined by geohydrologic constants, but also by the flow situation in the regional aquifer outside the area considered. In the comparison with the one-aquifer solutions for the feeding resistance, the value of  $H_{1,a}$  has

been varied over a wide range, in order to assure that practically all possible realistic flow situations are taken into account.

*Derivation of the boundary conditions*

The heavy flow line in figure 6.3.5-a separates the flow as discussed in the former section. The groundwater flow above this line can be schematized as presented in figure 6.3.5-b.

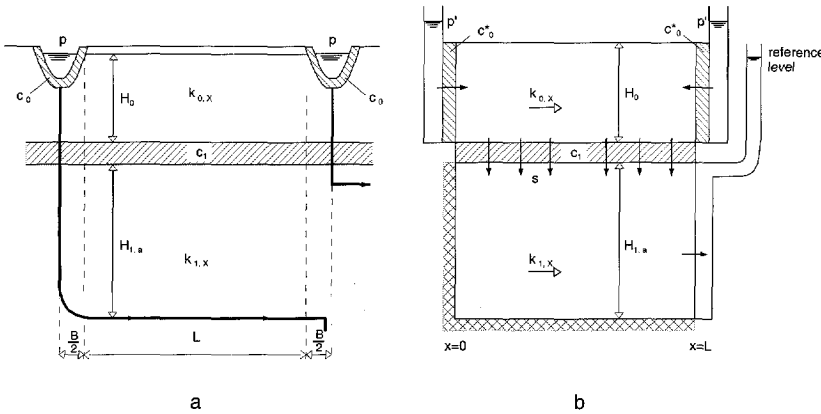


Figure 6.3.5 Detailed conceptual model with two aquifers (a) and its mathematical schematization (b) for the derivation of the feeding resistance

In the top aquifer, the boundary conditions at  $x = 0$  and  $x = L$  describe the interactions with the surface waters similar to those in figure 6.2.2, leading to expressions similar to (6.2.10):

$$\frac{p' - \varphi_0}{c_0^*} = -k_{0,x} \frac{d\varphi_0}{dx} \quad \text{at } x = 0 \quad (6.3.9)$$

$$\frac{p' - \varphi_0}{c_0^*} = k_{0,x} \frac{d\varphi_0}{dx} \quad \text{at } x = L \quad (6.3.10)$$

In the regional aquifer, the heavy flow line generates a no flow boundary on the left hand side and acts as the impermeable base of the flow system. On the right hand side, the head in the regional aquifer is specified equal to the reference level, because the analysis is focused on the feeding resistance.

$$\frac{d\varphi_0}{dx} = 0 \quad \text{at } x = 0 \quad (6.3.11)$$

$$\varphi_1 = 0 \quad \text{at } x = L \quad (6.3.12)$$

Using these four boundary conditions, the integration constants in (6.3.7) and (6.3.8) can be solved.

*Solution of integration constants.*

The integration constants are solved in three steps. In the first step the boundary conditions are combined with the general solution of the differential equation. Combination of (6.3.11) and the derivative of (6.3.8) with  $x = 0$  leads to:

$$C_3 = (C_2 - C_1)\lambda_{01}/\lambda_1^2 \quad (6.3.13)$$

Combination of (6.3.12) and (6.3.8) with  $x = L$  leads to:

$$C_4 = (C_1/\alpha + C_2\alpha)\lambda_{01}^2/\lambda_1^2 - C_3L \quad (6.3.14)$$

where:

$$\alpha = e^{L/\lambda_{01}} \quad (6.3.15)$$

Combination of (6.3.9) and (6.3.7) and its derivative with  $x = 0$  leads to:

$$C_4 = p' - (C_2 + C_1)\lambda_{01}^2/\lambda_0^2 + (C_2 - C_1)k_{0,x}c_0^*/\lambda_{01} \quad (6.3.16)$$

Combination of (6.3.10) and (6.3.7) and its derivative with  $x = L$  leads to:

$$C_3 = (p' - (C_1/\alpha + C_2\alpha))/k_{0,x}c_0^* + (C_1/\alpha - C_2\alpha)\lambda_{01}/\lambda_0^2 \quad (6.3.17)$$

In the second step, these four equations can be reduced to two equations with two unknowns in one step by choosing a particular combination of equations. The first equation is found by combination of (6.3.13) and (6.3.17) and the second equation is a combination of (6.3.13) and (6.3.16).

$$C_2\gamma_1 = p' + C_1\gamma_2 \quad (6.3.18)$$

$$C_2\gamma_3 = p' + C_1\gamma_4 \quad (6.3.19)$$

where:

$$\gamma_1 = \beta_3\beta_2 + \alpha + \alpha\beta_3\beta_1;$$

$$\gamma_2 = \beta_3\beta_2 - 1/\alpha + \beta_3\beta_1/\alpha$$

$$\gamma_3 = \beta_2\alpha + \beta_2L/\lambda_{01} + \beta_1 - \beta_3;$$

$$\gamma_4 = -\beta_2/\alpha - \beta_2L/\lambda_{01} + \beta_1 - \beta_3$$

$$\beta_1 = k_{1,x}H_{1,a}/(k_{0,x}H_0 + k_{1,x}H_{1,a});$$

$$\beta_2 = k_{0,x}H_0/(k_{0,x}H_0 + k_{1,x}H_{1,a})$$

$$\beta_3 = k_{0,x}c_0^*/\lambda_{01}$$

Because the thickness of the considered part of the regional aquifer is  $H_{1,a}$  (figures 6.3.4 and 6.3.5),  $H_1$  in (6.3.3) has been replaced by  $H_{1,a}$ . In the third step, the combination of equation (6.3.18) and (6.3.19) leads to the integration constants  $C_1$  and  $C_2$ .

$$C_1 = p' \quad (6.3.20)$$

$$C_2 = p' \quad (6.3.21)$$

where:

$$\epsilon_1 = (\gamma_3 - \gamma_1)/(\gamma_1\gamma_4 - \gamma_3\gamma_2); \quad \epsilon_2 = (\gamma_4 - \gamma_2)/(\gamma_1\gamma_4 - \gamma_3\gamma_2)$$

The integration constants  $C_3$  and  $C_4$  can be solved using (6.3.13) and (6.3.14) respectively.

$$C_3 = p'(\epsilon_2 - \epsilon_1)\lambda_{01}/\lambda_1^2 \quad (6.3.22)$$

$$C_4 = p'[(\epsilon_1/\alpha + \epsilon_2)\lambda_{01} - (\epsilon_2 - \epsilon_1)L]\lambda_{01}/\lambda_1^2 \quad (6.3.23)$$

*Derivation of the feeding resistance.*

In section 6.2, the feeding resistance (expression (6.2.13)) is defined by using either the average value of the flux through the separating layer and the constant head in the regional aquifer or the constant flux through the separating layer and the average value of the head in the regional aquifer. In the present case, both this flux and head vary and their average values are to be used, leading to:

$$c^* = (p - \phi_{1,Lav})/s_{Lav} \quad (6.3.25)$$

where  $\phi_{1,Lav}$  is the average over  $L$  of the head in the regional aquifer [ $L$ ], which is derived by integration of (6.3.8) over  $0 \leq x \leq L$ .

$$\phi_{1,Lav} = p'\epsilon_3 \quad (6.3.26)$$

where  $\epsilon_3 = \beta_2[(\epsilon_1/\alpha + \epsilon_2)(1 - \alpha)\lambda_{01}/L + (\epsilon_1 - \epsilon_2)L/2\lambda_{01} + \epsilon_1/\alpha + \epsilon_2\alpha]$ .

The average flow through the separating layer  $s_{Lav}$  is found from the water balance in the regional aquifer.

$$s_{Lav}L = -k_{1,x}H_{1,a} \frac{d\phi_1}{dx} \quad \text{at } x = L \quad (6.3.27)$$

leading to:

$$s_{Lav} = p'\epsilon_4 k_{1,x}H_{1,a}/\lambda_{01}L \quad (6.3.28)$$

where  $\epsilon_4 = (\epsilon_1/\alpha + \epsilon_2)(\alpha - 1)\beta_2$ .

Combination of (6.3.25), (6.3.26) and (6.3.28) and using (6.2.11) leads to the expression for the feeding resistance:

$$c^* = \lambda_{01}L/k_{1,x}H_{1,a}(c_1 + c_0)/c_0(1 - \epsilon_3)/\epsilon_4 \quad (6.3.29)$$

which again is a function of geohydrologic constants only. In subsection 6.3.4, this expression will be compared with the expressions derived in section 6.2.

### 6.3.4 Comparison of the expression for the feeding resistance based on flow in both the top aquifer and the regional aquifer with the simple expression presented in section 6.2.

#### Context and premises

The feeding resistance derived in subsection 6.3.3 is compared with the simple expression for the feeding resistance derived in subsection 6.2.1. The comparison concerns the differences and similarities between expression (6.3.29) and expression (6.2.15). Expression (6.2.15) is used instead of expression (6.2.23), because the effects of the resistance to vertical flow have been left out in the conceptual model of section 6.3.3 (figure 6.3.5). Beforehand, it is concluded from subsection 6.2.4 that, if expression (6.3.29) and expression (6.2.15) compare well, the condition at the lower boundary (constant head in the regional aquifer) used in the derivation of expression (6.2.15) is to be preferred above the boundary condition (constant flux to the regional aquifer) used in the derivation of expression (6.2.47).

In the comparisons of the feeding resistances, the same variations of parameter values are used as in subsection 6.2.4 for  $B$ ,  $c_0$ ,  $c_1$  and  $k_{0,x}H_0$ . Because the resistance to vertical flow is not taken into account  $k_{0,z}$  is omitted in the comparison and (6.2.15) is used instead of (6.2.20). The transmissivity of the regional aquifer  $k_{1,x}H_1$  is added to the set of parameters (table 6.3.1). The values of  $k_{1,x}H_1$  are taken rather small because, in general, only a small part of the thickness of the regional aquifer is occupied by the outflow from the individual surface waters (see figure 6.3.4). In order to assure that practically all possible realistic situations are taken into account, a wide range of values is taken.

Table 6.3.1 Parameter values applied in the comparison

parameter	low value	standard value	high value
$c_0$ d	.01	1	100
$c_1$ d	.1	10	1000
$k_{0,x}H_0$ m <sup>2</sup> /d	.1 × .5	1 × 5	10 × 50
$k_{1,x}H_{1,a}$ m <sup>2</sup> /d	.2 × .5	20 × .5	20 × 50
$B$ m	.1	2	10

The result of the comparison is presented in the diagrams in figure 6.3.6, where the y-axes express the ratio between two feeding resistances and x-axes represent the distance between the (parallel) surface waters. This ratio is chosen in such a way that the large differences between both feeding resistances appear as a ratio smaller than 1.

#### Comparison

All diagrams in figure 6.3.6 show, that for small and for large values of the distance between the surface waters  $L$ , the ratios between the feeding resistances are almost constant with  $L$ . Apparently, the relationship be-

tween the cases is consistent. The ratio remains within 0.85 and 1.0, except for extremely low values of the transmissivity of the regional aquifer (*figure 6.3.6-d*). In that situation the two-aquifer schematization is no longer valid (see later). So, the feeding resistances in the comparison can be considered to be about equal taking into account that their values vary from less than 1 to more than  $10^6$  days.

Looking more in detail at *figure 6.3.6*, the following remarks can be made.

The condition of the constant head in the one-aquifer case of subsection 6.2.1 corresponds to an infinitely large transmissivity of the regional aquifer. As shown in *figure 6.3.6*, the feeding resistance (6.2.15) is equal to (6.3.29) if the transmissivity of the regional aquifer is large compared to the transmissivity of the top aquifer (*figure 6.3.6-d*). In that case, the regional aquifer acts like an aquifer with an infinitely large transmissivity. The same applies to the situation in which the transmissivity of the top aquifer is small compared to the transmissivity of the regional aquifer (*figure 6.3.6-b*). The opposite situation, where the transmissivity of the top aquifer is much larger than that of the regional aquifer, is comparable to that with the absence of the regional aquifer. The two-aquifer model is reduced to a one-aquifer model and becomes, in fact, not valid. Therefore, the line expressing the low hydraulic conductivity in the regional aquifer in *figure 6.3.6-d* should be disregarded in the comparison.

In situations where the entrance resistance (*figure 6.3.6-a*) is large, the local effect on the head in the regional aquifer is small, because the fluxes to or from the surface water are small. The constant head in the regional aquifer used in the one-aquifer case is nearly correct then and both cases are almost equal. A small entrance resistance causes a large flux and generates a relevant effect on the head in the regional aquifer and causes the difference between the compared feeding resistances shown in *figure 6.3.6-a*.

An increase in the width of the surface water (*figure 6.3.6-e*) shows similar behaviour as a decrease in the entrance resistance and vice versa, which also can be deduced from (6.3.32). So, the larger the width the greater the differences in the feeding resistances will be.

In situations where the resistance of the separating layer is small (*figure 6.3.6-c*), the effects of the flux from or to the surface water will be very local, as the characteristic lengths in both aquifers are small. The flux through the separating layer will be affected by the surface water only over a small distance. Therefore, the ratio between the feeding resistances for large values of  $L$  (compared to the characteristic length) will be about constant. The higher the resistance of the separating layer, the larger the characteristic length will be and the larger the length will be over which the flow is different in both cases. Then, the feeding resistances for large  $L$  will differ more and more. The shift of the sloping part in the curves of *figure 6.3.6-c* indicates this relationship via the characteristic length. However, the ratios remain constant with  $L$  for large  $L$ .

It is concluded that the results of both expressions for the feeding resistance in the comparison are very similar, except in situations of minor importance. By this conclusion, the verification of the simple expression for the feeding resistance presented in subsection 6.2.1 is completed.

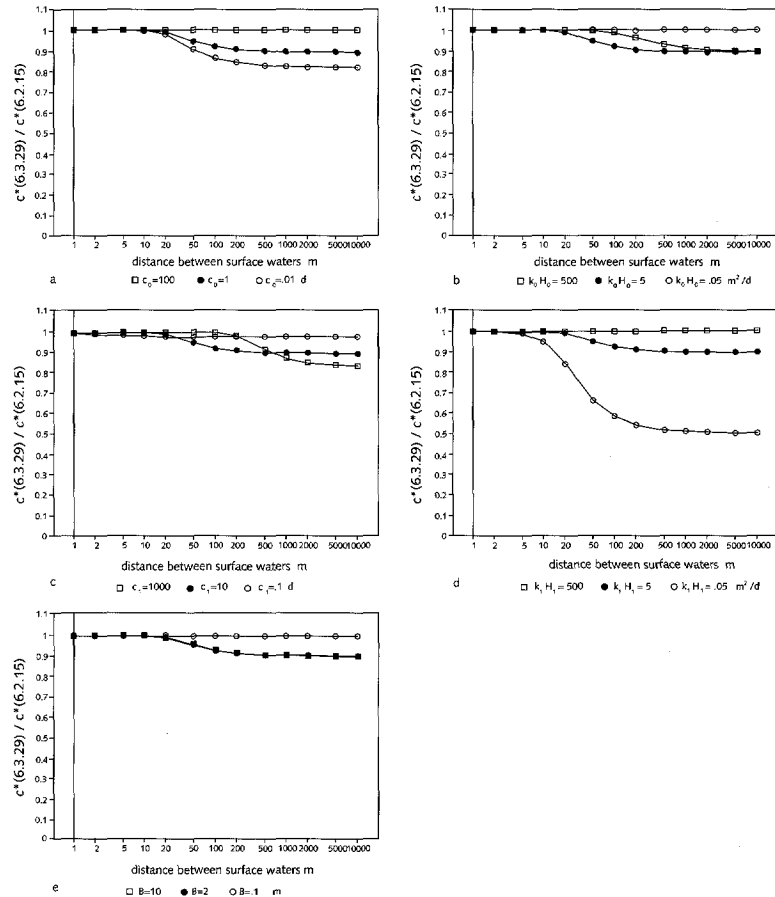


Figure 6.3.6 Ratios between the feeding resistances of (6.3.29) and (6.2.15).

#### 6.4 An expression for the feeding resistance based on a conceptual model with surface waters connected to both the top aquifer and the regional aquifer and its comparison with a more practical expression

##### 6.4.1 Derivation of an expression for the feeding resistance based on a conceptual model with surface waters connected to both the top aquifer and the regional aquifer

Sometimes, the surface waters cut through the top aquifer and even through the separating layer. In such situations, they are in direct contact with the regional aquifer. Once the expression for the feeding resistance for the conceptual model of subsection 6.3.3 was found, it was a small step to find boundary conditions for another two-aquifer conceptual

model. The expression for the feeding resistance is derived similar to the way it was done in subsection 6.3.3.

### Boundary conditions

Figure 6.4.1 shows the conceptual model with the surface waters connected to both aquifers and its mathematical schematization. The direct contact between the surface waters and the regional aquifer is generated by the boundary conditions for the regional aquifer at  $x = 0$  and  $x = L$ . Also, the boundary conditions of the top aquifer are different from that in the previous subsection, because the Cauchy boundary conditions in the top aquifer express the connection of the surface water with that aquifer over its entire thickness. In these boundary conditions, the entrance resistances  $c_0$  are used as they reflect the actual boundary of the surface water.

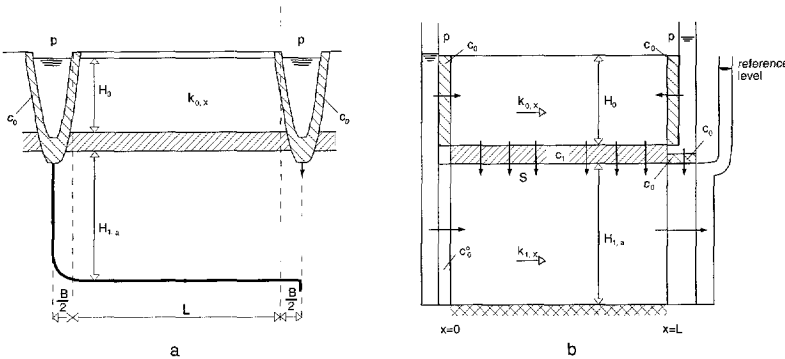


Figure 6.4.1 Detailed conceptual model (a) with surface waters connected to two aquifers and the schematization (b) for the derivation of the feeding resistance.

So, the boundary conditions in the top aquifer are:

$$\frac{p - \varphi_0}{c_0} = -k_{0,x} \frac{d\varphi_0}{dx} \quad \text{at } x = 0 \quad (6.4.1)$$

$$\frac{p - \varphi_0}{c_0} = k_{0,x} \frac{d\varphi_0}{dx} \quad \text{at } x = L \quad (6.4.2)$$

Similar to the way it was done in the case of subsection 6.3.3 (figure 6.3.5), the boundary condition on the left side in the regional aquifer is based on the separating flow line sketched in figure 6.4.1-a. The flow to the regional aquifer through the bottom of the surface water occurs over a width  $B/2$ . This flow is included in the schematization on the left side of figure 6.4.1-b, where it occurs over the entire aquifer thickness  $H_{1,a}$ . The head in the regional aquifer is assumed to be constant over the small width  $B$ . Then, it follows that:

$$(p - \varphi_1)B/2c_0 = (p - \varphi_1)H_{1,a}/c_0^0 \quad \text{at } x = 0$$



and hence:

$$c_0^o = 2H_{1,a}c_0/B \quad (6.4.3)$$

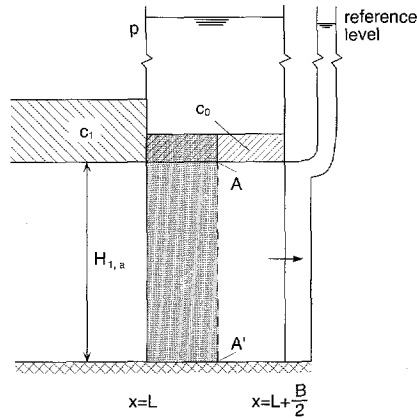


Figure 6.4.2 Scheme for the derivation of the boundary condition at  $x=L$ .

So, the boundary condition on the left side is expressed by:

$$\frac{p - \phi_1}{c_0^o} = -k_{1,x} \frac{d\phi_1}{dx} \quad \text{at } x = 0 \quad (6.4.4)$$

The derivation of the boundary condition on the right hand side in the regional aquifer is based on a difference approach around the section A-A' at  $x = L + B/4$  in figure 6.4.2. Both the flow from the surface water into the regional aquifer and the specified head are included in this boundary condition.

The flux through the vertical section A-A' is determined by the water balance in the shaded domain left of section A-A' in figure 6.4.2.

$$q_1(A)H_{1,a} = q_1(L)H_{1,a} + s_{Bav}'' B/4 \quad (6.4.5)$$

where:

$q_1(A)$  = flux per unit thickness through vertical section over point A [L/T]

$q_1(L)$  = flux per unit thickness through vertical section at L [L/T]

$s_{Bav}''$  = average flux through bottom of surface water over width B/4 in the shaded domain in figure 6.4.2 [L/T]

Assuming that the head  $\phi_1$  is linear between  $x = L$  and  $x = L + B/2$  (figure 6.4.2), the head in the centre of the shaded domain in figure 6.4.2 at  $x = L + B/8$  becomes  $(\phi_1(L) - 0) * 3/4$ , where  $\phi_1(L)$  is the head [L] at  $x = L$  and the reference level at  $x = L + B/2$  equals 0 as mentioned before. The vertical flow from the surface water into the shaded domain in figure 6.4.2 is:

$$s_{Bav}'' = [p - (\phi_1(L) - 0)3/4] / c_0 \quad (6.4.6)$$

Darcy's equation in terms of differences over section A-A' in figure 6.4.2 is expressed by:

$$q_1(A) = k_{1,x}(\varphi_1(L) - 0) / (B/2) \quad (6.4.7)$$

Combination of equations (6.4.5), (6.4.6) and (6.4.7) and using (6.3.12) leads to a Cauchy boundary condition.

$$q_1(L) = (\varphi_1(L) - p\beta_p)/c_1^0 \quad (6.4.8)$$

where:

$$c_1^0 = (16c_0H_{1,a}B)/(32k_{1,x}H_{1,a}c_0 + 3B^2)$$

$$\beta_p = (4B^2)/(32k_{1,x}H_{1,a}c_0 + 3B^2)$$

So, at the right hand side in the regional aquifer, the following Cauchy condition is valid:

$$\frac{p\beta_0 - \varphi_1(L)}{c_1^0} = k_{1,x} \frac{d\varphi_1}{dx} \quad (6.4.9)$$

#### *Solution of integration constants*

In four steps, the four boundary conditions (6.4.1), (6.4.2), (6.4.4) and (6.4.9) are used to solve the four integration constants in the general solution of the differential equations (6.3.7) and (6.3.8). In the first step, the boundary conditions are combined with these differential equations.

Combination of (6.3.7) and its derivative with (6.4.1) and  $x = 0$  lead to:

$$(C_1+C_2)\lambda_{01}^2/\lambda_0^2 + C_4 - p = [(C_2-C_1)\lambda_{01}^2/\lambda_0^2 + \lambda_{01}C_3]k_{0,x}c_0/\lambda_{01} \quad (6.4.10)$$

Combination of (6.3.8) and its derivative with (6.4.4) and  $x = 0$  lead to:

$$-(C_1+C_2)\lambda_{01}^2/\lambda_1^2 + C_4 - p = [(C_1-C_2)\lambda_{01}^2/\lambda_0^2 + \lambda_{01}C_3]k_{1,x}c_0^0/\lambda_{01} \quad (6.4.11)$$

Combination of (6.3.7) and its derivative with (6.4.2) and using (6.3.15) and  $x = L$  lead to:

$$-(C_1/\alpha + \alpha C_2)\lambda_{01}^2/\lambda_0^2 - C_3L - C_4 + p = [(C_2\alpha - C_1/\alpha)\lambda_{01}^2/\lambda_0^2 + \lambda_{01}C_3]k_{0,x}c_0/\lambda_{01} \quad (6.4.12)$$

Combination of (6.3.8) and its derivative with (6.4.9) and using (6.3.15) and  $x = L$  leads to:

$$-(C_1/\alpha + \alpha C_2)\lambda_{01}^2/\lambda_1^2 + C_3L + C_4 - p\beta_p = [(C_2\alpha - C_1/\alpha)\lambda_{01}^2/\lambda_1^2 - \lambda_{01}C_3]k_{1,x}c_1^0/\lambda_{01} \quad (6.4.13)$$

The second step is the elimination of  $C_4$ , leading to three equations with  $C_1, C_2$  and  $C_3$ . The first equation is derived by combination of (6.4.10) and

(6.4.11), the second by combination of (6.4.12) and (6.4.13) and the third by combination of (6.4.10) and (6.4.12).

$$C_1\gamma_5 + C_2\gamma_6 = \lambda_{01}C_3\gamma_7 \quad (6.4.14)$$

$$C_1/\alpha\gamma_8 + C_2\alpha\gamma_9 + p(1-\beta_p) = \lambda_{01}C_3\gamma_{10} \quad (6.4.15)$$

$$C_1(\gamma_{11}-\gamma_{12}/\alpha) + C_2(\gamma_{12}-\alpha\gamma_{11}) = \lambda_{01}C_3\gamma_{13} \quad (6.4.16)$$

where:

$$\beta_4 = k_{1,x}c_0/\lambda_{01}$$

$$\beta_5 = k_{1,x}c_1/\lambda_{01}$$

$$\beta_6 = k_{0,x}c_0/\lambda_{01}$$

$$\gamma_5 = 1 + \beta_1\beta_6 + \beta_2\beta_4$$

$$\gamma_6 = 1 - \beta_1\beta_6 - \beta_2\beta_4$$

$$\gamma_7 = \beta_1 - \beta_4$$

$$\gamma_8 = -1 - \beta_1\beta_6 - \beta_1\beta_5$$

$$\gamma_9 = -1 + \beta_1\beta_6 + \beta_2\beta_5$$

$$\gamma_{10} = \beta_6 - \beta_5$$

$$\gamma_{11} = \beta_1(1 + \beta_6)$$

$$\gamma_{12} = \beta_1(1 - \beta_6)$$

$$\gamma_{13} = L/\lambda_{01} + 2\beta_6$$

In the third step,  $C_3$  is eliminated resulting in two equations with  $C_1$  and  $C_2$ . The first equation is derived by combination of (6.4.14) and (6.4.15) and the second by combination of (6.4.14) and (6.4.16).

$$C_1\delta_1 + C_2\delta_2 = p\delta_5 \quad (6.4.17)$$

$$C_1\delta_3 + C_4\delta_2 = 0 \quad (6.4.18)$$

where:

$$\delta_1 = \gamma_5\gamma_{10} - \gamma_7\gamma_8/\alpha$$

$$\delta_2 = \gamma_6\gamma_{10} - \gamma_7\gamma_9\alpha$$

$$\delta_3 = \gamma_{11} - \gamma_{12}/\alpha - \gamma_5\gamma_{13}/\gamma_7$$

$$\delta_4 = \gamma_{12} - \gamma_{11}\alpha - \gamma_6\gamma_{13}/\gamma_7$$

$$\delta_5 = (1-\beta_p)\gamma_7$$

In the fourth step, the integration constants  $C_1$  and  $C_2$  are solved by the combination of (6.4.17) and (6.4.18). After that,  $C_3$  is derived by using (6.4.14) and  $C_4$  is found by using (6.4.10).

$$C_1 = p\epsilon_5 \quad (6.4.19)$$

$$C_2 = p\epsilon_6 \quad (6.4.20)$$

$$C_3 = p\epsilon_7/\lambda_{01} \quad (6.4.21)$$

$$C_4 = p(\epsilon_8 + 1) \quad (6.4.22)$$

where:

$$\epsilon_5 = -\delta_5\delta_4/(\delta_2\delta_3 - \delta_4\delta_1)$$

$$\epsilon_6 = \delta_5\delta_3/(\delta_2\delta_3 - \delta_4\delta_1)$$

$$\epsilon_7 = (\gamma_5\epsilon_5 + \gamma_6\epsilon_6)/\gamma_7$$

$$\epsilon_8 = \beta_3\epsilon_7 - \gamma_{11}\epsilon_5 - \gamma_{12}\epsilon_6$$

*Determination of the feeding resistance.*

The feeding resistance is derived in a similar way as in the previous case, so using (6.3.25). The equation for  $\varphi_{1,Lav}$  is derived by integration of (6.3.8) over  $L$  and dividing by  $L$ , and using (6.4.19) to (6.4.22). This leads to:

$$\varphi_{1,Lav} = (1 + \epsilon_9)p \quad (6.4.23)$$

where:

$$\epsilon_9 = (\epsilon_5/\alpha + \epsilon_6)(1 - \alpha)\beta_2\lambda_{01}/L + \epsilon_7L/2\lambda_{01} + \epsilon_8$$

The total flux leaving the regional aquifer above the separating flow line at  $x = L + B/2$  (figure 6.4.2) equals the flux through the separating layer  $s_{Lav}$  between the centres of the surface waters and also equals the sum of the flux through the regional aquifer above the separating flow line at  $x = L$  and the flux through the separating layer between  $x = L$  and  $x = L + B/2$ .

$$s_{Lav}(L + B) = q_1(L)H_{1,a} + s_{Bav}B/2 \quad (6.4.24)$$

where:

$s_{Bav}$  = average flux through the bottom of the surface water with width  $B/2$  [L/T]

The horizontal flux at  $x = L$  is found by using (6.4.18) with the derivative of (6.3.8).

$$q_1(L) = p\epsilon_{10}k_{1,x}/\lambda_{01} \quad (6.4.25)$$

where:

$$\epsilon_{10} = [(\alpha\epsilon_6 - \epsilon_5/\alpha)\beta_2 - \epsilon_7]$$

Similar to expression (6.4.6), the flux through the bottom of the surface water  $s_{Bav}$  can be described by (reference level = 0):

$$s_{Bav} = [p - (\phi_1(L) - 0)/2]/c_0 \quad (6.4.26)$$

Application of (6.3.8) with  $x = L$  leads to:

$$s_{Bav} = p\epsilon_{11}B/(2c_0) \quad (6.4.27)$$

where:

$$\epsilon_{11} = 1 + (\alpha\epsilon_6 + \epsilon_5/\alpha)\beta_2/2 - \epsilon_7L/2\lambda_{01} - \epsilon_8/2$$

Combination of equations (6.4.24), (6.4.25) and (6.4.27) leads to an equation for  $s_{Lav}$ . The substitution of this equation for  $s_{Lav}$  and (6.4.23) for  $\phi_{1,Lav}$  in (6.3.25) leads to the following equation for the feeding resistance.

$$c^* = -\epsilon_9(L + B)/(\epsilon_{10}k_{1,x}H_{1,a}/\lambda_{01} + \epsilon_{11}B/(2c_0)) \quad (6.4.28)$$

At first sight, it might be concluded from (6.4.28) that  $c^*$  is linearly related with  $L$ . However, the parameters  $\gamma_{13}$ ,  $\delta_3$  and  $\delta_4$  contain the factor  $L/\lambda_{01}$  and, therefore, the parameters  $\epsilon_5$  to  $\epsilon_{11}$  also contain this factor and  $c^*$  in (6.4.28) is not strictly linear related with  $L$ . In subsection 6.4.2, the results of this expression will be compared with the length-weighted harmonic mean of the resistance of the layer at the bottom of the surface water and the feeding resistance.

## 6.4.2 Comparison of the expression based on a conceptual model in which the surface waters are connected to both the top aquifer and the regional aquifer with a more practical expression

### *Context and premises*

The expression, based on a conceptual model in which the surface waters are connected to both the top aquifer and the regional aquifer, is compared with a more practical expression based on the simple expression presented in subsection 6.2.1. Expression (6.4.28) is compared with the (length-weighted) harmonic mean of the feeding resistance (6.2.15) and the resistance of the layer at the bottom of each surface water (see next).

The situation of *figure 6.4.1-a* occurs many times in thin top aquifers, but expression (6.4.28) is too complex for modeling practice. Therefore, this expression is compared with "the hydrologists first order estimation".

In *figure 6.4.1-a*, the flow in the top aquifer can be separated into two parts, being:

- 1 - Below the surface water the flow is approximately vertical through the bottom layer of the surface water.
- 2 - In the domain between the borders of the surface waters the flow is largely similar to the flow is sketched in *figure 6.1.2-b* describing the situation in which the feeding resistance is determined.

So, the flow from the surface water to the regional aquifer in flow system above the separating flow line in *figure 6.4.1* partly meets the vertical resistance  $c_0$  over twice the length  $B/2$  and partly meets the feeding resistance  $c^*$  over the length  $L$ . Assuming that the head in the regional aquifer is about constant, the difference between this head and the surface water level is equal in the two parts. Then, the combined feeding resistance  $c^*B + L$  over the entire length  $B + L$  can be estimated by the length-weighted harmonic mean of the entrance resistance and the feeding resistance  $c^*$  (6.2.15).

$$c^*_{B+L} = (B + L)/(B/c_0 + L/c^*) \quad (6.4.29)$$

This simple expression for the combined feeding resistance  $c^*_{B+L}$  is compared with the complex expression (6.4.28). The results of this comparison are presented in *figure 6.4.3*.

In this comparison, the variation of the values of the constants is equal to that described in subsection 6.3.4 (table 6.3.1). Also, the ratio of the feeding resistances ( $= (6.4.28) / (6.4.29)$ ), presented in *figure 6.4.3*, is chosen in such a way that the large differences between these feeding resistances appear as a ratio smaller than 1.

### *Comparison*

The main differences between the results are caused by the approach of the length-weighted harmonic mean and by the assumption of a constant head in the regional aquifer used in the derivation of expression (6.2.15).

As mentioned before the constant head implies an infinitely large transmissivity of the regional aquifer.

The largest agreements in the results occur if the transmissivity of the regional aquifer is much larger than the transmissivity of the top aquifer (*figure 6.4.3-b and -d*). Then, the head in the regional aquifer will hardly be affected by the surface waters and will be about constant. In these cases, the differences in the ratio between the feeding resistances are about 20 per cent and remain constant with L.

If the transmissivity of the regional aquifer is much smaller than the transmissivity of the top aquifer (*figure 6.4.3-d*), the differences become large. Then, the regional aquifer is almost absent compared to the top aquifer and all expressions used in the comparison are no longer valid. Therefore, the line for the low transmissivity of the regional aquifer in *figure 6.4.3-d* and the line for the high transmissivity of the top aquifer in *figure 6.4.3-b* should be disregarded (similar to what is done with *figure 6.3.6-d*).

If the resistance of the separating layer is small (*figure 6.4.3-c*), the ratio between the feeding resistances is about 1. This can be explained in the same way as in the previous comparison (*figure 6.3.6-c*). In the other cases in *figure 6.4.3-c*, the ratios between both feeding resistances differ more from 1, but remain within .5 and 1 and for large L they become constant with L.

The larger the width of the surface water, the more effective the surface water will be (*figure 6.4.3-e*). Similar to the previous comparison (*figure 6.3.6-e*), a large width is comparable with a low value of the entrance resistance and vice versa.

From this analysis, it follows that the ratio of the feeding resistances of the considered cases remains generally within the range 0.5 - 2.0. In general, the geohydrological parameters are known not more accurate than with a factor 2 (transmissivity) or 10 (hydraulic resistance). Taking this into account together with the complexity of the situation considered, it may be concluded that the length-weighted harmonic mean is an acceptable estimation in many cases of groundwater modeling, for instance in a model for national groundwater management in which details are lumped.

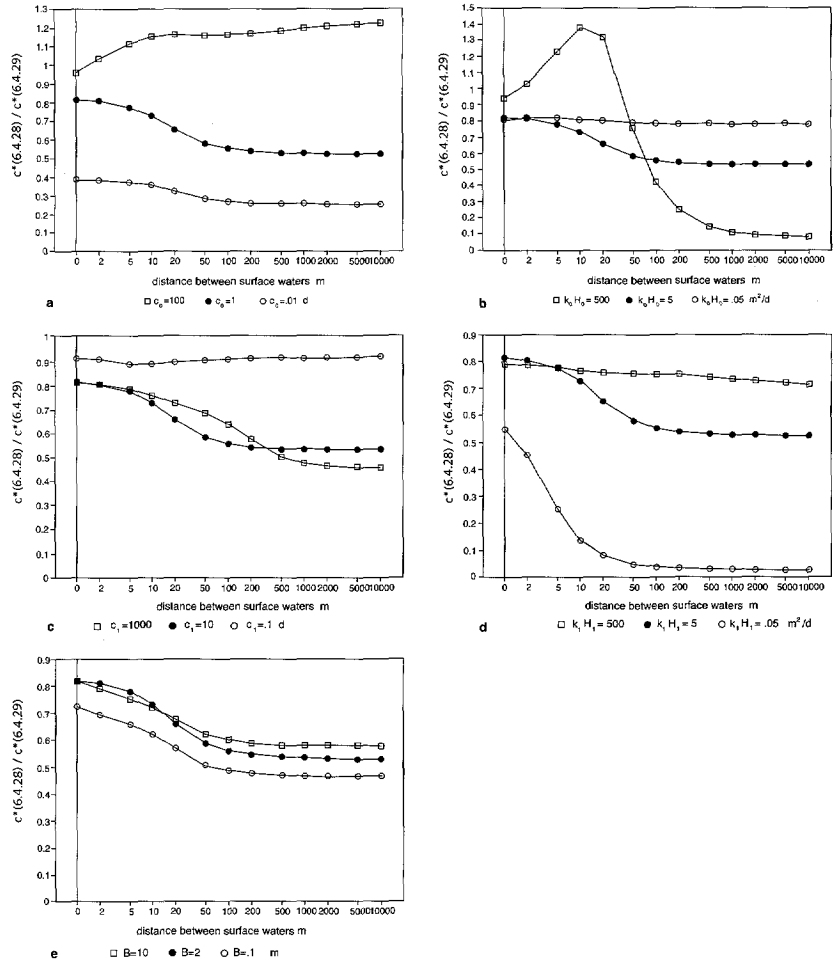


Figure 6.4.3 Ratios between the feeding resistances of equations (6.4.28) and (6.4.29)

## 6.5 Concluding remarks

The Cauchy boundary condition can be used to describe the interaction between many surface waters in a top aquifer and the groundwater in a regional aquifer (which is the upper aquifer of the actual computer model).

The two constants in the Cauchy boundary condition (6.2.13) are called the feeding resistance and the modified surface water level. The feeding resistance can be described in terms of the geohydrologic constants, whereas in the modified surface water level also the natural recharge is included.

Simple expressions are proposed for the feeding resistance (6.2.20) and the modified surface water level (6.2.21). These simple expressions can be implemented simply in computer programs such as spreadsheets and GIS manipulations. Also, these expressions can be used in mathematical manipulations (differentiation and integration) as will be shown in chapter 7.

The simplifications used in the derivation of these simple expressions are acceptable, which follows from a comparison with expressions ((6.2.38) and (6.2.39)) derived without these simplifications.

A change of the boundary condition at the separating layer (a constant flux to the regional aquifer instead of a constant head in the regional aquifer) causes results that are significantly different from the results of the proposed expressions, which follows from the comparison of expressions (6.2.20) and (6.2.21) with expressions (6.2.47) and (6.2.48).

The boundary condition at the separating layer (a constant head in the regional aquifer) leads to results of the feeding resistance ((6.2.15) as simplification of (6.2.20)) that compare well with the results of the feeding resistance (6.3.29) derived for a conceptual model that includes the flow in both the top aquifer and the regional aquifer.

A conceptual model for the derivation of the feeding resistance should include a net flux between the surface waters in the top aquifer and the groundwater in the regional aquifer.

Conceptual models of two aquifers with boundary conditions based on symmetry in the regional aquifer can not be used for the derivation of the feeding resistance, because no net flux between the surface waters in the top aquifer and the groundwater in the regional aquifer occurs.

In situations where the surface water is in direct contact with both the top and the regional aquifer, the feeding resistance often can be approximated by a simple expression (6.4.29) based on the simple expression for the feeding resistance and the resistance of the bottom layer of the surface water.

In the example of section 7.6, the application of the simple expression for the feeding resistance is demonstrated. In chapter 8, its application in NAGROM is described.



## **7 ON THE DETERMINATION OF THE FEEDING RESISTANCE IN CASES WITH ARBITRARY SITUATED SURFACE WATERS**

### **7.0 Summary**

A theoretical basis is presented for the determination of the feeding resistance in areas with arbitrary situated surface waters. In such areas, the groundwater flow is schematized as either predominantly parallel or predominantly axial-symmetric flow. In sub-areas with predominantly parallel flow, the representative feeding resistance can be based on the representative distance between arbitrary situated surface waters calculated from the drainage density. The drainage density is the length of surface waters in a sub-area divided by the size of that sub-area. In sub-areas with predominantly axial-symmetric flow, an expression for the feeding resistance is derived, which shows that this feeding resistance is not related to the drainage density. The representative feeding resistance of the entire area is the area-weighted harmonic mean of the feeding resistances of all the sub-areas.

Considering the complexity of the problem, the feeding resistance in an area with arbitrary situated surface waters can often be based on a simplified version of the drainage density and the simple expression for the feeding resistance that has been presented in chapter 6. The simplified version of the drainage density is the length of surface waters in the entire area divided by the size of that area. Doing this, the effects of the feeding resistance in areas with predominantly axial-symmetric flow are neglected. In an example based on reality, the results of this approach are compared to the results of the area-weighted harmonic mean of the feeding resistances of all the sub-areas. The results appear to be comparable in many cases, which also follows from a theoretical comparison of the same results.

### **7.1 Introduction**

As described in chapter 6, the feeding resistance is an important parameter in the Cauchy boundary condition that describes the interaction between many surface waters and the groundwater in a regional aquifer. The expressions for the feeding resistance in chapter 6 apply to parallel and equidistant surface waters only. In practice (Querner, 1993), these expressions are used also to determine the feeding resistance in situations with arbitrary situated surface waters. In these situations, the representative distance between the surface waters used in the expression for the feeding resistance is often taken equal to the reciprocal of the drainage density, which is defined as the length of surface waters in an area divided by the size of that area. Such an area should be bounded in such a way that the drainage density is approximately constant inside the area. Also, the geohydrologic parameters should be averaged over that area.

In this chapter, a theoretically based approach is presented for the determination of the feeding resistance in areas with arbitrary situated surface waters. In the derivation of this approach, the groundwater flow is assumed to be either predominantly parallel or predominantly axial-symmetric. In areas with predominantly parallel groundwater flow the feeding resistance is based on expression (6.2.20). For the feeding resistance in an area with predominantly axial-symmetric flow a new expression is derived. The so-called representative feeding resistance in an area with arbitrary situated surface waters is determined by the area-weighted harmonic mean of the feeding resistances in the different sub-areas in which either predominantly parallel or predominantly axial-symmetric flow is assumed. Next, the steps used in the derivation of the representative feeding resistance are introduced.

The derivation of the representative feeding resistance in an area with arbitrary situated surface waters starts with the subdivision of the area of concern in sub-areas - bounded by water divides, path lines and surface waters - with predominantly parallel flow or with predominantly axial-symmetric flow. These sub-areas are determined in such a way that they have simple shapes, such as triangles or rectangles (see example in section 7.6). For each different type of sub-area (so either a triangular or a rectangular shape with parallel flow or a triangular shape with axial-symmetric flow), an expression for the feeding resistance is derived.

In the sub-areas with parallel flow, it is assumed that the conceptual model for the feeding resistance (*figure 6.2.1*) can be used in sections along arbitrary but predominantly parallel path lines. In the analysis of the different expressions for the feeding resistance in chapter 6, it has been shown that the distance between the surface waters is an important parameter in the determination of the feeding resistance. In a sub-area with arbitrary situated surface waters, the distance between the surface waters may vary and a so-called representative distance between the surface waters is needed to determine the representative feeding resistance. In this thesis, the representative distance between the surface waters is defined as the distance that leads to the representative feeding resistance in that sub-area to be used in the Cauchy boundary condition (6.2.13).

In the first step concerning sub-areas with parallel flow, the feeding resistance and the representative distance between the surface waters is determined in the simple theoretical case of a triangular area (with predominantly parallel flow) between a straight surface water and a straight water divide forming a corner with an angle smaller than  $90^\circ$  (section 7.3). In this case, a relation between the feeding resistance and the representative distance between the surface waters will be derived based on expression (6.2.20).

In the following steps concerning sub-areas with parallel flow, relations between these two parameters will be derived for sub-areas with predominantly parallel flow between surface waters forming a rhomb and

forming a parallelogram. It appears that in these cases the representative distance between the surface waters can be based on the reciprocal of the drainage density. This relation can be used also in many situations of sub-areas with predominantly parallel flow. So, the drainage density is important in the determination of the representative feeding resistance. Therefore, it is discussed separately in section 7.2.

For (triangular) sub-areas with axial-symmetric flow, an expression for the feeding resistance will be derived based on the analytic solution for flow towards a well in a semi-confined aquifer (section 7.4). In this situation, the drainage density is not applicable.

Having the expressions for the feeding resistance in these sub-areas, any area with arbitrary situated surface waters can be covered completely by sub-areas with a value for the feeding resistance. Then, the overall feeding resistance in that area can be found (section 7.5). In an example with surface waters situated as it occurs in reality (section 7.6), the feeding resistance is compared with its practical version.

## 7.2 The drainage density

In his summary of drainage-basin characteristics Horton (1932) mentions that the drainage density has first been suggested by Newman (1900) as an important parameter in drainage applications. Horton defined the drainage density as the sum of the lengths of all surface waters in a drainage basin divided by the area of that basin. He also mentioned, that "the reciprocal of the drainage density is the average distance between the surface waters" and that "one-half the reciprocal of the drainage density is the average horizontal distance between streams and appurtenant watershed-lines". However, no proof of this is given and it is assumed by the author that the boundaries of the drainage basins are the surface watershed-lines.

In this thesis, the definition of the drainage density  $M$  [1/L] is adapted for the use in the determination of the feeding resistance in arbitrary situations and is expressed by:

$$M = \sum^J (\sum^I l_{i,j}) / \sum^J A_j \quad (7.1)$$

where  $\sum^I l_{i,j}$  is the sum of the lengths of all surface waters (I) in sub-area  $A_j$  and  $A_j$  is a sub-area in which expression (6.2.20) can be used to determine the feeding resistance. Expression (7.1) applies to situations with predominantly parallel flow only. If the sub-area  $A_j$  is bounded by groundwater divides and path lines, the surface waters are completely inside that sub-area and the lengths of these surface waters  $l_{i,j}$  can be used straight forward in the summation  $\sum^I l_{i,j}$ . If the sub-area  $A_j$  is (partly) bounded by a surface water, only half of the width of the surface water is draining inside the sub-area. In other words this means that half of the "draining

capacity" of the surface water is used. Because only the length of the surface water is taken into account here, the half of the "draining capacity" is included by taking half of the length of this surface water (so  $l_{i,j}/2$ ) in the summation  $\sum l_{i,j}$ .

The reciprocal of the drainage density is exactly equal to the distance between parallel equidistant surface waters. This can easily be shown by taking  $J = 1$  in (7.1) between any pair of water divides. Because in this situation expression (6.2.20) holds in any (rectangular) area between water divides, in (7.1) the sum of the lengths of  $I$  surface waters with equal lengths is divided by the product of  $I$  times the distance between the parallel surface waters and the length of the surface waters. The reciprocal of this result is the distance between each pair of the surface waters. This distance is the representative distance to be used for the determination of the representative feeding resistance, because all distances between the surface waters are equal. So in this situation, the representative distance between the surface waters  $L_{rep}$  (see definition in section 7.1) is exactly equal to the reciprocal of the drainage density, which is expressed by:

$$L_{rep} = 1/M \tag{7.2}$$

Next, it will be shown that this relation is approximately exact also for use in the determination of the representative feeding resistance in a situation of an area with parallel non-equidistant surface waters (figure 7.1).

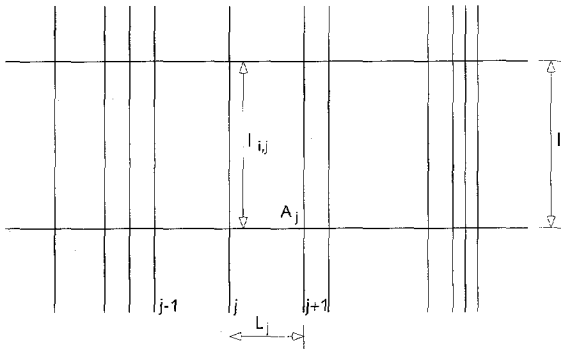


Figure 7.1 Arbitrary set of parallel surface waters

Consider a strip in normal direction to an arbitrary combination of infinitely long parallel surface waters (figure 7.1). In this strip (with width  $l$ ), the length of each surface water  $l_{i,j}$  equals  $l$ . In sub-domain  $A_j$  between the surface waters  $j$  and  $j + 1$  inside the strip expression (6.2.20) holds, because the path lines are parallel and their lengths are equal. Because each sub-domain  $A_j$  is bounded by two surface waters, expression (7.1) can be used in each sub-domain  $A_j$  by taking half of the length ( $l_{i,j}/2$ ) of the two ( $I = 2$ ) bounding surface waters in the summation  $\sum l_{i,j}$ .

The representative feeding resistance  $c^*_i$  (|| indicates parallel flow) for the entire area  $A_{tot}$  equals the area-weighted harmonic mean of the feeding resistance  $c^*_j$  of the sub-domains  $A_j$ , which rule is based on summation of parallel resistances:

$$A_{tot}/c^*_i = \sum^J (A_j/c^*_j) \quad (7.3)$$

The area of each sub-domain can be expressed by  $A_j = L_j \sum^I l_{i,j}$ , where  $L_j$  is the distance between surface water  $j$  and surface water  $j + 1$  (figure 7.1). Similarly, the entire area  $A_{tot}$  can be described by the expression  $A_{tot} = L_{rep} l_{sum}$ , where the meaning of  $l_{sum}$  will become clear in expression (7.4). As described in the text with expression (6.2.20), under certain conditions, the feeding resistance is approximately linearly related with the (representative) distance between the surface waters. In this derivation, it is assumed that both  $c^*_i$  and  $c^*_j$  are linearly related with  $L_{rep}$  and  $L_j$  respectively by one and the same constant  $C$ . This implies that  $c^*_i = CL_{rep}$  and  $c^*_j = CL_j$ , where  $C$  is determined in expression (6.2.23). The expressions for  $A_{tot}$ ,  $c^*_i$ ,  $A_j$  and  $c^*_j$  derived in this paragraph are substituted in expression (7.3), leading to:

$$l_{sum} = \sum^J (\sum^I l_{i,j}) \quad (7.4)$$

So,  $l_{sum}$  appears to be the sum of the lengths of all surface waters in the entire area. In expression (7.1), the denominator equals  $A_{tot}$ , which leads to the following elaboration:

$$M = \sum^J (\sum^I l_{i,j}) / A_{tot} = l_{sum} / L_{rep} l_{sum} = 1/L_{rep} \quad (7.5)$$

which shows that, also in this situation, the drainage density equals the reciprocal of the representative distance between the surface waters.

The distances between the surface waters may vary so much in the area of concern that the feeding resistance is not linearly related with the distance between the surface waters as mentioned above (see also text with expression (6.2.23)). Then, the following steps can be carried out to derive the representative feeding resistance. (1) The drainage density is determined for a sub-area taken so small that the linear relation can be used. (2) The representative feeding resistances for these sub-areas are determined. (3) The representative feeding resistance over the entire area of concern is determined using (7.3), in which the summation applies to the sub-areas in which the linear relation holds.

### 7.3 The representative feeding resistance in areas with predominantly parallel flow

#### 7.3.1 The representative feeding resistance in an area between a straight surface water and a straight water divide forming a corner with an angle smaller than $90^\circ$

In *figure 7.2-a*, a situation is presented of groundwater flow between two surface waters in the top aquifer. This flow pattern is similar to that sketched in the sectional profile of *figure 6.1.2-b* and is computed with a model of analytic elements. The surface waters are simulated by numerous line-elements with a specified head (= surface water level, see subsection 3.3.2), by which the variation in the flux to the surface water is accounted for.

In *figure 7.2-a*, the path lines start along the bisector representing the water divide (with almost stagnant flow), then curve (in the zone with very slow flow) to become more and more parallel before entering the surface waters in normal direction. The groundwater flow in the situation of *figure 7.2-a* occurs mainly near the surface waters. In this part of the area, the path lines are approximately parallel. So, the larger part of the resistance to flow is felt in the area with approximately parallel path lines. Therefore, the flow is schematized as presented in *figure 7.2-b*. The greatest differences between the flow patterns in parts a and b of *figure 7.2* appear near the water divide, where the flow is negligible compared to the flow near the surface waters.

In real situations, it may occur that the water infiltrated in the top aquifer at some distance from the surface waters directly flows to the underlying regional aquifer. The larger the area in which this occurs, the shorter the path lines to the surface waters in the top aquifer and the more the remaining parts are approximately straight. Then, the approximation of straight path lines becomes more and more realistic. For the picture of *figure 7.2-a*, the parameters in the model are chosen such that all path lines in the top aquifer cover the full range between the water divide and the surface water.

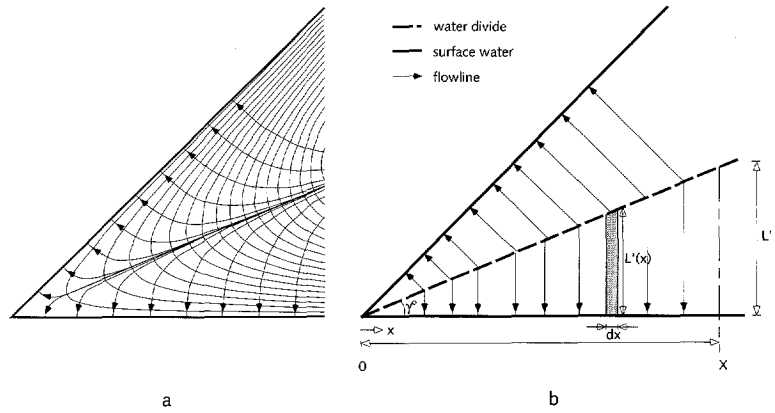


Figure 7.2 Flow (a) between two straight surface waters, schematized (b) to determine the feeding resistance.

In the case with the schematized flow pattern (figure 7.2-b), the flux to the surface water (e.g. over an infinitesimal distance  $dx$ ) increases with the distance to the corner, because the inflow area increases. This agrees with the distribution of the flux to the surface water in the situation of figure 7.2-a.

The representative feeding resistance is determined for the triangular domain between the surface water, the water divide and the bounding path line at distance  $X$  from the corner (figure 7.2-b). Along each path line in this triangular domain, the conceptual model of figure 6.2.1-a is assumed to be valid. The vertical flux  $s(x)$  through the separating layer (figure 6.2.1) in the triangular domain is defined as a function of the distance  $x$  to the corner by using expressions (6.2.13) and (6.2.20). It follows from (6.2.13), that  $s(x)$  is constant (the line-average flux) along each path line. The area-average flux  $s_{av}$  is determined by integration of  $s(x)$  over the triangular domain and divided by the area of that domain. This area-average flux is substituted in expression (6.2.13) to determine the representative feeding resistance over the triangular domain.

In a strip of width  $dx$ , representing a flow conduit along which the conceptual model of figure 6.2.1-a is assumed to be valid, the flux  $dS$  through the separating layer [ $L^3/T$ ] is:

$$dS = s(x)L'(x)dx \quad (7.6)$$

where  $L'(x)$  is the distance between the surface water and the water divide along the schematized path line at  $x$ . The flux  $s(x)$  is derived from (6.2.13) in which  $c^*$  comes from (6.2.20). With  $L'(x) = x \tan \gamma^0$  (where  $\gamma^0$  is the corner between the surface water and the water divide), this leads to:

$$d[S/(p^* - \varphi_0)] = R_2 dx' / [R_1 + c \tanh(x')] \quad (7.7)$$

where:

$$\begin{aligned}
 R_1 &= 2\lambda_0 R_3 / R_4 && [-] \\
 R_2 &= \lambda_0^2 / (R_4 \tan \gamma^0) && [L^2/T] \\
 R_3 &= (1 + \beta) c_0 / B + r_{rad} && [T/L] \\
 R_4 &= (c_0 + c_1') && [T] \\
 x' &= (x \tan \gamma^0) / \lambda_0 && [-]
 \end{aligned}$$

where  $\beta$ ,  $\lambda_0$ ,  $B$ ,  $c_0$ ,  $c_1'$  and  $r_{rad}$  have been explained in subsection 6.2.2. After rewriting  $\text{ctnh}(x')$  in exponential functions with  $x'$ , integration for  $0 \leq x \leq X$ , so for  $0 \leq x' \leq X'$  with  $X' = X \tan \gamma^0 / \lambda_0$  leads to:

$$\begin{aligned}
 \frac{S}{p^* - \phi_1} = R_0(X') = R_2 X' & \left[ \frac{2R_1}{R_1^2 - 1} + \frac{R_2}{2(R_1 + 1)} \ln \left| \frac{(R_1 + 1) + (1 - R_1)e^{-2x'}}{2} \right| + \right. \\
 & \left. + \frac{R_2}{2(1 - R_1)} \ln \left| \frac{(1 - R_1) + (R_1 + 1)e^{-2x'}}{2} \right| \right] \quad (7.8)
 \end{aligned}$$

where  $R_0(X')$  is defined to simplify the expressions in the forthcoming part of the derivation. The representative feeding resistance for parallel (index  $\parallel$ ) flow in a corner (index  $\angle$ ) between the water divide and the surface water  $c^*_{\parallel}$  is determined by using (6.2.13) in which  $s_{av}$  is the average flux over the triangular domain A:

$$c^*_{\parallel} = (p^* - \phi_1) / s_{av} \quad (7.9)$$

Using  $s_{av} = S/A$ ,  $A = XL'/2$ ,  $X = L'/\tan \gamma^0$  and (7.8) in (7.9), the expression for the representative feeding resistance becomes:

$$c^*_{\parallel} = L'^2 / 2R_0(X') \tan \gamma^0 \quad (7.10)$$

This expression describes the representative feeding resistance for the triangular domain and is valid if the corner between the surface water and the water divide has an angle smaller than  $90^\circ$ , because then the path line closes a triangular domain (figure 7.2-b). This means that the corner between the surface waters is restricted to an angle smaller than  $180^\circ$ . In the example of subsection 7.6, it will be shown that surface waters forming a corner with an angle larger than  $180^\circ$  cause essentially non-parallel flow to the edge of the corner (along the rest of the line parallel flow occurs). This flow situation is classed in the category of cases with predominantly axial-symmetric flow. The feeding resistance for areas with this type of flow will be derived in section 7.4.

The expression (7.10) does not give a simple relation between the representative feeding resistance and the representative distance between the surface waters  $L_{rep}$ . After some numerical experiments with the distances used in expression (6.2.20), it appeared that the results of (7.10) can be compared with the results of (6.2.20) if the distance between the surface waters  $L_{rep}$  is replaced by the maximum distance  $L'$  between the



surface water and the water divide in the observed area (see figure 7.2-b). As shown in figure 7.3, the ratio between the results of expression (7.10) and of (6.2.20) with  $L_{rep} = L'$  remains within 1 and 1.15 for an arbitrary range of values of  $c_1$ . Similar distributions of this ratio are found for all other parameters, including  $\gamma^p$ . Apparently both expressions behave similar for large and small values of  $L_{rep}$  and only deviate in a minor sense in the in between range for  $L_{rep}$ .

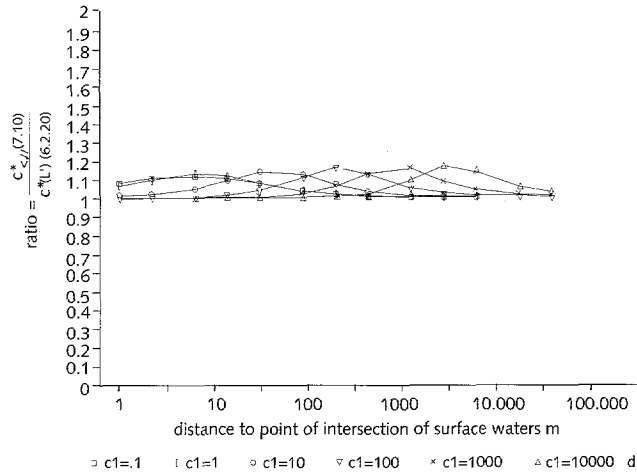


Figure 7.3 Ratio between feeding resistance of (7.10) and of (6.2.20) with  $L_{rep} = L'$ .

This use of  $L'$  in (6.2.20) implies that the "representative distance between the surface water and the water divide" (see scheme of figure 6.2.1) will be equal to  $L'/2$ , which "occurs" at  $X/2$  in figure 7.2. Although this seems like linear averaging, it does not necessarily mean that a simple linear relation between  $L'$  and  $c^*$  has to exist in the entire corner area, because both feeding resistances in the ratio of figure 7.3 are partly non-linear with  $L'$ .

From the fact that the ratios in figure 7.3 (where  $L_{rep} = L'$ ) are close to 1, it is concluded that the representative distance between surface waters as used for the calculation of the representative feeding resistance in a triangular area - bounded by a path line, a surface water and a water divide - with predominantly parallel flow can be estimated by the maximum distance between the surface water and the water divide in that area.

### 7.3.2 The representative feeding resistance in the situation of parallel flow in quadrangular areas bounded by surface waters

For the determination of the representative feeding resistance, the ground-water flow between four surface waters forming a rhomb is presented in figure 7.4-a in a situation similar to that in figure 7.2-a. The path lines have been computed using a model of analytic elements (figure 7.4-a) and schematized afterwards (figure 7.4-b). As shown in figure 7.4-b, the rhomb can be subdivided into eight triangular sub-domains with predominantly parallel flow. Each of these sub-domains is bounded by a surface

water, a water divide and a path line similar to the situation in *figure 7.2-b*. The maximum distance between the water divides and the surface waters is equal for all eight triangular sub-domains. Using the final conclusion in subsection 7.3.1, it follows that the representative distances between surface waters are equal in all eight triangular sub-domains and, therefore, the representative feeding resistances in these areas are equal. So, the representative feeding resistance of the rhomb area becomes equal to the feeding resistance of each of these triangular sub-domains.

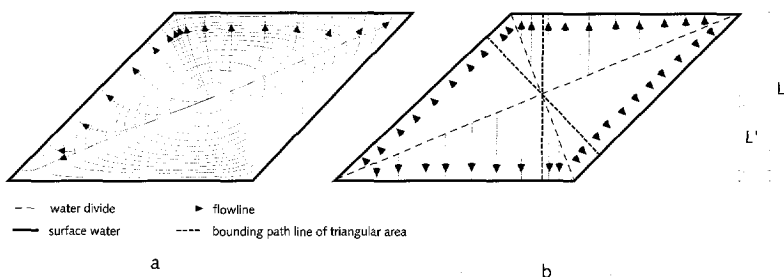


*Figure 7.4* Flow (a) between four surface waters forming a rhomb, schematized (b) to determine the feeding resistance.

The feeding resistance for the rhomb area can be based on (6.2.20) taking the representative distances in the sub-areas equal to the distance between the surface waters and the point of intersection of the water divides. This distance also equals half the distance between each pair of parallel surface waters. The representative distance between the surface waters resulting from the drainage density of the rhomb area agrees with this: *Figure 7.4* represents a part of an area with two crossing sets of equidistant parallel surface waters. The length of surface waters in any rhomb-shaped area bounded by surface waters is twice as large as in the case of parallel surface waters in *figure 7.1*. This results in a representative distance that is half the distance between two parallel surface waters. So, the drainage density leads to the correct representative distance for the representative feeding resistance in the rhomb area.

In *figure 7.5-a*, the flow between four surface waters forming a parallelogram is presented in a situation similar to that in *figure 7.2-a* and this computed flow pattern is schematized in *figure 7.5-b*. The latter figure forms the basis for the derivation of the representative feeding resistance in a parallelogram area. The parallelogram area can be subdivided in eight triangles forming two "half-rhombs" and two rectangular areas. In the two "half-rhombs", the representative feeding resistance can be derived as described in the paragraph above, which means that it can be based on the representative distance following from the drainage density. In the rectangular sub-domains the flow is equal to flow between two parallel surface waters (section 7.2). The feeding resistance in each of these sub-domains agrees with the representative length based on the drainage density. So, the feeding resistance in each sub-domain of the parallelogram area can be based on the respective drainage densities.

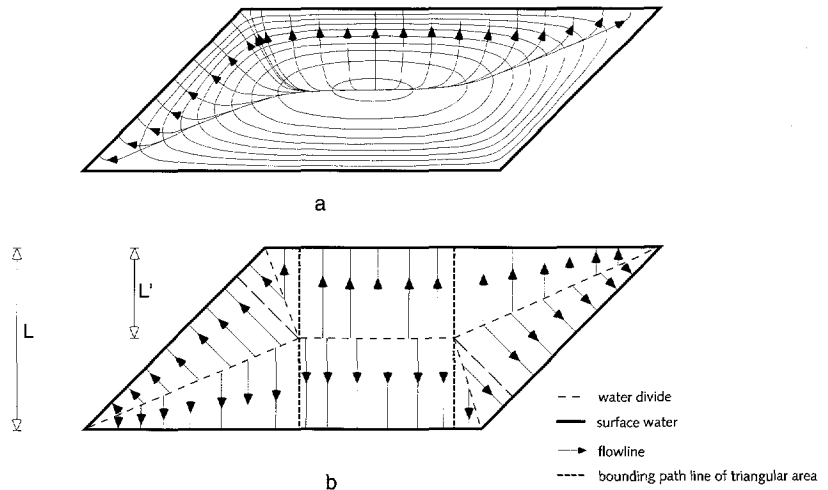


Figure 7.5 Flow (a) between four surface waters forming a parallelogram, schematized (b) to determine the feeding resistance.

The representative feeding resistance  $c^*_1$  of the entire parallelogram area  $A_1$  is determined by the area-weighted harmonic mean of the feeding resistances of the sub-domains, expressed by:

$$A_1/c^*_1 = \sum_{\square} A_{\square j}/c^*_{\square j} + \sum_{\Delta} A_{\Delta j}/c^*_{\Delta j} \quad (7.11)$$

where  $c^*_{\square j}$  is the feeding resistance of the rectangular (= index  $\square$ ) sub-domain  $A_{\square j}$  and  $c^*_{\Delta j}$  is the feeding resistance of the triangular (= index  $\Delta$ ) sub-domain  $A_{\Delta j}$ .

Expression (7.11) will be reworked in a way that is similar to the derivation of expression (7.4) from expression (7.3). The areas of the two ( $J_{\square} = 2$ ) rectangular sub-domains are described by  $A_{\square j} = L_j \sum l_{ij}$  and those of the eight ( $J_{\Delta} = 8$ ) triangular sub-domains by  $A_{\Delta j} = L_j \sum l_{ij}/2$ . The area of the parallelogram is described by  $A_1 = L_{rep} l_{sum}$ , where  $l_{sum}$  will be determined in expression (7.12). Again, it is assumed that one linear relation exists between the different feeding resistances  $c^*$  and the distances between the surface waters in the different sub-areas. So,  $c^*_{\square j} = CL_j$  is taken for the rectangular sub-domains,  $c^*_{\Delta j} = CL_j/2$  is taken for the triangular sub-domains (see last paragraph of sub-section 7.3.1) and  $c^*_1 = CL_{rep}$  is taken for the parallelogram area. Substitution of these expressions in expression (7.11) leads to:

$$l_{sum} = \sum_{\square} \frac{I}{\sum l_{ij}} + \sum_{\Delta} \frac{I}{\sum l_{ij}} \quad (7.12)$$

So,  $l_{sum}$  is equal to the total length of all surface waters in the parallelogram, which means that expression (7.12) is equal to expression (7.4).

Substitution of this expression and of  $A_{||} = L_{rep}l_{sum}$  in expression (7.1) leads to expression (7.5). So, the drainage density can be used to determine the representative distance between surface waters for the computation of the representative feeding resistance in the parallelogram area, as long as one linear relation (so a single value of  $C$ ) exists between the different feeding resistances and the representative distances for all sub-domains as well as for the entire parallelogram area. In situations where this linear relation is not valid, the approach described in the last paragraph of subsection 7.3.1 can be used.

### **7.3.3 The representative feeding resistance for an arbitrary area with predominantly parallel flow bounded by surface waters making corners with angles smaller than 180°**

Any arbitrary area bounded by surface waters making corners with angles smaller than 180° can be subdivided in triangles and rectangles similar to the way shown for the parallelogram area. If again, the linear relation mentioned in the last paragraph of subsection 7.3.2 exists, expression (7.11) leads to expression (7.12). The resulting  $l_{sum}$  can be used in expression (7.4), which leads to expression (7.5) and the drainage density is again the reciprocal of the representative distance between the surface waters. So, the drainage density (7.1) can be used to determine the representative distance in any area with predominantly parallel flow bounded by surface waters forming corners with angles smaller than 180°. If the linear relation does not exist, the approach described in the last paragraph of subsection 7.3.1 can be used.

### **7.3.4 Discussion of flow pattern analysis in literature**

Youngs (1992) analyses patterns of flow to surface waters forming amongst others a rectangle and a parallelogram by using both analytic and numerical solutions. He presents the distribution of the horizontal flux in the area together with that of the discharge potential (expression (3.5)). His pattern of the discharge potential in the case of the parallelogram is essentially the same as the pattern of the groundwater head in *figure 7.5*, which is to be expected because in both cases the transmissivity is constant, so a linear relation between the discharge potential and the groundwater head exists (see equation 3.6).

Youngs mentions that the flow to the surface waters decreases to zero in edges of corners between surface waters with angles smaller than 90°. For corners with angles greater than 90°, he mentions that the flux to the corner is non-zero but remains finite. In his text, he does not mention that the angles should be smaller than 180°. The analysis in this thesis agrees with Youngs observations concerning the flux to the edges of the corners (between surface waters) with angles smaller than 90° and for corners with angles greater than 180° (which case will be discussed in section 7.4). For corners with angles between 90° and 180°, the schematized models of *figures 7.2-b*, *7.4-b* and *7.5-b* result in no flow to the edge of these corners, which is most likely because of the following. Both in the cases of

Youngs (1992) and in the cases discussed in this section, the surface waters form a head-specified boundary, which causes that all path lines enter or leave in the direction perpendicular to the surface waters. In all cases, the water divide is along the bisector between the surface waters starting from the edge of the corner. In the edge of the corner the distance between the surface water and the water divide is zero, so the length of the path line in the edge in perpendicular direction to the surface water is zero. So, no path line can exist to or from the edge of the corner between the surface water and the water divide with an angle smaller than  $90^\circ$ . Therefore, there can not be any flow from (or to) the edge of a corner between surface waters that is smaller than  $180^\circ$ . This is opposite to Youngs statement mentioned above. It is most likely, that Youngs conclusions are affected by numerically-based solutions e.g. for the case of flow in a parallelogram area.

#### 7.4 The feeding resistance in situations with predominantly axial-symmetric flow

Figure 7.6-a shows the flow pattern between infinitely long parallel surface waters which are all interrupted over an equal distance, computed by a model of analytic elements. This flow is schematized in figure 7.6-b, which shows that axial-symmetric flow is assumed near the tips of the surface waters and parallel flow in the rest of the area. Similar to the flow pattern in figure 7.2, the flow close the surface waters predominantly determines the schematized flow pattern. The flow near each tip is approximately axial-symmetric and is assumed to be centred at that tip.

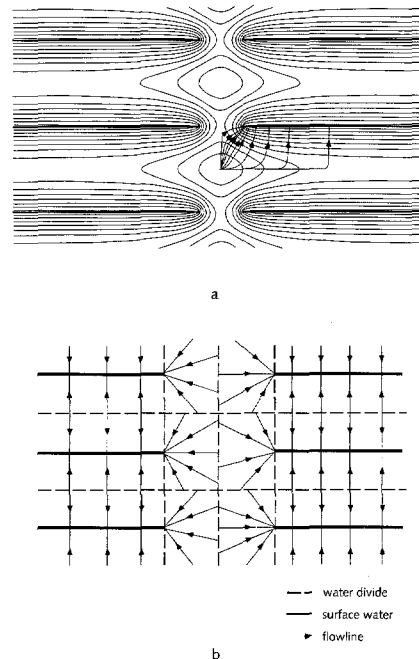


Figure 7.6 Flow between infinitely long, parallel surface waters with equal interruptions (a), schematized to determine the feeding resistance (b).

Also, if the angle between surface waters is greater than  $180^\circ$ , the flow to the edge of the corner is approximately axial-symmetric (see example in section 7.6).

In this section, an expression for the feeding resistance in an arbitrary area with axial-symmetric flow will be derived, which is based on a conceptual model that is comparable to the one used in the derivation of (6.2.20). The flow to the tip of the surface waters is schematized as flow to a well. The flow in the top aquifer is bounded by an impermeable circular boundary at a certain distance of the well. So, along a radius between the well and the impermeable boundary the schematization of figure 6.2.1-b can be used. The derivation of the expression for the feeding resistance starts with the case of axial-symmetric flow in a segment of the circular domain. The expression for the feeding resistance derived for this case is used to derive an expression in the case of axial-symmetric flow in a triangular area. The expression for the feeding resistance in an arbitrary area with axial-symmetric flow is derived based on the expression for the feeding resistance in a triangular area.

#### 7.4.1 The feeding resistance in a situation of axial-symmetric flow in a circular area

For the derivation of an expression for the feeding resistance for axial-symmetric flow, the flow from a tip of a surface water is considered (figure 7.7). The groundwater flows axial-symmetric via the top aquifer and the separating layer to the regional aquifer. Similar to in derivation of (6.2.20) (compare the text with expression (6.2.3)), it is assumed that the piezometric head  $\phi_1$  in the regional aquifer is not affected by this flow. This assumption is acceptable if the flux from the well is small compared to the flux in the regional aquifer.

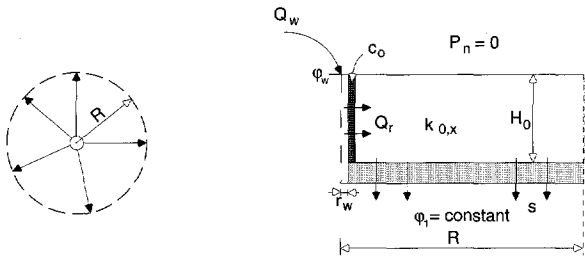


Figure 7.7 Conceptual model to determine the feeding resistance in a situation with axial-symmetric flow.

The analytic solution for the case of figure 7.7 can be deduced from the general solution of a well in a semi-confined aquifer by changing the place of the separating layer from the top to the bottom of this aquifer (which is the actual top aquifer). The general solution for this case can be found e.g. in Strack (1989, pp. 165-169) and is expressed by:

$$\Phi(r) = C_1 I_0(r/\lambda_0) + C_2 K_0(r/\lambda_0) \quad (7.13)$$

$$Q(r) = [-C_1 I_1(r/\lambda_0) + C_2 K_1(r/\lambda_0)]/\lambda_0 \quad (7.14)$$

where  $I_0$  and  $K_0$  are modified Bessel functions of the first and second kind and of order zero,  $I_1$  and  $K_1$  are the same functions of order one,  $C_1$  and  $C_2$  are the integration constants,  $\Phi(r)$  is the discharge potential at  $r$  [ $L^3/T$ ], and  $Q(r)$  is the total flux through the circle at  $r$  [ $L^3/T$ ]. The well simulates the tip of the surface water which leads to the following condition at the well radius (see expression (14.47) on page 169 in Strack, 1989):

$$\Phi(r_w) = k_0 H_0 (\varphi_0(r_w) - \varphi_1) \quad (7.15)$$

Here, the surface water level  $p$  is renamed to the groundwater head  $\varphi_0(r_w)$  in the top aquifer at the well radius  $r_w$  and  $\varphi_1$  is the head in the regional aquifer. The outer boundary at  $r = R$  is impermeable (compare figure 6.2.1-b), leading to the condition:

$$Q(R) = 0 \quad (7.16)$$

Solution of the integration constants leads to:

$$C_1 = \Phi(r_w)/IK_1 \quad (7.17)$$

$$C_2 = \Phi(r_w)/IK_2 \quad (7.18)$$

where:

$$IK_1 = I_0(r_w/\lambda_0) K_1(R/\lambda_0) / I_1(R/\lambda_0) + K_0(r_w/\lambda_0)$$

$$IK_2 = I_0(r_w/\lambda_0) + K_0(r_w/\lambda_0) I_1(R/\lambda_0) / K_1(R/\lambda_0)$$

The total flux through the separating layer in the circular domain inside  $r = R$  equals the flux  $Q(r_w)$  through the well radius  $r_w$ . This flux becomes ((7.17) and (7.18) in (7.14)):

$$Q(r_w) = \Phi(r_w)IK_3/\lambda_0 \quad (7.19)$$

where:

$$IK_3 = K_1(r_w/\lambda_0)/IK_1 - I_1(r_w/\lambda_0)/IK_2$$

From numerical experiments, it follows that  $IK_3$  is approximately constant for  $R > 4\lambda_0$  and  $r_w \ll \lambda_0$ . The average flux  $s_{Rav}$  through the separating layer [ $L/T$ ] inside the circular area with radius  $R$  becomes:

$$s_{Rav} = Q(r_w)/\pi R^2 \quad (7.20)$$

This average flux is valid in any segment of the circular area. The feeding resistance is based again on the Cauchy boundary condition (6.2.13), which is adapted to the axial-symmetric case.

$$s_{Rav} = (\varphi_0(r_w) - \varphi_1)/c_{\underline{v},R}^* \quad (7.21)$$

where  $c_{\underline{v},R}^*$  is the feeding resistance for axial-symmetric flow in a circular area [ $T$ ]. Combination of (7.15), (7.19), (7.20) and (7.21) leads to:

$$c_{\underline{v},R}^* = c_1 (R/\lambda_0)^2 \pi \lambda_0 / IK_3 \quad (7.22)$$

In this case, the tip of the surface water is in direct contact with the top aquifer. Between the top aquifer and the surface water an entrance resistance  $c_0$  may occur (see *figure 7.7-b*). This resistance is assumed to occur at the boundary of the well and the thickness of the layer generating the entrance resistance is neglected. The groundwater head at the boundary between the entrance resistance layer and the top aquifer is defined as  $\varphi_0(r_w')$ . Continuity of flow across this layer gives:

$$Q(r_w) = 2\pi H_0 r_w (\varphi_0(r_w) - \varphi_0(r_w')) / c_0 \quad (7.23)$$

In order to account for the entrance resistance  $c_0$ ,  $\varphi_0(r_w)$  in (7.21) is replaced by  $\varphi_0(r_w')$ . Combination of this modified (7.21) with (7.19), (7.20) and (7.23) leads to:

$$c_{y,R}^* = R^2 \pi K_R \quad (7.24)$$

where:

$$\begin{aligned} K_R &= 1/\epsilon + 1/\kappa \\ \epsilon &= 2\pi r_w H_0 / c_0 \\ \kappa &= k_0 H_0 / K_3 / \lambda_0 \end{aligned}$$

This expression for the feeding resistance in the case of axial-symmetric flow is comparable with expression (6.2.20), except for that the radial resistance (6.2.17) is not included (which should account for the partial penetration of the surface water if present). In the following, it is assumed that the radial resistance is accounted for by an adaption in the value of the entrance resistance  $c_0$ .

Because the case is axial-symmetric, expression (7.24) is valid in any segment bounded by two path lines and the circular boundary at  $R$ . This will be used in the following step (sub-section 7.4.2) on the way to an expression for the feeding resistance in an arbitrary area with axial-symmetric flow.

#### 7.4.2 The feeding resistance for axial-symmetric flow in a triangular area bounded by path lines and a straight water divide

In this sub-section, expression (7.24) will be used to derive an expression for the feeding resistance for axial-symmetric flow in a triangular area bounded by path lines and a straight water divide as presented in *figure 7.8*. In this figure, expression (7.24) holds in the segment with angle  $d\gamma^\circ$ . The area  $dA$  of this segment equals  $R(\gamma)^2 d\gamma^\circ / 2$  and the total flux through the separating layer in the segment  $dS$  is:

$$dS = s_{Rav} R(\gamma)^2 d\gamma^\circ / 2 \quad (7.25)$$

Combination of the expressions (7.21), (7.24) and (7.25) leads to:

$$d[S / (\varphi_{0,w} - \varphi_1)] = R(\gamma)^2 d\gamma^\circ / 2 c_{y,R}^* = 1/2 \pi K_R d\gamma^\circ \quad (7.26)$$



In the forthcoming integration over  $\gamma^0$ ,  $K_R$  is assumed to be constant within the triangular sub-domain. Because  $IK_3$  is the only term in expression (7.24) that varies with  $\gamma$ ,  $IK_3$  is implicitly assumed to be constant. Following from expression (7.19), it is needed that either  $R(\gamma)$  is larger than  $4\gamma_0$  or  $R(\gamma)$  should be about constant inside this area. (If  $IK_3$  is not constant, the integration should be carried out over smaller triangular sub-domains in which  $R(\gamma)$  is constant. After that step 3 described in the last paragraph of section 7.2. should be carried out). Integration of expression (7.26) between  $0 \leq \gamma^0 \leq \gamma^0$  (figure 7.8) gives:

$$S/(\varphi_{0,w} - \varphi_1) = \gamma^0/2\pi K_R \quad (7.27)$$

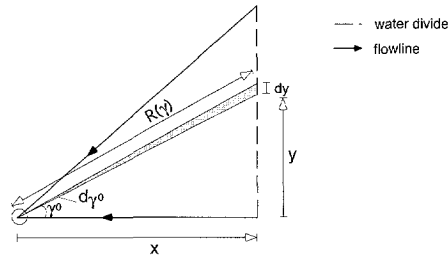


Figure 7.8 Triangular area with axial-symmetric flow bounded by two path lines and a water divide.

The feeding resistance  $c^*_{\underline{v},\Delta}$  for axial-symmetric (index  $\underline{v}$ ) flow inside a triangular (index  $\Delta$ ) area is derived from (compare expression (7.9)):

$$c^*_{\underline{v},\Delta} = (\varphi_{0,w} - \varphi_1)/s_{av} \quad (7.28)$$

and with  $s_{av} = S/A_{\underline{v}}$ , where  $A_{\underline{v}}$  is the area with axial-symmetric flow, and expression (7.27) this leads to:

$$c^*_{\underline{v},\Delta} = 2\pi K_R A_{\underline{v}}/\gamma^0 \quad (7.29)$$

This is the expression of the feeding resistance for a triangular area bounded by path lines and a water divide with axial-symmetric flow.  $K_R$  is assumed to be constant in expression (7.29), which means that a representative value for  $R(\gamma)$  (called  $R'$ ) over the area  $A$  should be determined. This  $R'$  can be estimated by using the facts that  $K_R$  applies to a circle segment (because it originates from expression (7.24)) and that expression (7.29) applies to a triangular area. Stating that  $K_R$  should generate the same value of the feeding resistance in both areas, the criterium for  $R'$  is expressed by the equation  $c^*_{\underline{v},\Delta} = c^*_{\underline{v},R}$ , which leads to:

$$R' = \sqrt{(2A_{\underline{v}}/\gamma^0)} \quad (7.30)$$

Expression (7.26) also follows from the statement that the size of the circle segment should be equal to the size of the triangular area.

### 7.4.3 The feeding resistance for axial-symmetric flow in an arbitrary area bounded by path lines and water divides

The area with axial-symmetric flow in figure 7.6-b can be subdivided into triangles each being comparable to the one in figure 7.8. In each triangular sub-domain (index  $j$ ), expression (7.29) in combination with expression (7.30) can be applied to determine the feeding resistance  $c_{\underline{v},\Delta,j}^*$ . In expression (7.29) the parameters  $A_{\underline{v}}$ ,  $K_r$  and  $\gamma^0$  are replaced by respectively  $A_j$ ,  $K_{r,j}$  and  $\gamma_j^0$ . The representative feeding resistance  $c_{\underline{v}}^*$  over the entire area  $A_{\underline{v}}$  with axial-symmetric flow is again based on the area-weighted harmonic mean of the feeding resistances of the sub-domains  $c_{\underline{v},\Delta,j}^*$ , leading to:

$$A_{\underline{v}}/c_{\underline{v}}^* = \sum(A_j/c_{\underline{v},\Delta,j}^*) = \sum(\gamma_j^0/2\pi K_{r,j}) \quad (7.31)$$

or:

$$c_{\underline{v}}^* = A_{\underline{v}}/\sum(\gamma_j^0/2\pi K_{r,j}) \quad (7.32)$$

If  $R'$  is approximately equal for all sub-domains, this can be rewritten as:

$$c_{\underline{v}}^* = 2\pi K_{r,j} A_{\underline{v}} / (\sum \gamma_j^0) \quad (7.33)$$

So, as a first approximation the feeding resistance for axial-symmetric flow can be determined from the constant  $K_r$ , the size of the entire area  $A_{\underline{v}}$  and the sum over all angles of axial-symmetric flow  $\sum \gamma_j^0$ . Obviously, the feeding resistance for areas with axial-symmetric flow is not at all related to the drainage density, because the tip of the surface water has no length. As expression (7.33) shows, the feeding resistance for an area with predominantly axial-symmetric flow is proportional to its area  $A_{\underline{v}}$  and that it is certainly not linearly related with the distance between the surface waters as the feeding resistance is in the case of an area with predominantly parallel flow. From expression (7.30), it may be concluded that  $A_{\underline{v}}$  is quadratically related with  $R$  (see also the example in section 7.6).

### 7.5 The representative feeding resistance in an area with both axial-symmetric and parallel flow and a comparison with its determination in modeling practice.

The representative feeding resistance for an arbitrary area is derived as a combination of the feeding resistances in the distinguished sub-areas. These sub-domains can be either rectangles and triangles with parallel flow or triangular areas with axial-symmetric flow (see example in section 7.6). For each of these sub-areas, an expression for the feeding resistance is found in sections 7.3 and 7.4. The representative feeding resistance  $c_{rep}^*$  for the entire area  $A_{tot}$  is the area-weighted harmonic mean (see section 7.1) of all feeding resistances in the sub-domains (expression (7.3)). For the comparison between this representative feeding resistance and the one derived in common practice, the feeding resistances in all sub-domains with axial-symmetric flow are combined to one with a representative feeding resistance  $c_{\underline{v}}^*$  for the total area  $A_{\underline{v}}$  with axial-symmetric flow by taking the area-

weighted harmonic mean of the feeding resistance in all these sub-domains. The same applies for the feeding resistances in all sub-domains with parallel flow leading to the representative feeding resistance  $c_{\parallel}^*$  for the total area with parallel flow  $A_{\parallel}$ . Then, in the area  $A_{tot}$  including both axial-symmetric flow and parallel flow, the following relation holds:

$$A_{tot}/c_{rep}^* = A_{\parallel}/c_{\parallel}^* + A_{\underline{v}}/c_{\underline{v}}^* \quad (7.34)$$

In this relation, the difference between the feeding resistance based on the drainage density ( $c_{\underline{v}}^*$ ) and the feeding resistance without any relation to the drainage density ( $c_{\parallel}^*$ ) is made explicit. In the following part of this section, the determination of the feeding resistance based on (7.34) is called the accurate approach.

In modeling practice, the representative feeding resistance for an arbitrary area  $c_{rep}^*$  (adding " to distinguish from  $c_{rep}^*$  in (7.34)) is determined by using an approximate representative distance between surface waters  $L$  in (6.2.20). For this approximate representative distance, the drainage density is simply determined by taking the sum of the lengths of all surface waters in the entire area divided by the size of that area. Because this representative feeding resistance is an approximate of  $c_{\parallel}^*$ , it is called  $c_{\parallel}^*$ . So, in this so-called "practical approach", expression (7.34) simplifies to:

$$A_{tot}/c_{rep}^* = A_{tot}/c_{\parallel}^* \quad (7.35)$$

Next, this practical approach will be compared to the accurate approach by analysis of the ratio  $c_{rep}^*/c_{rep}^*$ . By using  $A_{tot} = A_{\parallel} + A_{\underline{v}}$ , (7.34) and (7.35) can be combined to:

$$c_{rep}^*/c_{rep}^* = A_{\parallel}/A_{tot} \times c_{\parallel}^*/c_{\parallel}^* \times (1 - c_{\parallel}^*/c_{\underline{v}}^*) + c_{\parallel}^*/c_{\underline{v}}^* \quad (7.36)$$

If  $A_{\underline{v}}$  is small compared to  $A_{\parallel}$ ,  $A_{tot}$  is almost equal to  $A_{\parallel}$ . Because the total length of all surface waters in the area are also equal, the drainage density (7.1) is almost equal in both cases and so the representative distance between the surface waters is also almost equal. Therefore,  $c_{\parallel}^*$  is almost equal to  $c_{\parallel}^*$  and the right hand side of expression (7.36) becomes almost equal to 1. So,  $c_{rep}^*$  is almost equal to  $c_{rep}^*$ , which means that the practical approach is as good as the accurate approach.

If  $A_{\underline{v}}$  is not small compared to  $A$  (so  $A_{\underline{v}} \geq A_{\parallel}$ ), three cases are distinguished:

(1)  $c_{\underline{v}}^* > c_{\parallel}^*$ , (2)  $c_{\underline{v}}^* \approx c_{\parallel}^*$  and (3)  $c_{\underline{v}}^* < c_{\parallel}^*$ .

Case 1:

If  $c_{\underline{v}}^* > c_{\parallel}^*$  and  $A_{\underline{v}} \geq A_{\parallel}$  expression (7.34) reduces to:

$$A_{tot}/c_{rep}^* = A_{\parallel}/c_{\parallel}^* \quad (7.37)$$

and divided by (7.35), this leads to a different form of (7.36):

$$c_{rep}^*/c_{rep}^* = A_{\parallel}/A_{tot} \times c_{\parallel}^*/c_{\parallel}^* \quad (7.38)$$

Assuming that both feeding resistances are linear with their representative distances between surface waters (so  $c_{II}^* = CL_{rep}$  and  $c_{II}^* = CL_{rep}$ ) and using the derivation of these distances as described above (so  $L_{rep} = A_{tot} / \sum l_i$  and  $L_{rep} = A_{II} / \sum l_i$ ) the right hand side of (7.38) becomes 1, which means that the practical approach leads to the accurate feeding resistance.

Case 2:

If  $c_{v}^* \approx c_{II}^*$  and  $A_v \geq A_{II}$  expression (7.36) can be simplified to

$$A_{tot}/c_{rep}^* = A_{tot}/c_{II}^* \quad (7.39)$$

and divided by (7.37), this leads to the following simplification of expression (7.36):

$$c_{rep}^*/c_{rep}^* = c_{II}^*/c_{II}^* \quad (7.40)$$

Because  $A_{tot}$  is always larger than  $A_{II}$  and in both cases the same length of the surface waters is used in the drainage density, the representative distance between the surface waters will be larger in the practical case than in the more accurate case. Because in both cases (6.2.20) is used,  $c_{II}^*$  is larger than  $c_{II}^*$ . Then, from (7.40) it is concluded that  $c_{rep}^*$  is larger than  $c_{rep}^*$ . This overestimation of  $c_{rep}^*$  is larger, the larger  $A_{tot}$  is compared to  $A_{II}$ .

Case 3:

If  $c_{v}^* < c_{II}^*$  and  $A_v \geq A_{II}$  expression (7.34) reduces to:

$$A_{tot}/c_{rep}^* = A_v/c_{v}^* \quad (7.41)$$

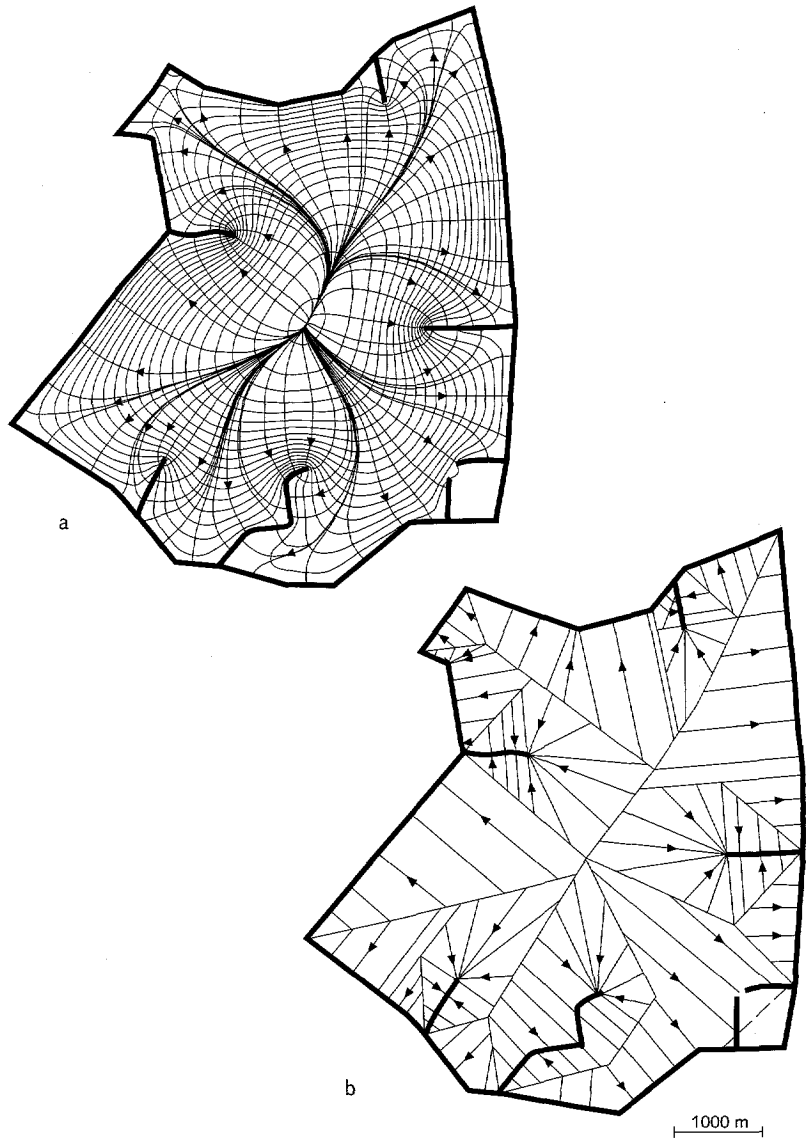
which shows that in this case the representative feeding resistance is actually not related with  $c_{II}^*$  and therefore it is not related with the drainage density at all. So, the practical approach will lead to an inaccurate feeding resistance and should not be used.

From this analysis it is concluded, that the practical approach is valid if  $c_{v}^*$  is not small compared to  $c_{II}^*$ .

## 7.6 Examples of the calculation of the feeding resistance for an arbitrary area

As an example, the feeding resistance is determined for a small area in the northern part of the Netherlands (figure 7.9-a), which is bounded by a closed chain of surface waters. The sizes, shapes and entrance resistances of these surface waters are assumed to be about equal (see section 6.1), which means that the situation can be used straight-forwardly for the determination of the drainage density.

Also in this complex situation, a model of analytic elements (figure 7.9-a) is used. In this model, the shapes of the surface waters are simulated in detail by numerous line-elements (subsection 3.3.2). The parameters ( $k_0H_0$  and  $c_1$ ) in the model are taken in such a way that the boundaries of the sub-areas become clear from the pattern of path lines (figure 7.9-a). The Figure



7.9 Flow between arbitrary surface waters (a) schematized to determine the feeding resistance (b).

boundaries of the schematized sub-areas (figure 7.9-b) are surface waters, path lines and water divides. (Actually, the place of these boundaries should preferably be determined based on measurements of heads and/or path lines.) Figure 7.9-b shows that in about 20% of the area, the flow accumulates in axial-symmetric flow to the tips of the surface water or to the edges of corners between surface waters with an angle larger than  $180^\circ$ .

The value of the representative feeding resistance based on the practical approach (so using the drainage density applied to the total area) is compared to the value of the accurate approach based on (7.36). The drainage density in this area is determined, by using half the length of the border surface waters and the full length of the surface waters within these

borders (see subsection 7.2). In the computation (table 7.1),  $c^*_i$  comes from (6.2.20),  $L$  from (7.1) and (7.2),  $c^*_v$  from (6.2.20) using  $L^*$ ,  $L^*$  from (7.1) and (7.2) with  $J = 1$ ,  $c^*_v$  from (7.3) with  $R'$  in  $K_R$  determined by (7.30),  $c^*_{rep}$  from (7.34) and  $c^*_{rep}$  from (7.35).

The first example in table 7.1 represents the actual situation of figure 7.9. In the second example  $k_{0,x}$ ,  $k_{0,z}$  and  $H_0$  are multiplied by 10 and  $c_1$  by 100. In the third example, the length scale of the model is changed in such a way that kilometers become hectometers and in the fourth example the value of  $c_0$  is multiplied by 10.

From the results presented in table 7.1, the following conclusions are drawn for these examples:

- The practical approach leads to acceptable values of the representative feeding resistance in all examples, because  $c^*_v \geq c^*$ .
- A change in the scale of the situation with a factor 10 (case 3) does change the value of the feeding resistance for parallel flow with a factor 10 and the feeding resistance for axial-symmetric flow with a factor 100. This example complies with  $L > 3\lambda_0$  and  $R > 4\lambda_0$ , which leads to a linear relation between  $L$  and  $c^*$  (see comments to expression 6.2.20) and to a linear relation between  $A_v$  and  $c^*_v$  (see expression (7.3) and the text near expression (7.19)).

Table 7.1. Computation of the feeding resistance in four examples based on figure 7.9 (see text).

Parameters	example 1	example 2	example 3	example 4
$B (=2r_w)$ m	2	2	2	2
$c_0$ d	1	1	1	10
$c_1$ d	10	1000	10	10
$H_0$ m	5	50	5	5
$k_{0,x}$ m/d	3	30	3	3
$k_{0,z}$ m/d	.3	3	.3	.3
$\lambda_0$ m	20	1235	20	20
$A$ km <sup>2</sup>	44	44	.44	44
$A_v$ km <sup>2</sup>	11	11	.11	11
$\sum l_i$ km	20	20	2	20
$\sum \gamma_i$ rad	$6\pi$	$6\pi$	$6\pi$	$6\pi$
$R$ m	1080	1080	108	1080
$L$ m	2200	2200	220	2200
$L^*$ m	2750	2750	275	3750
$IK_3$ m	6.3	14	6.3	6.3
$c^*_i$ d	2926	2376	293	13400
$c^*_v$ d	893000	227000	8927	1943000
$c^*_{rep}$ d	3655	2962	362	16750
$c^*_{rep}$ d	3657	2786	366	16780

## 7.7 Concluding remarks

A theoretical basis is derived for the determination of the representative feeding resistance in areas with arbitrary situated surface waters.

In the determination of the feeding resistance, areas with predominantly parallel flow should be distinguished from areas with predominantly axial-symmetric flow.

The feeding resistance for areas with predominantly parallel flow can often be based on the drainage density, which is the sum of the lengths of all surface waters in a certain area divided by the size of that area.

The feeding resistance for areas with predominantly axial-symmetric flow is independent of the drainage density.

The representative feeding resistance for an area consisting of sub-areas with both predominantly parallel and predominantly axial-symmetric flow is the area-weighted harmonic mean of the feeding resistances of all sub-areas.

The practical approach for the determination of the feeding resistance (taking the drainage density equal to the total length of all surface waters in the entire area divided by the size of that area and using only an expression for the feeding resistance for parallel flow) is allowed as long as the representative feeding resistance for all areas with predominantly axial-symmetric flow is not small compared to the representative feeding resistance for all areas with predominantly parallel flow or if the total size of all areas with axial-symmetric is negligible compared to the size of the entire area.





## **8. ON THE MODELING OF LARGE DOMAINS WITH ANALYTIC ELEMENTS**

### **8.0 Summary**

The modeling of large domains using the concept of geohydrologic features is introduced. The four main steps in modeling of large domains are presented, which are based on the coupling and refining of model parts. A model for national groundwater management should give comparable results everywhere, but is generally developed by different modelers. Therefore, an approach to build comparable models of different areas by different modelers is presented.

### **8.1 Introduction**

An analytic element is a mathematical function meant to model a specific geohydrologic feature (section 3.1). These features can be abstraction wells, polders, infiltration areas, parts of separating layers, parts of aquifers, surface waters, lakes, etc. Modeling with analytic elements is modeling in terms of geohydrologic features. In the modeling process, features have to be selected and the appropriate analytic elements have to be chosen. The application of the relation between geohydrologic features and analytic elements in this process of choosing is a continuation of the chapters 5, 6 and 7.

The modeling process is discussed with special attention to the modeling of large domains. This is a selection of the reports on NAGROM (De Lange, 1991, De Lange and Van der Meij 1994), in which the applicability of the theory presented in this thesis has been demonstrated.

A model such as NAGROM is large compared to the scale of the included geohydrologic features, which implies that it will be developed using sub-models (sections 2.3 and 2.4). The different sub-models of NAGROM have been developed by different modellers during different periods. In order to derive one combined model for national water management, these sub-models should be comparable. This will be elaborated in subsection 8.3.1. Therefore, an approach to develop comparable models of different areas by different modellers is presented, which is an elaboration of thoughts that appears to be useful in practice rather than a sound theory. This approach is based on geohydrologic features which closely agrees with analytic element modeling.

## 8.2 The approach for modeling of large domains with analytic elements

### 8.2.1 Modeling with analytic elements using the concept of geohydrologic features

Modeling with analytic elements is modeling with geohydrologic features. In the modeling process, geohydrologic features are selected in accordance with their importance for the groundwater flow in the model area. An indicator for the presence and importance of several types of features is the change of the hydraulic gradient in vertical as well as in horizontal direction. For instance, differences in place in the hydraulic gradient may indicate differences in place in the transmissivity of an aquifer in horizontal direction or in the resistance of a separating layer in vertical direction. Also, the importance of the effect of a well, of the spatial difference in the groundwater recharge, or of a spatial difference in the surface water level are indicated by the distribution of the hydraulic gradient. The larger the change in place in the gradient the more important the feature will be. In the search for such a change, the scale of the model should be taken into account. A limitation of this indicator is that features are only recognized if they affect the groundwater flow in the present (measured) situation. Geohydrologic features that do not affect the flow at present are hard to determine and often are left out or modeled by using the experts guess.

Geohydrologic features can be simulated using one analytic element per feature (e.g. a well-element representing an abstraction well) or using several analytic elements per feature (line-sinks simulating a river) or even one analytic element for several features (e.g. one inhomogeneity-element embracing several areas in which the transmissivity is different from in the rest of the aquifer). So, there is not a one to one relation between the number of geohydrologic features and the number of analytic elements (although it sometimes seems to turn out that way).

Some types of geohydrologic features may be simulated by more than one type of analytic element.

As a first example, a very low permeability boundary in an aquifer (e.g. a sheet-pile wall) can be modeled by using impermeable wall elements (subsection 3.3.5), by using leaky wall elements (subsection 3.3.5) or by using (nested) inhomogeneity elements (subsection 3.3.6). The leaky and the impermeable wall elements are actually developed for this feature, but the straight elements can not be connected (section 5.3). Therefore, the inhomogeneity elements have been used until the curvilinear elements became available in the cases of curved low permeable boundaries.

As a second example, the anisotropic behaviour in a part of an aquifer can be simulated using line elements with a specified relatively high transmissivity (cracks) or with line elements with a specified resistance (leaky walls). As has been explained in subsections 5.2.5 and 5.2.6, the leaky wall elements are to be preferred to model anisotropic behaviour.

The third example illustrates that the choice of a type of analytic element may depend on the scale of modeling (subsection 8.3.1). The interaction between surface water and groundwater can be simulated both by area-sinks using the approach developed in chapters 6 and 7 and by line-sinks simulating each individual surface water. In areas with many surface waters, the area-sinks are used in large modeling areas while the line-sinks are used in small modeling areas. In other words, if a large amount of similar geohydrologic features is present in a domain of interest (the actual modeling area), these features are lumped but if the amount is small, the features are modeled individually.

The choice of which analytic element should be used to model a certain geohydrologic feature is a typical aspect of modeling with analytic elements (section 5.1). This aspect also enables to change the elements in the model during the calibration process. After the experience of the author, the possibility to choose leads to relevant knowledge on the properties of geohydrologic features. Also, the need (following from the measured values) to change to an other analytic element may lead to the conclusion that the type of geohydrologic feature is different from the expected one.

The distribution of analytic elements depends on the possible shapes of the elements as presented in chapters 3 and 4, on the distribution of the geohydrologic features and on constraints to the combination of different types of elements as presented in section 5.3. The sizes of (the segments of) the elements are based on the scale of the model and on the desired accuracy for which several rules have been presented in section 5.2.

The geohydrologic parameters used to specify a certain type of analytic element belong to the specific class of geohydrologic features for which that type of elements has been developed specifically (chapters 3 and 4). Often, an analytic element can also be used for a class of features that is different from the one it originally has been developed for e.g. curvilinear leaky walls to model anisotropic behaviour, as described in subsection 5.2.5. As shown in that subsection, a relation between the geohydrologic parameters to specify these elements and the parameters that describe the geohydrologic feature has to be determined.

So, the value of the parameters belonging to analytic elements in a model are directly related to the properties of geohydrologic features. This is different from the data in a common model based on the finite element or finite difference technique that are often seen as mutually independent cell-values of the standard parameters (such as the transmissivity of the aquifers and the vertical resistances of the separating layers).

### **8.2.2 The approach to model large domains**

The approach for the modeling of large domains has been developed for NAGROM (De Lange, 1991; De Lange and Van der Meij, 1994). Here, this approach is summarized by a discussion of the four main steps. These steps describe the modeling process that begins with the global modeling of a

large area around the domain of interest and ends up with the refinement of model parts in order to meet the desired scale of modeling (subsection 8.3.2). The approach is based on the coupling and refining of models which is easy when modeling with analytic elements.

*Step 1; the boundary zone*

In a model of analytic elements, the domain of interest is "separated" from the rest of the infinite aquifer by a boundary zone. The analytic elements in this boundary zone generate the behaviour of the geohydrologic features in that area in a coarse way and as simple as possible. So, large elements are used. Only the main geohydrologic features are included such as large rivers (modeled by line-sinks) and infiltration areas (modeled by area-sinks). Other analytic elements such as inhomogeneities and leaky walls are hardly used and generally with (very) large segments. At the boundary of the domain of interest, the elements in the boundary zone should give a proper description of the "outside world" with respect to the present and forthcoming situations in the domain of interest.

*Step 2; the "coarse" model*

The domain of interest is covered by analytic elements that simulate the most important geohydrologic features when looking at the domain as a whole. The "coarse" model covers the entire large domain and represents the main geohydrologic features. This model can be seen as the "first try" of filling up the model area with elements. Only very large geohydrologic features are included by using relatively large elements. The result is a very global description of the groundwater flow. This model does not need to serve any purpose but being the boundary zone for the model parts to be refined in the next steps. All types of elements can be used but as simple as possible.

*Step 3; the refinement of model parts*

The domain of interest is split up in several parts, which are refined one after another. When a certain part is refined, the elements in the rest of the large domain are taken from the "coarse" model. After the refinement of all parts, the entire large domain of interest can be covered by the combination of all elements at the refined level (scale of the model), which may or may not be the final scale of modeling. If the domain of interest is modeled on the final scale, the analytic elements are refined and adapted until the optimal accuracy is obtained (see examples in section 5.3). All types of elements are used as extensive as needed for this optimization. During the optimization, the amount of geohydrologic features included in the model remains the same.

*Step 4; repeated refinement in sub-parts*

Each model part of step 3 can be split up again in sub-parts. Each sub-part can be refined while taking the elements in the rest of the model part from the refinement of step 3. Outside that model part,

the elements of either step 3 or step 2 can be taken. As in step 3, after the refinement of the entire model part, all sub-parts can be combined to cover the entire model part at the repeated refined level. This step can be repeated over and over in all parts, sub-parts, sub-sub-parts etc. of the model.

During this step, the amount of geohydrologic features is increased within the area of refinement. After the increase of the amount of geohydrologic features, the optimization with respect to the accuracy should be carried out (see step 3). So, the refinement of the elements to meet the desired modeling scale (so adding geohydrologic features) has an aim (adding information) different from the adaptation of the elements for the optimization (adding accuracy).

During the optimization of the elements and a refinement, the changes in a model may consist of the common adjustments of element parameters. But, they may also consist of changes of the shapes and types of individual analytic elements, which is uncommon in other techniques. For instance, elements may be split up in order to comply with the rules for the combination of elements presented in chapter 5.

### **8.3 An approach to build comparable models of different areas by different modellers**

#### **8.3.1 On the relation between the accuracy and the comparability of models**

A model of a large domain for water management purposes is used to compare the effects of different measures that occur in different places (section 2.1). This implies that the computed effects e.g. in terms of differences in heads and/or fluxes should be comparable all over the model. In this, comparability means that similar changes imposed in different areas with similarly schematized geohydrologic systems of aquifers and aquitards should lead to similar effects computed by the model. Similar changes in different areas with differently schematized systems should lead to effects of which the differences in the results can be deduced from the differences in the geohydrologic schematization only. So, the translation of geohydrologic features in analytic elements should not lead to differences in computed results.

Because NAGROM has been developed by different modellers during different periods, an approach was needed to arrive at comparable models of different areas. Before this approach is presented (in the next subsection), some aspects of comparability in relation with accuracy of models are discussed. This discussion focuses on (stationary) models for quantitative effects (fluxes, heads) such as NAGROM rather than on models for qualitative effects (travel times, transport of pollutants).

The comparability with respect to computed effects of the different parts of a groundwater model is often assumed to be related with the accuracy in terms of heads and fluxes of the model in those parts. In this, the accuracy is the

commonly used measure that describes how the computed values of the fluxes and heads compare to the measured values. Next, it will be illustrated that this accuracy in the case of a stationary model can not be used to arrive at comparable models, but that (where it is possible) the differences in the heads and fluxes in at least two different situations observed in reality should be compared to the differences in the same two situations simulated by the model.

During the calibration of a stationary model, the distribution of a variable (head, flux) is compared with the spatial distribution of a representative time-average of the measured values of that variable. In NAGROM, the measured head (steady state) is defined as the average head during the last weeks of the wet season which is approximately the month april (De Lange and Van der Meij 1994).

The natural variation in time can be used to determine the range of discrepancies between computed and measured values that are allowed in the model due to the concept of steady flow. In each sub-model of NAGROM, the variations of the heads at different places throughout ten or more years have been used to estimate the allowed discrepancies between the measured and computed heads. For instance, the variations in time in the area of the NAGROM model of the eastern part of the Netherlands have led to the acceptance of discrepancies of several decimeters at some places and of several meters at other places.

The natural variation in place may lead to the conclusion that certain computation results might be acceptable for a large domain model but not for a detailed model. For instance, the variation in place in the groundwater head in the ice-pushed ridge in the Veluwe-region in the central part of the Netherlands may be many meters within a distance of several hundreds of meters. Therefore, discrepancies between measured and computed heads are accepted in the order of meters in those areas in NAGROM (De Lange and Van der Meij, 1994), because the scale of the model is in the order of kilometers. If the area should be detailed further (say on a scale in the order of hectometres), this variation in the groundwater head should be simulated by including more and smaller geohydrologic features.

In the flat valleys and polders in the NAGROM model of the same Veluwe-region, the variation in the groundwater head gradually changes with only a few decimeters per kilometre, which leads to the constraints to the deviations in the head following from the variation in time as discussed above.

The results of a model for water management purposes are usually expressed in terms of differences between computed values in two situations. During a calibration the discrepancies between the measured and computed values are observed in a single situation. The comparability of the results in different parts a large model such as NAGROM is based on differences between the values in two situations. So, the discrepancies used in the calibration can not be used to express the internal model comparability. Only by using the differences in heads or fluxes between two situations such as the calibration and the verification situation, the computed differences can be used to

determine the comparability. However, it appeared that too few large areas can be found in the

Netherlands in which two situations are known to check the comparability of NAGROM.

Therefore, an approach is developed for NAGROM to arrive at comparability based on the concept of geohydrologic features (subsection 8.3.2).

### **8.3.2 An approach to build comparable models of different areas (based on their scale and using geohydrological features)**

In the former section it has been concluded, that the comparability should be interpreted in terms of comparable reactions to imposed stresses. The reaction of a model to imposed stresses is largely determined by the geohydrologic features included. This forms the basis of the approach to build comparable models of different areas by different modelers. It is important to realize that this approach is an elaboration of thoughts that appears to be useful in practice rather than a sound theory. It is described here in order to give an idea how different modelers arrived at the comparable models of NAGROM, but the basis of the theory needs to be elaborated further.

In the modeling of large domains, the most important features are included first, because they determine the main part of the reactions to imposed stresses. During the calibration, geohydrologic features can be adapted and even be added in the model (subsection 8.2.2). The more features will be included, the less important the last ones will be when looking at the original scale of modeling. At a certain point in the modeling process, the addition of more features may cause that part of the model to become so detailed that it actually has changed to a different scale. When the refinements are not carried out all over the model, the modeling scale may vary strongly from one part to another and the differences in the sizes of the elements within one model can become extreme. In the early stage of development of NAGROM, this has occurred several times in order to arrive at equal accuracy in the measured heads and fluxes in the calibration situation. The models appeared to be not internally comparable. This problem has been tackled using the following approach, which is slightly different from the approach presented in De Lange (1991).

The geohydrologic features are selected using their size in relation to the size of the domain of interest. The length of a line-shaped feature (e.g. a canal) to be included should be at least  $1/10$  of the square root of the size of the domain of interest and the size of an area-shaped feature (e.g. a polder) should be at least  $1/100$  of the size of the domain of interest. In practice, a number between 20 and 50 features is used depending on the number of aquifers and the complexity of the area features, with an average of about 30 features.

For the modeling approach used for NAGROM, a relation between the scale and the size of a domain of interest has been defined (De Lange, 1991).

In table 8.1, the most important part for modeling of large domains is presented. This table expresses: LOCAL is thinking in hectares, REGIONAL in square kilometers, FLUVIAL in areas of (several) countries and MONDIAL concerns the whole earth. In general, the word 'scale' means 'standard'. Therefore, a scale can also be related with the size of an area.

Table 8.1 Relation between scale and domain of interest

name of scale prefix	size of domain of interest [km <sup>2</sup> ]		
	sub-	-	supra-
local	10 <sup>2</sup>	10 <sup>1</sup>	10 <sup>0</sup>
regional	10 <sup>1</sup>	10 <sup>2</sup>	10 <sup>3</sup>
fluvial	10 <sup>4</sup>	10 <sup>5</sup>	10 <sup>6</sup>
mondial	10 <sup>7</sup>	10 <sup>8</sup>	10 <sup>9</sup>

This naming of scales may replace the existing habit to name models after the scale of the topographic map they are based on (say 1:100.000). The scales of topographic maps can be related to the scale names presented in table 8.1 by considering that the size of the area covered by one sheet of a map has the same order of magnitude as the domain of interest of the model. Sheets of maps as used in the Netherlands generally cover 0.5 m × 0.7 m = 0.35 m<sup>2</sup>. On a scale of 1:100,000 this 0.35 m<sup>2</sup> represents an area of 3,500 km<sup>2</sup> and is in the range of a supra-regional scale. The same sheet on a scale of 1:25,000 then covers 220 km<sup>2</sup>, which is in the regional scale and a sheet on the scale of 1:10,000 covers 35 km<sup>2</sup>, which is in the sub-regional scale. Such a sheet on the scale of 1:1000 covers .35 km<sup>2</sup> and is local scale. So, these names agree with common practice.

In the practice of NAGROM, the modeling of the domain of interest is started at supra-regional scale, which means that about 30 geohydrologic features are included in domains of interest with sizes of about 1000 to 10,000 km<sup>2</sup>. In the second step, the modeling is carried out at regional scale, using the supra-regional model as a framework. The area of the supra-regional model is split up in 5 to 10 regional models (areas of interest) each with a size about 100 to 1000 km<sup>2</sup>. In each of these areas of interest again about 30 features are included. Once all the regional models have been built, the entire supra-regional area can be covered by elements on supra-regional scale as well as by the combination of all regional elements. The latter step can be repeated: in the third modeling step, the regional models might be split up again in 5 to 10 sub-regional models with a domain of interest with a size of about 10 to 100 km<sup>2</sup>.

So in the approach presented here, the geohydrologic features in the domain of interest are determined depending on the scale of the model. These geohydrologic features are simulated by analytic elements in such a way that the accuracy is optimum. This means that in different areas the response to stresses of the geohydrologic features should be comparable and the computation results should not differ due to the applied analytic elements. Doing this, the computed changes in heads or fluxes due to imposed stresses will be comparable in different areas.



## 9. CONCLUSIONS AND RECOMMENDATIONS

### 9.1 Conclusions

The modeling approach developed for the NATIONAL GROundwater Model (NAGROM) is unique because it is based on coupling and refining of models. This approach is mainly due to the application of the analytic element modeling technique.

In a model of analytic elements boundary conditions are defined on outside boundaries as well as on inside boundaries. The latter is uncommon in modeling with other techniques.

The development of proper combinations of analytic elements desires a thorough understanding of the analytic elements used and of their interaction.

Analytic elements generating a higher transmissivity inside than outside (inhomogeneity, crack, drain) are relatively easy to use in models. However, their effect on the groundwater flow is not only related to their relative transmissivities and to their sizes but also to the flow situation generated by the rest of the model. Because of this, a crack or drain can hardly be used to model anisotropic behaviour. On the contrary, analytic elements generating a lower transmissivity (or hydraulic conductivity) inside than outside (inhomogeneity, leaky wall, impermeable wall) are relatively difficult to use in models. Their effect on the groundwater flow is only related to that relative low transmissivity and to their sizes and not to the flow situation. Therefore, the leaky wall can well be used to model anisotropic behaviour.

The effect of a leaky wall on the groundwater flow can be characterized by a simple parameter.

The accuracy of the flux and the head generated by an area-sink can be often simply related to the size of that element.

Modeling with analytic elements is complex compared to modeling with classical (finite element or finite difference) techniques and should be carried out following the rules for modeling derived in chapter 5. These rules mainly concern the strength distribution generated by elements and the response of other elements to this. In general, overlapping elements should be avoided.

The interaction between surface water systems and the groundwater in regional aquifers are included in NAGROM by lumping the effects of the individual surface waters in an area-representative Cauchy boundary condition. It is shown in this thesis, that in a Cauchy boundary condition in

which the feeding resistance is used, the modified surface water level should be applied also. New and simple expressions for both the feeding resistance and the modified surface water level are presented in this thesis.

The feeding resistance and the drainage resistance should not be based on conceptual models in which the flux across the separating layer below the top aquifer is constant.

The feeding resistance can not be derived by adding the vertical resistance of a separating layer to the drainage resistance, because then the flux across the separating layer below the top aquifer is assumed to be constant.

The use of multi-aquifer models for the computation of the feeding resistance as well as the drainage resistance is limited to conceptual models in which the conditions at the boundary in the lower aquifer allow for a net flow between the groundwater in the top aquifer (included in the Cauchy boundary condition) and the groundwater in the regional aquifer (the upper aquifer of the actual model).

The feeding resistance for the situation in which the surface waters cut through the separating layer can often be determined by a simple expression.

The feeding resistance in an area with arbitrary situated surface waters can often be derived by using the drainage density in the determination of the representative distance between the surface waters in that area. The derivation of this representative distance has been based on the new and simple expression for the feeding resistance presented in this thesis.

The following conclusions are directly related to this thesis, but not based on presented theory or developments.

The computation of heads, velocities and fluxes using analytic expressions provides exact and consistent values at any point in a model. In this the effects of density variation can be included analytically too. Although the AEM is not developed far enough yet to model transport of pollutants including dispersion, it provides a base for "clean" computation without numerical dispersion.

The two-dimensional mathematics of the AEM has properly been extended (by Strack) for use in semi-three-dimensional computation of groundwater flow.

The use of the discharge potential has opened new ways to model several aspects of groundwater flow (e.g. density-driven flow) by analytic expressions.

The growth of new type of analytic elements and new applications of the discharge potential appears to be almost unlimited.

## 9.2 Recommendations

The approach for scale-dependent modeling as discussed in chapter 8, should be developed further. As yet, it has led to the comparability of models developed by different modelers.

In the coming years, the theory for several aspects in computations concerning groundwater quality, such as transport of pollutants, should be implemented in the analytic element technique.



## SUMMARY

At the end of the 1980's, modeling of large domains was quite cumbersome using the classical (finite element and finite difference) techniques. By the appearance of Strack's analytic element technique, the coupling of models became easy to perform. The necessity to have the disposal of a groundwater model covering the entire country of the Netherlands at Rijkswaterstaat initiated the development of "NAGROM", which stands for NAtional GROundwater Model.

This thesis describes the basis of the modeling approach developed for NAGROM. After the first two introductory chapters, in the first main part (chapters 3, 4 and 5), rules are developed for the application of the analytic element technique as developed by Strack. In the second main part (chapters 6 and 7), the interaction between a system of surface waters and the groundwater in the regional aquifer in the same area are described by a simple formula, of which the general applicability is shown. In the last main part (chapter 8), an approach is presented to arrive at the point that the different models of NAGROM give comparable results.

NAGROM is based on the analytic element technique of Strack (University of Minnesota, U.S.A.). Analytic elements are solutions of the Laplace (and in special cases of the Poisson) differential equation. The elements are combined using the principle of superposition. Different elements impose different boundary conditions. Analytic elements can be point-, line-, or area-elements. Point-elements are used to model wells. Line-elements may simulate for instance brooks, rivers, sheet-pile walls, cracks and by using line-polygons, inhomogeneities in the aquifer properties can be included. Area-elements are used to simulate leakage through layers as it occurs below lakes and polders and through layers separating aquifers. Also, infiltration can be simulated by area-elements.

Strack developed a solution technique, which enables to compute the unknown strengths of elements in models with more than one aquifer. The analytic element technique can be used to model complex multi-aquifer models including anisotropy (using an approach described in this thesis), three-dimensional density-driven flow, horizontally-layered aquifers and partially penetrating wells (using an approach described in this thesis). In each arbitrary volume in a model of analytic elements the water balance is exact and at any point the head and its derivative comply exactly with the velocity. So, numerical dispersion is absent in the derivation of the velocity. At this moment (1995), the analytic element technique used in NAGROM is limited to stationary flow and excludes diffusion, dispersion and chemical reactions of solvents in the groundwater.

In modeling with analytic elements, it is important to choose the right type of analytic element to include the geohydrologic properties (transmissivity,

resistance, anisotropy, etc.) as well as to combine the elements correctly. The more complex the model, the more interactions appear in the model that may generate so-called physical errors. Physical errors are errors caused by the erroneous use or erroneous combination of analytic elements. These errors can be prevented by applying the modeling rules developed in this thesis. Most of these modeling rules have been found by analyzing the combination of each two types of elements. The most important rules are based on the proper use of the strength distribution belonging to each type of analytic element.

A well-known example of a physical error is the following. The strength of an element depends on the transmissivity at the point where that strength is computed or specified. If the element covers partly an area with a different transmissivity, this strength is wrong either inside or outside in that area.

From the stepwise construction of relatively complex models it is concluded, that analytic element models should be built from large to small and from coarse to detailed. This means that the distribution of elements is adapted during the modeling process. This is fundamentally different from modeling with classical (finite difference or finite element) techniques. The refinement of (a part of) an analytic element model is repeated until the desired accuracy is derived. From the examples presented in this thesis and from the experience of the author, it is concluded that physical errors are not present in a model if they do not show up explicitly in the results.

In the Netherlands, areas with many surface waters have been modeled since long by using methods in which the effects of the individual surface waters on the groundwater flow in the underlying regional aquifer are lumped in a simple area-representative boundary condition. In this, a *Cauchy boundary condition* is used, which describes a linear relation between the flux through the boundary layer and the potential at the inner side of that boundary layer. In the Cauchy boundary condition often either the so-called drainage resistance or the feeding resistance in combination with a representative value of the potential at the outer side of the boundary layer are used. The drainage resistance describes the situation in which the surface waters are in direct contact with the upper aquifer in the model. The feeding resistance is used in the situation with the surface waters in a top aquifer which is separated by a resistance layer from the upper aquifer in the model. The choice between both resistances depends on the situation to be modeled.

In this thesis, a new and simple formula for the feeding resistance is presented. Comparisons have been carried out concerning the differences between formulas for one-dimensional and two-dimensional flow and concerning the effects of different boundary conditions at the bottom of the top aquifer. In the comparison of these latter boundary conditions, a solution for a two-aquifer model is used. From these comparisons, it is concluded that the new and simple formula appears to be generally applicable.

Apart from this, a new analytic solution for the feeding resistance in the situation with the surface waters cutting through the separating layer at the bottom of the top aquifer appears to compare well with the length-weighted harmonic mean of the feeding resistance (following from the simple formula applied between the surface waters) and the resistance of the bottom of the surface waters. So, the latter can often be used.

The representative distance between the surface waters is important for the value of both the drainage resistance and the feeding resistance. It is known by several hydrologists in the Netherlands that this representative distance can be determined using the so-called drainage density, which is the sum of the length of all surface waters in a domain divided by the area of that domain. An explanation for this has never been presented before. By using the new formula for the feeding resistance, it is shown that this approach is acceptable in the situations where the feeding resistance is linearly related with the distance between the surface waters. In areas with many open ends of surface waters, the application of this approach may lead to a significant error in the value of the representative feeding resistance and the approach presented in this thesis should be used to determine the overall feeding resistance in areas with arbitrary situated surface waters.

The knowledge on modeling of large domains with analytic elements described above has been used during the development of NAGROM and is mentioned in chapter 8. A complete description is presented in various documents (De Lange, 1991; De Lange and Van der Meij 1994) and is not described in this thesis.

The results of NAGROM should be comparable all over the country. In order to meet this constraint, the models of NAGROM have been developed on a specified scale. In chapter 8, the scale of a model is defined by the size of its domain of interest. In each defined domain of interest, a standard amount of geohydrologic features (units in which the geohydrologic properties are constant) is defined. Doing this, the degree of detail varies with the scale, but is equal in domains modeled on the same scale. Geohydrologic features can be well related with analytic elements. This approach appeared to be useful during the development of NAGROM.





## SAMENVATTING

Het modelleren van grote gebieden met een redelijke mate van detail was eind jaren tachtig vrijwel ondoenlijk met de toen bestaande modeltechnieken (eindige elementen techniek en eindige differentie techniek). Tot aan het verschijnen van Strack's analytische elementen methode, was er geen modelleer techniek waarmee bestaande modellen rechtstreeks en eenvoudig aan elkaar gekoppeld konden worden. De noodzaak voor Rijkswaterstaat om te kunnen beschikken over een landsdekkend grondwater model voor landelijke beleidsanalyse heeft ertoe geleid dat een nieuwe ontwikkeling in gang gezet werd, die uiteindelijk heeft geleid tot NAGROM (NATionaal GRONdwater Model).

In dit proefschrift wordt de modelleer aanpak van NAGROM theoretisch onderbouwd. Na de twee inleidende hoofdstukken wordt in het eerste hoofdgedeelte (hoofdstukken 3, 4 en 5) het modelleren met analytische elementen, zoals deze zijn ontwikkeld door Strack, onderbouwd met regels. In het tweede hoofdgedeelte (hoofdstukken 6 en 7) wordt de interactie tussen het stelsel van oppervlaktewateren in een gebied en het grondwater in het regionale watervoerend pakket eronder beschreven met een eenvoudige formule waarvan de algemene toepasbaarheid op de belangrijkste punten onderbouwd wordt. In het laatste hoofdgedeelte (hoofdstuk 8) wordt een benadering gepresenteerd om de verschillende NAGROM deelmodellen vergelijkbare resultaten te laten produceren.

NAGROM is gebaseerd op de analytische elementen technique van Strack (Universiteit van Minnesota, V.S.). Analytische elementen zijn oplossingen van de Laplace (en in bijzondere gevallen van de Poisson) differentiaal-vergelijking. Op basis van het superpositie beginsel worden de elementen gecombineerd. Met verschillende typen elementen kunnen verschillende randvoorwaarden worden opgelegd. Analytische elementen kunnen punt-, lijn- of oppervlakte-elementen zijn. Punt-elementen worden gebruikt om onttrekkingen te modelleren. Met lijn-elementen kunnen beken, rivieren, damwanden, zeer sterk doorlatende langgerekte gebieden (karstverschijnselen) worden gemodelleerd en met polygonen kunnen inhomogeniteiten in de eigenschappen van het watervoerend pakket worden gemodelleerd. Met oppervlakte-elementen wordt lek van of naar het watervoerend pakket gesimuleerd, zoals dat optreedt onder polder- of infiltratiegebieden en bij scheidende lagen.

Door Strack is een oplossingstechniek ontwikkeld waardoor onbekende sterkten van elementen kunnen worden bepaald in modellen met meerdere watervoerend pakketten. Met de analytische elementen techniek kunnen complexe meerlagen modellen worden gebouwd met horizontale anisotropie (met behulp van een benadering beschreven in dit proefschrift), drie-dimensionale dichtheidstroming, gelaagdheid binnen watervoerende pakketten en onvolkomen putten en waterlopen (met behulp van de benadering

beschreven in dit proefschrift). De waterbalans in elk willekeurig volume in een model is exact en numerieke dispersie in het bepalen van de snelheidsverdeling treedt niet op vanwege het gebruik van analytische formuleringen. Vooralsnog (1995) is de voor NAGROM gebruikte techniek beperkt tot stationaire stroming zonder diffusie, dispersie of chemische omzettingen in het transport van opgeloste stoffen.

Bij het modelleren met analytische elementen is het belangrijk om de juiste elementen voor de op te nemen geohydrologische eigenschappen (doorlaatvermogen, weerstand, anisotropie, etc.) te kiezen en om de elementen op correcte wijze samen te laten werken. Hoe complexer het model des te meer interacties tussen elementen een rol gaan spelen die, bij verkeerd gebruik, kunnen leiden tot zogenaamde fysische modelleerfouten in de resultaten. Dit zijn fouten die ontstaan door het onjuist gebruik of onjuiste combinatie van analytische elementen. Dit kan worden voorkomen door het opvolgen van regels voor het combineren van elementen die zijn afgeleid in dit proefschrift. De meeste van deze regels zijn gebaseerd op analyse van de combinaties van twee analytische elementen van verschillend of gelijk type. De belangrijkste regels voor het modelleren hebben betrekking op het juiste gebruik van de sterkteverdelingen, die zijn gedefinieerd per type element.

Een bekend voorbeeld hiervan is het feit dat een sterkte berekend voor een element afhangt van het doorlaatvermogen ter plaatse van het controlepunt (het punt waar de sterkte bepaald wordt aan de hand van de opgelegde randvoorwaarde) en dus tot onjuiste resultaten leidt als het element een relevant deel van een gebied met een ander doorlaatvermogen bedekt.

Aan de hand van een stapsgewijze opbouw naar meer complexe modellen wordt geconcludeerd dat het, bij gebruik van de analytische elementen methode, voor de hand ligt om van groot naar klein en van grof naar fijn te modelleren. Dit betekent dat tijdens het modelleerproces de verdeling van de elementen wordt aangepast in de opeenvolgende stappen. Dit is een fundamenteel verschil met het modelleren met klassieke (eindige elementen, eindige differentie) technieken. Het verfijnen wordt in principe zo vaak herhaald als nodig is om de gewenste nauwkeurigheid te verkrijgen bij de schaal waarin gemodelleerd wordt. De gepresenteerde voorbeelden en de ervaring van de schrijver laten de conclusie toe dat indien geen duidelijke tekenen van fysische fouten worden geconstateerd, deze ook niet in het model voorkomen.

Bij het modelleren van gebieden waarin vele oppervlaktewateren voorkomen, wordt in Nederland reeds gedurende decennia gebruik gemaakt van methoden om de individuele effecten van die oppervlaktewateren op de grondwaterstroming samen te trekken in een eenvoudige gebiedsgemiddelde randvoorwaarde. In de daarbij gebruikte Cauchy randvoorwaarde - die een lineaire relatie tussen de flux door een rand en de potentiaal net binnen die rand beschrijft - wordt meestal de zogeheten drainageweerstand danwel de zogeheten voedingsweerstand gebruikt in combinatie met een representatieve waarde van de potentiaal net buiten die rand (meestal het

gemiddelde oppervlaktewater peil). De drainageweerstand beschrijft de situatie waarin de oppervlaktewateren direct liggen in het bovenste watervoerend pakket van het model. De voedingsweerstand beschrijft de situatie met oppervlaktewateren liggend in een toplaag boven het bovenste watervoerende pakket in het model, welke gescheiden zijn door een weerstandbiedende laag. De modelleur kan kiezen uit beide weerstandstypen aan de hand van het bijbehorende conceptuele model.

In dit proefschrift wordt een eenvoudige nieuwe formule gepresenteerd voor de voedingsweerstand. Uit vergelijkingen betreffende ondermeer de verschillen tussen een twee-dimensionale en een een-dimensionale benadering en de effecten van de voorwaarde op de rand tussen de toplaag en het bovenste watervoerende pakket van het model blijkt de nieuwe formule zeer goede eigenschappen te bezitten. Bij deze laatste vergelijking wordt gebruik gemaakt van een nieuwe analytische oplossing van een tweelagenprobleem.

Daarnaast wordt uit een vergelijking met een analytische oplossing geconcludeerd dat in het geval waarin de oppervlaktewateren insnijden door de weerstandbiedende laag onder de toplaag, het lengte-gewogen harmonische gemiddelde van de voedingsweerstand en de bodemweerstand van het oppervlaktewater een voldoende representatieve waarde voor de weerstand in de Cauchy randvoorwaarde geven.

Bij het bepalen van de waarde van zowel de drainageweerstand als de voedingsweerstand is de representatieve afstand tussen de oppervlaktewateren een belangrijke parameter. Het is bij sommige hydrologen bekend dat deze representatieve afstand kan worden gebaseerd op de zogeheten drainagedichtheid, de som van de lengten van alle oppervlaktewateren (of andere drainage middelen) binnen een bepaald gebied gedeeld door de oppervlakte van dat gebied. Een onderbouwing voor deze aanpak is echter nooit gegeven. Door gebruik te maken van de nieuwe formule voor de voedingsweerstand wordt aangetoond dat deze aanpak acceptabel is in gevallen waarin de voedingsweerstand een lineaire relatie heeft met de afstand tussen de oppervlaktewateren. In gebieden met veel open einden van oppervlaktewateren kan het gebruik van de drainagedichtheid tot significant afwijkende waarden voor de voedingsweerstand leiden en kan gebruik worden gemaakt van de in dit proefschrift aangegeven methode voor de berekening van de voedingsweerstand in gevallen met willekeurig gelegen oppervlaktewateren.

De bovenbeschreven kennis over het modelleren van grote gebieden met analytische elementen is bij het bouwen van NAGROM in praktijk gebracht en is aangestipt in hoofdstuk 8. De volledige beschrijving van NAGROM valt buiten dit proefschrift en is verwoord in diverse documenten (De Lange, 1991; De Lange en Van der Meij, 1994).

De resultaten van NAGROM moeten over het hele land vergelijkbaar zijn. Om dit te verkrijgen worden de deelmodellen van NAGROM op een van te voren vastgestelde schaal gebouwd. In hoofdstuk 8 is aan zo'n schaal een modelgebied met gedefinieerde grootte (kortweg schaal-gebieds-

grootte) gekoppeld. Door een vaste hoeveelheid grondwater-eenheden (eenheden met gelijke eigenschappen ten aanzien van grondwater stroming) per schaalgebiedsgrootte te nemen varieert de mate van detail per schaal, maar verschillende deelmodellen op een en dezelfde schaal bezitten dezelfde mate van detail. De verschillende typen grondwater eenheden kunnen goed gerelateerd worden aan de verschillende typen van analytische elementen. Het definiëren van de mate van detail, gebaseerd op grondwater-eenheden per gebiedsgrootte afhankelijk van de schaal, is bij NAGROM een bruikbare werkwijze gebleken voor het modelleren met analytische elementen.

## REFERENCES

- Abramowitz, M. and I.A. Stegun, 1965, Handbook of mathematical functions, Dover Publications, New York.
- Arnold, G.E., MOZART, een landsdekkend model voor de stroming in de onverzadigde zone, RIZA note in prep., RIZA Lelystad
- Bakker, M., 1991, Two analytic solutions for groundwater flow with varying density, report for Strack Consulting, Inc, North Oaks, Minnesota, USA.
- Bear, J., 1972, Dynamics of fluids in porous media, American Elsevier, New York
- Bear, J., 1979, Hydraulics of groundwater, McGraw Hill, New York
- Bear J. and A. Verruijt, 1987, Modeling Groundwater Flow and Pollution, D.Reidel Publ. Comp, Dordrecht, The Netherlands
- Brown, T.P. and R.J. Barnes, 1994, Stochastic analytic elements for groundwater modeling, in: proceedings of "Analytic element modeling of groundwater flow, University of Indiana School for Public and environmental affairs, Bloomington, Indiana.
- Bruggeman, G.A., 1972, Twee dimensionale stroming in een semi afgesloten watervoerend pakket, Appendix 5 of: Onderzoek voor ontrekkingen nabij "De Groeve", National Institute for Water Supply, Leidschendam, The Netherlands.
- CHO-TNO, 1964, Steady flow of groundwater towards wells, Versl. en Meded. Comm. hydrologisch onderzoek TNO no. 10, Delft.
- Dagan, G, 1964, Spacings of drains by an approximate method, J.Irr and Drainage Div. Proc. ASAE Paper 3824, pp 41-46
- De Lange, W.J., 1986, Application of the Boundary Integral Element Method to analyse the behaviour of a fresh water salt water interface calculating three-dimensional groundwater flow, in Proceedings of the 9th SWIM, pp 361-378, R.H. Boekelman, J.C. van Dam, M. Evertman and W.H.C. ten Hoorn, eds, Delft University of Technology, Delft.
- De Lange, W.J., 1991, A groundwater model of the Netherlands, RIZA note 90.066, RIZA Lelystad, The Netherlands.
- De Lange, W.J. and J.L. van der Meij, 1994, Reports on NAGROM, TNO-GG Delft, RIZA Lelystad.

Diersch, H-J., 1988, Finite element modeling of recirculating density-driven salt water intrusion processes in groundwater, *Adv. Water Resources*, vol 11, pp 25-43.

Douben, N.S.M., 1994, H.B. Bos and G.G.A. Meijers, MER Uitwijkhaven Weurt, RIZA note 94.018, RIZA, Lelystad.

Ernst, L.F., 1961, Grondwater stromingen in the verzadigde zone en hun berekening bij aanwezigheid van horizontale evenwijdige open leidingen, *Versl. Landbouwk Onderz.* 67.15, Pudoc, Wageningen, The Netherlands

Ernst, L.F., 1978, Drainage of undulating sandy soils with high groundwater tables, *J Hydrol.* 39(1/2), pp 1-50

Ernst, L.F., 1983, Infiltratie en kwel; de grondwaterstroming van hogere naar lagere gebieden, Report 7, Winand Staring Centre, Wageningen, The Netherlands.

Fitts, C.R., 1991, Modeling three-dimensional flow about ellipsoidal inhomogeneities with application to flow to a gravel-packed well and flow through lens-shaped inhomogeneities, *Water Resour. Res.*, 27(5), pp. 815-824.

Girinski, N.K., 1946, Complex potential of flow with free surface in a stratum of relatively small thickness and  $k = f(z)$ , (in Russian). *Dkl. Akad. Nauk SSSR*, 58(4), pp 559-561.

Haitjema H.M., 1985, Modeling three-dimensional flow in confined aquifers by superposition of both two- and three-dimensional analytic functions, *WRR* 21(10), pp 1557-1566.

Haitjema, H.M. and S.R. Kraemer, 1988, A new analytic function for modeling partially penetrating wells, *WRR* 25(5) pp.681-690

Hardy, R.L., Theory and application of the Multiquadric-Biharmonic Method, *Computers Math. Appl*, Vol 19 (8,9), pp. 163-208.

Heini M., and P.J. Brinkman, 1989, A groundwater model of the Nubian aquifer system, *Journ. of Hydr.Sc.*, 34,4,8, pp 425-447

Hooghoudt, S.B., 1940, Bijdragen tot de kennis van enige natuurkundige grootheden van de grond, No. 7, *Versl Landbouwk. Onderz.* 46, pp515-707, Pudoc, Wageningen, The Netherlands

Horton, R.E., 1932, Drainage-basin Characteristics, *Trans. AGU*, (13), pp. 350-361

Huisman L., 1972, *Groundwater Recovery*, MacMillan, New York.

IWACO, 1987, Eindrapport geohydrologisch onderzoek Centrale Slenk, fase 2, IWACO, Boxtel

IWACO, 1992, Projektgroep Grondwaterbeheer Midden-Nederland, Modelleringswatersystemen, IWACO Rotterdam & Prov Gelderland Arnhem.

Kirkham, D., 1960, An upper limit for the height of the water table in drainage design formulas, 7th Int. Congres of Soil Sci. Madison I, pp 486-492

Kontis, A.L and R.J. Mandle, 1988, Modifiactions of a three dimensional ground-water flow modl to account for variable density and effects of multiaquifer wells, US Geological Survey Water-Resources Investigations Rep. 87-4265, Madison, Wisconsin.

Maas C., 1986, The use of matrix differential calculus in problems of multiple aquifer flow, J. Hydrol, 88, 43-67.

Maas, C., 1994, On convolutional processes and dispersive groundwater flow, PhD-thesis, Univ. of Delft, Delft , The Netherlands.

Maas, C. and M.J. Emke, 1989, Solving varying density groundwater problems with a single density computer program, Proc. 10th SWIM, Natuurw. Tijdschrift, 70 pp 143-154, W. de Breuck and L. Walschot, eds, Ghent, Belgium.

Mazure, J.P., 1936, Geohydrologische gesteldheid van de Wieringermeer. Rapp. en Meded Zuiderzeewerken 5: 67-131.

McDonald, M.G., Harbaugh, A., 1984, A modular three-dimensional finite-difference groundwater flow model, U.S. Geological Survey, Reston, Virginia.

Newman, 1900 Zeitschrift fuer Gewässerkunde, (not found by the author)

Olsthoorn, T.N and J.H.N Moorman, 1991, Eerste resultaten MLAEM en toelaatbare grootte van oppervlakte-elementen in het Bethune model, Gem. Waterl. Amsterdam.

Pastors, M.J.H., 1992 Landelijk grondwater model, conceptuele modelbeschrijving, RIVM report 714305004, Bilthoven

Power, B.F. and R.J. Barnes, 1993, Model calibration techniques for use with analytic element method, Groundwater, 31(1), pp 91-97.

Pulles, J.W., 1985, PAWN, Policy Analysis for the Water management in the Netherlands, Rijkswaterstaat, the Hague.

Province of Drenthe, 1985, Grondwaterplan Drenthe, reports III and +, Province of Drenthe, Assen, The Netherlands.

Querner, E., 1993, Aquatic weed control within an integrated water management framework, PhD thesis Wageningen Agricultural University,

Report 67, DLO Winand Staring Centre, Wageningen, The Netherlands

Rand Corporation, 1982, Appendix XII of the Policy Analysis of Water Management for the Netherlands, N-1500/12-NETH, Rand Corporation, Santa Monica, USA.

Raudkivi A.J. and R.A. Callander, 1976, Analysis of Groundwater Flow, Edward Arnold Ltd, London.

Strack, O.D.L., 1981, Assessment of effectiveness of geologic isolation systems; analytic modeling of flow in a permeable fissured medium, Pacific Northwest Lab., Richmond, Washington.

Strack, O.D.L., 1984, Three-dimensional streamlines in Dupuit-Forchheimer models, Water Resour. Res., 20(7), pp 812-822.

Strack, O.D.L., 1986, Curvilinear analytic elements, Report on research done for the U.S. Bureau of Mines, Minneapolis, Strack Consulting Inc., North Oaks, Minnesota, USA.

Strack, O.D.L., 1989a, Groundwater Mechanics, Prentice Hall, New Jersey

Strack, O.D.L., 1989b, Multi-layer aquifer modeling using the analytic element method, Proc. 4th Int. Conf. on the use of models to find working solutions to groundwater problems, Nat. Water well Ass., Dublin Ohio, USA

Strack, O.D.L., 1990, Unconfined two-fluid flow, Report pursuant to contract DB-612, Strack Consulting Inc., North Oaks, Minnesota, USA.

Strack, O.D.L., 1991a, An area-sink for modeling leakage near wells, Report pursuant to contract DB-612, Strack Consulting Inc., North Oaks, Minnesota, USA.

Strack, O.D.L., 1991b, A Dupuit-Forchheimer model for variable density flow, Report pursuant to contract DB-612, Strack Consulting Inc., North Oaks, Minnesota, USA.

Strack, O.D.L., 1992a, Dupuit-Forchheimer solution for flow with density that varies horizontally, Report pursuant to contract DB-612, Strack Consulting Inc., North Oaks, Minnesota, USA.

Strack, O.D.L., 1992b, A Multi-Quadratic area-sink, Report pursuant to contract DB-612, Strack Consulting Inc., North Oaks, Minnesota, USA.

Strack, O.D.L., 1992c, The superblock analytic element model, Report pursuant to contract DB-612, Strack Consulting Inc., North Oaks, Minnesota, USA.

Strack, O.D.L., 1992d, An area element for leakage near streams, Report



pursuant to contract DB-612, Strack Consulting Inc., North Oaks, Minnesota, USA.

Strack, O.D.L., 1993, An area-sink with multi-logarithmic density distribution, Report pursuant to contract DB-612, Strack Consulting Inc., North Oaks, Minnesota, USA.

Strack, O.D.L. and H.M. Haitjema, Modeling double aquifer flow using a comprehensive potential and distributed singularities, 2 Solution for inhomogeneous permeabilities, *Water Resour. Res.*, 17(5), pp 1551-1560.

Van den Akker, C., 1982, Numerical flow analysis of the streamfunction in plane groundwater flow, PhD-thesis, Delft University of Technology, Delft, The Netherlands

Van der Veer, P., 1978, Calculation methods for two-dimensional groundwater flow, PhD Thesis, Delft University of Technology, Delft, The Netherlands.

Van Drecht, G., 1983, Berekening van stationaire grondwaterstroming naar sloten, RID-rep 83-1, National Institute for Water Supply, Leidschendam, The Netherlands.

Verhagen, F., 1992, Een MLAEM model van het Plateau van Margraten, MSc. thesis, Wageningen Agricultural University, Wageningen.

Verruijt, A., 1982, Groundwater flow, 2<sup>nd</sup> edition Macmillan

Wassiyng, A., 1982, Solving  $Ax = b$ ; A method with reduced storage requirements, *SIAM J. Numer. Anal.* 19(1), pp 197-204.

Youngs, E.G., 1992, Patterns of steady groundwater movement in bounded unconfined aquifers, *Journal of Hydrology*, 131, pp. 239-253

Zaadnoordijk, W.J., 1988, Analytic elements for transient groundwater flow, PhD-thesis, Univ. of Minnesota, Minnesota.



## LIST OF SYMBOLS

symbol	defined in chapter	meaning
$a$	6	anisotropy factor [-]
$a_c$	4	constant [-]
$a_m$	4	constant $m = 1, M$
$a_w$	5	distance between the line of observation and the well [L]
$A$	7	size of area [L <sup>2</sup> ]
$A_k$	7	size of sub-area $k$ [L <sup>2</sup> ]
$A_{tot}$	7	total observed area [L <sup>2</sup> ]
$A_o$	7	sum of all rectangular sub-areas with parallel flow [L <sup>2</sup> ]
$A_\Delta$	7	sum of all triangular sub-areas with parallel flow [L <sup>2</sup> ]
$A_i$	7	size of area between surface waters $i$ and $i + 1$ [L <sup>2</sup> ]
$A_{  }$	7	total area with parallel flow [L <sup>2</sup> ]
$A_{\underline{v}}$	7	total area with radial flow [L <sup>2</sup> ]
$b_j, b_m$	3	base level of layer $j$ resp. $m$ in a stratified aquifer [L]
$B$	6	width of the surface water [L]
$B_{cr}$	5	width of the crack [L]
$B_{tr}$	5	width of the through at upper side of the aquifer [L]
$B_1$	5	width of strip with constant strength [L]
$c$	5	resistance of separating top layer [T]
$c'$	5	specific resistance to groundwater flow [T]
$c''$	5	specific resistance to groundwater flow inside strip $dx$ under trough [T]
$c^*$	6	feeding resistance [T]
$c^*_{B+L}$	6	combination of feeding resistance and entrance resistance [T]
$c^*_{rep}$	7	representative feeding resistance over an area with both radial and parallel flow [T]
$c^*_{r  }$	7	representative feeding resistance for parallel flow in a corner between a water divide and a surface water [T]
$c^*_{  }$	7	representative feeding resistance over an area with parallel flow [T]
$c^*_{\underline{v}}$	7	representative feeding resistance over total area with radial flow [T]

symbol	defined in chapter	meaning
$c_{\underline{v},R}^*$	7	feeding resistance for radial flow inside the circular area with radius R [T]
$c_{\square}^*$	7	representative feeding resistance for the rectangular sub-areas [T]
$c_{\triangle}^*$	7	representative feeding resistance for the triangular sub-areas [T]
$c_{\underline{v},\triangle}^*$	7	feeding resistance for radial flow inside a triangular area [T]
$c_{\text{drain}}$	6	drainage resistance [T]
$c_{\text{lkw}}$	5	resistance of the leaky wall against horizontal flow [T]
$c_{\text{rad}}$	6	radial resistance [T/L]
$c_{\text{tr}}$	5	total resistance generated by trough in the aquifer [T]
$c_0$	6	resistance of bottom layer of surface water [T]
$c_0^{\circ}$	6	resistance parameter with $c_0$ [T]
$c_0''$	6	resistance parameter with $c_0$ [L]
$c_0^*$	6	resistance between surface water and boundary at $x = 0$ or at $x = L$ in the upper aquifer [T]
$c_1$	6	resistance of separating layer between upper, local aquifer and regional aquifer [T]
$c_1^{\circ}$	6	resistance parameter with $c_1$ [T]
$c_1'$	6	resistance of the separating layer combined with the vertical resistance in the upper aquifer [T]
$c_1''$	6	resistance parameter with $c_1$ [L]
$c_2$	3	resistance of separating layer between two regional aquifers [T]
$C$	6	parameter in the derivation [T/L]
$C_c$	3	integration constant for confined situation [ $L^3/T$ ]
$C_i$	5	integration constants, $i = 1, \dots, 4$ [-] or [L]
$C_u$	3	integration constant for unconfined situation [ $L^3/T$ ]
$D$	3	distance between top of aquifer and the reference level [L]
$D_s$	3	depth of interface compared to the reference level [L]
$E$	5	relative difference between fluxes [-]
$F(n,z)$	6	function [-]
$F(\delta_w, \epsilon_w, H, r_w)$	5	function given in (CHO-TNO, 1964, p 82) [-]
$h$	3	thickness over which the groundwater flow occurs [L]
$H$	3	thickness of confined aquifer [L]
$H_{\text{inh}}$	5	thickness of aquifer inside inhomogeneity [L]

symbol	defined in chapter	meaning
$H_j$	3	thickness of layer $j$ in a stratified aquifer [L]
$H_{tr.}$	5	maximum thickness of the through [L]
$H_0$	6	thickness of the upper, local aquifer [L]
$H_0^*$	6	thickness of phreatic aquifer directly contributing to the surface water [L]
$H_1$	6	thickness of the lower, regional aquifer [L]
$H_{1,a}$	6	thickness of the lower, regional aquifer above separating flow line [L]
$H(x)$	5	thickness under the trough at $x$ [L]
$i_z$	4	unit vector in vertical direction [-]
$I_{ki}$	7	parameter in derivation including modified-Bessel functions, $i = 1,2,3$ [-]
$k$	3	hydraulic conductivity [L/T]
$k_{cr}$	5	hydraulic conductivity of the crack [L <sup>2</sup> /T]
$k_{high}$	5	highest hydraulic conductivity in anisotropic aquifer [L/T]
$k_{inh}$	5	hydraulic conductivity inside the inhomogeneity [L/T]
$k_j, k_m$	3	hydraulic conductivity of layer $j$ resp. $m$ in a stratified aquifer [L/T]
$k_{low}$	5	lowest hydraulic conductivity in anisotropic aquifer [L/T]
$k_x(\rho_f)$	4	hydraulic conductivity in terms of $\rho_f$ in $x$ -direction [L/T]
$k_y(\rho_f)$	4	hydraulic conductivity in terms of $\rho_f$ in $y$ -direction [L/T]
$k_z(\rho_f)$	4	hydraulic conductivity in terms of $\rho_f$ in $z$ -direction [L/T]
$k_{0,x}$	6	hydraulic conductivity in horizontal direction in the upper aquifer [L/T]
$k_{0,z}$	6	hydraulic conductivity in vertical direction in the upper aquifer [L/T]
$k_{1,x}$	6	hydraulic conductivity in horizontal direction in the lower aquifer [L/T]
$K_R$	6	parameter including modified Bessel function [-]
$K_0$	4	modified Bessel functions of the second kind and of order zero
$K_1$	4	modified Bessel functions of the second kind and of order one
$l_a$	7	length of surface waters at the border of a rectangular area [L]
$l_\Delta$	7	length of surface waters at the border of a triangular area [L]
$l_{i,j}$	7	length of the surface water $i$ [L]

symbol	defined in chapter	meaning
$l_{tot}$	7	total length of surface waters in the observed area [L]
$L$	6	distance between the borders of the parallel surface waters [L]
$L'$	7	distance between the surface water and the water divide [L]
$L''$	7	L determined using the practical approach in sub-section 6.4.5 [L]
$L$	7	distance between parallel surface waters in a rectangular area [L]
$L_{\Delta}$	7	distance between parallel surface waters in a triangular area [L]
$L'(x)$	7	distance between the surface water and the water divide at x [L]
$L_i$	7	distance between surface water i and surface water i + 1 [L]
$L_k$	7	distance between surface water and waterdivide [L]
$L_{k-low}$	5	length in direction of lowest hydraulic conductivity over which leaky wall represents anisotropic behaviour [L]
$L_{cr}$	5	length of the crack [L]
$L_{lkw}$	5	length of the leaky wall [L]
$L_{rep}$	7	representative distance between the surface waters [L]
$M$	7	drainage density [1/L]
$p$	3	surface water level [L]
$p'$	6	constant including surface water level and resistances [L]
$p^*$	6	modified surface water level [L]
$P_m$	3	observation point [-]
$P_n$	6	natural recharge [L/T]
$q_x$	4	specific discharge in x direction [L/T]
$q_y$	4	specific discharge in y direction [L/T]
$q_z$	4	specific discharge in z direction [L/T]
$q_0(0)$	6	flux at x = 0 [L/T]
$q_1(A)$	6	flux per unit thickness through vertical section at A [L/T]
$q_1(L)$	6	flux per unit thickness through vertical section at L [L/T]
$Q_{cr,m}$	5	flux in the middle of the crack [L <sup>3</sup> /T]
$Q_{cr}(r_{Qmx})$	5	maximum flux through the crack at $r_{Qmx}$ [L <sup>3</sup> /T]
$Q_l$	3	line-sink discharge [L <sup>3</sup> /T]
$Q_n$	5	normal flux across line [L <sup>3</sup> /L.T]

symbol	defined in chapter	meaning
$Q_R$	7	volume per unit time across the circular boundary at radius $R$ ( $L^3/T$ )
$Q_w$	3	abstraction rate (strength) of the well [ $L^3/T$ ]
$Q_{w,i}$	5	the abstraction rate of the well affected by $i = 0, 1, 2, 3, 4$ crack(s) [ $L^3/T$ ]
$Q_{w,inh}$	5	the abstraction rate of the well affected by an inhomogeneity [ $L^3/T$ ]
$Q_x, Q_y$	3	discharge vector per unit width in x- respectively y- direction [ $L^3/L.T$ ]
$Q_{x,in}$	5	flux component in x-direction per unit width (in y-direction) inside inhomogeneity [ $L^3/L.T$ ]
$Q_{x,out}$	5	flux component in x-direction per unit width (in y-direction) outside inhomogeneity [ $L^3/L.T$ ]
$Q(0)$	5	flux over entire thickness at $x = 0$ per unit width perpendicular to the section [ $L^3/L.T$ ]
$Q(r_{Qmx})$	5	flux through circle at $r = r_{Qmx}$ outside the crack [ $L^3/T$ ]
$Q(B_1)$	5	flux over entire thickness at $x = B_1$ per unit width [ $L^3/L.T$ ]
$r$	3	distance between well and observation point [L]
$r_{inh}$	5	radius of circular inhomogeneity [L]
$r_{lkw}$	5	distance from well to concentric circular leaky wall [L].
$r_{Qmx}$	5	distance from the well to the point of maximum flux in the crack [L]
$r_{rad}$	6	specific radial resistance [T/L]
$r_{ref}$	3	distance from the well to the reference point [L]
$r_w$	3	well radius [L]
$r_1$	5	distance from well to closest tip of the crack [L]
$r_2$	5	distance from well to farthest tip of the crack [L]
$R$	7	radius of circular area [L]
$R_i$	7	parameters in derivation $i = 0, 1, 2, 3, 4, 5$ [ $L^2/T$ ], [-], [ $L^2/T$ ], [T/L], [T], [T]
$s$	6	flux through separating layer [L/T]
$s_{Lav}$	6	average over $L$ of flux through the separating layer [L/T]
$s_{Bav}$	6	average flux through bottom of surface water with width $B/2$ [L/T]
$s_{Bav}''$	6	average flux through bottom of surface water over width $B/4$ [L/T]
$s_{Rav}$	6	average flux through the separating layer over circular area with radius $R$ [L/T]
$s_1$	6	flux through bottom layer of surface water [L/T]
$s_2$	6	flux through separating layer below surface water [L/T]

symbol	defined in chapter	meaning
$S$	6	volume per unit time through the separating layer over the area of concern [ $L^3/T$ ]
$S_j$	3	strength of element $j$ [ $L^3/T$ ]
$S_{F_{m,j}}$	3	shape function of element $j$ [-]
$S(0, B_1)$	5	the total flux through the separating layer between $x = 0$ and $x = B_1$ per unit width perpendicular to the section [ $L^3/L.T$ ]
$T$	5	transmissivity of the aquifer [ $L^2/T$ ]
$T_{an}$	5	equivalent transmissivity in an annular domain including the effect of the crack(s) [ $L^2/T$ ]
$T_{eq}$	5	equivalent transmissivity for domain between reference point and well [ $L^2/T$ ]
$T''$	5	transmissivity at $x$ inside the strip $dx$ under the trough [ $L^2/T$ ]
$U_s$	5	flux component in the direction of the crack generated by the uniform flow independent of the crack [ $L^2/T$ ]
$U_s(r)$	5	flux component at $r$ in the direction of the crack generated by the well independent of the crack [ $L^2/T$ ]
$v$	5	valuator to determine effect of a leaky wall [-]
$x$	5	coordinate with the origin at the point of projection of the well on the line of observation [L]
$x'$	6	modified coordinate [L]
$x_m, y_m, z_m$	4	coordinates of point $m$ [L]
$X$	5	parameter [-]
$X'$	6	modified coordinate [L]
$Y$	5	parameter [-]
$Z$	4	observation level [L]
$Z_{ref}$	4	level of reference plane [L]
$\alpha$	6	parameter in derivation [-]
$\alpha_c$	5	constant [-]
$\alpha_i$	6	parameters in derivation $i = 1, 2, 3$ [-]
$\alpha^\circ$	3	$\beta^\circ + 1/2 \pi$ , orientation of dipoles at line-doublet [-]
$\beta$	6	parameter in derivation [-]
$\beta_c$	5	constant [-]
$\beta_i$	6	parameters in derivation, $i = 1, 5$ [-]
$\beta_p$	6	parameter in derivation [-]
$\beta^\circ$	3	orientation of dipole, line-dipole [-].



symbol	defined in chapter	meaning
$\gamma$	3	vertical flow or strength per unit area [L/T]
$\gamma_c$	5	constant [-]
$\gamma_i$	6	parameters in derivation, $i = 1, 13$ [-]
$\gamma^\circ$	7	corner between the surface water and the water divide [-]
$\delta_i$	6	parameters in derivation, $i = 1, 5$ [-]
$\delta_w$	5	length of the well screen [L]
$\Delta$	4	smoothing parameter [L]
$\Delta^\circ$	5	angle between line-sink and considered line [-]
$\epsilon$	7	parameter in derivation [L <sup>2</sup> /T]
$\epsilon_i$	6	parameters in derivation, $i = 1, 11$ [-]
$\epsilon_p$	6	parameter including $p$ [-]
$\epsilon_{scale}$	4	scale parameter [-]
$\epsilon_w$	5	excentricity of the well screen [L]
$\kappa$	7	parameter in derivation [L <sup>2</sup> /T]
$\kappa_i$	6	constant $i = 1, 2, 3$ [T], [T], [-]
$\lambda$	4	characteristic length [L]
$\lambda_{01}$	6	combined characteristic length [L]
$\lambda_0$	6	characteristic length in the upper aquifer [L]
$\lambda_0'$	6	"minor" characteristic length in the upper aquifer [L]
$\lambda_1$	6	characteristic length in the lower aquifer [L]
$\nu$	3	relative density [-]
$\nu_0$	4	constant related to relative density [-]
$\rho$	4	density, varying with place [M/L <sup>3</sup> ]
$\rho_f$	3	density of fresh water [M/L <sup>3</sup> ]
$\rho_s$	3	density of salt water [M/L <sup>3</sup> ]
$\tau_{dip}$	3	strength of dipole [L * L <sup>3</sup> /T]
$\sigma_{dip}$	3	strength of line-dipole per unit length [L <sup>3</sup> /L.T]
$\sigma_{dou}$	3	strength of line-doublet [L <sup>3</sup> /L.T]
$\sigma_{inh}$	3	strength of inhomogeneity [L <sup>3</sup> /L.T]
$\sigma_{lin}$	3	strength of line-sink per unit length [L <sup>3</sup> /L.T]
$\varphi$	3	head [L]
$\varphi(\rho_f)$	4	head in the regional aquifer in terms of $\rho_f$ [L]
$\varphi_i$	3	head in aquifer $i = 0, 1, 2, 3, \dots$ [L]

symbol	defined in chapter	meaning
$\phi_l$	3	head in the lower part of an aquifer with impermeable laminae [L]
$\phi_{ref}$	5	head at the reference point [L]
$\phi_{Zref}(\rho_f)$	4	head at reference level in terms of $\rho_f$ [L]
$\phi_s$	3	head (in terms of $\rho_s$ ) in the saline part of the aquifer [L]
$\phi_u$	3	head in the upper part of an aquifer with impermeable laminae [L]
$\phi_w$	5	head at the well radius [L]
$\phi_0$	6	head in the upper, local aquifer [L]
$\phi_0(0)$	6	head in the upper, local aquifer at $x = 0$ [L]
$\phi_0(-B/2)$	6	head in the upper, local aquifer at $x = -B/2$ [L]
$\phi_0(r_w)$	6	head at the boundary between the entrance resistance layer and the top aquifer [L]
$\phi_{0,Bav}$	6	average of $\phi_0$ over $-B/2 < x < 0$ [L]
$\phi_{0,Lav}$	6	average of $\phi_0$ over $0 < x < L/2$ [L]
$\phi_1$	6	head in the regional aquifer [L]
$\phi_{1,Lav}$	6	average of $\phi_1$ over $L$ [L]
$\phi_1(L)$	6	head in the regional aquifer at $x = L$ [L]
$\phi_1(x)$	5	head in the regional aquifer at $x$ [L]
$\phi_1(0)$	5	head in the regional aquifer at $x = 0$ [L]
$\phi_2$	3	head in the second (lowest) aquifer [L]
$\Phi$	3	discharge potential [ $L^3/T$ ]
$\Phi_{ref}$	3	discharge potential at the reference point [ $L^3/T$ ]
$\Phi_m$	3	discharge potential in an observation point $P_m$ generated by all elements in the model [ $L^3/T$ ]
$\Phi_{m,j}$	3	discharge potential in observation point $P_m$ , generated by element $j$ [ $L^3/T$ ]
$\Phi(r)$	3	discharge potential at distance $r$ from the well [ $L^3/T$ ]
$\Phi^-$	3	discharge potential at the outside of the inhomogeneity boundary [ $L^3/T$ ]
$\Psi$	3	stream function [ $L^3/T$ ]
$\Omega$	3	complex potential [ $L^3/T$ ]

## CURRICULUM VITAE

Willem Jan de Lange werd op 22 december 1953 in Semarang (Indonesië) geboren. In 1975 runde hij de studie weg- en waterbouwkunde aan de toenmalige Hogere Technische School te Leeuwarden af, waarna hij tot 1981 Civiele Techniek studeerde aan de toenmalige Technische Hogeschool te Delft. In de afstudeerfase ontwikkelde hij onder meer een drie-dimensionaal model met een scherp grensvlak tussen zoet en zout grondwater gebaseerd op de rand-elementen methode. Na zijn militaire dienst werkte hij vanaf 1983 bij de provinciale Waterstaat van Zuid-Holland als geohydroloog aan diverse projecten op het gebied van bescherming van waterwinningen en bodembescherming. Daar onderzocht hij onder andere het voorlopen van de getijbeweging in het grondwater op de getijbeweging in de Hollandse IJssel nabij Gouderak. In die periode is ook de ontwikkeling van een theorie voor het combineren van risico's met betrekking tot grondwater gestart, die verder mede door hem is uitgewerkt bij het Rijksinstituut voor Integraal Zoetwaterbeheer en Afvalwaterbehandeling te Lelystad. Daar begon hij in 1986 als senior-geohydroloog en startte eind 1987 met de bouw van NAGROM, het landsdekkende grondwatermodel van Rijkswaterstaat. Dit proefschrift vormt een belangrijk deel van de onderbouwing van dit model.





